Dissertation

Morphological PAT tools for filamentous bioprocesses

Monitoring and control enhanced for fungal morphology

ausgeführt zum Zwecke der Erlangung des akademischen Grades eines Doktors der technischen Wissenschaften unter der Leitung von

Univ.Prof. Dipl.-Ing. Dr.techn. Christoph Herwig
Institut 166/4
Institut für Verfahrenstechnik, Umwelttechnik und Technischen Biowissenschaften

eingereicht an der Technischen Universität Wien
Fakultät für Technische Chemie

von

Dipl.-Ing. Lukas Veiter
Matrikelnummer: 00927445

_____ _____

Wien, am eigenhändige Unterschrift

Meinem Opa gewidmet.

Danksagung

An dieser Stelle möchte ich zuallererst Prof. Christoph Herwig für die wohlwollende Aufnahme in sein Team und die damit verbundenen, an Ressourcen reichen Arbeitsbedingungen danken. Wissenschaftlicher Fortschritt verlangt nach frischen Ideen. Besonders sei ihm daher dafür gedankt, dass er mir stets mit den richtigen Impulsen zur Seite stand, um meiner Arbeit den letzten Schliff zu geben.

Ich möchte mich bei den Mitarbeitern von Sandoz für die großartige Zusammenarbeit bedanken, im Besonderen bei Michael Weiner und Ivo Zadra für die Möglichkeit, meine Methoden und Ideen auch vor Ort in Kundl testen zu können.

Im Lauf meiner Dissertation durfte ich mit vielen Post-Docs zusammenarbeiten, ich danke daher Jens Fricke, Ines Stelzer und Vignesh Rajamanickam für ihre Unterstützung! Natürlich bin ich auch dem institutsübergreifenden Elan von Christoph Slouka zu Dank verpflichtet, der viele Forschungen erst möglich gemacht hat. Danke auch an Markus Kubicek, für seine Geduld und seine verlässliche Unterstützung hierbei! Julian Kagers Expertise in Fermentation und Prozesskontrolle war immens wichtig, um den Kreis zwischen den Bereichen Analytik und Kontrolle zu schließen.

Anschließend möchte ich mich bei Oliver Spadiut und der gesamten „OSP-Group' insbesondere bei David Wurm, Britta Eggenreich, Thomas Gundinger, Julian Quehenberger und Alexander Pekarsky für Freundschaft und Hilfe bedanken. Außerdem konnten mir meine Studenten und Studentinnen Thomas Hartmann, Maximilian Podsednik, Marija Simonovic und Thomas Seper sehr erfolgreich bei den Laborarbeiten helfen. Für die Unterstützung im Labor bin ich natürlich allen derzeitigen und ehemaligen Kolleginnen und Kollegen zu Dank verpflichtet.

Abschließend möchte ich meine Familie nicht unerwähnt lassen, die mir weit über das Studium hinaus stets unter die Arme gegriffen hat.

Besonderer Dank gebührt auch der Corina für ihr Helfen, nicht zuletzt auch bei Erstellung des Layouts dieser Dissertation.

Zusammenfassung

Biomasse ist die wohl essenziellste Prozessvariable in Bioprozessen. Prozesskontrolle, Effizienz und Produktivität hängen in filamentösen Bioprozessen direkt von zellulären Aspekten ab. So können morphologische Eigenschaften der Biomasse und deren Konsequenzen stark variieren, daher muss die Morphologie stets individuell betrachtet werden. Hierbei umfasst der Begriff der „Qualität“ ganz eindeutig auch die Qualität der Biomasse, sprich ihre vorteilhafte Morphologie als Garant für dauerhaft erhöhte Viabilität und Effizienz im Prozess.

Filamentöse Pilze bilden eine Vielzahl an morphologischen Formen: homogen verteilte Hyphen, stark verzweigte Konstrukte aus Hyphen-Aggregaten und schließlich das filamentöse „Pellet“, bestehend aus einem Agglomerat an Hyphen mit dichtem Kern. Morphologie, Viabilität und Produktivität sind eng miteinander verbunden. Je nach Ziel des Bioprozesses, können unterschiedliche Charakteristiken der Morphologie von Vorteil sein, die umfassend analysiert und quantifiziert werden müssen.

Morphologie und Viabilität können mit unterschiedlichsten Methoden untersucht werden, jede Methode ist hierbei gewissen Limitationen unterworfen. So ist die Bildanalyse als ein sehr gängiges, meist auf Mikroskopie basierendes Verfahren sehr arbeits- und zeitintensiv. Typische Methoden zur Bestimmung der Viabilität umfassen die dielektrische Spektroskopie oder die Verwendung von fluoreszierenden Farbstoffen, was hinsichtlich der komplexen filamentösen Morphologie oft zu Problemen führt. Daher war unser Ziel in dieser Dissertation, eine respektable Anzahl an alternativen, zeitsparenden und statistisch robusten Methoden zur Bestimmung von Morphologie und Viabilität entwickeln. Dabei kamen Durchflusszytometrie sowie fluoreszierende Farbstoffe zum Einsatz, bei deren Verwendung wurden neuartige morphologische Einblicke in die Pellet-Biomasse erhalten, wie beispielsweise „Pellet Kompaktheit“ und „viable Pelletschicht“. Zusätzlich konnten wir mittels ortaufgelöster Massenspektrometrie den Metabolismus und die produktiven Regionen in filamentösen Pellets mittels einer neuartigen Methode analysieren.

Unsere übergeordnete Ambition war der Einsatz obgenannten analytischer Methoden, um neuartige morphologische Aspekte der Biomasse zugänglich zu machen. Mit diesem Wissen war eine Optimierung der Prozessführung während der Fermentation inklusive verbesserter Viabilität und Produktivität möglich. Dabei wurden weitere Kontrollmechanismen angewandt und entwickelt: beispielsweise zur Kontrolle der Wachstumsrate und der spezifischen Substrat-Aufnahmerate in *Penicillium chrysogenum* Fermentationen. Durch statistische Versuchsplanung unter Variation der Faktoren Leistungseintrag, Gelöstsauerstoff-Konzentration und spezifische Substrataufnahmerate konnte ein mit neuartigen, morphologischen Daten getriebenes Modell erstellt werden. Damit ist eine optimierte Prozessführung zugänglich geworden, die nachweislich eine erhöhte Viabilität und spezifische Produktivität in der Fermentation erreicht.

Die entstandene Methodensammlung, unterteilt in die Bereiche „Analytik“ und „Kontrolle“ soll dabei als Werkzeug im Rahmen der Prozess Analytischen Technologie (PAT) dienen - speziell entwickelt für die Erfordernisse der filamentösen Morphologie. Um die Vielseitigkeit unserer Methodik zu demonstrieren, haben wir ausgewählte Methoden auch bei nicht filamentösen Organismen erfolgreich angewandt.

Abstract

Biomass is one of the most essential process variables in bioprocesses. Process performance, process controls strategies and productivity in filamentous processes highly depend on cellular aspects, such as morphological elements of the biomass which calls for a segregated view of biomass. In filamentous bioprocesses, quality of the biomass is of prime importance. Hereby one strives to ensure high biomass viability and productivity.

Filamentous fungi display a large variety of morphological forms in submerged cultures. These range from dispersed hyphae to denser hyphal aggregates, the so-called pellets. Morphology, viability and productivity are tightly interlinked. Depending on the objective function of the bioprocess, different characteristics of morphology are favourable and need to be quantified accordingly.

Morphology and viability can be determined via a variety of methods, each limited to specific areas of application. The most common method to characterize morphology is image analysis based on microscopy, which is work intensive and time consuming. Typical methods to determine viable biomass encompass di-electric spectroscopy or staining reagents, which is troublesome regarding the complex fungal morphology. Therefore, our objective was to develop several alternative, robust and statistically sound methods based on flow cytometry and fluorescent staining for at-line application capable of assessment of morphology and viability. Furthermore, novel morphological characteristics describing pellet biomass are assessable via these methods: ‘pellet compactness’ and ‘viable pellet layer’. Additionally, spatially resolved mass spectrometry was used in a novel technique to study metabolism and productive zones in fungal pellets.

Our superior goal was to apply said analytical methods to study novel morphological responses and use this knowledge to determine a process design space in fermentation ensuring optimal morphology, viability and productivity. To achieve this, we employed and developed additional control strategies to regulate the growth rate or specific substrate uptake during *Penicillium chrysogenum* fermentations. In a design of experiments (DOE) approach, fermentation factors power input, dissolved oxygen concentration and specific substrate uptake rate were varied to feed a data-driven model including novel morphological responses. Thereby an optimised process design could be obtained which resulted in enhanced biomass viability and specific productivity.

We envision that the methods compiled in the comprehensive ‘Analytics’ and ‘Control’ chapters of this Thesis will serve as process analytical technology (PAT) tools specifically enhanced for complex fungal morphology and providing novel morphological descriptors. Additionally, we have successfully tested our methodology on other agglomerate-forming organisms like yeast to demonstrate versatility and transferability.

Table of Content

Chapter 1.
Introduction

Process analytical technology in filamentous bioprocesses

Process analytical technology (PAT) was defined as a framework for 'designing, analysing, and controlling manufacturing through timely measurements of critical quality and performance attributes' by the U.S. Food and Drug Administration (FDA) in 2004 (FDA 2004).

The goal of this initiative can be summarised as an improvement of product quality through comprehensive process understanding (Langemann et al. 2016). This approach encompasses design, analysis and control of manufacturing processes via 'timely measurement of critical quality and performance attributes of raw and in-process materials' (Langemann et al. 2016). 'Timely' or 'real-time' is used in this context to demonstrate that measurement responses are generated before the next process stage is initiated (Read et al. 2010). The industrial implementation of this initiative has been defined by the International Conference on Harmonization (Simon et al. 2015) in the documents: ICH Q8.

PAT is intrinsically connected to Quality by Design (QbD) as defined in the aforementioned ICH Q8 guideline (Rathore and Winkle 2009) describing QbD as 'a systematic approach to development that begins with predefined objectives and emphasises product and process understanding and process control, based on sound science and quality risk management'.

Thereby the characterisation of product attributes which define safety and efficacy is summarised as critical quality attributes (CQA) such as biological activity, impurities and immunochemical properties (Rathore et al. 2017). However, QbD also includes all relevant process aspects such as process design, control and monitoring strategies, as well as validation techniques (Rathore and Devine 2008). The key aspect of QbD is that quality is not merely defined as a single product characteristic but is considered already in process design and during production. Consequently, a continuity of understanding in all process phases must be ensured via identification of critical material attributes (QMA) and critical process parameters (CPP) (Herwig 2010). PAT tools provide the means to achieve this complex task: process design, analysis and control are facilitated through real-time monitoring of the aforementioned critical parameters: CMAs, CPPs and CQAs. The generation of process understanding from a PAT perspective is illustrated in Figure 1.1.

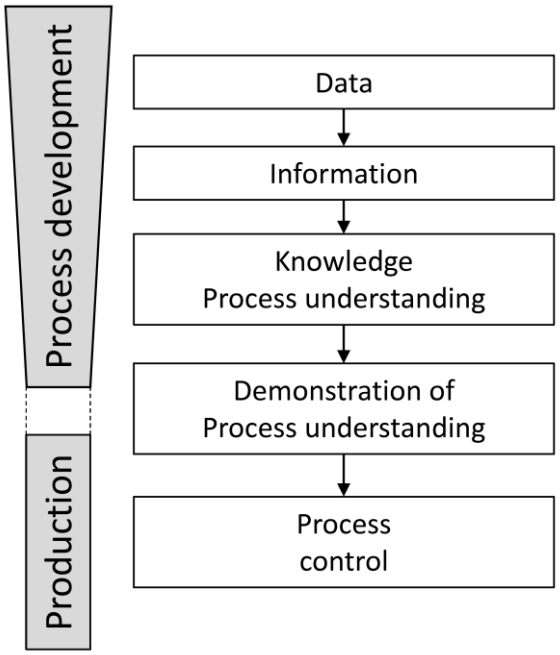

Figure 1.1. Generation of process understanding in accordance with PAT from process development towards production, adapted from Herwig 2010.

Naturally, an industrial manufacturer will strive for enhanced productivity and reduction of variability as soon as process quality can be ensured. Subsequent process optimisation should be performed within a defined design space including all critical process parameters which have previously been shown to affect quality (Kager 2019). In filamentous bioprocesses such a design space must consider biomass as a form of quality attribute: process performance, process control strategies and productivity in filamentous processes highly depend on biomass morphology which calls for a segregated view of biomass. Consequently, in filamentous bioprocesses the term quality also encompasses the 'quality' of the biomass itself.

Challenges regarding PAT and filamentous morphology

Hyphal growth is characterised by cells which grow from a germination point and later branch into various macroscopic structures (Simon et al. 2015). These structures might include homogeneously distributed hyphae known as filamentous growth or compact agglomeration of hyphae commonly known as fungal pellets (Zhang and Zhang 2016). All these morphological forms exhibit complex effects on biomass growth and viability, process control and productivity, making them an essential factor in process design. Furthermore, while the taking of representative samples is a general burden in a large bioreactor, morphological heterogeneity poses additional monitoring challenges (Simon et al. 2015). Examples of PAT related applications in filamentous bioprocesses are provided in Table 1.

Table 1. Examples for PAT related applications in filamentous bioprocesses.

Application	Method(s)	Conclusion	Reference
Real-time monitoring of filamentous biomass	Dielectric spectroscopy, software sensors fluorescence spectroscopy, turbidity probe	Combination of dielectric spectroscopy and turbidity measurements yielded favourable prediction errors over a broad biomass range	Sarra et al. 1996 Neves et al. 2001 Ronnest et al. 2011
Cell mass and lipase activity in *Aspergillus oryzae* cultivations	multi-wavelength fluorescence analysis	Monitoring fed-batch cultivations of filamentous fungi	Haack et al. 2007
Customization of *Aspergillus niger* morphology	Addition of inorganic insoluble micro particles	Control of fungal morphology	Wucherpfennig et al. 2012
Physiological description of interdependencies between process parameters	Definition of CPPs followed by study of interdependencies by DoE.	Novel, scalable key process parameter for pellet morphology and process performance established	Posch and Herwig 2014
Morphological and physiological bioprocess characterization of filamentous organisms	Microscopy, dielectric spectroscopy, MALDI intact cell mass spectrometry, FTIR spectroscopy, multivariate data mining	Enhanced understanding of morphological and physiological behaviour	Posch et al. 2013
Determination of *Penicillium* spore inoculum quality	Flow cytometry combined with fluorescent staining	Detection of viable spores with intact growth potential enables reproducible inoculum	Ehgartner et al. 2016
Real-rime monitoring of penicillin production	Raman spectroscopy and off-gas analysis	Online estimation of the biomass concentration, specific growth rate, and specific penicillin production rate.	Golabgir and Herwig 2016
Micromorphology of *Trichoderma reesei* and its relationship with cellulase production	Confocal laser-scanning microscopy (CLSM) and the computer-aided image analysis	Analytical tool for enzyme production by *T. reesei* on lignocellulosic substrate	Novy et al. 2016
Prediction of filamentous process performance attributes by raw material quality assessment	Mid-infrared spectroscopy and chemometrics	Combination quality assessment and correlation with process performance to establish risk-based criteria	Hofer et al. 2018

Quantitative image analysis pipeline for the characterization of filamentous fungal morphologies	Microscopy and automated image analysis	Flexible approach to quantify diverse fungal morphologies	Cairns et al. 2019
Analysis of the three-dimensional morphology of fungal pellets	X-ray microtomography using freeze-dried pellets obtained from submerged cultivations	Optimize pellet structures by means of appropriate process or genetic control in biotechnological applications.	Schmideder et al. 2019

A prominent aspect in filamentous bioprocesses is the determination of viable biomass, which involves the online use of sensors and at-line application of analytical instruments to obtain relevant information in real-time or at least 'timely' as defined by Read et al. 2010. Typical PAT online monitoring techniques in this context include dielectric spectroscopy, infrared spectroscopy and fluorescence (Ronnest et al. 2011). However, inline sensors are prone to high measurement noise and require chemometric knowledge to establish measurement procedures. Furthermore, morphology is not considered. In order to assess these morphological aspects, other techniques are necessary. The most common method is still microscopy combined with some form of image analysis, preferably in an automated fashion (Posch et al. 2012, Veiter et al. 2018). To additionally assess viability, some form of a fluorescent staining technique is generally used in combination with a device to record said fluorescence like plate readers or confocal laser scanning microscopy. More advanced analytical techniques are summarized in our published review (Veiter et al. 2018) on fungal pellet morphology to be found in 'Chapter 4. State of the Art' of this Thesis. From a PAT perspective however, the majority of these methods can only be utilized in an at-line or offline capacity.

In recent years, the combination of flow cytometry with fluorescent staining (Ehgartner et al. 2017) was introduced as a potent tool to overcome previously mentioned obstacles, the most relevant advantage is statistical robustness due to fast measurement of thousands of particles in a matter of minutes. Flow cytometry provides a comprehensive assessment of morphological characteristics and biomass viability, however detailed information on hyphal structures and branching cannot be obtained as in microscopic techniques. The complexity and segregated nature of filamentous pellet structures requires even more enhanced analytics to shed light on physiology and productive zones in a spatially resolved way.

In the scope of this Thesis, we have developed several PAT tools to meet the aforementioned challenges. All methods are specifically designed to take fungal morphology into account. At the same time, we were following the specific methodology (Sagmeister et al. 2014) developed in scope of the Christian Doppler Laboratory funding the studies in this Thesis. This 'method cycle' is displayed in Figure 1.2 and will be explained in the following:

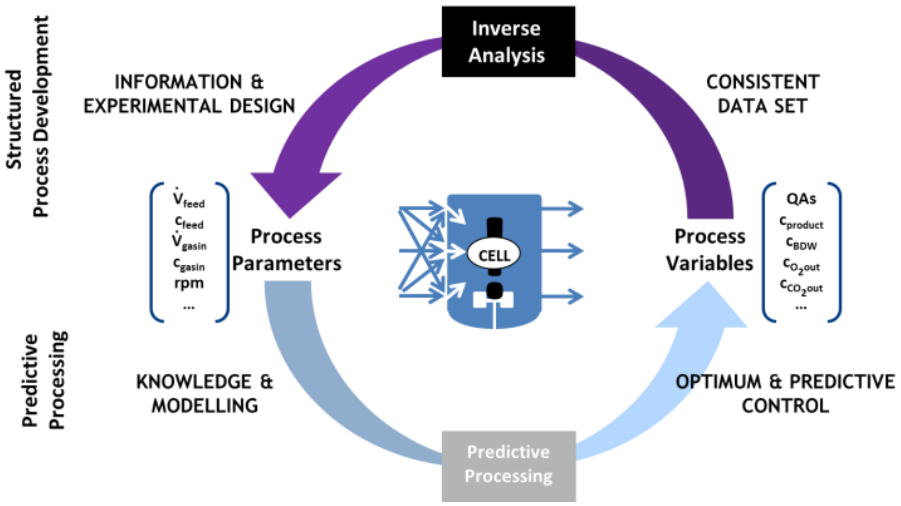

Figure 1.2. Method cycle as the central tool for the execution of the CD laboratory tasks.

The idea behind this approach is methodological synergy between methods (Sagmeister et al. 2014). Successful process development encompasses the enhancement of quality attributes (QAs) like product amount via an optimisation of process variables. To achieve this goal, experiments are executed which are defined by variation process parameters (PPs) and resulting process variables like product concentration. Through inverse analysis the relationship between QAs and PPs can be obtained and used identify critical process parameters (CPPs).

This methodology is started by analytical development (Figure 1.2, upper right) with the objective to achieve a reliable dataset. In filamentous bioprocess development this could be a reliable method to measure viable biomass combined with morphological assessment. In the following step this data can be transformed into knowledge in the form of physiological descriptors like yields (Ys) and specific rates (q_s) which are independent of experimental conditions. Consequently, these descriptors can be used in experimental design. For instance, the effect of a specific substrate uptake rate (q_s) on QAs like productivity can be tested (Figure 1.2, upper left).

As mechanistic hypotheses and correlations can be extracted from experimental data, a data-driven or mechanistic model can be formulated (Figure 1.2, lower left). In our case this was done in order to obtain an optimal operating range for enhanced process productivity and efficiency. In the end, this favourable operating range can be achieved through predictive processing and control strategies (Figure 1.2, lower right). We have employed methods to control either the growth rate or the specific substrate uptake rate in *Penicillium chryosgenum* bioreactor cultivations.

Methods described in ‘Chapter 5. Analytics’ and ‘Chapter 6. Control’ of this Thesis follow this methodology closely and will be explained in detail in the respective chapters. In the following section, the relationship between fungal morphology and productivity will be briefly discussed, as it is a prerequisite for process optimisation in filamentous cultivations. A detailed review of these interlinks can be found in ‘Chapter 4. State of the Art’.

Relationship between morphology and productivity

There is a close relationship between fungal morphology, biomass viability and productivity. As mentioned in the previous section, filamentous fungi can either grow in filamentous or pelleted form, which greatly affects process performance in a bioreactor. In turn, said morphology and physiology are influenced by fermentation process parameters like power input, dissolved oxygen content and substrate availability. Relevant factors need to be studied in a combined fashion to detect and describe possible inter-dependencies.

In general, we see enhanced viability and productivity in homogeneously dispersed hyphae or loose hyphal agglomerates. This comes at the expense of process control because dense hyphal entanglements lead to rheological challenges and issues regarding substrate and gas transfer. Pellet morphology is favoured in industrial bioprocesses due to their sphere-like form featuring tightly packed mycelium. This results in lower broth viscosity enabling higher cell densities due to facilitated gas-liquid mass transfer. However, pellet morphology is characterised by a dense core, which typically impairs oxygen and substrate penetration. Consequently, a dense pellet is degrading from the inside out with higher metabolic activity and productivity in the outer a.k.a. 'hairy' pellet region. We have thoroughly reviewed all relevant aspects of these interlinks (Veiter et al. 2018), our complete publication can be found in 'Chapter 4. State of the Art'.

When working with fungal pellets, the goal in process development is to enable a morphological compromise: The ideal pellet features (i) a loose morphology enabling oxygen diffusion into all biomass sections, at the same time it is (ii) dense enough to ensure all rheological advantages previously mentioned. In order to achieve this compromise, analytical techniques capable of measuring all relevant morphological and physiological characteristics are necessary.

In this Thesis we have utilized our previously developed analytical methods (see 'Chapter 5. Analytics') to study effects of fermentation parameters on *P. chrysogenum* pellet morphology. This approach enabled us to define an operating range for bioreactor cultivations to ensure optimal morphology, viability and productivity. These aspects will be discussed in 'Chapter 6. Control'.

References Introduction

Cairns TC, Feurstein C, Zheng XM, Zheng P, Sun JB, Meyer V (2019) A quantitative image analysis pipeline for the characterization of filamentous fungal morphologies as a tool to uncover targets for morphology engineering: a case study using aplD in *Aspergillus niger*. Biotechnol Biofuels 12.

Ehgartner D, Herwig C, Fricke J (2017) Morphological analysis of the filamentous fungus *Penicillium chrysogenum* using flow cytometry - the fast alternative to microscopic image analysis. Appl Microbiol Biotechnol 101: 7675-7688

Ehgartner D, Herwig C, Neutsch L (2016) At-line determination of spore inoculum quality in *Penicillium chrysogenum* bioprocesses. Appl Microbiol Biotechnol 100: 5363-5373.

FDA (2004) Guidance for Industry. PAT—a framework for innovative pharmaceutical development, manufacturing and quality assurance. Department of Health and Human Services - Food and Drug Administration. http://www.fda.gov/downloads/Drugs/Guidances/ucm070305.pdf (accessed 04/23/2014)

Golabgir A, Herwig C (2016) Combining Mechanistic Modeling and Raman Spectroscopy for Real-Time Monitoring of Fed-Batch Penicillin Production. Chem-Ing-Tech 88: 764-776

Haack MB, Lantz AE, Mortensen PP, Olsson L (2007) Chemometric analysis of in-line multi-wavelength fluorescence measurements obtained during cultivations with a lipase producing *Aspergillus oryzae* strain. Biotechnol Bioeng 96: 904-913

Herwig C (2010) Prozess Analytische Technologie in der Biotechnologie. Chem Ingen Tech 82: 405-414

Hofer A, Kamravamanesh D, Bona-Lovasz J, Limbeck A, Lendl B, Herwig C, Fricke J (2018) Prediction of filamentous process performance attributes by CSL quality assessment using mid-infrared spectroscopy and chemometrics. J Biotechnol 265: 93-100

Kager J (2019) The deployment of mechanistic models for advanced bioprocess monitoring and control. Vienna University of Technology

Langemann T, Mayr UB, Meitz A, Lubitz W, Herwig C (2016) Multi-parameter flow cytometry as a process analytical technology (PAT) approach for the assessment of bacterial ghost production. Appl Microbiol Biotechnol 100: 409-418

Neves AA, Pereira DA, Vieira LM, Menezes JC (2001) Real time monitoring biomass concentration in *Streptomyces clavuligerus* cultivations with industrial media using a capacitance probe. J Biotechnol 84: 45-52

Novy V, Schmid M, Eibinger M, Petrasek Z, Nidetzky B (2016) The micromorphology of *Trichoderma reesei* analyzed in cultivations on lactose and solid lignocellulosic substrate, and its relationship with cellulase production. Biotechnol Biofuels 9: 169

Posch AE, Herwig C (2014) Physiological description of multivariate interdependencies between process parameters, morphology and physiology during fed-batch penicillin production. Biotechnol Progr 30: 689-699

Posch AE, Koch C, Helmel M, Marchetti-Deschmann M, Macfelda K, Lendl B, Allmaier G, Herwig C (2013) Combining light microscopy, dielectric spectroscopy, MALDI intact cell mass spectrometry, FTIR spectromicroscopy and multivariate data mining for morphological and physiological bioprocess characterization of filamentous organisms. Fungal Genetics and Biology 51: 1-11

Posch AE, Spadiut O, Herwig C (2012) A novel method for fast and statistically verified morphological characterization of filamentous fungi. Fungal Genet Biol 49: 499-510

Rathore AS, Devine R (2008) PDA workshop on 'Quality by Design for Biopharmaceuticals: Concepts and Implementation'. May 21-22, 2007, Bethesda, Maryland. PDA J Pharm Sci Technol 62: 380-390

Rathore AS, Garcia-Aponte OF, Golabgir A, Vallejo-Diaz BM, Herwig C (2017) Role of Knowledge Management in Development and Lifecycle Management of Biopharmaceuticals. Pharm Res 34: 243-256

Rathore AS, Winkle H (2009) Quality by design for biopharmaceuticals. Nat Biotechnol 27: 26-34

Read EK, Shah RB, Riley BS, Park JT, Brorson KA, Rathore AS (2010) Process analytical technology (PAT) for biopharmaceutical products: Part II. Concepts and applications. Biotechnol Bioeng 105: 285-295

Ronnest NP, Stocks SM, Eliasson Lantz A, Gernaey KV (2011) Introducing process analytical technology (PAT) in filamentous cultivation process development: comparison of advanced online sensors for biomass measurement. J Ind Microbiol Biotechnol 38: 1679-1690

Sagmeister P, Jazini M, Klein J, Herwig C (2014) Bacterial Suspension Cultures: Wiley

Sarra M, Ison AP, Lilly MD (1996) The relationships between biomass concentration, determined by a capacitance-based probe, rheology and morphology of *Saccharopolyspora erythraea* cultures. J Biotechnol 51: 157-165

Schmideder S, Barthel L, Friedrich T, Thalhammer M, Kovacevic T, Niessen L, Meyer V, Briesen H (2019) An X-ray microtomography-based method for detailed analysis of the three-dimensional morphology of fungal pellets. Biotechnol Bioeng 116: 1355-1365

Simon LL, Pataki H, Marosi G, Meemken F, Hungerbuhler K, Baiker A, Tummala S, Glennon B, Kuentz M, Steele G, Kramer HJM, Rydzak JW, Chen ZP, Morris J, Kjell F, Singh R, Gani R, Gernaey KV, Louhi-Kultanen M, O'Reilly J, Sandler N, Antikainen O, Yliruusi J, Frohberg P, Ulrich J, Braatz RD, Leyssens T, von Stosch M, Oliveira R, Tan RBH, Wu HQ, Khan M, O'Grady D, Pandey A, Westra R, Delle-Case E, Pape D, Angelosante D, Maret Y, Steiger O, Lenner M, Abbou-Oucherif K, Nagy ZK, Litster JD, Kamaraju VK, Chiu MS (2015) Assessment of Recent Process Analytical Technology (PAT) Trends: A Multiauthor Review. Org Process Res Dev 19: 3-62

Veiter L, Rajamanickam V, Herwig C (2018) The filamentous fungal pellet - relationship between morphology and productivity. Appl Microbiol Biotechnol 102: 2997-3006

Wucherpfennig T, Lakowitz A, Driouch H, Krull R, Wittmann C (2012) Customization of *Aspergillus niger* Morphology Through Addition of Talc Micro Particles. Jove-J Vis Exp

Zhang J, Zhang J (2016) The filamentous fungal pellet and forces driving its formation. Crit Rev Biotechnol 36: 1066-1077

Chapter 2. Hypotheses and Goal of the Thesis

Hypotheses

1. There is a close relationship between morphology, viability and productivity.
2. Morphology and viability are affected by fermentation parameters and assessable via advanced analytical methods enhanced for fungal morphology.
3. Morphology, viability and productivity can be controlled through optimisation of fermentation parameters.

Goal

The goal of this Thesis is to provide analytical methods enhanced for fungal morphology as monitoring tools to be used in fermentation to ensure optimal morphology, viability and productivity through optimization of cultivation parameters.

Morphology, viability and productive are to be:

- depicted via analytics
- predicted via data-driven modelling
- controlled through adaption of fermentation parameters

Chapter 3. Structure of the Thesis

This is a cumulative Thesis comprising five published peer reviewed papers, one manuscript under peer review at the time this was written and one report in the scope of the Christian Doppler Laboratory project. The Thesis is divided into two main chapters corresponding to the tasks of a typical upstream process development for filamentous fungi, specifically for *P. chrysogenum*, dealing with (i) analytical challenges regarding fungal morphology and (ii) aspects of fermentation control to ensure efficient bioprocesses.

Figure 3.1 provides an overview on the Thesis, highlighting the pillars 'Analytics' and 'Control' which are connected through the underlying hypotheses and goals.

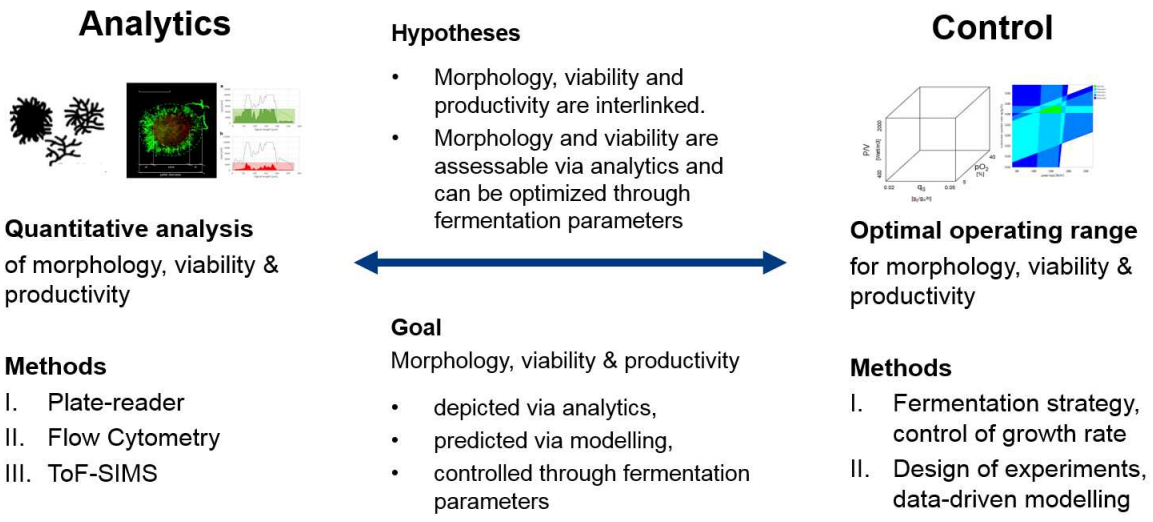

Figure 3.1. Overview of the Thesis. Hypotheses and goal are formulated in the middle. To achieve these goals the pillars 'Analytics' and 'Control' are needed, both pillars can be summarized by the respective methods. The blue arrow represents the interconnection between 'Analytics' and 'Control' which signifies that control can be achieved through employment of analytical methods.

The structure of this Thesis is depicted in Figure 3.2 and will be explained in the following:

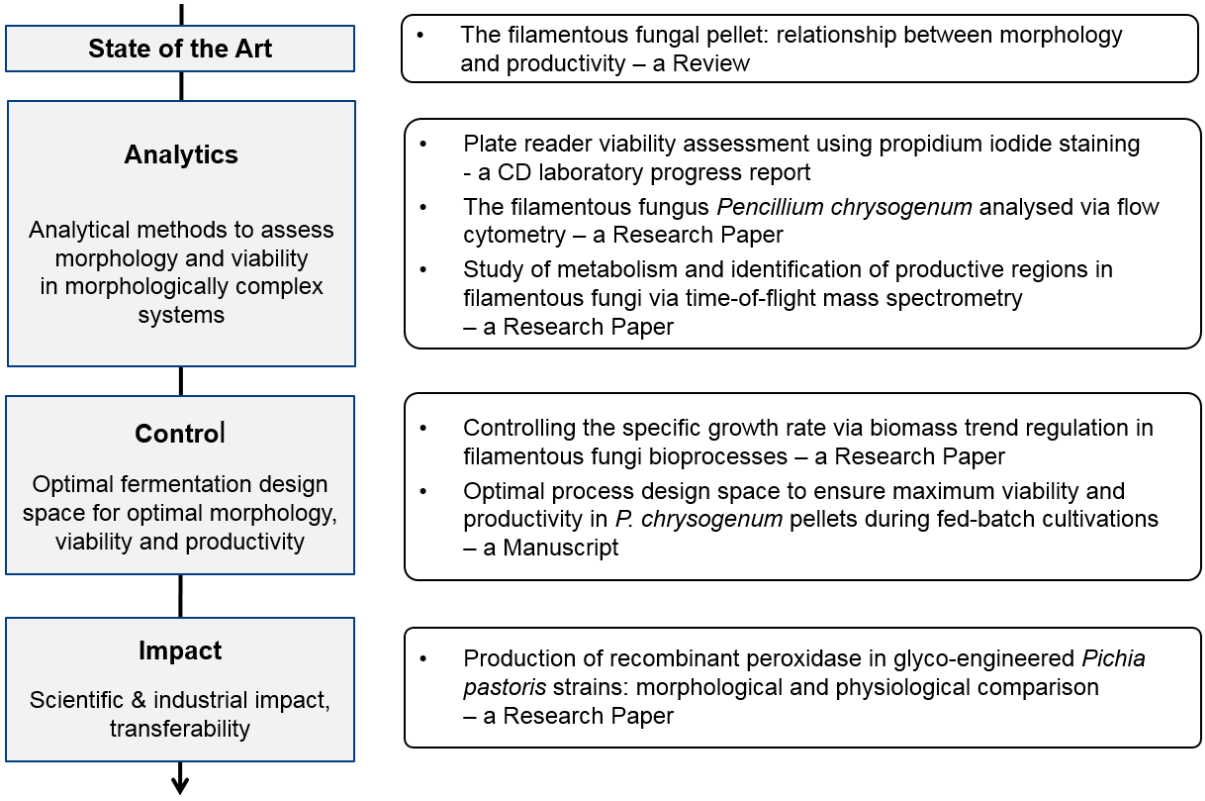

Figure 2.2. Structure of Thesis.

In ‘Chapter 4. State of the Art’ a review on the filamentous fungal pellet provides an overview on the State of the Art in filamentous bioprocess development including interlinks between fungal morphology and viability.

‘Chapter 5. Analytics’ compiles all analytical methods developed in the scope of this Thesis. These methods were used to measure morphological and physiological responses in the development of an optimal fermentation design space in *P. chrysogenum* bioreactor cultivations as described in ‘Chapter 6. Control’. Both chapters and related research papers are summarised in this chapter.

The impact and transferability of the developed methodology is examined in ‘Chapter 7. Impact’.

In the following, the material compiled in Chapter 5 and 6 will be summarized to give an overview on each developed method and its potential impact as well as my specific contribution to those methods.

Material in ‘Chapter 5. Analytics’

The aim of Chapter 5 is to provide analytical methods which shed a light on the main research hypothesis: morphology, viability and productivity are interlinked. Each analytical method is designed to illuminate one or more of the three aforementioned aspects, namely (i) to quantitatively assess the impact of morphology on viable biomass and (ii) to identify productive biomass regions in complex fungal morphology according to research hypotheses:

1. There is a close relationship between morphology, viability and productivity.
2. Morphology and viability are affected by fermentation parameters and assessable via advanced analytical methods enhanced for fungal morphology.

In the following an overview on the challenge, the state of the art and the findings of each method and lists the corresponding titles and authors of the manuscripts are provided. Also the impact and applicability of the methods are discussed and linked to bioprocess development tasks.

Method 1.

Plate reader viability assessment

Challenge

A plate-reader method for viability assessment was developed in the course of the CD-Laboratory. Preliminary results when applying this method indicated that the propidium iodide (PI) concentration is insufficient to stain dead cells completely. Thus, the estimation of viability might be influenced by the amount of biomass used in the assay. The appropriate amount of PI in relation to biomass concentration in the assay has to be determined to obtain trustworthy results.

State-of-the-art

The membrane impermeable dye PI binds to DNA. If subsequently excited at wavelengths of 488 nm, PI will emit in the red spectral section. This characteristic is used for viability assessment according to the following method: Viability is estimated as a ratio between fluorescence intensity of an untreated sample versus a microwaved hence non-viable negative control. Viability assessment via staining methods is commonly used as a simple analytical at-line tool, but complex fungal morphology frequently leads to complications regarding the appropriate amount of staining dyes.

Findings

Viability assessment via staining methods is commonly used as a simple analytical at-line tool, but complex fungal morphology makes it necessary to adapt the appropriate amount of fluorescent dye at cell densities exceeding 25 g/L.

Impact of method

The here-presented method is a fast and simple approach to estimate viability in an at-line fashion using established tools such as fluorescent staining and plate reader measurements. Recent improvements enable the application at higher cell densities with corresponding adaption of fluorescent dye concentration.

Citation

The method is summarized in the CD - Laboratory progress report from September 6th, 2018.

My contribution

I planned the study, performed and analysed the required experiments together with Thomas Hartmann and wrote the report.

Method 2.

The filamentous fungus *Penicillium chrysogenum* analysed via flow cytometry – a fast and statistically sound insight into morphology & viability

Challenge
P. chrysogenum comprises several morphological forms when growing in submerged culture, ranging from homogenously dispersed hyphae to pellets. Each morphological class affects viability, productivity and performance in different ways. Naturally, these variations across all morphological forms complicate viability estimation and by extension determination of growth rate, substrate uptake rates and yields.

State-of-the-art
Morphology is generally analysed via microscopy which is time consuming and statistically not robust. Common methods for viability assessment are staining methods which only provide an overview on viability without morphological aspects. Confocal laser microscopy can be used in combination with fluorescent staining for in-depth characterisation of single pellets.

Findings
Within this contribution, we present a flow cytometry–based method employing fluorescent staining. Thereby, we can assess filamentous biomass in a statistically sound way according to (i) morphology and (ii) viability of each detected morphological form.

Impact of method
The developed method is at-line and potentially online applicable, statistically sound due to the high number of measured particles within minutes, and can estimate viable layers in specific morphological classes, such as pellets and large hyphal agglomerates. This viability data is enhanced by morphological parameters like pellet and large element compactness. This method can shed light on the complex relationship between fungal morphology, viability and productivity—in both process development and routine manufacturing processes.

Citation
Veiter, L. and C. Herwig (2019). 'The filamentous fungus *Penicillium chrysogenum* analysed via flow cytometry - a fast and statistically sound insight into morphology and viability.' Appl Microbiol Biotechnol 103:6725–6735. https://doi.org/10.1007/s00253-019-09943-4.

My contribution
I developed the method, designed and performed all experiments, analysed the data and wrote the paper.

Method 3.

Study of metabolism and identification of productive regions in filamentous fungi via spatially resolved time-of-flight secondary ion mass spectrometry

Challenge
Industrial filamentous fungi processes typically favour the pellet morphology comprising compact hyphal agglomerates. Inherently these tightly packed entanglements lead to inactive, degrading sections within the pellet's core because of limitations. Optimal process design requires detailed knowledge of the nature of the limitations and localization of productive zones in the complex morphology of the biomass.

State-of-the-art
Knowledge on productive regions and metabolism is generally obtainable through modelling and complex analytical methods such as the use of oxygen microelectrodes and histological investigations.

Findings
In this study, we used time-of-flight secondary ion mass spectrometry in combination with oxygen and glucose tracer substrates, requiring little effort for sample preparation and measurement. Our method is capable of analysing oxygen and substrate uptake in various morphological structures by the use of ^{18}O as tracer. In parallel, we can assess productive biomass regions through identification of penicillin mass fragments to simultaneously study oxygen diffusion, substrate incorporation, and productive biomass sections.

Impact of method
This method is a potent tool to facilitate industrial process design and strain characterization by shedding light on C-source incorporation and respiratory limitations within complex fungal biomass agglomerates. This information could also be used in the generation of flux-based models. An additional benefit is the simultaneous localization of productive biomass regions, which does not require further effort in sample preparation or measurement.

Citation
Veiter, L., Kubicek, M., Hutter, H., Pittenauer, E., Herwig C. and C. Slouka (2019). 'Study of metabolism and identification of productive regions in filamentous fungi via spatially resolved time-of-flight secondary ion mass spectrometry.' Anal Bioanal Chem. https://doi.org/10.1007/s00216-019-01980-2.

My contribution
I co-designed the study, performed all experiments, analysed the data and wrote the paper.

Material in ‘Chapter 6. Control’

The aim of Chapter 6 is to utilize previously developed analytical methods to measure novel morphological and physiological responses in the development of an optimal fermentation design space in *P. chrysogenum* bioreactor cultivations. In Chapter 6 the third hypothesis of this Thesis is being addressed:

3. Morphology, viability and productivity can be controlled through optimisation of fermentation parameters.

In the following, an overview on the challenge, the state of the art and the findings of each method and lists the corresponding titles and authors of the manuscripts are provided. It also shows the impact and applicability of the methods and links it to bioprocess development tasks.

Method 4.

Controlling the specific growth rate via biomass trend regulation in filamentous fungi bioprocesses

Challenge
The PAT and QbD initiatives push process control into focus in pharmaceutical cultivation processes. Online biomass estimation in filamentous bioprocesses is a complex challenge due to morphological inhomogeneity in fungi. Further challenges encompass the application of said biomass estimation for control of the organism's growth rate.

State-of-the-art
Biomass estimation via dielectric spectroscopy is applicable for filamentous fungi. However, most contributions identify a growth and decline phase over process time, the latter is especially error-prone regarding biomass estimation. Furthermore, control of the specific growth rate in filamentous cultures is challenging as growth rate levels are rather low compared to other organisms. Furthermore, changing biomass yields during the penicillin production process appeared to be a main issue in μ control.

Findings
In the here presented study, we developed a control strategy for the specific growth rate based on online estimation of viable biomass via dielectric spectroscopy. The method was constantly verified using an at-line staining method for viability measurement (see Method 1) to account for changing biomass yields during either growth or decline phases.

Impact of method
The online viable biomass estimation is applicable in the growth and decline phase, coping with physiological and morphological changes of filamentous fungi. The method is applicable for control of the specific growth rate during growth phase and adapts to changing biomass yields.

Citation
Ehgartner D., Hartmann T., Heinzl S., Frank M., Veiter L., Kager J., Herwig C. and J. Fricke (2017). 'Controlling the specific growth rate via biomass trend regulation in filamentous fungi bioprocesses.' Chem Eng Sci. https://doi.org/10.1016/j.ces.2017.06.020

My contribution
I co-performed bioreactor cultivations experiments, co-analysed the data and assisted in paper revision before publication.

Method 5.

Optimal process design space to ensure viability and productivity in *Penicillium chrysogenum* pellets during fed-batch cultivations through morphological and physiological control

Challenge

Biomass growth of *P. chrysogenum* is characterised by a distinct pellet morphology consisting of compact hyphal agglomerates. Fungal pellets are advantageous in industrial process control due to rheological advantages. The challenge is to find an optimal operating range for enhanced pellet viability and productivity at beneficial morphological conditions.

State-of-the-art

Several fermentation parameters are known to affect key pellet characteristics regarding morphology, viability and productivity. Pellet morphology and size are affected by agitation. Biomass viability and productivity are tightly interlinked with substrate uptake and dissolved oxygen concentration.

Findings

We studied the impact of the fermentation parameters power input, dissolved oxygen content and specific substrate uptake rate on morphology, biomass viability and productivity. A design of experiments (DOE) approach was conducted and corresponding responses were analysed using a previously established flow cytometry method. Results clearly display inverse correlations between power input and pellet size, specific morphological parameters related to pellet density can be increased in direct proportion to power input. Biomass viability and productivity are negatively affected by high specific substrate uptake rates.

Impact of method

From an industrial point of view, our approach ensures a high space-time-yield via an optimised operating range of several factors: a feed regime dependent on q_s ensures a sound compromise between productivity and viability, at the same time favourable morphological conditions can be ensured through controlled power input.

Citation

This manuscript is currently under review at Microbial Cell Factories.

My contribution

I co-designed the study, performed all experiments, performed and evaluated flow cytometry measurements, analysed the data and wrote the paper.

Chapter 4.
State of the Art

The filamentous fungal pellet – relationship between morphology and productivity

Lukas Veiter[1,2], Vignesh Rajamanickam[1,2] and Christoph Herwig[1,2*]

[1] CD Laboratory on Mechanistic and Physiological Methods for Improved Bioprocesses, Vienna University of Technology, Gumpendorferstrasse 1a/166, 1060 Vienna, Austria

[2] Research Area Biochemical Engineering, Institute of Chemical, Environmental and Bioscience Engineering, Vienna University of Technology, Gumpendorferstrasse 1a/166, 1060 Vienna, Austria

*Corresponding author:
christoph.herwig@tuwien.ac.at; Tel (Office): +43 1 58801 166400
Gumpendorferstrasse 1a / 166-4
1060 Wien, Austria

Published in 'Applied Microbiology and Biotechnology':

Veiter, L., Rajamanickam V. and C. Herwig (2019). 'The filamentous fungi pellet – relationship between morphology and productivity.' Appl Microbiol Biotechnol.

Abstract

Filamentous fungi are used for the production of a multitude of highly relevant biotechnological products like citric acid and penicillin. In submerged culture, fungi can either grow in dispersed form or as spherical pellets consisting of aggregated hyphal structures.

Pellet morphology, process control and productivity are highly interlinked. On the one hand, process control in a bioreactor usually demands for compact and small pellets due to rheological issues. On the other hand, optimal productivity might be associated with less dense and larger morphology. Over the years, several publications have dealt with aforementioned relations within the confines of specific organisms and products. However, contributions which evaluate such interlinkages across several fungal species are scarce. For this purpose, we are looking into methods to manipulate fungal pellet morphology in relation to individual species and products. This review attempts to address, i) how variability of pellet morphology can be assessed and ii) how morphology is linked to productivity. Firstly, the mechanism of pellet formation is outlined. Subsequently, the description and analysis of morphological variations are discussed to finally establish interlinkages between productivity, performance and morphology across different fungal species.

Keywords

Fungal pellet morphology, interlinks between productivity and morphology, variability and alteration of morphology, analysis of morphology

Introduction

In submerged culture filamentous fungi either grow in spherical pellets, consisting of compact hyphal aggregation, or in filamentous form, featuring homogeneously dispersed hyphae (Pirt 1966). A pellet forming cultivation system is necessarily heterogenous and aerobic (Wosten et al. 2013; Amanullah et al. 2001). The morphological state of filamentous fungi has a large impact on process performance in a bioreactor. Morphology, physiology and productivity of filamentous fungi are influenced by process parameters on many levels (Ehgartner 2017). These characteristics are highly interlinked with each other and therefore have to be addressed collectively to understand the interdependencies between them. For example, in free mycelia high biomass concentrations result in highly viscous fermentation media, resulting in issues with gas−liquid mass transfer, liquid mixing and a generally complex rheology in *Aspergillus terreus* (Porcel et al. 2005). However, pellet morphology also comes with disadvantages: within *Penicillium chrysogenum* pellets, problems with internal transport of substrates and products may occur, depending on size and compactness of pellets (Dynesen and Nielsen 2003). Therefore, it is highly important to individually assess each production task.

This review strives to provide a general overview across several pellet forming fungal species. In the following, basic forces that trigger pellet formation are briefly summarised. Subsequently, description and analysis of pellet morphology is outlined. This provides the basis for understanding interlinks between productivity, performance and morphology, as will be discussed in the final chapter of this review.

Mechanism of pellet formation

Traditionally fungal pellets are attributed to either coagulative or non-coagulative types of formation (Nielsen et al. 1995, Pirt 1966). Table 1 available on page 42 provides an overview on pellet classification across several species.

In the coagulative type, spores aggregate fast and subsequently germinate involving hyphal tip growth (Zhang and Zhang 2016). Finally, a great number of spores of the coagulative type form pellets. On the contrary, spores of the non-coagulative type germinate before pellet formation. Therefore, one pellet theoretically can be formed by one single spore. Non-coagulative pellet formation is interlinked with agitation and aeration (Pazouki and Panda 2000). It should be noted however that depending on cultivation factors fungal species will exhibit different morphological behaviour. Therefore, a final classification of coagulation type is difficult (Zhang and Zhang 2016; Pazouki and Panda 2000). For instance, *P. chrysogenum* exhibits characteristics of both types, as agglomeration of hyphal elements leads to hyphal clumps which form pellets in the end (Wilkinson 1998; Nielsen et al. 1995). Wilkinson (1998) therefore suggested a new term for *P. chrysogenum*: hyphal element agglomerating type.

Electrostatics, hydrophobicity and interactions between spore wall components are main triggers for pellet formation (Zhang and Zhang 2016). Fungal spores generally exhibit negative surface charges (Douglas et al. 1959) which are affected by pH and ionic strength (Akriba et al. 1994). In a simplified view higher pH values are considered to cause negative charges which in turn decrease spore aggregation (Zhang and Zhang 2016). However, conflicting observations suggest that electric repulsion is not the only driving factor. For *Aspergillus niger* it was proposed that mainly single conidia are affected by surface charge, aggregated conidia might additionally be stabilized through higher electric charges (Grimm et al. 2005). Wargenau et al. (Wargenau et al. 2011) further found that the electrostatic surface potential of *A. niger* spores is considerably affected by pH-dependent release of melanin pigment.

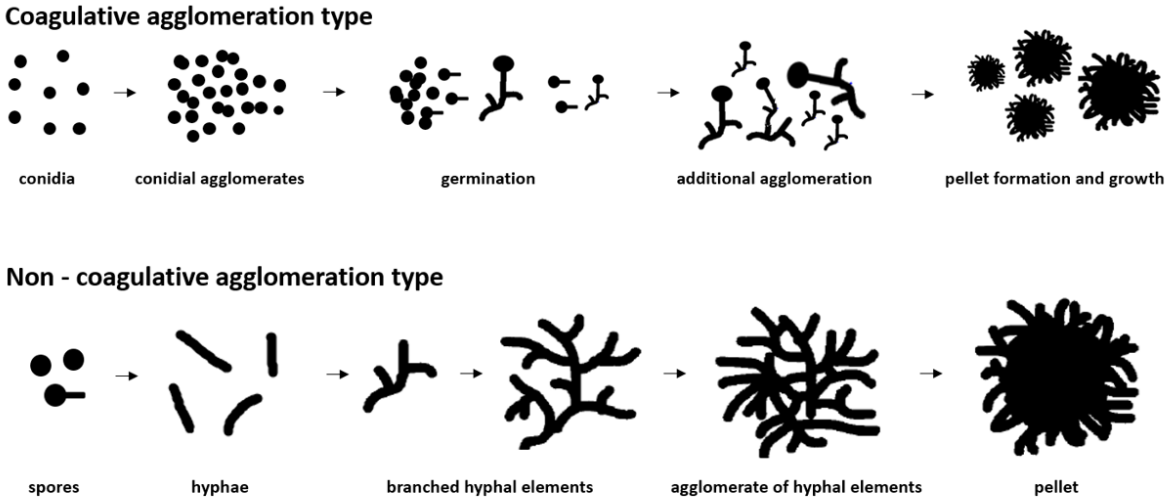

Figure 1. Illustration depicting the coagulative and non-coagulative model of pellet formation.

They concluded that thickness and accessibility of surface coating, as well as ionic strength of the medium have additional effects on pH-dependent spore repulsion. Furthermore, pH also heavily affects hydrophobicity of proteins (Pascual et al. 2000). Especially hydrophobins strongly influence adhesion forces. For instance, deletion in different hydrophobin encoding genes in *A. nidulans* mutants leads to a decrease in pellet biomass and size (Dynesen and Nielsen 2003).

Another important contribution to pellet formation are interactions between spore wall components, notably salt bridging between polysaccharides (Zhang and Zhang 2016). Gerin et al. (Gerin et al. 1993) even stated that aggregation is only dependent on salt bridging between polysaccharides in *Phanerochaete chrysosporium*. Depending on respective physiological conditions, spores undergo several changes in spore wall components and properties (Zhang and Zhang 2016): In the beginning, water uptake combined with the swelling of spores leads to an increase of metabolic activiteis leads to water uptake combined with swelling of spores. This is followed by germination of conidia, which represents the beginning of fungal growth. After germination hyphal elongation takes place and the fungus can initiate hyphal branching which is critical for the formation of the mycelium (Paul and Thomas 1996). These initial steps in fungal development strongly affect spore aggregation: shortly after incubation spore aggregation occurs due to electrostatic and hydrophobic interactions. However, as soon as the swelling of spores leads to polysaccharides being exposed, hydrophobic interactions decrease in favour of interactions between cell wall components (Priegnitz et al. 2012; Zhang and Zhang 2016).

Recently efforts to describe aggregation kinetics via population dynamics modelling were made (Grimm et al. 2004; Lin et al. 2008). Via an in-line particle size analyser two distinct aggregation steps of coagulating fungi *A. niger* could be described. In the first step, conidial aggregates are formed from individual conidia. Population dynamics in this first step combine formation and disappearance of particles through aggregation and breakage. The second step considers germination of conidia, thereby hyphal growth greatly increases the surface area necessary for aggregation. This process is closely related to the specific length growth rate and the rate of germination (Grimm et al. 2005). More recently Priegnitz et al. (Priegnitz et al. 2012) concluded that germination of conidia within the second step is essential for pellet formation in *A. niger*.

All of these findings signify that specific aggregation triggers vary during the pellet formation process. When summarizing influences on electrostatic and hydrophobic interactions, it can be concluded that pH is the driving factor for both. Regarding interactions between spore wall components, no definite conclusions can be drawn from the scientific literature. However, publications

suggest that it is mostly driven by the presence of polysaccharides (Zhang and Zhang 2016).

Description and analysis of pellet morphology

Pellet diameters extend from a few hundred micrometres up to one millimetre. The basic morphology of fungal pellets is characterized by the compact inner core consisting of densely packed hyphae (Cox et al. 1998). The existence of such a core is the distinction between pellets and clumps. The core is surrounded by a less dense hyphal layer, known as the hairy region (Krull et al. 2010). Core region and hairy region can be defined by parameters, mostly derived from microscopic analysis as displayed in Table 2 (Paul and Thomas 1998; Posch et al. 1998, Daniela Ehgartner 2017). Figure 2 displays images related to respective parameter estimation.

The most common method to analyse pellet morphology is microscopy (Cox et al. 1998, Paul and Thomas 1998, Posch et al. 2012). Usually image recording is combined with some form of automated image analysis software to ensure statistical verification. Thereby most parameters described in Table 2 can be determined. However, sample preparation on microscopy slides is problematic as it affects fungal biomass dimensions due to potential squeezing between cover slide and specimen slide. In this process also all three-dimensional information is lost.

Confocal laser scanning microscopy (CLSM) in combination with staining is a powerful method for visualisation of metabolically active regions in pellets. Furthermore, biomass segregation, density and growth could by monitored via this technique (Villena et al. 2010). Wargenau et al. (Wargenau et al. 2010) were able to directly measure *A. niger* spore adhesion forces at different pH and ionic strength values by further employing atomic force microscopy (AFM). Information on hydrophobic and hydrophilic domains can be obtained via adhesion force mapping across spore surfaces. This technique also provides information on the role of hydrophobins on adhesion (Krull et al. 2013). Via scanning electron microscopy (SEM) Villena et al. (Villena and Gutierrez-Correa 2007) were able to differentiate highly intertwined superficial hyphae and densely packed deep mycelium in *A. niger* pellets.

In recent years flow cytometry in combination with fluorescent staining (Golabgir et al. 2015) was also used to depict morphological distributions in filamentous fungi samples. Limitations of this technique are also related to large pellet dimensions, consequently, flow cytometers must be adapted for large particle size ranges. Flow cytometry is very fast and statistically robust as a large number of particles can be measured in low time spans. When compared with microscopic image analysis Ehgartner et al. were able to obtain similar size parameters as well as enhanced characterization of fungal pellet compactness and hyphal region (Daniela Ehgartner 2017). Potential issues include size exclusion effects at the sampling tube.

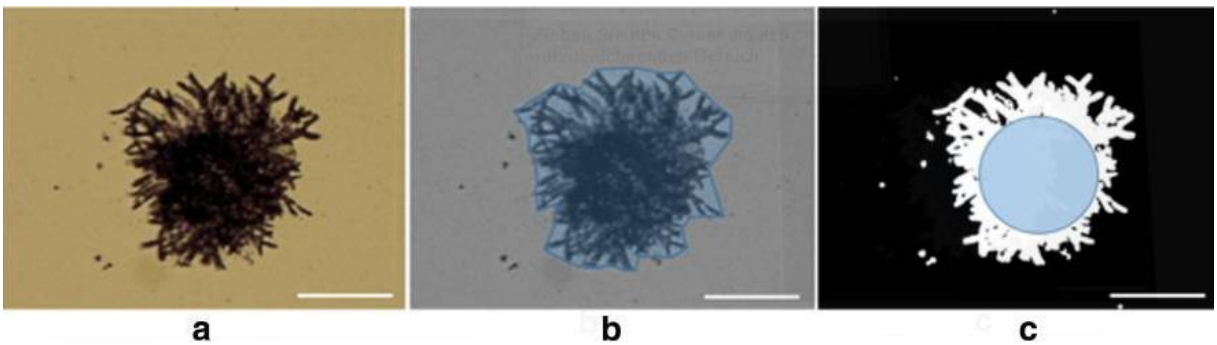

Figure 2. Light microscopic images of the same P. chrysogenum pellet, white line = 100 µm; parameters for depiction of core region and hairy region. Blue line (B): perimeter for estimation of roughness, blue area (B): convex area for fullness calculation, blue circle (C): core area.

Table 2. Parameters for pellet characterisation

	Parameter	Definition
Core region	Fullness	Ratio of actual area of the particle to convex area; = 1 for pellets without hairy regions
	Circularity	Deviation from a true circle, derived from area and perimeter
	Core area	Encompasses core equivalent diameter
Hairy region	Roughness	Irregularity of the perimeter of an object, obtained from circularity measurement around an object boundary
	Equivalent diameter	Diameter of a circle having the same area as the pellet

Other methods successfully used for macroscopic analysis of *A. niger* include focused beam reflectance measurement (FBRM), a size-determining optical method based upon backscattering laser light (Krull et al. 2013). Grimm et al. (Grimm et al. 2004) characterized conidial inocula to determine effects on the conidial aggregation process. Lin et al. (Lin et al. 2010) analysed pellet slices of several pellet regions via microscopy in order to determine regularity/circularity and surface structures. Furthermore, the impact of pellet surface structure on sedimentation behaviour in water was described. Although optical methods involving microscopy and flow analysis can be used to determine macro-morphological features, characterization of pellet morphology and physiology remains challenging. This is mainly due to the fact that common macro-morphological parameters do not cover all important pellet characteristics (Hille et al. 2006). Regarding physiology, diffusion of substrates into pellets needs to be considered dependent on varying degrees of compactness and roughness, which cause variable oxygen uptake rates (Krull et al. 2010). If homogeneous biomass distribution is assumed, oxygen concentration gradients are the same for pellets of equal size. However, while mean biomass density may be similar for pellets from different cultivations, their inner structures could differ considerably. Hille et al. (Hille et al. 2006) describe variations in biomass density between *A. niger* pellets related to inoculum conditions. The authors used CLSM to measure fluctuating density distributions in the outer layers. Dense outer pellet sections strongly impact oxygen delivery and consumption in two ways: (i) oxygen consumption is increased and (ii) substrate diffusion is restricted. Furthermore, hydrodynamics significantly affect substrate diffusion and internal oxygen concentration profiles. In their periphery, loosely structured pellets exhibit convective tendencies in substrate transport, whereas in tightly packed core regions, diffusion is predominant. If the number of hyphal tips is the essential factor for oxygen conversion, dense pellets are favoured despite restricted oxygen transport (Hille et al. 2005). Related oxygen concentration profiles in fungal pellets obtained via microelectrodes were successfully correlated with hyphal distribution in outer pellet regions (Grimm et al. 2005).

Consequently, a major task when characterizing morphology is to come up with novel or expanded parameters also depicting micro-morphological and physiological characteristics. Such parameters must come from robust analytical tools and have to consider culture conditions as well, thereby deepening understanding of fungal morphology and physiology.

Effects of pellet morphology on productivity

There have been several attempts to specify definite links between morphology and productivity (Walisko et al. 2015), but no simple relationship that would favour a specific morphology has been identified. Grimm et al. (Grimm et al. 2005) identified the large amount of process parameters affecting morphology as an important factor. Consequently, any reported co-dependencies are limited to individual processes with specific organisms and products. When comparing these various results, it becomes clear that there are no generally applicable rules. In fact, different morphologies are in favour of different products, conflicting reports are available even for the same species. Consequently, comprehensive process design must align morphology with metabolism and productivity (Grimm et al. 2005). For fungal pellets, the following relationship to metabolism has been proposed (Grimm et al. 2005): Biomass density is inhomogeneous and inversely proportional to pellet porosity, which in turn leads to limited accessibility for nutrients. Such complex hyphal networks hinder

substrate uptake thereby directly affecting metabolism. Within this context, oxygen has been identified as the prime limiting substrate.

Interlinkages between pelletized morphology and productivity were studied intensively for *A. niger* (Papagianni 2007). While it is not entirely clear if pelletized or filamentous morphology is more appropriate for citric acid production, it has been proven that productivity is linked to short, swollen hyphal branches that may have swollen tips. Available literature (Papagianni 2007; Papagianni and Mattey 2006; Zhang and Zhang 2016) mainly favours compact agglomerates and pellets (< 0.5 mm), but conflicting reports also find pellet growth disadvantageous. More detailed studies (Papagianni et al. 1998) have suggested that the so-called clump form would be most suitable. Such clumps are stable agglomerates of filaments, but do not exhibit a compact core (Papagianni 2007) as opposed to pellets. Driouch et al. (Driouch et al. 2012) were able to stir *A. niger* pellet morphology towards a reduced thickness of biomass layer via smaller pellets as well as altered core shell structure to enhance productivity. Such a trend was also established for *A. terreus* as smaller pellets are deemed more compact, hence more stable (Porcel et al. 2005). However, for *A. oryzae* filamentous growth achieved higher α-amylase productivity (Carlsen et al. 1996).

For *P. chrysogenum* Paul and Thomas (Paul and Thomas 1998) discriminated between different parts of hyphae: actively growing regions, non-growing cytoplasm, vacuolised hyphae and inactive regions (Justen et al. 1998). Penicillin production is happening in the non-growing cytoplasm (equivalent to subapical hyphal cells). This differentiation can be expanded to larger pellet structures: also pellets feature distinct active regions (Baumgartl et al. 1984). Such an active region is found in the outer layer of the pellet, which contains high quantities of cytoplasm. Cytoplasm content is decreasing in the inner regions. The pellet's centre exhibits hyphal degradation (Ehgartner 2017). Therefore, the largest possible active layer would characterize the optimal pellet form for Penicillin production in bioreactors.

Pellet formation greatly enhances lactic acid production and fumaric acid when compared to clump-like morphological structures for *R. oryzae* (Liao et al. 2007). This is especially interesting as less compact morphology usually displays more productivity as viability is apparently not hindered by diffusion through dense structures. Fu et al. (Fu et al. 2014) also found that low-density pellets exhibiting a hollow core greatly decreased lactic acid production. However, pellet densities over 60 kg/m^3 were identified to be disadvantageous as this led to a generally limited mass transfer.

Kim et al. (Kim et al. 2009) found that pellet size of white rot fungus *Pleuratus ostreatus* affects its biodegrading capacity. The overall biodegradation rates were closely related to laccase and esterase activity. Small-pelleted cultures were determined as favourable morphology for optimal activity of both degradative enzymes.

In general, any enhanced productivity of mycelia and clumps is due to easier supply of oxygen and substrates. Consequently, the ideal pellet is a large agglomeration of productive sections that have open access to substrates and oxygen. As mentioned, such a loose structure is associated with highly viscous fermentation media, resulting in issues with gas−liquid mass transfer, liquid mixing and complex rheology. Therefore, morphological optimisation must consider the following: rheological requirements for the bioprocess on the one hand and ideal pellet compactness for enhanced productivity on the other hand. Possible options to favourably alter pellet morphology are discussed below.

Alteration of pellet morphology

In this section, we take a closer look at factors, which affect pellet formation and morphology. All these potential factors are interdependent. Therefore, any form of morphological control strategy is highly complex.

Agitation

The general rule states that strong agitation results in smaller pellets. If pellet formation is proceeded by spore aggregation, strong agitation could decrease pellet growth (Prosser and Tough 1991). If pellets have already formed, they are affected by agitation in two ways (Tanaka et al. 1975): (1) hyphal elements on the pellet surface can be shaved off, (2) there is also the possibility of total pellet rupture. In general, the shaving of hyphal elements is preferred, as opposed to total pellet rupture.
For several *Aspergillus* species strong agitation forces facilitate a morphology of short, thick and

highly branched filaments advantageous for citric acid production (Pagagianni 2007). Fragmentation of filaments can also occur but is mainly limited to old and heavily vacuolated parts. Therefore, there is a leeway for beneficial breakage of filaments through agitation: a balance between new growth and fragmentation of inactive sections (Pagagianni 2007).

P. chrysogenum also displays clear relations between morphology and agitation. Agglomeration of hyphal elements and thereby pellet formation is negatively affected by strong agitation (Walisko et al. 2015). Nielsen et al. (Nielsen et al. 1995) have reported that a shift from pellet morphology to disperse mycelia could be achieved for fed-batch cultivations.

Pellet size of *P. ostreatus* is predominantly controlled via agitation, Kim et al. (Kim et al. 2009) were able to obtain either large-pelleted or small-pelleted morphology at respective agitation speeds. Tinoco-Valencia et al. (Tinoco-Valencia et al. 2014) further studied agitation and aeration effects on *P. ostreatus* growth. They observed predominantly pellet morphology. High agitation in combination with high aeration flow rates led to increased oxygen mass transfer and decreased pellet size, respectively. Consequently, growth rate and maximum biomass concentration were increased.

To recapitulate, agitation considerably alters morphology, especially during agglomeration. If pellets have already formed, strong agitation could lead to adverse effects like pellet rupture. Several production processes favour thin biomass layers and loose core structures in pellets due to strong agitation, for example citric acid production in *A. niger* or lignin peroxidase production in *Phanerochaete chrysosporium.*

Broth viscosity, medium composition and pH

In general, an inverse relation between pellet size and broth viscosity has been reported. For example, Prosser and Tough (Prosser and Tough 1991) state that adjustment of broth viscosity via carbohydrates is advantageous for cultivations of *Blakeslea* and *Choanephora*. The use of anionic polymers has been shown to hinder spore aggregation prior to germination. Thereby organisms that usually favour pellet growth can be stirred towards dispersed growth and vice versa. Trinci (Trinci 1983) reported this effect for *Aspergillus* and some basidiomycetes. These findings might also apply to naturally formed polysaccharides as has been speculated for *P. chrysogenum* (Prosser and Tough 1991).

Kisser et al. (Kisser et al. 1980) studied the effect of manganese sufficient or deficient cultivation on *A. niger* morphology and cell wall composition in citric acid production. Omission of manganese from the nutrient medium results in 'abnormal morphological development which is characterised by increased spore swelling and bulbous hyphae'. Only compact pellets produce citric acid, consequently manganese deficiency is to be avoided. The same effects of manganese deficiency have also been confirmed by Papagianni et al. (Papagianni et al. 1998). Sensitivity to the presence of trace metals equals that there is also sensitivity for metal complexing ions like EDTA (Prosser and Tough 1991).

Wucherpfennig et al. (Wucherpfennig et al. 2011) studied the effect of osmolality on *A. niger* morphology and productivity. Culture broth osmolality was increased by the addition of sodium chloride. It was found that pellet size declined with osmolality. However, it was determined that the culture was also becoming more homogenous.

Investigations into optimal medium composition for *R. oryzae* implied that peptone had a positive effect on pellet formation. The addition of metal ions as well as interaction of metal ions and peptone impeded pellet formation (Liao et al. 2007). Through the concentrations of potato dextrose broth, soybean peptone, and calcium carbonate in the medium pellet size were controlled. Fu et al. (Fu et al. 2014) additionally state that pellet density is positively affected by addition of peptone. Under low peptone concentrations, low-density pellets with hollow structures were observed.

For *P. chrysogenum,* addition of Corn Steep Liquor (CSL) to the culture medium is known to have positive effects on pellet formation at an early stage and penicillin production (Sajjad et al. 2012). There is still ongoing research if the state-of-the-art penicillin fermentation medium (composed of CSL, glucose, lactose, minerals, oil, nitrogen source and precursor) can be modified and improved. Cultivation in buffered medium had positive effects on biomass growth for several *Penicillium* species: pellets displayed greater diameters as well as smaller hyphae on the surface (Walisko et al. 2015).

Studies using SEM indicate that the morphology of *P. chrysogenum* is affected by CO_2 presence in the medium: at low CO_2 concentrations (up to 8 %) the filamentous form was predominant, higher concentrations led to the formation of swollen and stunted hyphae affecting pellet morphology (Ho and Smith 1986).

As noted previously, pH is a driving factor on electrostatic and hydrophobic interactions. For citric acid production pH of culture medium is preferably low and strongly affects production, simply because of the pH sensitivity of enzymes in the TCA cycle (Papagianni 2007). Morphological development of small pellet aggregates and short filaments is best sustained at pH values of 2.0 ± 0.2. Liu and Wu (Liu and Wu 2012) also found pH-related effects on the morphology of *C. sinensis*. The mycelial pellets became less uniform at lower pH (< 6.0). Filamentous growth was observed at higher pH (8–9). The growth of ascomycete fungus *Neurospora intermedia* in uniform pellet form can be achieved using a pH range of 3.0 -4.0 (Nair et al. 2016).

In recent years, the effect of surfactants has been tested. Liu and Wu (Liu and Wu 2012) found that Tween exhibited a promoting effect on production of exopolysaccharide in the fungus *Cordyceps sinensis*. Improved productivity was combined with medium inhibited pellet formation leading to small and loose pellets. More recently Kurukake et al. (Kurukake et al. 2017) observed that *A. oryzae* pellets became mall and spherical on addition of Tween surfactant. Furthermore, production of fructosyl-transferase could be enhanced. Addition of Tween also led to an increased specific surface area of *Pleurotus eryngii* pellets (Wu et al. 2016). Antecke et al. (Antecke et al. 2016) successfully applied a morphological engineering technique to a laccase production process in basidiomycetes. The authors found that the addition of Al_2O_3 microparticles led to a decrease of pellet size, shape and structure in *Cerrena unicolor* and *Pleurotus sapidus*. Similar morphological engineering techniques – namely the use of magnesium silicate microparticles - were also successful for oleaginous fungus *Mortierella isabellina* (Gao et al. 2014).

To summarise, effects of medium composition on morphology and productivity are highly diversified and entirely dependent on species and process conditions. According to the available literature, we can only assume that pH has considerable impact across several species. Nevertheless, a selection of preferred medium compositions is available for several fungal pellet processes.

Spore inoculum level and other inoculation strategies

Generally, an inverse relationship between spore number and pellet size has been identified for several *Aspergillus* species (Prosser and Tough 1991). Citric acid production in *A. niger* is particularly affected by spore inoculum. Papagianni and Mattey (Papagianni and Mattey 2006) found studied spore development and morphology in a bioreactor in relation to spore inoculum concentrations. They classified four morphological classes: globular pellets, elongated pellets, clumps and free mycelia. Glucosamine formation and release was clearly related to spore inoculum level. At higher inoculum levels (10^8 – 10^9 spores/mL) lower dissolved oxygen levels were measured which led to mycelium developed in dispersed morphologies. For *Caldariomyces fumago* aforementioned relationships were also found. Additionally, pellet density was reported to be inversely related to pellet size (Carmichael and Pickard 1989).

For *P. chrysogenum* it was reported that with low spore inoculum concentrations only few agglomerations of hyphal elements happen which in turn leads to pellets with small diameters (Nielsen et al. 1995). At very high concentrations (> 10^5 spores/mL) the hyphal element size is small and agglomeration respectively pellet formation does not occur in the first place. For a spore inoculum concentration of $3.7 * 10^4$ spores/mL maximum pellet concentration was measured which amounts to roughly $1.5 * 10^4$ pellets/mL. In a different study, Posch and Herwig (Posch and Herwig 2014) describe a positive effect of spore inoculum concentration on penicillin formation during early production phases, which feature excess substrate, biomass growth and overflow metabolism. Simultaneously a negative effect on pellet morphology is observed: Pellets develop larger structures at reducted spore inocula, consequently pellet breakage resulting in dispersed morphology is more likely.

In recent years the so-called pellet-dispersion strategy has brought promising results for seed cultivation of *A. niger niger* (Wang et al. 2017). Thereby pellets were used to substitute spores during inoculation.

Traditionally long time spans are needed for spore preparation of seed culture. This drawback was avoided through the development of a novel seed-recycling process. The morphological structure displayed 'densely intertwined hyphae' and pellet compactness increased considerably. A 48-hour pellet inoculum was also advantageous for growth of a newly isolated nitrifying fungus defined as *Penicillium* sp. L1. When compared to inoculation with spore suspension, pellet size could be increased significantly by using a pellet inoculum (Liu et al. 2017).

Other factors – aeration and growth rate

A. niger generally features an indirect relation between pellet compactness and aeration rate. However, using an 1:1 oxygen/air mixture leads to dense growth and increased hyphal branching (Prosser and Tough 1991). Krull et al. (Krull et al. 2013) state that *A. niger* pellets derived from high aeration rates have overall a much larger structure and have unstructured and irregular outer sections. Low aeration results in rather compact peripheral structures. By comparison, it was found that agitation effects are less severe.

Some *Aspergillus* species are associated with filamentous morphology at low growth rates and reversibly produce pellets at higher rates (Prosser and Tough 1991). High growth rates in *P. chrysogenum* cultivations lead to an increase in hyphal branching (Nielsen et al. 1995). Decreasing the specific growth rate was followed by pellet breakage. In addition, hyphal elements were torn away from the surface. Nielsen et al. assume that such pellet breakage happens due to cell lysis within the pellet, which leads to a loss in stability. Posch et al. (Posch et al. 2014) were able to describe parameter effects on pellet morphology through morphological and physiological bioprocess modelling approaches. In the beginning, high growth rates yield large pellet fractions. If pellet growth reaches a critical level, a transition phase leads to dispersed growth due to increasing pellet erosion and breakage.

Summarizing, factors such as agitation and media pH have universal impact on pellet morphology. However, the effect of most factors described in this section only applies to specific species and processes. In general, definite guidelines for morphological alteration or control cannot be given.

Conclusions

Any preference in fungal pellet morphology depends on species and specific task at hand. To timely assess current process morphology, novel techniques like flow cytometry combined with fluorescent staining are convenient. Once desired relations between pellet form and productivity have been established, one can draw from a multitude of options to favourably alter and optimise morphology. Some of these possibilities are summarised in Table 1: In this table, pellet forming species are divided into coagulative or non-coagulative type. Based upon this distinction preferred pellet morphologies are cited, extended by possible techniques to favourably alter morphology.

From our perspective, modelling approaches involving raw data from morphological classification seem promising to increase process understanding. We envision a combination of timely morphological assessment with specific morphological alteration in order to favourably stir fungal pellet processes towards increased productivity.

Compliance with Ethical Standards

Conflict of Interest: The authors declare that they have no conflict of interest.

Ethical approval: This article does not contain any studies with human participants or animals performed by any of the authors.

Table 1. Overview on several fungal species: agglomeration type, variations in pellet morphology and possibilities of morphological alteration; if not mentioned otherwise, preferred morphology refers to cultivation.

Type	Species	Preferred morphology	Alteration of morphology	References
Coagulative type	*Aspergillus* *A. niger* *A. nidulans* *A. oryzae*	For citric acid production: Swollen hyphal branches, compact agglomerates = clumps, pellets featuring thin biomass layers and loose core For production of fructosyl-transferase: Small, spherical	Strong agitation (filament fragmentation wanted) Aeration using oxygen/air 1:1 mixture, high growth rate low pH (2.0 ± 0.2), Manganese presence Spore inoculum level Pellet dispersion instead of spore inoculum Surfactant: Tween 20	Wilkinson 1998 Papagianni 2007 Papagianni and Mattey 2006 Prosser and Tough 1991 Wamg et al. 2017 Kurakake et al 2017
	Phanerochaete chrysosporium	Small pellet size (~ 5.5 mm^3) for lignin peroxidase production	High shear rate	Zhang and Zhang 2016 Zmak et al. 2006
	Blakeslea and *Choanephora*	Compact pellet form	Anionic polymers hinder spore aggregation prior to germination	Prosser and Tough 1991
	C. unicolor	Compact star-shaped pellet form	Microparticle-enhanced cultivation (Al_2O_3 particles)	Antecka et al. 2016
	C. fumago	Compact pellet form	Small inoculum volume, carbon source (fructose)	Carmichael and Pickard 1989
	C. sinensis	Small and loose pellets	Surfactant: Tween 80 pH: optimum 6.0	Liu and Wu 2012
Non – coagulative type	*A. ochraceus*	Compact pellet form	Spore inoculum and agitation	Abd-Elsalam 2009
	R. oryzae	Loose pellets in lactic acid production	Medium: peptone, dextrose, calcium carbonate	Liao et al. 2007
Hyphal element agglomerating type	*P. chrysogenum*	'Fluffy' pellet to ensure largest possible active layer with high quantities of cytosol	Aeration using oxygen/air, controlled growth rate CSL in medium, CO_2 concentration Spore inoculum level Physiological process control based on morphological modelling approach	Wilkinson 1998 Nielsen et al. 1995 Prosser and Tough 1991 Ho and Smith 1986 Posch and Herwig (2014)
	P. sp. L1	Large pellet size	Pellet dispersion instead of spore inoculum	Liu et al. 2017

References

Akiba T, Nishi A, Takaoki M, Nagaoka S, Tomita F (1994) Electrophoretic free mobility and viability of microbial cells: a preliminary study in preparation for space experiments. Appl Theor Electrophor 4(2):65-9

Amanullah A, Leonildi E, Nienow AW, Thomas CR (2001) Dynamics of mycelial aggregation in cultures of *Aspergillus oryzae*. Bioproc Biosyst Eng 24(2):101-107 doi:10.1007/s004490100235

Baumgartl H, Wittler R, Lubbers DW, Schugerl K (1984) Oxygen profiles and structure of *Penicillium chrysogenum* pellets. Adv Exp Med Biol 169:793-9

Camici L, Sermonti G, Chain EB (1952) Observations on *Penicillium chrysogenum* in submerged culture. 1. Mycelial growth and autolysis. Bull World Health Organ 6(1-2):265-75

Carlsen M, Spohr AB, Nielsen J, Villadsen J (1996) Morphology and physiology of an alpha-amylase producing strain of *Aspergillus oryzae* during batch cultivations. Biotechnology and bioengineering 49(3):266-76

Carmichael RD, Pickard MA (1989) Continuous and Batch Production of Chloroperoxidase by Mycelial Pellets of *Caldariomyces fumago* in an Airlift Fermentor. Appl Environ Microbiol 55(1):17-20

Christiansen T, Spohr AB, Nielsen J (1999) On-line study of growth kinetics of single hyphae of *Aspergillus oryzae* in a flow-through cell. Biotechnology and bioengineering 63(2):147-53

Cox PW, Paul GC, Thomas CR (1998) Image analysis of the morphology of filamentous micro-organisms. Microbiology 144 (Pt 4):817-27 doi:10.1099/00221287-144-4-817

Douglas HW, Collins AE, Parkinson D (1959) Electric Charge and Other Surface Properties of Some Fungal Spores. Biochim Biophys Acta 33(2):535-538 doi:Doi 10.1016/0006-3002(59)90145-3

Douma RD, Verheijen PJ, de Laat WT, Heijnen JJ, van Gulik WM (2010) Dynamic gene expression regulation model for growth and penicillin production in *Penicillium chrysogenum*. Biotechnology and bioengineering 106(4):608-18 doi:10.1002/bit.22689

Driouch H, Hansch R, Wucherpfennig T, Krull R, Wittmann C (2012) Improved enzyme production by bio-pellets of *Aspergillus niger*: targeted morphology engineering using titanate microparticles. Biotechnology and bioengineering 109(2):462-71 doi:10.1002/bit.23313

Driouch H, Sommer B, Wittmann C (2010) Morphology engineering of *Aspergillus niger* for improved enzyme production. Biotechnology and bioengineering 105(6):1058-68 doi:10.1002/bit.22614

Dynesen J, Nielsen J (2003) Surface hydrophobicity of *Aspergillus nidulans* conidiospores and its role in pellet formation. Biotechnol Prog 19(3):1049-52 doi:10.1021/bp0340032

Ehgartner D (2017) A Comprehensive Analytical and Process-Technological Toolbox for Improved Penicillin Production. Vienna University of Technology

Ehgartner D, Herwig C, Fricke J (2017) Morphological analysis of the filamentous fungus *Penicillium chrysogenum* using flow cytometry—the fast alternative to microscopic image analysis. Applied Microbiology and Biotechnology:1-14 doi:10.1007/s00253-017-8475-2

Fu YQ, Yin LF, Zhu HY, Jiang R, Li S, Xu Q (2014) Effects of pellet characteristics on L-lactic acid fermentation by *R. oryzae*: pellet morphology, diameter, density, and interior structure. Appl Biochem Biotechnol 174(6):2019-30 doi:10.1007/s12010-014-1146-1

Gao D, Zeng J, Yu X, Dong T, Chen S (2014) Improved lipid accumulation by morphology engineering of oleaginous fungus *Mortierella isabellina*. Biotechnology and bioengineering 111(9):1758-66 doi:10.1002/bit.25242

Gerin PA, Dufrene Y, Bellon-Fontaine MN, Asther M, Rouxhet PG (1993) Surface properties of the conidiospores of *Phanerochaete chrysosporium* and their relevance to pellet formation. J Bacteriol 175(16):5135-44

Golabgir A, Ehgartner D, Neutsch L, Posch AE, Sagmeister P, Herwig C (2015) Imaging Flow Cytometry and High-Throughput Microscopy for Automated Macroscopic Morphological Analysis of Filamentous Fungi. Fung Biol-Us:201-210 doi:10.1007/978-3-319-10503-1_17

Grimm LH, Kelly S, Hengstler J, Gobel A, Krull R, Hempel DC (2004) Kinetic studies on the aggregation of *Aspergillus niger* conidia. Biotechnology and bioengineering 87(2):213-8 doi:10.1002/bit.20130

Grimm LH, Kelly S, Krull R, Hempel DC (2005a) Morphology and productivity of filamentous fungi. Appl Microbiol Biotechnol 69(4):375-84 doi:10.1007/s00253-005-0213-5

Grimm LH, Kelly S, Volkerding, II, Krull R, Hempel DC (2005b) Influence of mechanical stress and surface interaction on the aggregation of *Aspergillus niger* conidia. Biotechnology and bioengineering 92(7):879-88 doi:10.1002/bit.20666

Hille A, Neu TR, Hempel DC, Horn H (2005) Oxygen profiles and biomass distribution in biopellets of *Aspergillus niger*. Biotechnology and bioengineering 92(5):614-623 doi:DOI 10.1002/bit.20628

Hille A, Neu TR, Hempel DC, Horn H (2006) Effect of morphology on transport of matter and conversion in *Aspergillus niger*-Pellets. Chem-Ing-Tech 78(5):627-632 doi:10.1002/cite.200600018

Ho CS, Smith MD (1986) Morphological Alterations of *Penicillium-Chrysogenum* Caused by Carbon-Dioxide. J Gen Microbiol 132:3479-3484

Justen P, Paul GC, Nienow AW, Thomas CR (1998) Dependence of *Penicillium chrysogenum* growth, morphology, vacuolation, and productivity in fed-batch fermentations on impeller type and agitation intensity. Biotechnology and bioengineering 59(6):762-775

Kim YM, Song HG (2009) Effect of fungal pellet morphology on enzyme activities involved in phthalate degradation. J Microbiol 47(4):420-4 doi:10.1007/s12275-009-0051-8

Kisser M, Kubicek CP, Rohr M (1980) Influence of manganese on morphology and cell wall composition of *Aspergillus niger* during citric acid fermentation. Arch Microbiol 128(1):26-33

Krull R, Cordes C, Horn H, Kampen I, Kwade A, Neu TR, Nortemann B (2010) Morphology of Filamentous Fungi: Linking Cellular Biology to Process Engineering Using Aspergillus niger. Adv Biochem Eng Biot 121:1-21 doi:10.1007/10_2009_60

Krull R, Wucherpfennig T, Esfandabadi ME, Walisko R, Melzer G, Hempel DC, Kampen I, Kwade A, Wittmann C (2013) Characterization and control of fungal morphology for improved production performance in biotechnology. J Biotechnol 163(2):112-123 doi:10.1016/j.jbiotec.2012.06.024

Kurakake M, Hirotsu S, Shibata M, Takenaka Y, Kamioka T, Sakamoto T (2017) Effects of nonionic surfactants on pellet formation and the production of beta-fructofuranosidases from *Aspergillus oryzae* KB. Food Chem 224:139-143 doi:10.1016/j.foodchem.2016.12.054

Liao W, Liu Y, Chen S (2007) Studying pellet formation of a filamentous fungus *Rhizopus oryzae* to enhance organic acid production. Appl Biochem Biotechnol 137-140(1-12):689-701 doi:10.1007/s12010-007-9089-4

Lin PJ, Grimm LH, Wulkow M, Hempel DC, Krull R (2008) Population balance modeling of the conidial aggregation of *Aspergillus niger*. Biotechnology and bioengineering 99(2):341-50 doi:10.1002/bit.21569

Lin PJ, Scholz A, Krull R (2010) Effect of volumetric power input by aeration and agitation on pellet morphology and product formation of *Aspergillus niger*. Biochem Eng J 49(2):213-220 doi:10.1016/j.bej.2009.12.016

Liu Y, Hu T, Zhao J, Lv Y, Ren R (2017) Simultaneous removal of carbon and nitrogen by mycelial pellets of a heterotrophic nitrifying fungus-*Penicillium* sp. L1. J Biosci Bioeng 123(2):223-229 doi:10.1016/j.jbiosc.2016.08.009

Liu YS, Wu JY (2012) Effects of Tween 80 and pH on mycelial pellets and exopolysaccharide production in liquid culture of a medicinal fungus. J Ind Microbiol Biotechnol 39(4):623-8 doi:10.1007/s10295-011-1066-9

Nair RB, Lennartsson PR, Taherzadeh MJ (2016) Mycelial pellet formation by edible ascomycete filamentous fungi, *Neurospora intermedia*. AMB Express 6(1):31 doi:10.1186/s13568-016-0203-2

Nielsen J, Johansen CL, Jacobsen M, Krabben P, Villadsen J (1995) Pellet formation and fragmentation in submerged cultures of *Penicillium chrysogenum* and its relation to penicillin production. Biotechnol Prog 11(1):93-8 doi:10.1021/bp00031a013

Papagianni M (2007) Advances in citric acid fermentation by *Aspergillus niger*: biochemical aspects, membrane transport and modeling. Biotechnol Adv 25(3):244-63 doi:10.1016/j.biotechadv.2007.01.002

Papagianni M, Mattey M (2006) Morphological development of *Aspergillus niger* in submerged citric acid fermentation as a function of the spore inoculum level. Application of neural network and cluster analysis for characterization of mycelial morphology. Microb Cell Fact 5 doi:Artn 310.1186/1475-2859-5-3

Papagianni M, Mattey M, Kristiansen B (1998) Citric acid production and morphology of *Aspergillus niger* as functions of the mixing intensity in a stirred tank and a tubular loop bioreactor. Biochem Eng J 2(3):197-205 doi:Doi 10.1016/S1369-703x(98)00032-1

Pascual S, De Cal A, Magan N, Melgarejo P (2000) Surface hydrophobicity, viability and efficacy in biological control of *Penicillium oxalicum* spores produced in aerial and submerged culture. J Appl Microbiol 89(5):847-853 doi:DOI 10.1046/j.1365-2672.2000.01189.x

Paul GC, Thomas CR (1996) A structured model for hyphal differentiation and penicillin production using *Penicillium chrysogenum*. Biotechnology and bioengineering 51(5):558-572

Paul GC, Thomas CR (1998) Characterisation of mycelial morphology using image analysis. Adv Biochem Eng Biotechnol 60:1-59

Pazouki M, Panda T (2000) Understanding the morphology of fungi. Bioprocess Eng 22(2):127-143 doi:DOI 10.1007/s004490050022

Pirt SJ (1966) A theory of the mode of growth of fungi in the form of pellets in submerged culture. Proc R Soc Lond B Biol Sci 166(1004):369-73

Porcel EMR, Lopez JLC, Perez JAS, Sevilla JMF, Chisti Y (2005) Effects of pellet morphology on broth rheology in fermentations of *Aspergillus terreus*. Biochem Eng J 26(2-3):139-144 doi:10.1016/j.bej.2005.04.011

Posch AE, Herwig C (2014) Physiological description of multivariate interdependencies between process parameters, morphology and physiology during fed-batch penicillin production. Biotechnol Progr 30(3):689-699 doi:10.1002/btpr.1901

Posch AE, Spadiut O, Herwig C (2012) A novel method for fast and statistically verified morphological characterization of filamentous fungi. Fungal Genetics and Biology 49(7):499-510 doi:10.1016/j.fgb.2012.05.003

Priegnitz BE, Wargenau A, Brandt U, Rohde M, Dietrich S, Kwade A, Krull R, Fleissner A (2012) The role of initial spore adhesion in pellet and biofilm formation in *Aspergillus niger*. Fungal Genet Biol 49(1):30-8 doi:10.1016/j.fgb.2011.12.002

Prosser JI, Tough AJ (1991) Growth mechanisms and growth kinetics of filamentous microorganisms. Crit Rev Biotechnol 10(4):253-74 doi:10.3109/07388559109038211

Sajjad Ur R, Rasool MH, Rafi M (2012) Penicillin production by wild isolates of *Penicillium chrysogenum* in Pakistan. Braz J Microbiol 43(2):476-81 doi:10.1590/S1517-83822012000200007

Serrano-Carreon L, Galindo E, Rocha-Valadez JA, Holguin-Salas A, Corkidi G (2015) Hydrodynamics, Fungal Physiology, and Morphology. Adv Biochem Eng Biotechnol 149:55-90 doi:10.1007/10_2015_304

Tanaka H, Mizuguchi T, Ueda K (1975) Studies on Effect of Agitation on Mycelia in Submerged Mold Culture .5. Index Representing Mycelial Strength to Maintain Physiological-Activity on Mechanical Agitation. J Ferment Technol 53(1):35-43

Tinoco-Valencia R, Gomez-Cruz C, Galindo E, Serrano-Carreon L (2014) Toward an understanding of the effects of agitation and aeration on growth and laccases production by *Pleurotus ostreatus*. J Biotechnol 177:67-73 doi:10.1016/j.jbiotec.2014.02.013

Trinci APJ (1983) Effect of Junlon on Morphology of *Aspergillus-Niger* and Its Use in Making Turbidity Measurements of Fungal Growth. T Brit Mycol Soc 81(Oct):408-412

Villena GK, Fujikawa T, Tsuyumu S, Gutierrez-Correa M (2010) Structural analysis of biofilms and pellets of *Aspergillus niger* by confocal laser scanning microscopy and cryo scanning electron microscopy. Bioresource Technol 101(6):1920-1926 doi:10.1016/j.biortech.2009.10.036

Villena GK, Gutierrez-Correa M (2007) Morphological patterns of *Aspergillus niger* biofilms and pellets related to lignocellulolytic enzyme productivities. Lett Appl Microbiol 45(3):231-237 doi:10.1111/j.1472-765X.2007.02183.x

Walisko R, Moench-Tegeder J, Blotenberg J, Wucherpfennig T, Krull R (2015) The Taming of the Shrew--Controlling the Morphology of Filamentous Eukaryotic and Prokaryotic Microorganisms. Adv Biochem Eng Biotechnol 149:1-27 doi:10.1007/10_2015_322

Wang B, Chen J, Li H, Sun F, Li Y, Shi G (2017) Pellet-dispersion strategy to simplify the seed cultivation of *Aspergillus niger* and optimize citric acid production. Bioprocess Biosyst Eng 40(1):45-53 doi:10.1007/s00449-016-1673-y

Wargenau A, Fleissner A, Bolten CJ, Rohde M, Kampen I, Kwade A (2011) On the origin of the electrostatic surface potential of *Aspergillus niger* spores in acidic environments. Res Microbiol 162(10):1011-7 doi:10.1016/j.resmic.2011.07.006

Wargenau A, Kwade A (2010) Determination of Adhesion between Single *Aspergillus niger* Spores in Aqueous Solutions Using an Atomic Force Microscope. Langmuir 26(13):11071-11076 doi:10.1021/la100653c

Wilkinson MHFH (1998) Digital Image Analysis of Microbes: Imaging, Morphometry, Fluorometry, and Motility Techniques and Applications 1st John Wiley & Sons, Inc. New York, NY, USA

Wosten HAB, van Veluw GJ, de Bekker C, Krijgsheld P (2013) Heterogeneity in the mycelium: implications for the use of fungi as cell factories. Biotechnol Lett 35(8):1155-1164 doi:10.1007/s10529-013-1210-x

Wu M, Xu Y, Ding W, Li Y, Xu H (2016) Mycoremediation of manganese and phenanthrene by *Pleurotus eryngii* mycelium enhanced by Tween 80 and saponin. Appl Microbiol Biotechnol 100(16):7249-61 doi:10.1007/s00253-016-7551-3

Wucherpfennig T, Hestler T, Krull R (2011) Morphology engineering - Osmolality and its effect on *Aspergillus niger* morphology and productivity. Microb Cell Fact 10 doi:10.1186/1475-2859-10-58

Zhang J, Zhang J (2016) The filamentous fungal pellet and forces driving its formation. Crit Rev Biotechnol 36(6):1066-1077 doi:10.3109/07388551.2015.1084262

Chapter 5.
Analytics

Plate reader method for viability assessment

Lukas Veiter[1,2]

[1] CD Laboratory on Mechanistic and Physiological Methods for Improved Bioprocesses, Vienna University of Technology, Gumpendorferstrasse 1a/166, 1060 Vienna, Austria

[2] Research Area Biochemical Engineering, Institute of Chemical, Environmental and Bioscience Engineering, Vienna University of Technology, Gumpendorferstrasse 1a/166, 1060 Vienna, Austria

This method was summarized as a Christian Doppler Laboratory progress report on September 6th, 2018. Formatting of figures according to the original report.

Problem Statement

Viability assessment via PI staining and subsequent measurement via Tecan plate reader is used to estimate viable biomass. A method developed in the CD Laboratory was transferred to Sandoz in August 2017, however an internal lab report from Sandoz (AIOD 30/2018) from July 2018 found the method to be inadequate. The findings of this report were investigated by the CD laboratory and the findings are summarized in this report.

Hypothesis and Goal

For at-line viability assessment, Propidium iodide (PI) is used. This membrane impermeant dye binds to DNA. If subsequently excited at wavelengths of 488 nm, PI will emit at a wavelength of 617 nm (red). This characteristic is used according to the following method:
Sample is washed via centrifugation and resuspension in PBS buffer. Subsequently sample is put on multi-well plate and PI is added. After 20 minutes of incubation, fluorescence intensity is measured via a Tecan plate reader. As negative control microwaved samples are used. Viability is estimated according to equation 1:

$$(1) \quad \text{Viability}\,[-] = \left(1 - \frac{\text{red fluorescence orginal sample}}{\text{red fluorescence in microwaved sample}}\right)$$

Hypothesis (taken from Lab report AIOD 30/2018)
The results shown in this report indicate that the PI concentration in the procedure developed in the CD Laboratory are insufficient to stain dead cells completely. Thus, the estimation of viability is influenced by the amount of biomass used in the assay.

Goal
The appropriate amount of PI in relation to biomass concentration in the assay has to be determined to obtain trustworthy results.

To achieve this goal and further investigate the following experiments were performed:

1. Verification of method robustness with different biomass and PI concentrations
2. Test of method on different ratios of microwaved samples

Materials and Methods

1.3.1. Shake flask cultivations

To generate biomass containing substantial pellet population the following media composition was used for all cultivations (see Table 1):

Table 1. Media composition

Pre culture media		
volume of solution	0.20	l
component	**conc.**	**unit**
Saccharose $C_{12}H_{22}O_{11}$	18	g/l
Glucose Monohydrate $C_6H_{12}O_6 \cdot H_2O$	3	g/l
Corn Steep Liquor	26	g/l
Calcium carbonate $CaCO_3$	3.8	g/l
Main culture media composition is confidential		
Volume of solution	1	l

Table 2 summarizes employed cultivation strategies:

Table 2. Cultivation strategy

Preculture Process Conditions	2x 500 ml shakeflask	
Batch starting volume	2 x 0.050	l
pH	uncontrolled	
Temp	25	°C
Initial agitation rate	300	rpm
Inoculation		
volume of innoculum	2.0	ml
Batch-end criteria	53.5 hours	
Estimated cell conc.	5	g/l
Fill / Harvest Volume Calculations		
volume at the end of batch	0.075	L
desired volume at start of fed-batch	0.075	L
Volume of medium in main culture	0.06375	L
Volume Batch culture transferred to main culture	0.01125	L
% of transferred batch culture in main culture	15	%
Main culture		
Temp	25	°C
Agitation rate	300	rpm

1.3.2. Standard viability assessment

Samples were taken at various points during main culture cultivation. For viability assessment 200 µL of sample was mixed with 800 µL of PBS buffer. Additionally, 1 mL of sample was added to 4 mL of PBS buffer (50 mL CaCl2, 0.2 g/L KCl, 0.2 g/L KH3PO4, 0.1 g/L MgCl * 6H2O, 8 g/L NaCl, 0.746 g/L Na2HPO4 * 2H2O) and microwaved for 30 s using 600 Watt. Afterwards microwaved and non-microwaved sample were treated identically. Samples were subsequently washed twice.
100 µL of re-suspended samples was pipetted as duplicates into individual wells of a 96 well microtiter plate. Propidium iodide (PI) working solution was added and the well plate was incubated in the dark for 20 min. Measurements were carried out using an Infinite M200 Pro (Tecan, Switzerland) multimode microplate reader after a previous shaking step (20 s, 2 mm amplitude, orbital mode). Fluorescence intensity was measured at an emission wavelength of 600 nm and an excitation wavelength of 535 nm. The fraction of viable cells was estimated according to equation 1.

1.3.3. Verification of method robustness with different biomass concentrations and of PI concentrations

Biomass in main culture medium was diluted using PBS according to the following scheme:

- Pure = 0: 5 ml biomass
- 1:4: 1.25 ml PBS and 3.75 ml biomass
- 1:2: 2.5 ml PBS and 2.5 ml biomass
- 3:4: 3.75 ml PBS and 1.25 ml biomass

Viability assessment was performed according to 1.3.2. Standard viability assessment, either 20 µM, 100 µM or 200µM PI were used.

1.3.4. Test of method on different ratios of microwaved samples

For this purpose, half the content of a shakeflask at varius cultivation times was microwaved at 700 W for 30 seconds using a loose cap to prevent volume loss due to evaporation. Subsequently this microwaved biomass was mixed with untreated biomass to produce solutions of 5 ml with 0, 25, 50, 75, 100 % microwaved (= dead) biomass. These biomass solutions were subjected to viability assessment according to 1.3.3. Verification of method robustness with different biomass concentrations and of using different PI concentrations (1 µl, 5 µl or 10 µl of PI). In total three experiments using different ratios of microwaved biomass were conducted.

Results and discussion

1.4.1. Verification of method robustness with different biomass concentrations and concentrations of PI

This experiment was conducted to study the influence of 1) biomass concentration as well as 2) PI concentration on viability assessment. Dilutions performed according to 1.3.3. resulted in different biomass concentrations (see Table 3). Additionally, the effect of PI concentration was tested by the use of different PI concentrations on these samples. The results of viability assessment are displayed in Figure 1.

Table 3. Biomass dilutions according to 1.3.3.

No.	Cultivation time [h]	Dilution	Biomass [g/l]
1:1	160	none	26.95
1:4		1.25 PBS / 3.75 biomass	20.19
1:2		2.5 PBS / 2.5 biomass	13.50
3:4		3.75 PBS / 1.25 biomass	6.73

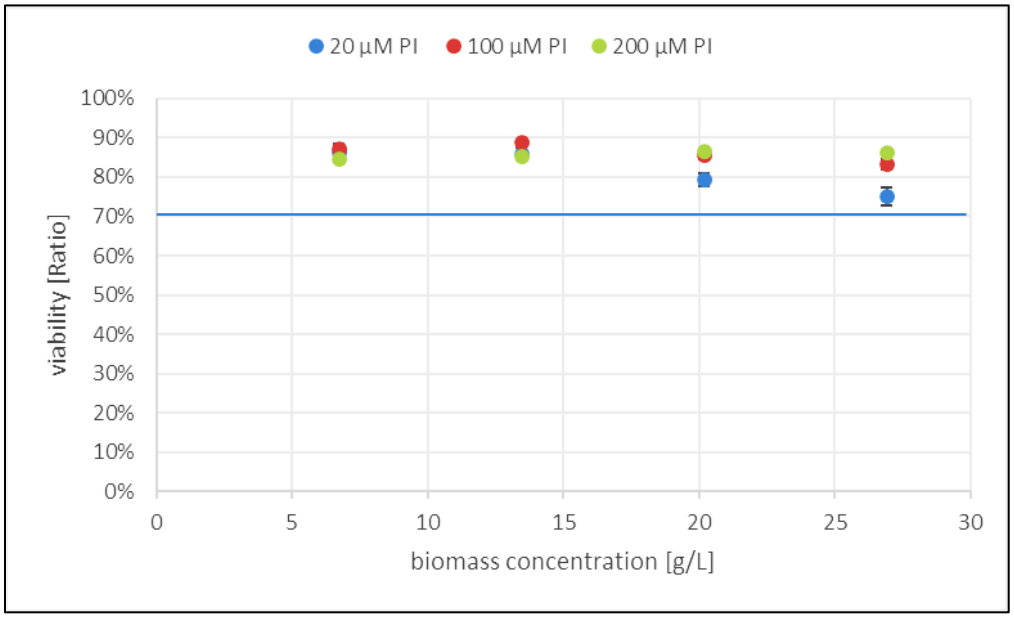

Figure 1. Viability assessment using different biomass concentrations and PI concentrations

As viability itself should not be affected by dilution of biomass, the overall result of viability assessment should remain constant for all biomass dilutions. This is generally the case, however at high biomass concentrations (no dilution, 26.95 g/L biomass) and low PI concentrations of 20 µM PI, viability assessment yields lower values by roughly 5 % (77 % vs. 82-83 %). This effect can be described linearly (see Figure 2).

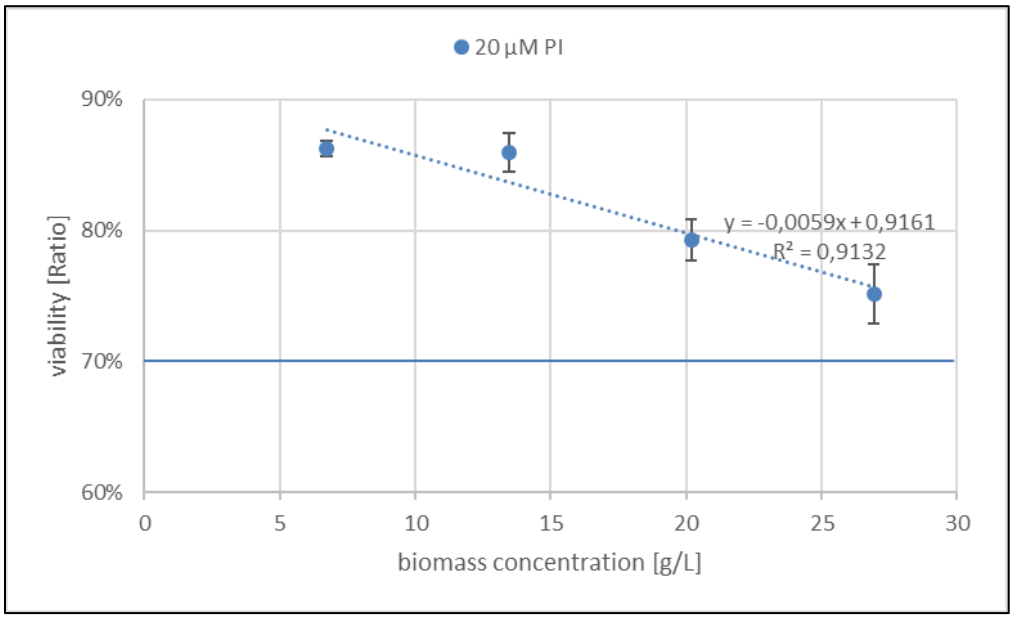

Figure 2. Drop in calculated viability as a result of high biomass concentration

Consequently, viability assessment would be off by 10 % at a biomass concentration of 36 g/L. This effect was not detected during method development because shake flask cultivations were primarily used with considerably lower biomass concentrations. At higher PI concentrations, no deviations in viability assessment are detectable as demonstrated in Figure 3.

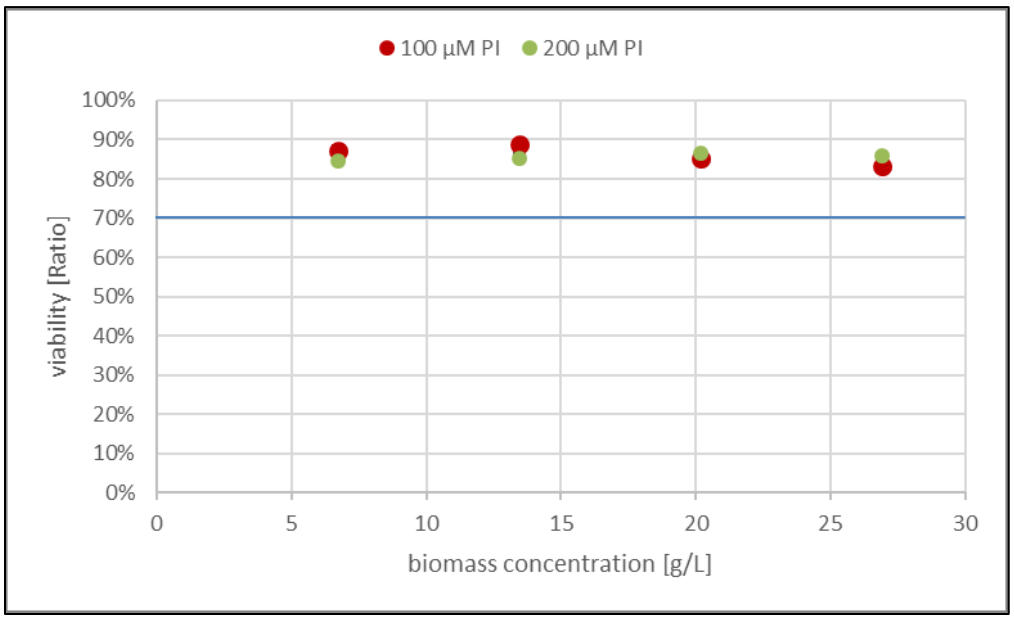

Figure 3. Viability assessment for different biomass concentrations using 100 µM or 200 µM PI

These results indicate that a concentration of 20 µM PI is indeed too low when biomass concentrations > 25 g/L are used. We suspect that the microwaved sample cannot be stained completely. Therefore, viability is underestimated according to equation 1.

Based on recent findings we recommend a concentration 100 µM PI (equals 5 µl of 0,2 mM PI stock solution in 100 µl of sample, see SOP 'PI staining' from August 2017).

Additional remark: According to Sandoz Lab report AIOD 30/2018 a 10-fold increase of PI concentration from 20 µM to 200 µM results in a 10-fold increase of fluorescence of microwaved biomass. As biomass concentrations are not stated in this report, it was not possible to replicate this experiment. In an effort to look into these results, we only detected a 2-fold increase of fluorescence at 20 g/L biomass concentration (data not shown).

1.4.2. Test of method on different ratios of microwaved samples

Figure 4 depicts fluorescence values dependent on (1) ratios of microwaved biomass and (2) PI concentration. A PI concentration of 100 µM PI (equals 5 µl of 0,2 mM PI stock solution in 100 µl of sample, see SOP 'PI staining' from August 2017) exhibits the lowest standard deviation and the best R^2 in contrast to 20 µM and 200 µM PI. Similar results to the descriptions in Sandoz Lab report AIOD 30/2018 were not observed (data not available for publishing). However, comparisons here are questionable, as biomass concentrations of Sandoz's experiments are unknown.

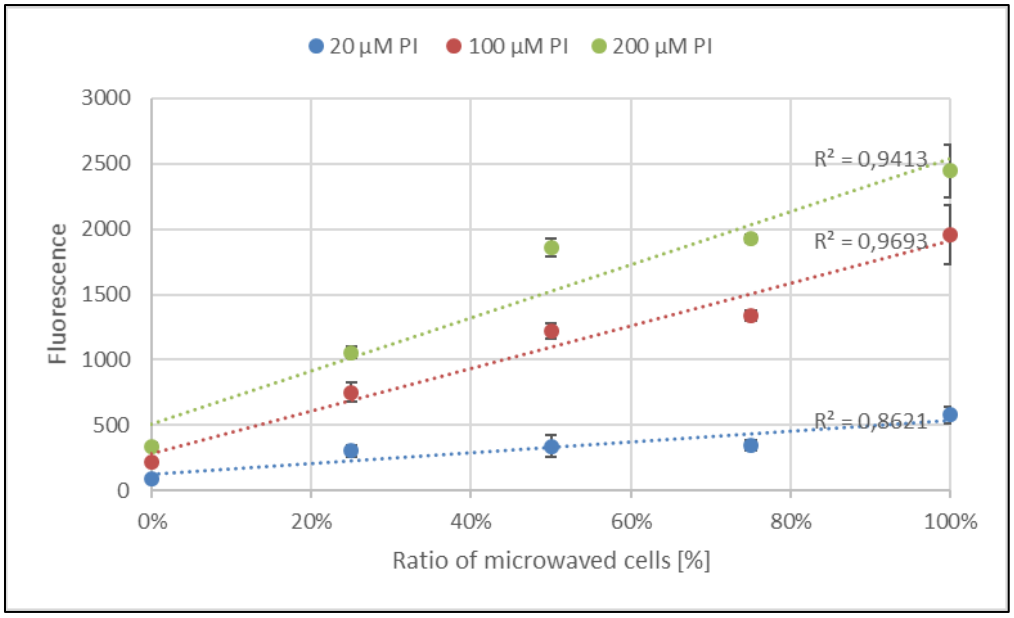

Figure 4. Viability assessment of biomass with different ratios of microwaved cells, biomass concentration 20 g/L.

In should be noted that PI degrades quickly as demonstrated by the following measurement (see Figure 5) of the same samples using a PI solution that was prepared the day before (24h before measurement). As mentioned in the SOP 'PI staining' from August 2017, a PI solution obtained by 1:100 dilution of 20 mM PI stock should be prepared daily to ensure consistently high fluorescence signals.

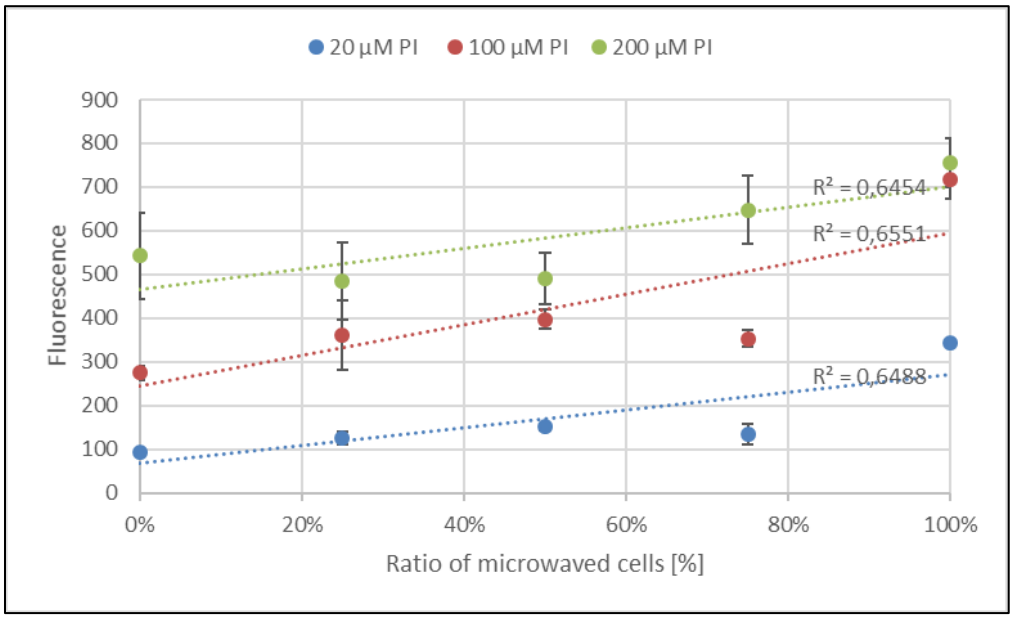

Figure 5. Viability assessment of biomass solutions with different ratios of microwaved cells, biomass concentration 20 g/L – PI solution prepared 24 h before measurement

1.5. Conclusions

Based on recent findings we recommend a concentration 100 µM PI when biomass concentrations > 25 g/L are used.

1.6. References

Sandoz Report Lab report AIOD 30/2018

Ehgartner D, Hartmann T, Heinzl S, Frank M, Veiter L, Kager J, Herwig C, Fricke J (2017) Controlling the specific growth rate via biomass trend regulation in filamentous fungi bioprocesses. Chem Eng Sci 172: 32-41

The filamentous fungus *Penicillium chrysogenum* analysed via flow cytometry - a fast and statistically sound insight into morphology and viability

Lukas Veiter[1,2] and Christoph Herwig*[,1,2]

*to whom the correspondence should be addressed to

[1] CD Laboratory on Mechanistic and Physiological Methods for Improved Bioprocesses, Vienna University of Technology, Gumpendorferstrasse 1a/166, 1060 Vienna, Austria
[2] Research Area Biochemical Engineering, Institute of Chemical, Environmental and Bioscience Engineering, Vienna University of Technology, Gumpendorferstrasse 1a/166, 1060 Vienna, Austria

*Corresponding author:
christoph.herwig@tuwien.ac.at; Tel (Office): +43 1 58801 166400
Gumpendorferstrasse 1a / 166-4
1060 Wien, Austria

Published in 'Applied Microbiology and Biotechnology':
Veiter, L. and C. Herwig (2019). 'The filamentous fungus *Penicillium chrysogenum* analysed via flow cytometry-a fast and statistically sound insight into morphology and viability.' Appl Microbiol Biotechnol.

Abstract

Filamentous fungi serve as production host for a number of highly relevant biotechnological products, like penicillin. In submerged culture morphology can be exceptionally diverse and is influenced by several process parameters, like aeration, agitation, medium composition or growth rate. Fungal growth leads to several morphological classes encompassing homogeneously dispersed hyphae and various forms of hyphal agglomerates and/or clump structures. Eventually, the so-called pellet structure can be formed, which represents a hyphal agglomerate with a dense core. Pellet structures can hinder oxygen and substrate transport, resulting in different states of viability, which in turn affects productivity and process control. Over the years, several publications have dealt with methods to either gain morphological insight into pellet structure or determine biomass viability.

Within this contribution, we present a way to combine both in a flow cytometry-based method employing fluorescent staining. Thereby we can assess filamentous biomass in a statistically sound way according to i) morphology and ii) viability of each detected morphological form. We are confident that this method can shed light on the complex relationship between fungal morphology, viability and productivity - in both process development and routine manufacturing processes.

Keywords

Filamentous fungi, *Penicillium chrysogenum*, flow cytometry, viability, morphology, pellets.

Introduction

Successful cultivation strategies involving filamentous fungi need to consider the organism's morphology. For example, *Penicillium chrysogenum* comprises several morphological forms when growing in submerged culture, ranging from homogenously dispersed hyphae to compact, hyphal agglomerates known as pellets (Veiter et al. 2018). Each morphological class affects viability, productivity and performance in different ways. From a process control standpoint, pellets are favoured as rheology, gas-liquid mass transfer and mixing are facilitated. However, pellet morphology also leads to active and non-active zones within the pellet due to limitations in transport of substrates and products, especially oxygen (Dynesen and Nielsen 2003). These zones also affect productivity, as production of penicillin is happening in the non-growing cytoplasm found in the pellet's outer layer (Baumgartl et al. 1984). In turn, the pellet's core exhibits hyphal degradation, a decline in viability and no productivity (Ehgartner 2017). Naturally, these variations across all morphological forms complicate viability estimation and by extension determination of growth rate, substrate uptake rates and yields.

Hence, a quantitative approach to assess viable biomass is of utmost importance. Determination of viability can be performed employing at-line chemical methods such as fluorescent staining or physical techniques using various sensors. Dielectric spectroscopy, infrared spectroscopy and fluorescence have been comprehensively studied in the scope of filamentous fungi (Ronnest et al. 2011, Ehgartner et al. 2017). While these methods enable real time measurement, they cannot take into account morphological aspects directly. In this respect, flow cytometry is a potent alternative. Biomass morphology can be classified according to size and form through analysis of light scatter signals (Dubelaar et al. 1999, Ehgartner et al. 2017, Pekarsky et al. 2018). To assess viability, fluorescent staining is regularly used in flow cytometry coupled with fluorescence detectors (Langemann et al. 2016, Attfield et al. 2000, Pekarsky et al. 2018). For filamentous fungi such studies are scarce, mainly due to the large particle sizes of fungal biomass (Dubelaar et al. 1999). Recent studies encompass *Aspergillus niger* microcolonies and *Trichoderma* (de Bekker et al. 2011, Delgado-Ramo et al. 2014), but are lacking detailed morphological analysis.

Specific applications of flow cytometry for morphological classification of *Penicillium chrysogenum* were recently published (Ehgartner et al. 2017), however they did not include viability assessment yet.

In this publication, we quantitatively employ flow cytometry to combine detailed morphological insights with viability assessment. The developed method is at-line and potentially online applicable, statistically sound due to the high number of measured particles and can estimate viable layers in specific morphological classes, such as pellets and large hyphal agglomerates. Furthermore, we have verified our results with established state-of-the-art methods such as a plate reader method for viability assessment as well as confocal laser microscopy for determination of viable pellet layer. In the following, these points will be discussed: (i) differentiation of viable biomass against complex media background, (ii) morphological analysis and assessment of viability, (iii) comparison of flow cytometry viability assessment with the state-of-the-art plate reader method, (iv) analysis of large element morphology and viable layer as well as (v) comparison of results from flow cytometry with confocal laser microscopy.

Materials and methods

Strain

Spore suspensions of the P-14 *P. chrysogenum* candidate strain for penicillin production descending from the P-2 *P. chrysogenum* candidate strain (American Type CulturCollection with the access number ATCC 48271) (Lein 1986) were provided by Sandoz GmbH (Kundl, Austria) and used for all experiments.

Bioreactor cultivations

Three cultivations (FB1 and FB2) were performed in a Techfors S bioreactor (Infors HT, Bottmingen, Switzerland) with 10 l working volume. The batch was cultivated with an initial volume of 6.5 l in the first mentioned bioreactor and inoculated with $2 \cdot 10^8$ spores/l. During batch phase pH was not controlled. The end of the batch was defined per default as an increase in pH of 0.5 by convention. After the batch, the broth was diluted with fed-batch medium (15% broth, 85% medium) and fed-batches were started with an initial volume of 6.5 l. Batch and fed-batch media were similar as described elsewhere Posch and Herwig (2014).

During fed-batch phase, pH was kept constant at 6.5 ± 0.1 by addition of 20% (w/v) KOH or 15% (v/v) H_2SO_4, respectively. pH was measured using a pH probe (Hamilton, Bonaduz, Switzerland). After additional 12 h nitrogen and phenoxyacetate feeds were started at constant rates (6.5 ml/h for nitrogen and 2 ml/h for phenoxyacetate). In the first 24 h of fed-batch, 500 g/l glucose solution was fed at a constant rate of 1.01 ml/(l·h). Afterwards, a three-times increase in feeding rate was carried out leading to a constant rate of 3 ml/(l/h). The stirrer was equipped with three six bladed Rushton turbine impellers, of which two were submersed and one was installed above the maximum liquid level for foam destruction. Fermentation temperature was kept at 25 °C via a cooling/heating jacket. Aeration was controlled at 1 vvm in batch and initial fed-batch with mass flow controllers (Vögtlin, Aesch, Switzerland). Dissolved oxygen concentration was measured using a dissolved oxygen probe (Hamilton, Bonaduz, Switzerland) and controlled between 40% and 90% during batch and between 40% and 60% during fed-batch, via adjustment of stirrer speed. The initial agitation conditions were 325 rpm stirring speed in batch and 500 rpm in fed-batch. CO_2 and O_2 concentration in the off gas were analysed with an off-gas analyser (M. Müller AG, Switzerland).

Both cultivations were similarly conducted in a standard manner to generate biomass for method development. Only in FB2 this strategy was slightly altered: In order to measure a sudden viability-decline, aeration was switched from air to N_2 for FB2 at a process time of 160 h, which caused an immediate drop in dissolved oxygen concentration and CO_2 concentration in the off gas.

Flow cytometry

Samples from fed-batch cultivations were diluted 1:10 into phosphate buffered saline (50 g/l of 2.65 g/l $CaCl_2$ solution, 0.2 g/l KCl, 0.2 g/l KH_2PO_4, 0.1 g/l $MgCl \cdot 6\ H_2O$, 8 g/l NaCl and 0.764 g/l $Na_2HPO_4 + 2\ H_2O$) and stained with propidium iodide (Sigma Aldrich, St. Louis, Missouri/USA; 20 mM stock dissolved in DMSO ≥ 99.9 %, diluted with phosphate buffered saline to a final concentration of 20 µM). In order to study different viability stages, some samples were subjected to microwave treatment for 30 s at 940 W in a microwave oven. After incubating 5 min, the sample was further stained with fluorescein diacetate (Sigma Aldrich, St. Louis, Missouri, USA; stock solution of 5 g/l dissolved in acetone ≥ 99.9% to a final concentration of 5 mg/l). After incubation of 5 min, the sample was further diluted (1:100 in the same buffer) for flow cytometric analysis. Metabolic activity is shown by FDA treatment resulting in green fluorescence through esterase activity. PI fluorescence is a result from DNA intercalation in cells with compromised membranes (Pekarsky et al. 2018).

A CytoSense flow cytometer (CytoBuoy, Woerden, Netherlands) with two forward scatter (FSC), one sideward scatter (SSC) and two fluorescence channels (green, red) was used for particle analysis. The implemented laser had a wavelength of 488 nm. The configuration of the filter set was 515-562 ± 5 nm for the green fluorescence channel (FL-green, used for fluorescein diacetate) and 605-720 ± 5 nm for the red fluorescence channel (FL-red, used for propidium iodide). The device was equipped with a PixeLINK PL-B741 1.3MP monochrome camera for in flow image acquisition. For data treatment, the software CytoClus3 (CytoBuoy, Woerden, Netherlands) was used.

The CytoSense flow cytometer provides multiple data points per channel per particle. This signal shape is achieved for both scatter channels as well as green and red fluorescence channels (Dubelaar et al. 1999).

These pulse shapes are the basis for multiple curve parameters (Ehgartner et al. 2017). Except for length parameters in µm, all parameters are in arbitrary units, as the user can set sensitivity levels SSC and fluorescence detectors. Setting of sensitivity levels was aligned with plate reader viability assessment. The most relevant parameters for the here presented study are the following parameters: Maximum (maximum of signal curve), Total (area under curve), Length (length of the signal), Sample length (length of signal above trigger level) and Fill factor (similarity of the curve to a block; 0-1; higher if block-shaped).

At-line viability measurement via plate reader

To investigate viability via propidium iodide (PI) staining, 200 µl of sample were diluted 1:5 with phosphate buffered saline (PBS, see (Ehgartner et al. 2017)). In addition, 1 ml of sample was diluted 1:5 with PBS and microwave treated by leaving it for 30 s at 940 W in a M510 microwave oven (Philips, Amsterdam, Netherlands). One millilitre of the microwave treated sample was used for further investigation. In a next step, duplicates of all samples (including microwave treated and untreated samples) were centrifuged for 15 min at 500 min^{-1} and 50 g. 800 µl of supernatant were removed and 800 µl of PBS buffer were added. The pellet was resuspended and the washing step repeated. 100 µl of the resuspended sample was pipetted into a microtiter well and 1 µl of 200 µM PI solution (Sigma Aldrich, St. Louis, Missouri/USA) was added. The PI was prepared by diluting a 20mM PI stock solution in DMSO, 1:100 in PBS. After an incubation time of 20 min at room temperature in darkness, the measurement was performed in a Tecan well-plate reader (Tecan, Männedorf, Switzerland; ex./em. 535/600 nm). Each sample was measured six times simultaneously using 96 well plates.

Viability is estimated according to Equation 1:

$$(2)\ \text{Viability}\,[-] = \left(1 - \frac{\text{red fluorescence orginal sample}}{\text{red fluorescence in microwaved sample}}\right)$$

Confocal laser fluorescence microscopy

Confocal fluorescence microscopy was used as method to distinguish between viable and dead parts of the pellets. FDA was used to stain metabolically active, viable hyphae while PI was used to stain dead cells. Microscopic images of the pellets were taken using a confocal fluorescent microscope (TE2000-E, Nikon, Japan).

100 µl of the bioreactor sample were diluted with 900 µl of PBS buffer and then centrifuged for 2 min at 500 rpm at room temperature. 800 µl of the supernatant were discarded and replaced with 800 µl of PBS buffer. Afterwards, 10 µl of 200 µM PI reagent (prepared from 20 mM stock solution by 1:100 dilution) were added and the sample was incubated for 10 min in the dark. 20 µl of the sample were then applied on a cover slide and the slide was then placed on the microscope table. After focusing, 2 µl of freshly prepared 50 mg/l FDA reagent (Sigma Aldrich, St. Louis, Missouri, USA; prepared with PBS buffer from a stock solution of 5 g/l dissolved in acetone) were added and a cover slide was placed on the sample. Lasers and the respective detector systems (PI: ex. 543 nm, em. 580 nm; FDA: ex. 488 nm, em. 507 nm) were activated separately. The gain for the 507 nm channel was adjusted according to FDA related fluorescence intensity increase. The pellet was focused with the maximum intension of the PI stained area as criterion. Pictures were taken for at least 10 pellets per sample.

Results

Differentiation of viable biomass against complex media background

Based on initial measurements of fed-batch medium with and without cells, a distinction of fungal cells from media background was possible. Particles exceeding a green fluorescence signal of 500 were classified as viable cells. Within previously set gates, viable cells and dead cells are easily differentiated from the media background as displayed in Figure S1. In principle, this differentiation is also possible without the use of fluorescent staining. However, results are negatively influenced by the media particle content (as demonstrated in Figure S2) making a sharp distinction impossible. Naturally, fluorescence intensity of unstained biomass is 10 – 50 times lower as well, which further complicates differentiation.

Morphological analysis and assessment of viability

Scatter plots from viable cell data were generated and gates were set for morphological classification as previously described by Ehgartner et al. 2017. This method enables classification according to the following forms: Hyphae, small clumps, large clumps and pellets. Summarising, gate setting is based on particle size in combination with SSC total. For differentiation between large clumps and pellets, saturation of FSC signals, respectively FSC Fill Factor values are considered. Exact definitions on the differentiation between morphological fractions are provided in Table 1. In the following, large clumps and pellets will frequently be characterised in a combined fashion as 'large elements'.

For large clumps and pellets, the parameter 'core compactness' representing the density of the pellet core can be derived from the following Equation 2:

$$(2)\quad \text{Compactness}_{\text{core}}\,[-] = \frac{\text{Length of saturated FSC signal in pellet core [µm]}}{\text{Core diameter [µm]}}$$

Similar knowledge can be obtained from the analysis of SSC signal length in combination with particle size, hereafter termed 'Compactness according to SSC' and calculated according to Equation 3:

$$(3)\quad \text{Compactness}_{\text{SSC}}\,[-] = \frac{\text{Length of SSC signal [µm]}}{\text{Particle diameter [µm]}}$$

Images of several pellet signal pulse shapes including FSC and SSC are displayed in Figure 1. These images are representative of several process stages in FB2. Figure 1A shows a pellet with rather low compactness according to the SSC signals, the pellet depicted in Figure 1B displays increased compactness. In Figure 1C and Figure 1D breakage can be observed from FSC signals in the pellet's core. Both of these degrading pellets display high compactness according to SSC signals. This is in accordance with literature, as highly compact pellets (as indicated by SSC signal saturation) exhibit hyphal degradation and a decline in viability in the pellet's core (Ehgartner et al. 2017).

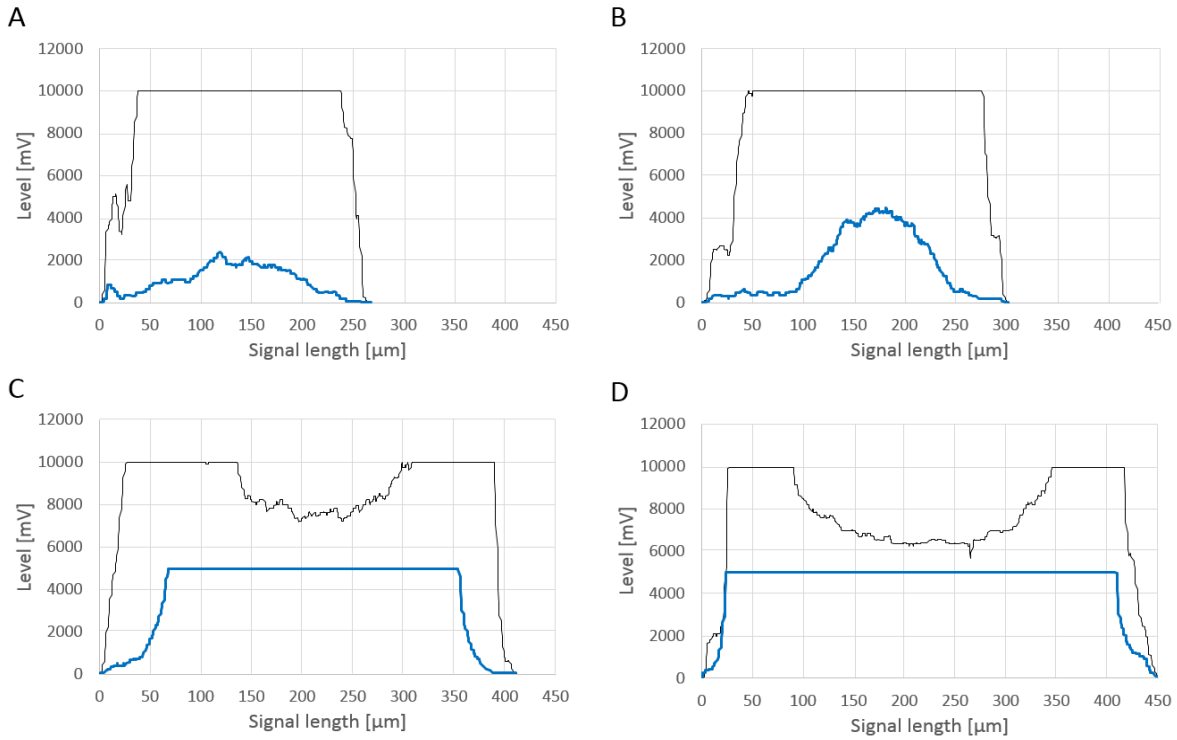

Figure 1. Pulse shape profiles of several pellets. Black line for FSC signal, blue line for SSC signal. Demonstration of compactness calculation according to Equation 1 and 2. Low diameter and low SSC signal, saturated FSC signal equals high core compactness (A). Low Diameter and increased SSC signal, saturated FSC signal (B). Saturated SSC signal and pellet breakage according to FSC signals at elevated pellet diameters equals low core compactness and high Compactness SSC (C, D).

These images are representative of several process stages in FB2. Figure 1A shows a pellet with rather low compactness according to the SSC signals, the pellet depicted in Figure 1B displays increased compactness. In Figure 1C and Figure 1D breakage can be observed from FSC signals in the pellet's core. Both of these degrading pellets display high compactness according to SSC signals. This is in accordance with literature, as highly compact pellets (as indicated by SSC signal saturation) exhibit hyphal degradation and a decline in viability in the pellet's core (Ehgartner 2017). Assessment of viability is based on individual particle pulse shapes, as demonstrated by Figure 2. In order to estimate contributions of both fluorescence signals to viability, the particle parameter 'fluorescence fill factor' (FL_{FF}) (see Equation 4) for green and red fluorescence was derived from fluorescence pulse shapes according to the following equation (Equation 4):

$$(4)\ FL_{FF}\ [-] = \frac{\text{Area under FL curve [mV*µm]}}{\text{Area under block shaped FL curve [mV*µm]}}$$

Individual particle viability can be estimated according to Equation 5.

$$(5)\ \text{Ind. via.}\ [-] = \frac{\text{Area under } FL_{green} \text{ curve / Area } FL_{red}}{1 + \text{Area under } FL_{green} \text{ curve / Area } FL_{red}}$$

In order to assess overall viability, the mean value of all particle viabilities in a certain morphological class or in all morphological classes can be calculated. Figure 3 provides an overview on the information to be obtained from individual morphological classes. Viable spores can be quantified in pre-culture media prior to inoculation (as described by Ehgartner et al. 2016). Viable hyphae and small clumps are detectable though staining in all process phases which were previously described in Materials and Methods under bioreactor cultivations. Large clumps and pellets can be identified in particle-free fed-batch media without staining due to auto-fluorescence (see Figure S2). Overall viability at different can also be subdivided into the viability of different morphological classes and vice versa (see Figure S3). Further information obtained from large elements comprises the viability ratio within biomass particles, the assessment of the viable layer as well as the parameter 'compactness' (as described by Ehgartner et al. 2017).

Typical pulse shape profiles are specifically obtainable by the CytoSense flow cytometer. They depict various viability states for each morphological class as displayed in Figure 4 for all four morphological classes. When analysing large structures, saturation of several signals was observed (see Figure 4D). This can be expected, as the system needs to be capable of measuring fluorescence in a wide range of particle sizes. Consequently, a compromise between the detection of low fluorescence due to high sensitivity settings and potential loss of information in large particles needs to be found. High green fluorescence also led to a 'bleeding' effect into the red fluorescence channel. However, this phenomenon was not prominent in microwaved negative control samples. Here, an increase in red fluorescence is not related to green fluorescence and indicated viability-declined agglomerates, as PI cannot cross the membrane of healthy cells (Soderstrom 1977, Pekarsky et al. 2018).

Comparing flow cytometry viability assessment with the state-of-the-art plate reader method

To compare viability assessment from flow cytometry data with a previously established at-line viability measurement via plate reader, hereinafter called state-of-the-art method (Ehgartner et al. 2017), two fed-batch cultivations were performed and samples were measured employing both at-line methods. Viability assessment data from cultivations FB1 and FB2 are displayed in Figure 5. For standard process conditions both methods show similar results. In FB2, a deliberate process deviation through a down regulation of dissolved oxygen at process time 160h (see Figure 5) was introduced which was immediately followed by a drop in offgas CO_2 signals (see Figure 5). Only the flow cytometry method immediately registered the impact on viability assessment.

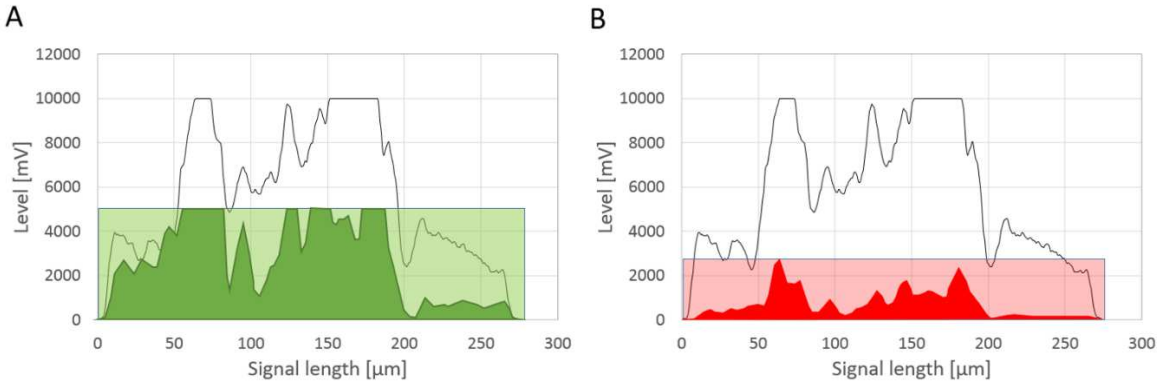

Figure 2. Pulse-shape signal profiles for assessment of viability according to Equation 3-4. Light green area indicates block shape of green fluorescence for Fill Factor calculation; dark green area indicates area under green fluorescence curve (A). Light red area indicates block shape of red fluorescence for Fill Factor calculation; dark red area indicates area under red fluorescence curve (B).

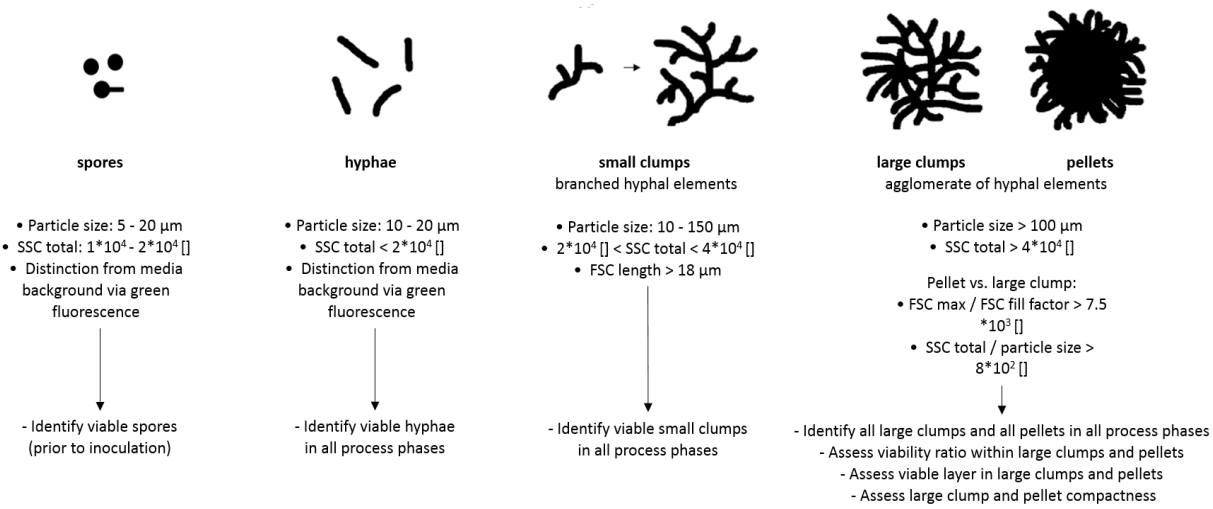

Figure 3. Information gain from individual morphological classes with definition of morphological classes according to flow cytometry.

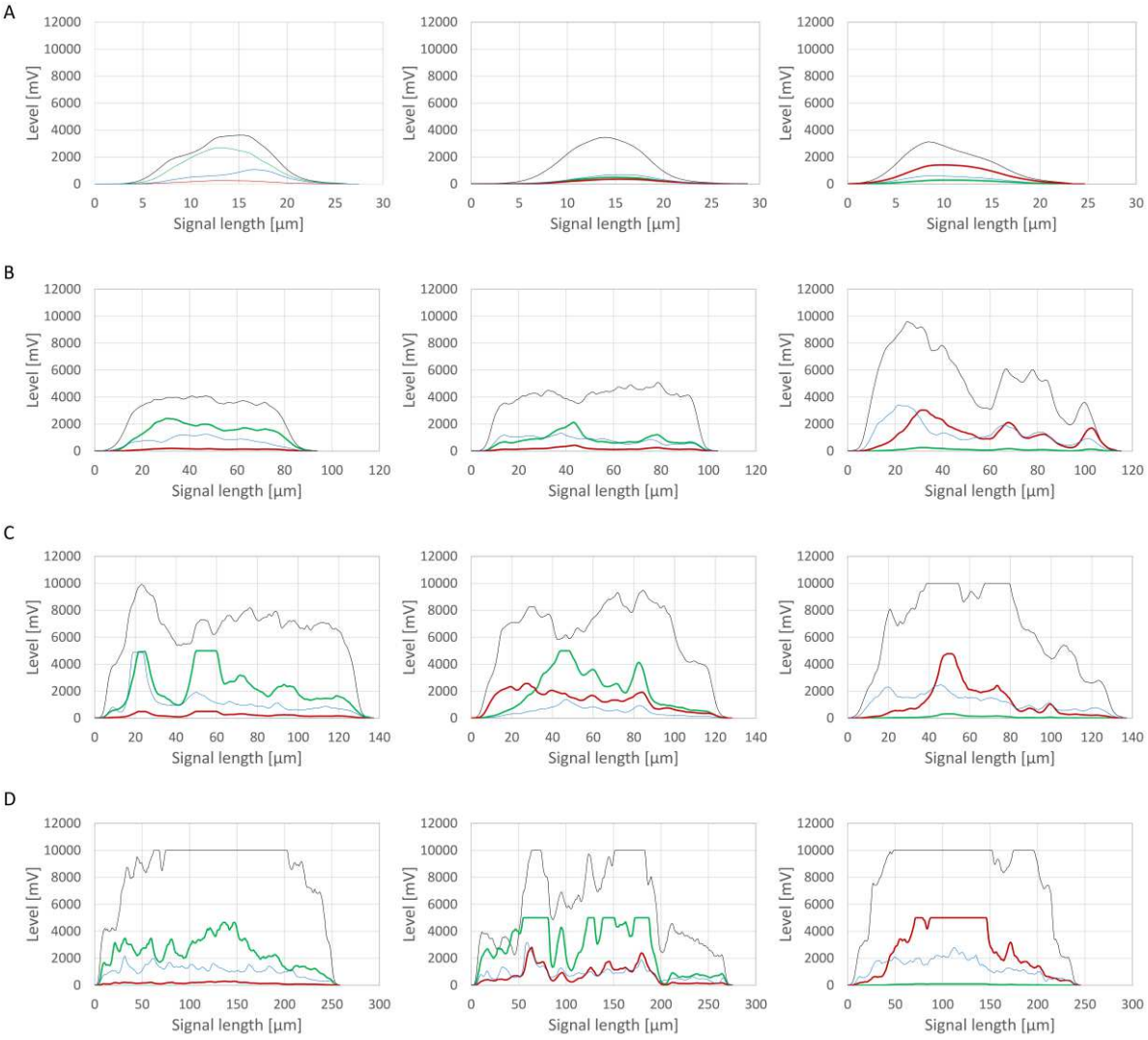

Figure 4. Pulse shape profiles of several morphological classes. Hyphae (A), small clumps (B), large clumps (C), pellets (D). High viability (left column), reduced viability (middle column), low viability in microwaved samples (right column). FSC signal (black line), SSC signal (blue line), FL-green signal (green line), FL-red signal (red line). Lines top to bottom: Increases in FSC and SSC signal indicate rise in particle size and compactness due to morphological class defined in Figure 3. Columns left to right: a decline in viability is seen with increasing FL-red signals and decreasing FL-green signals.

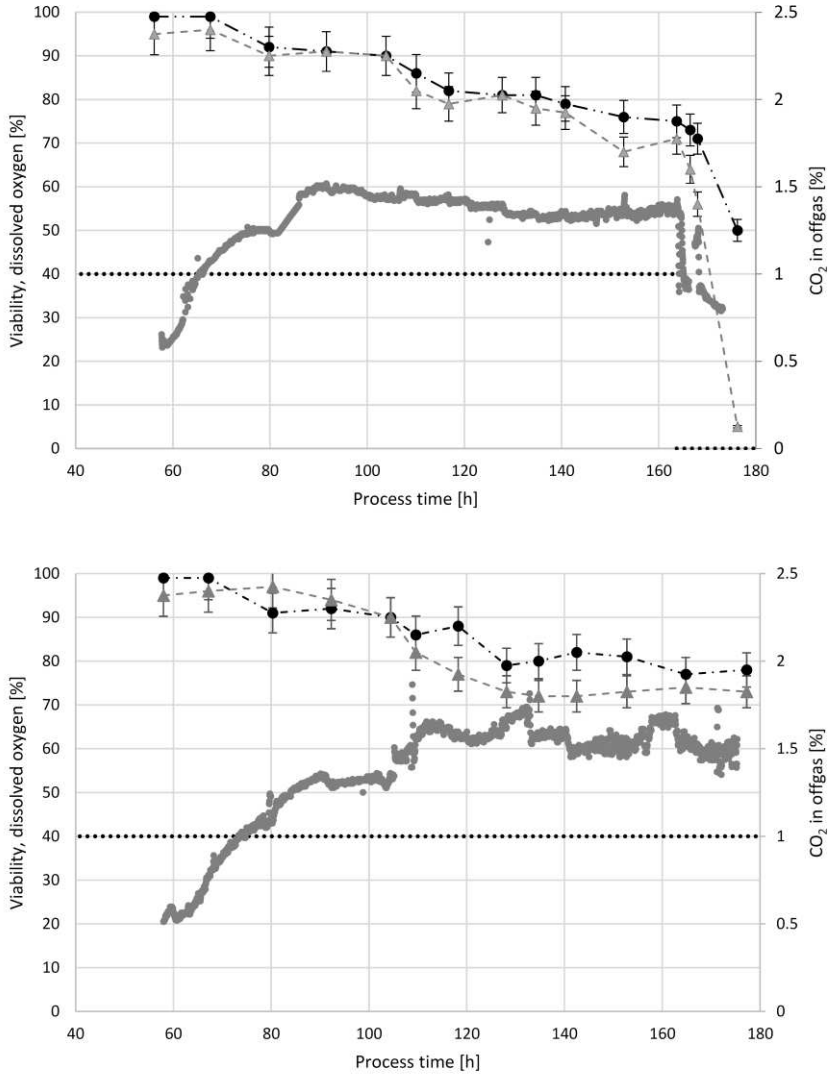

Figure 5. Comparison of flow cytometry viability assessment with state-of-the-art plate reader method. FB1 (top), FB2 (bottom). Plate reader (black). Flow cytometry (grey). Dissolved oxygen set point (dotted line), CO_2 in off-gas (grey points). Dissolved oxygen set point for FB2 was decreased to 0 % at process time 160 h to cause drop in viability.

After 3 hours, a 10 % decrease in viability is depicted, after 10 hours overall viability is estimated at only 5%. This is consistent with offgas and productivity data (data not shown). The viability drop is also observable in the plate-reader viability assessment, but less prominent and observable only in a delayed manner. This can be explained by the nature of the stain used in the plate-reader method: with PI, an immediate drop in metabolic activity as found through the use of FDA cannot be detected as PI can indicate viability loss only through DNA intercalation in cells with compromised membranes (Soderstrom 1977, Pekarsky et al. 2018).

Analysis of large element morphology and viable layer

A more detailed assessment of viability is possible in large elements due to signal length and associated information. On the one hand, the viable layer can be obtained from a comparison of green fluorescence derived from FDA staining with the particle's FSC signal. In combination with the known particle size, the viable layer (vl) can be estimated according to Equation 6. On the other hand, red fluorescence from PI staining indicates viability loss. The pellet's centre should harbour an increased amount of degenerated hyphal structures. Red fluorescence signals behave accordingly and display strong values or even saturation, usually in the core area. Consequently, vl

can be defined via the setting of a threshold value (see Equation 7) which indicates degradation when exceeded. This approach comes with the disadvantage that setting of the threshold is arbitrary and therefore needs to be aligned with data from other methods (eg. confocal laser microscopy see next section). In both approaches the factor 0.5 is added to calculate vl according to radius and not diameter when assuming the pellet to be a sphere/circle.

(6) $$\text{viable layer vl [µm]} = \frac{\text{Area under FLG [mV*µm]}}{\text{Area under FSC [mV*µm]}} * \text{average size [µm]} * 0.5$$

(7) $$\text{viable layer vl [µm]} = 0.5 * (1 - \text{Length of FLR} > \text{threshold [µm]})$$

Both approaches are outlined in Figure 6. Assessment according to Equation 6 is more reliable, as effects of particle size on fluorescence signals across all particles cannot be considered by the setting of a fixed threshold.

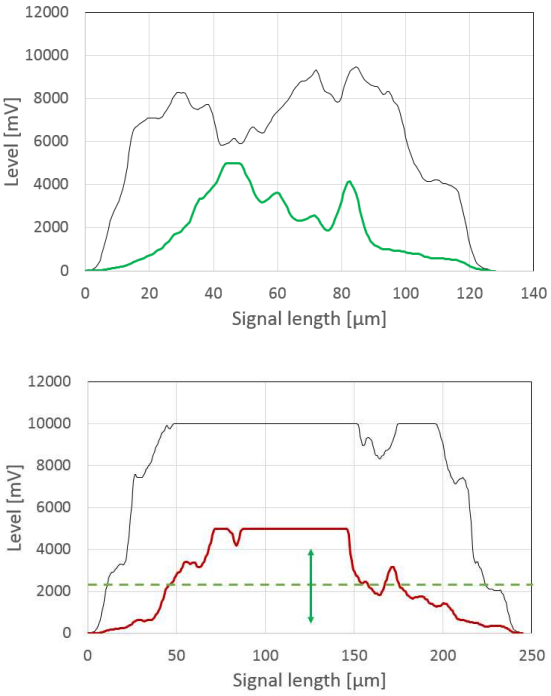

Figure 6. Approaches for determination of viable layer. Assessment via FL-G (top) or FL-R signal (bottom).

Comparing results from flow cytometry with confocal laser microscopy

Samples from FB1 were analysed to compare both methods for determination of viable layer. Exemplary pellet analysis using confocal layer microscopy employing FDA and PI staining is shown in Figure 7. A three-dimensional structure of viable regions can be estimated from this image, as red fluorescence harboured in the centre is partly overlaid by viable hyphal entanglements. Assuming a simplified two-dimensional cross section, a green fluorescent viable layer located around the outer hairy region is clearly distinguishable from the core, which exhibits degradation.

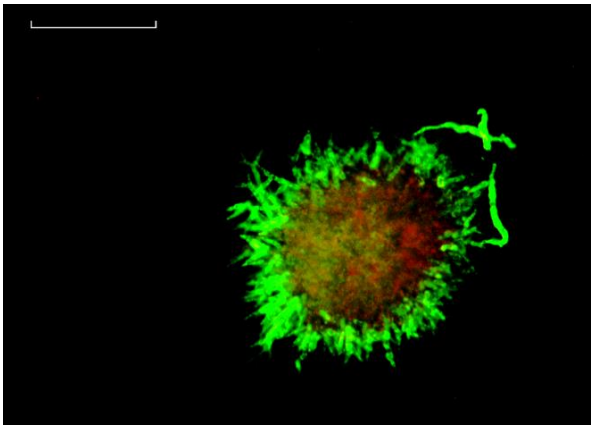

Figure 7. Confocal microscopy of pellet with enhanced contrast. Sample was taken from FB1 at a process time of 80h after transfer. Green fluorescence from FDA staining represents viable pellet layer, red fluorescence from PI staining in pellet core. White line = 50 µm.

After confocal analysis of at least six pellets per sample, the average viable pellet layer in five different samples was determined and compared to flow cytometry results as depicted in Figure 8. Both methods displayed similar values, apart from some deviations in the earlier process phases. In all samples viable layer was determined at roughly one third whole pellet radius, which is in agreement with literature (Posch et al. 2012, Baumgartl et al. 1984, Nielsen et al. 1995, Justen et al. 1998). The mean pellet diameter in FB1 was 251.5 ± 25 µm.

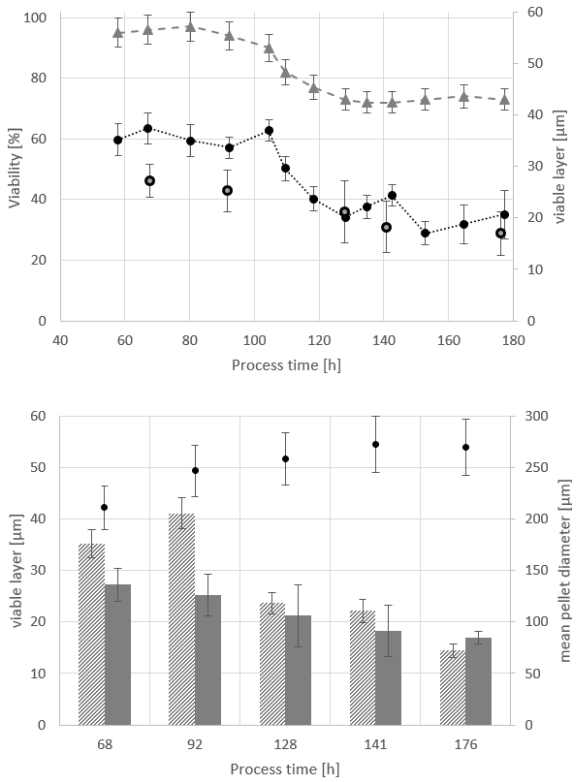

Figure 8. Comparison of confocal microscopy and flow cytometry, both methods employed to determine viable layer in large elements taken from FB1 samples. Top: viability from flow cytometry (grey triangles), viable layer from flow cytometry (black circles) and viable layer from confocal microscopy (grey squares). Bottom: viable layer determined via flow cytometry (patterned bars), viable layer determined via confocal microscopy (grey bars), average pellet diameter (black dots). Standard deviation in confocal microscopy calculated from at least six pellets analysed per sample.

Discussion

Advantages, disadvantages and comparability to other methods

Within this contribution, we present a novel combination of morphological analysis and viability assessment based on flow cytometry. This signifies a faster alternative to image analysis via microscopy and more statistical reliability due to the large number of particles being measured in sort time spans (as previously established by Ehgartner et al. 2017). In addition, enhanced insight into viability is generated simultaneously through fluorescent staining: Overall viability, viability of morphological classes and the viable layer of large elements can be determined. This viability data is enhanced by morphological parameters like pellet compactness.

To verify this technique, results were compared to data from respective state-of-the-art methods, namely at-line viability measurement via plate-reader for overall viability and confocal laser microscopy for determination of viable pellet layer. To generate sufficient amounts of biomass with diverse morphology and viability states, bioreactor cultivations in fed-batch mode were conducted and extensively sampled. Each sample was subjected to flow cytometry and plate-reader viability measurement. For determination of overall viability, the flow cytometry method was superior as the effects of a sudden drop of dissolved oxygen were registered more reliably. A selection of samples from FB1 was also analysed using confocal laser microscopy to determine viable layers across pellets. Results of the flow cytometry method were in accordance with reference measurements. Furthermore, the method was applicable in complex media with high particle background.

The main distinguishing feature of the flow cytometry method is that viability in different morphological classes can be determined, even down to individual particles. Other methods generally only provide an overview on viability. This is especially useful in later process stages: small hyphal elements tend to be viable, while degradation in larger agglomerates and pellets is observable over time. Such large elements can be analysed in detail, thereby viable and non-viable biomass sections are identified and quantified over each particle. However, a diverse morphology is a challenging thing and needs to be addressed: To guarantee comparable information content across all process phases, a compromise in fluorescence detector sensitivity settings must be found for individual strain/media combinations: in early process phases detectors must be sensitive enough to detect viable biomass, in later stages signal saturation needs to be avoided when possible. Furthermore, it should be noted that fluorescence spectral overlap might result in misleading signals. This is especially true for large elements harbouring considerable green fluorescence from FDA, which can also be registered by the red fluorescence detector as a misleading artefact (Bagwell and Adams 1993). The ratio between red and green fluorescence needs to be checked regularly. Deviations in this ratio occur due to saturation effects from green fluorescence signals, due to spectral overlap or might indicate viability decline.

Disadvantages also include size-exclusion effects: due to the large size and compact nature of fungal pellets, they might be excluded at the opening of the sampling tube. As a result, small elements are generally over-represented while more information can be obtained from the evaluation of large elements. If the measurement goal is characterisation of large elements, a simple solution to the size-exclusion issue would be to increase measurement times or set trigger factors in the software according to particle size. However, a representative overview on morphology respecting all size classes of morphology is more challenging. Depending on the fungal species and/or strain to be analysed certain adjustments of the sampling tube could be considered, like a wider tubing or a cone at the end of the sampling tube.

Table 1 compares measurement errors of all described methods for several parameters.

Table 1. Measurement errors of common parameters determined by previously described methods

Parameter	Plate reader staining method		Flow cytometry		Confocal laser microscopy	
	%	absolute	%	absolute	%	absolute
Viability overall	7	-	5	-		
Viability - Hyphae	2	-	4	-		
- Small clumps	2	-	3	-		
- Large clumps	-	-	6	-		
- Pellets	-	-	6	-		
Viable layer large elements			13	6 µm	-	-
Viable layer pellets			7	2 µm	11	3 µm

Applicability of the method

We envision this method to be a further milestone in the at-line characterisation of complex fungal biomass (with a clear potential for online application through automated sampling systems) in process development and routine manufacturing processes. Based upon previous method development (as published by Ehgartner et al. 2017) we enhanced morphological classification to analyse viability across all morphological forms with a special emphasis on the pellet's viable layer. As a result, we are now able to combine morphological analysis with viability assessment in an at-line environment with potential online applicability through the use of automated sampling and sample processing. For this purpose, sampling, dilution and addition of fluorescent dyes needs to be performed in a modular process analytical system (PAT) with a flow cytometer connected.

We are confident that this method can shed a light on the complex and extensively researched relationship between fungal morphology, viability and productivity (Veiter et al. 2018, Wucherpfennig et al. 2011, Krull et al. 2013).

While this method was developed for *P. chrysogenum,* we see the possibility to broaden applicability towards other filamentous fungi and by extend further agglomerate forming organisms such as yeast (Pekarsky et al. 2018).

Acknowledgements

We thank the Austrian Federal Ministry of Science, Research and Economy in course of the Christian Doppler Laboratory for Mechanistic and Physiological Methods for Improved Bioprocesses for financial support. Strains for the experiments were gratefully provided by Sandoz GmbH (Kundl, Austria).

Compliance with Ethical Standards

Funding: This study was funded by Austrian Federal Ministry of Science, Research and Economy in course of the Christian Doppler Laboratory for Mechanistic and Physiological Methods for Improved Bioprocesses (grand number 171).

Conflict of Interest: The authors declare that they have no conflict of interest.
Ethical approval: This article does not contain any studies with human participants or animals performed by any of the authors.

References

Attfield PV, Kletsas S, Veal DA, van Rooijen R., Bell PJL (2000) Use of flow cytometry to monitor cell damage and predict fermentation activity of dried yeasts. J Appl Microbiol Biochem 89(2): 207-214

Bagwell CB, Adams EG (1993) Fluorescence Spectral Overlap Compensation for Any Number of Flow-Cytometry Parameters. Ann N Y Acad Sci 677: 167-184

Baumgartl HR, Wittler D, Lubbers W, Schugerl K (1984) Oxygen Profiles and Structure of *Penicillium Chrysogenum* Pellets. Adv Exp Med Biol 169: 793-799

de Bekker C, van Veluw GJ, Vinck A, Wiebenga LA, Wosten HA (2011) Heterogeneity of *Aspergillus niger* microcolonies in liquid shaken cultures. Appl Environ Microbiol 77(4): 1263-1267

Delgado-Ramos L, Marcos AT, Ramos-Guelfo MS, Sanchez-Barrionuevo L, Smet F, Chavez S, Canovas D (2014) Flow cytometry of microencapsulated colonies for genetics analysis of filamentous fungi. G3 (Bethesda) 4(11): 2271-2278

Dubelaar GB, Gerritzen PL, Beeker AE, Jonker RR, Tangen K (1999) Design and first results of CytoBuoy: a wireless flow cytometer for in situ analysis of marine and fresh waters. Cytometry 37(4): 247-254

Dynesen J, Nielsen J 2003 Surface hydrophobicity of *Aspergillus nidulans* conidiospores and its role in pellet formation. Biotechnol Prog 19(3): 1049-1052

Ehgartner D, Hartmann T, Heinzl S, Frank M, Veiter L, Kager J, Herwig C, Fricke J (2017). 'Controlling the specific growth rate via biomass trend regulation in filamentous fungi bioprocesses.' Chem Eng Sci 172: 32-41.

Ehgartner D, Herwig C, Fricke J (2017) Morphological analysis of the filamentous fungus *Penicillium chrysogenum* using flow cytometry-the fast alternative to microscopic image analysis. Appl Microbiol Biotechnol 101(20): 7675-7688

Ehgartner D, Herwig C, Neutsch L (2016) At-line determination of spore inoculum quality in *Penicillium chrysogenum* bioprocesses. Appl Microbiol Biotechnol 100(12): 5363-5373

Justen P, Paul GC, Nienow AW, Thomas CR (1998) Dependence *of Penicillium chrysogenum* growth, morphology, vacuolation, and productivity in fed-batch fermentations on impeller type and agitation intensity. Biotechnol Bioeng 59(6): 762-775

Krull R, Wucherpfennig T, Esfandabadi ME, Walisko R, Melzer G, Hempel DC, Kampen I, Kwade A, Wittmann C (2013) Characterization and control of fungal morphology for improved production performance in biotechnology. J Biotechnol 163(2): 112-123

Langemann T, Mayr UB, Meitz A, Lubitz W, Herwig C (2016) Multi-parameter flow cytometry as a process analytical technology (PAT) approach for the assessment of bacterial ghost production. Appl Microbiol Biotechnol 100(1): 409-418

Lein J (1986) The Panlabs penicillin strain improvement program. Vanek Z, Hostalek Z (eds) Overproduction of microbial metabolites. Butterworths, Boston, pp 105–139

Nielsen J, Johansen CL, Jacobsen M, Krabben P, Villadsen J (1995) Pellet formation and fragmentation in submerged cultures of *Penicillium chrysogenum* and its relation to penicillin production. Biotechnol Prog 11(1): 93-98

Pekarsky A, Veiter L, Rajamanickam V, Herwig C, Grunwald-Gruber C, Altmann F, Spadiut O (2018) Production of a recombinant peroxidase in different glyco-engineered *Pichia pastoris* strains: a morphological and physiological comparison. Microb Cell Fact 17(1): 183.

Posch AE, Spadiut O, Herwig C (2012) A novel method for fast and statistically verified morphological characterization of filamentous fungi. Fungal Genet Biol. 49(7):499-510 doi:10.1016/j.fgb.2012.05.003

Posch AE, Herwig C (2014) Physiological description of multivariate interdependencies between process parameters, morphology and physiology during fed-batch penicillin production. Biotechnol Prog 30(3): 689-699.

Ronnest NP, Stocks SM, Eliasson Lantz A, Gernaey KW (2011) Introducing process analytical technology in filamentous cultivation process development: comparison of advanced online sensors for biomass measurement. J Ind Microbiol Biotechnol 38(10): 1679-1690

Soderstrom BE (1977) Vital Staining of Fungi in Pure Cultures and in Soil with Fluorescein Diacetate. Soil Biol Biochem. 9(1): 59-63

Veiter L, Rajamanickam V, Herwig C (2018) The filamentous fungal pellet-relationship between morphology and productivity. Appl Microbiol Biotechnol 102(7): 2997-3006

Supplementary Figures

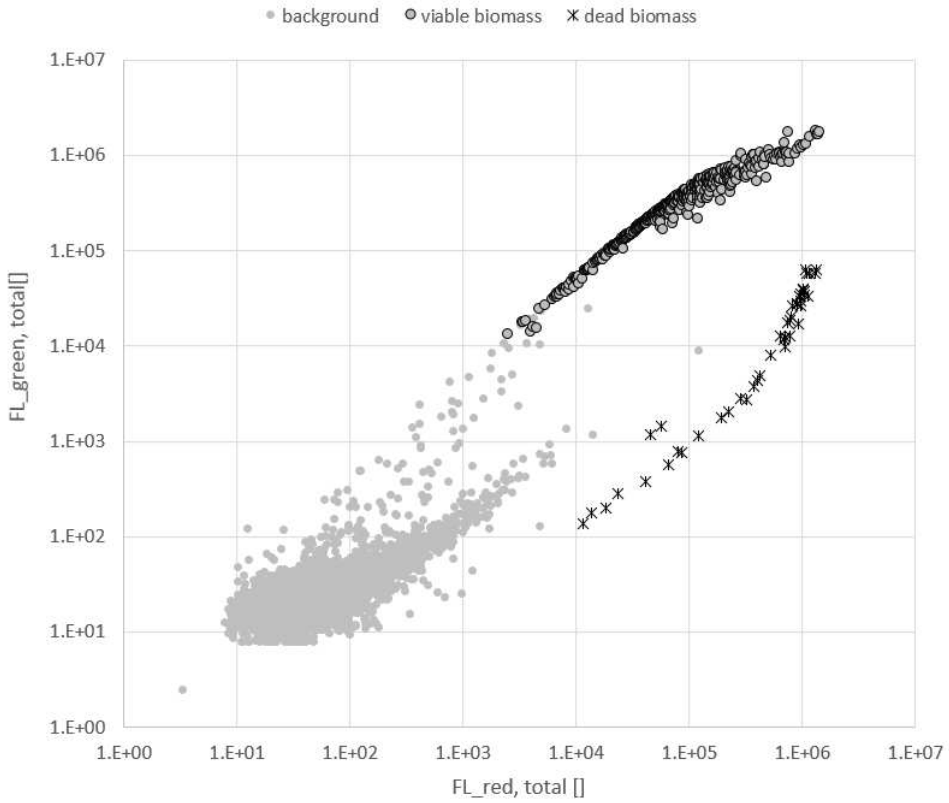

Figure S1. Sample from FB2 fed-batch phase 80h after transfer with overall viability of 90 % measured via flow cytometry and confirmed by plate reader staining measurements**.** Differentiation between complex media background, viable and dead biomass through gate setting employing fluorescent staining with FDA/PI. Viable biomass (framed circles), dead biomass (framed triangles) and background (grey circles).

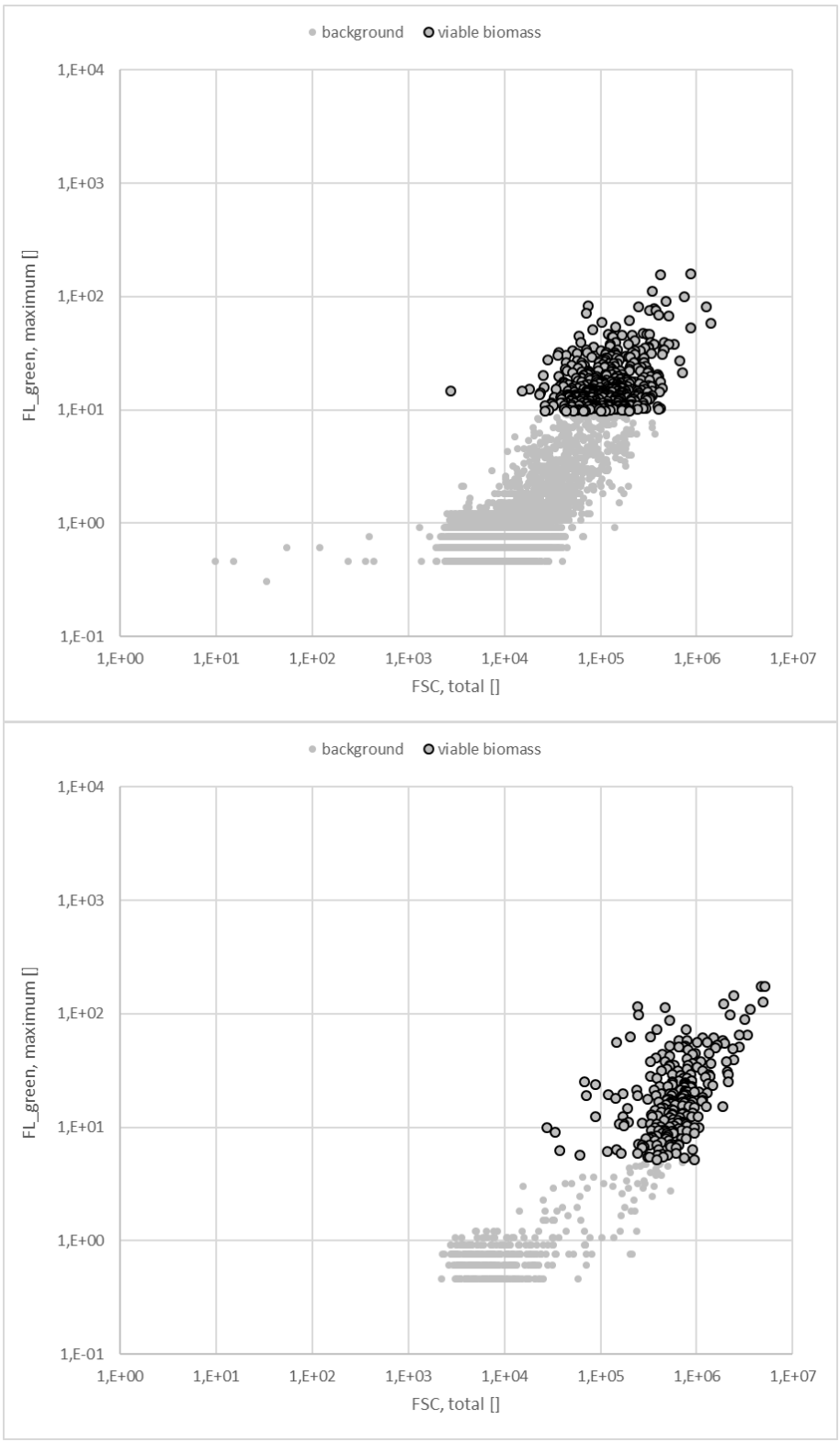

Figure S2. Comparison of biomass differentiation in different media without the use of fluorescent staining. High media particle content (top), low media particle content (bottom).

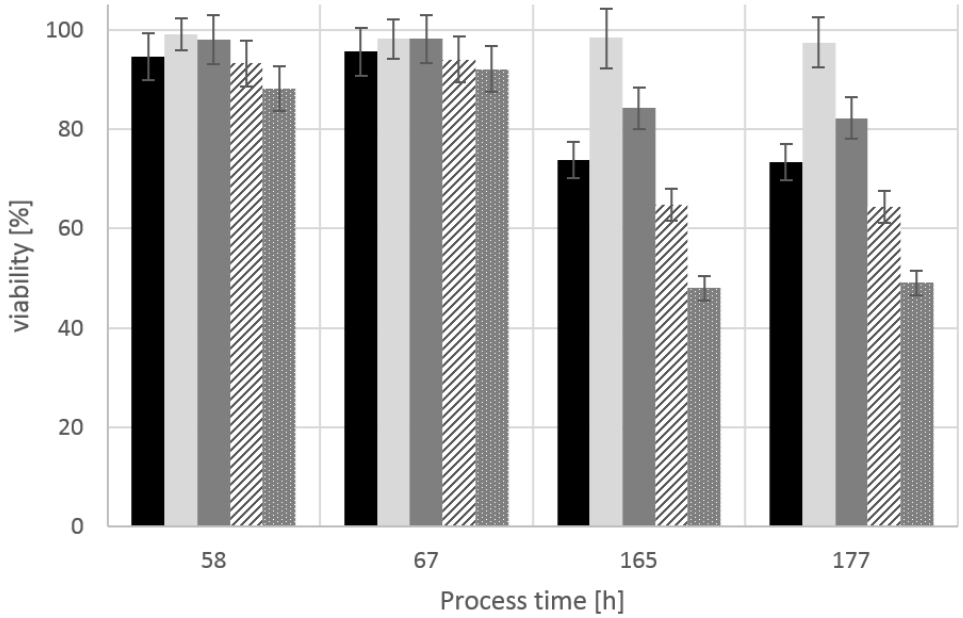

Figure S3. Viability determination via flow cytometry. Overall viability (black bars) at different process times subdivided into different morphological classes: hyphae (light grey bars), small clumps (dark grey bars), large clumps (patterned bars), pellets (dotted bars). Data from FB1 displaying beginning and end of fed-batch cultivation phase.

Study of metabolism and identification of productive regions in filamentous fungi via spatially-resolved Time-of-Flight Secondary Ion Mass Spectrometry

Lukas Veiter[1,2], Markus Kubicek[3], Herbert Hutter[3], Ernst Pittenauer[3], Christoph Herwig[1,2] and Christoph Slouka[1,2]

[1] Technische Universität Wien, Institute of Chemical, Environmental and Bioscience Engineering, Research Area Biochemical Engineering, Gumpendorfer Strasse 1a, 1060 Vienna, Austria

[2] Christian Doppler Laboratory for Mechanistic and Physiological Methods for Improved Bioprocesses, TU Wien, Gumpendorfer Straße 1a, 1060 Vienna, Austria

[3] Institute of Chemical Technologies and Analytics, Technische Universität Wien, Getreidemarkt 9/164EC, 1060 Vienna, Austria

[*] Correspondence: Christoph Slouka, TU Wien, Institute of Chemical, Environmental and Bioscience Engineering, Research Area Biochemical Engineering, Gumpendorfer Strasse 1a

Published in 'Analytical and Bioanalytical Chemistry'

Veiter L., Kubicek M., Hutter H., Pittenauer E., Herwig C. and C. Slouka (2019) 'Study of metabolism and identification of productive regions in filamentous fungi via spatially-resolved Time-of-Flight Secondary Ion Mass Spectrometry.' Anal Bioanal Chem.

Abstract

Filamentous fungi are well-established production hosts that feature a strong interconnection between morphology, physiology and productivity. For penicillin production in *Penicillium chrysogenum*, industrial processes frequently favour pellet morphology comprising compact hyphal agglomerates. Inherently these tightly packed entanglements lead to inactive, degrading sections within the pellet's core due to limitations. Optimal process design requires detailed knowledge on the nature of limitations and localisation of productive zones in the biomass – generally obtainable through modelling and complex analytical methods like oxygen microelectrodes and histological investigations. Methods, which combine physiological and morphological insight, are crucial yet scarce for filamentous fungi. In this study, we employed Time-of-Flight Secondary Ion Mass Spectroscopy in combination with oxygen and glucose tracer substrates, requiring little effort in sample preparation and measurement.

Our method is capable of i) analysing oxygen and substrate uptake in various morphological structures via the use of heavy ^{18}O tracer. In parallel, we can ii) assess productive biomass regions through identification of penicillin mass fragments to simultaneously study oxygen diffusion, substrate incorporation and productive biomass sections.

Keywords

Penicillium chrysogenum, pellet, oxygen diffusion, substrate incorporation, productivity, Time-of-Flight Secondary Ion Mass Spectrometry, ToF-SIMS

Introduction

Filamentous fungi are important industrial production organisms for a wide range of products ranging from bulk chemicals to therapeutic proteins. Morphology, physiology and productivity are tightly interlinked (Veiter et al. 2018). In submerged culture, morphology is generally characterized as either pelleted, consisting of compact hyphal agglomerates, or filamentous, displaying homogeneously dispersed hyphae. In *Penicillium chrysogenum* hyphal elements agglomerate to form clumps and eventually pellets (Nielsen and Krabben 1995). These various morphological forms lead to varying biomass characteristics with advantages and disadvantages. Compact pellet morphology facilitates process control regarding rheology, aeration and agitation. However, limitations in the pellet's core due to diffusion issues with oxygen and substrate leads to a decline in biomass viability (Walisko et al. 2015, Nielsen and Krabben 1995, Zhang and Zhang 2016). For optimal process design, a compromise between compact and loose morphology is required. To achieve this, comprehensive insight into morphology dependent incorporation of substrate and oxygen as well as the identification of productive regions is necessary. Thereby biomass degradation and/or over-feeding can be avoided. There are two ways of gaining insight, as discussed in the following paragraph: modelling approaches and advanced analytical methods.

Regarding the interlink between morphology and productivity, several studies have identified active regions for penicillin production (Nielsen and Krabben 1995). Growing regions in long, branching filamentous structure known as hyphae are continuously formed through branching from non-growing regions. In time, these apical regions become subapical regions with related vacuolisation. Penicillin production is happening in the non-growing cytoplasm, while growing regions and degenerated zones are non-productive (Paul and Thomas 1998, Zangirolami et al. 1997). When expanding this hypothesis to pellets, the outer layer is deemed the productive zone containing high quantities of cytoplasm (Wittler et al. 1986, Baumgartl et al. 1984). Consequently, productive regions in hyphal agglomerates of *P. chrysogenum* cannot be expected in the outermost, loose entanglements. Analytical methods to verify these hypotheses employ oxygen microelectrode measurements.

Viable zones within fungal pellets can be characterised via confocal laser microscopy (CLSM) in combination with staining (Hille et al. 2009, Hille et al. 2005). Secondary ion mass spectrometry (SIMS) is a powerful technique to obtain information on spatially resolved material composition. As a specimen surface is subjected to a primary ion beam, secondary ions (SI) reveal elemental and molecular information with high lateral or mass resolution (Walker 2008, Fearn 2015). Application on biological samples is often hindered by a limited desorption of ions with m/z > 500 and corresponding issues with the measurement of large molecules. Matrix assisted laser desorption/ionisation (MALDI) has been regarded as more suitable for with large intact biomolecules with very large molecular weights up to 10 000 Da. However, the development of cluster ion sources in the past decade has greatly improved secondary ion yields of high masses (Walker 2008, Kayser et al. 2013). Consequently, applications for biological samples have grown in importance (Fearn 2015). Of all SIMS methods, Nano-SIMS offers the highest lateral resolution (< 50 nm) but is limited to elemental ions and small fragments (Nunez et al. 2017). Featuring a comparatively good ion detection between 1500 – 2500 Da at a lateral resolution suitable for subcellular structures (~300 nm), Time-of-Flight Secondary Ion Mass Spectroscopy (ToF-SIMS) is a valid alternative (Fearn 2015). In the field of filamentous fungi, ToF-SIMS has been used to detect and quantify nutrients contained in individual hyphae (Cliff et al. 2002, Couturier et al. 2015). An application to study oxygen diffusion and substrate incorporation in specific morphological regions of filamentous biomass is currently unknown to us. For this purpose, the 'collimated burst alignment' (CBA) operation mode (Kubicek et al. 2014) is highly suitable as it is optimized for oxygen isotope analysis and capable of sub 100 nm lateral resolution.

In this study, we used ToF-SIMS in CBA operation mode combined with oxygen and glucose tracer substrates to develop a novel analytical method for spatially resolved analysis of substrate and oxygen incorporation into biomass. Additional capabilities include the measurement of spatial-resolved precursor incorporation of phenoxyacetic acid for penicillin production in surface biomass regions and allows identification of productive hyphal areas. To

the best of our knowledge, the here-presented method is unprecedented in terms of application and broad information gain.

Materials and methods

Strain, medium and cultivation

Spore suspensions of the P-14 *P. chrysogenum* candidate strain for penicillin production descending from the P-2 *P. chrysogenum* candidate strain (American Type CulturCollection with the access number ATCC 48271) were provided by Sandoz GmbH (Kundl, Austria) and used for all experiments.

All shake-flask cultivations were performed in an Infors HT Multitron shaker (Infors, Bottmingen, Switzerland) at 25 °C at 300 rpm. Fifty milliliters of an autoclaved complex pre-culture culture medium (sucrose 18 g/l, glucose 3 g/l, corn steep liquor 26 g/l and 3.8 g/l $CaCO_3$) in a 500-ml shake flask were inoculated using 1×10^9 spores/ml. By convention after 53.5 h in pre-culture medium, 10 vol.% of pre-culture broth were transferred to 50 ml of a main-culture medium similar as described by Posch et al. 2014.

HPLC analytics

High performance liquid chromatography (HPLC) using a Thermo Scientific UltiMate 3000 system (Thermo Fisher Scientific, Massachusetts, United States) with a Zorbax Eclipse AAA C18 column (Agilent Technologies, Santa Clara, USA) was used to quantify penicillin V and phenoxyacetic acid concentration with eluents as described elsewhere. (Ehgartner et al. 2016) A flow rate of 1.0 ml/min was applied and the temperature of the column oven was 30 °C. The wavelength of the UV/VIS detector for determining penicillin and phenoxyacetic acid peaks via absorption was set to 210 nm.

Oxygen Tracer Diffusion experiments

20 – 30 ml broth from pre-culture shake-flask cultivations was transferred to a sterile 100-ml vessel equipped with a dissolved oxygen pO_2 probe (EasySense O2 21, Mettler-Toledo, Switzerland) as well as ports for sterile aeration and sampling. ^{18}O-tracer pulses (Campro Scientific, Germany) were conducted for 5 – 10 s until the pO_2 signal reached oxygen saturation at a value of > 99.9 %. The isotope enrichment of the used oxygen was 97 atom % ^{18}O, the O_2 purity 99.9991%. Over the course of the experiment, the pO_2 signal was monitored and additional pulses were administered if the pO_2 value decreased under 10 %. Samples were taken after various timespans up to 24 h and aliquots of subsequent ToF-SIMS measurement were immediately quenched using liquid nitrogen. As CO_2 is produced in fungal metabolism and our aperture was essentially closed, we checked pH values of each sample (see Supplementary Figure 1). In general, pH values in main-culture medium were ranging from pH 5.8 up to pH 6.5, which would not drastically influence fungal activity as fed-batch bioreactor cultivations of the same strain care performed at similar pH values.

Substrate Incorporation Experiments

50 ml broth from main-culture shake-flask cultivations was transferred to a custom-made sterile 100-ml vessel equipped with a dissolved oxygen pO_2 probe (EasySense, Mettler-Toledo) as well as ports for sterile aeration and sampling. D-[1-18O] glucose (Omicron Biochemicals) was added in an amount to match 10 % of total glucose concentration in the main-culture medium. Dissolved oxygen concentration was controlled at a level higher than 40% via adjustment of aeration rate. Total cultivation time was 40 h, samples were taken at 0 h, 20 h and 40 h. Aliquots of subsequent ToF-SIMS measurement were immediately quenched using liquid nitrogen.

Sample preparation and ToF-SIMS measurements

Samples were thawed and 1 ml was centrifuged for 5 min at 50 g to generate a loose biomass pellet. Supernatant was removed and pellet was re-suspended in 0.1 % w/v saline. This step was repeated; however, 0.01 % w/v was used for repeated re-suspension. 100 µl of re-suspended broth was pipetted onto a cut silicone weaver specimen holder. The sample was subsequently sputtered on a sputter coater (Agar Scientific, UK) with 20 mA at 0.1 mbar oxygen partial pressure, which resulted in 20 -50 nm of Au, in order to inactivate exchange of tracer oxygen with ambient air and to inactivate the biomass metabolism. Subsequent analysis of the oxygen isotope distribution was performed on a TOF.SIMS 5 instrument (IonTof, Münster, Germany) using 25 kV Bi^+ primary ions (~0.03 pA), 1 kV Cs^+ for sputtering (~75 nA), and a low-energy electron gun (20 V) for charge compensation. Negative secondary ions in the mass range 1-146 u were measured. Areas of 100 µm × 100 µm or smaller were analysed. For sequential sputtering a 2 kV Cs+ sputter gun with 300 × 300 μm^2 sputter area, was

used. All measurements were performed in static SIMS conditions. Charge compensation was achieved by 20 eV electrons. The $^{18}O^-$ fractions were determined by operating the instrument in the 'Collimated Burst Alignment' (CBA) mode. Additional details on the used CBA measurement mode for imaging are given in references (Kubicek et al. 2014, Holzlechner et al. 2013).

MS measurements

Low-resolution mass spectra and low-energy (LE) CID-MS2 spectra of penicillin standard and phenoxyacetic acid in solid form were acquired on an Esquire 3000plus 3D-quadrupole ion trap mass spectrometer (Bruker Daltonics, Bremen, Germany) in negative-ion mode by means of electrospray ionization (ESI). The mass calibration was done with a commercial mixture of perfluorinated trialkyl-triazines (ES Tuning Mix, Agilent Technologies, Santa Clara, CA, USA). All analytes were dissolved in methanol Hypergrade LC-MS (Merck, Darmstadt, Germany): UHQ-water = 1 to 1 to form a concentration of roughly 1 mg/mL. Direct infusion experiments were carried out using a Cole Parmer model 74900 syringe pump (Cole Parmer Instruments, Vernon Hills, IL, USA) at a flow rate of 5 l/min. Full scan and LE-CID MS2 scans were measured in the range m/z 50-500 with the target mass set to the m/z value of the respective precursor ion. Further experimental conditions include: drying gas temperature: 200 °C; capillary voltage: 4 kV; skimmer voltage: 40 V; octapole and lens voltages: according to the target mass set. Mass spectra were averaged during data acquisition time of 1 min and one analytical scan consisted of three successive microscans resulting in 50 and 100 analytical scans, respectively, for final full scan mass spectra or MS2-spectra.

Results

We tested two different tracer materials based on oxygen-18, both detectable in high sensitivity by ToF-SIMS within biomass samples. Subsequently we evaluated their applicability for detection of substrate limitations in *P. chrysogenum.*

Oxygen Tracer Diffusion in *P. chrysogenum* using gaseous $^{18}O_2$

We tested feasibility of oxygen tracer incorporation in hyphal structures to detect ^{18}O within the fungal biomass in order to test for oxygen limitation in different fungal regions. We tested different time intervals starting with 15, 30 minutes to a maximum of 24 hours. Only at increased time intervals, ^{18}O could be detected in amounts that exceed natural abundance. Results for 24-hours are given in Figure 1. With 20 °C ambient temperature we exposed the cells to 0.103 mol of ^{18}O during the 24 hours of the experiment. The $^{18}O/(^{16}O+^{18}O)$ fraction in biomass samples is very low at average values of 0.0025 as seen in Figure 1.

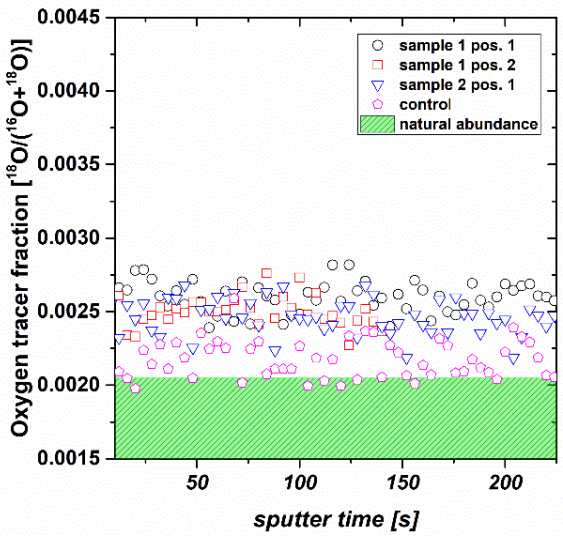

Figure 1. ^{18}O-incorporation normalized to ^{16}O after 24 h of incorporation time. Values are slightly higher when compared to the control sample and natural abundance, which indicates almost no incorporation of oxygen through respiration into biomass. Two samples (sample 1 and 2) with ^{18}O incorporation were measured, in sample 1 two distinct positions were analysed. Furthermore, data from a control sample without ^{18}O as well as natural abundance data is displayed.

Oxygen incorporation into biomass can also be estimated in more quantitative terms according to Equation 1:

(1)

$$\text{mmol } {}^{18}O = \text{Ratio}_{\frac{\text{oxygen}}{\text{biomass}}} * \text{g biomass}_{\text{total}} * \frac{10^3}{18\,\frac{\text{g}}{\text{mol}}} * \text{fraction}\,\frac{[{}^{18}O]}{[{}^{18}O+{}^{16}O]}$$

$$\text{Ratio}_{\frac{\text{oxygen}}{\text{biomass}}} \ldots 0.31 \text{ for the utilized strain}$$

The previously established average biomass composition of the utilized strain is: C=47%, N= 7.5%, H=6.5%, O=31%. Using offline measurements of dry cell weight after 24 hours, we can conclude that 0.03 mmol of ^{18}O can be estimated within 1 g of biomass, leaving the vast majority being converted to $C^{18}O_2$. As fixation of the biomass requires evacuation steps, residual $C^{18}O_2$ in the cell is lost as vapour in the preparation and cannot be analysed subsequently. Hence, the

analysis is restricted to oxygen incorporated into biomass. These tracer profiles normalized to ^{16}O in the biomass for two samples in three different regions show profiles (see Figure 1) with only a slight increase of ^{18}O integrated over the entire biomass, compared to the natural abundance. The $^{18}O/(^{16}O+^{18}O)$ fraction depicted in Figure 1 increases by $5*10^{-4} \pm 1*10^{-4}$.

As most of the incorporated tracer oxygen is converted to $C^{18}O_2$ gas exchange high spatial resolution during the monitoring of viable regions in the fungal structure is not possible using this method. However, it may be used for metabolic flux analysis in combination with mass spectroscopy in the gas phase to identify breathing capacity in different process stages during antibiotic production.

Oxygen incorporation into *P. chrysogenum* biomass using ^{18}O-marked glucose

As incorporation of gaseous tracer oxygen only resulted in very low amounts of incorporation, we used ^{18}O-marked glucose to test whether changes in the incorporation could be detected on a time dependent basis and in spatial resolution as displayed in Figure 2. Samples were taken at three characteristic time points t =0, t =20 and t = 40 hours. Spatial resolved analysis of the sample after t=20 hours is presented in Figure 2. The C_2H_2-signal is used to detect biomass covered areas on the sample holder, Figure 2a. Figure 2b shows the signal of total ^{16}O signal in the biomass and Figure 2c only the incorporated ^{18}O signal originating from the traced glucose in the sample.

Despite only 10% of total glucose being tracer-marked and only one marked oxygen out of six oxygen, a clear spatial-resolved image of incorporation could be already detected after 20 hours of cultivation (5 generation times in non-limited batch phase). The time-dependence of incorporation is given in Figure 3 for the three different time stages. The sample at t=0 hours shows an unexpected increase compared to the natural abundance at a first glance. As the media is already containing tracer-marked glucose low amounts of media attached to the surface may cause the deviations in the sample.

However, a clear time dependence can be dedicated from the depth profiles in Figure 3 with an increase of about a factor of 1.5 in tracer oxygen content for every 20 hours based on Equation 2.

(2)

$$ratio = \frac{[^{18}O]_{t=x} - n.a}{[^{18}O]_{t=x+20} - n.a}$$

$n.a.$ … natural abundance

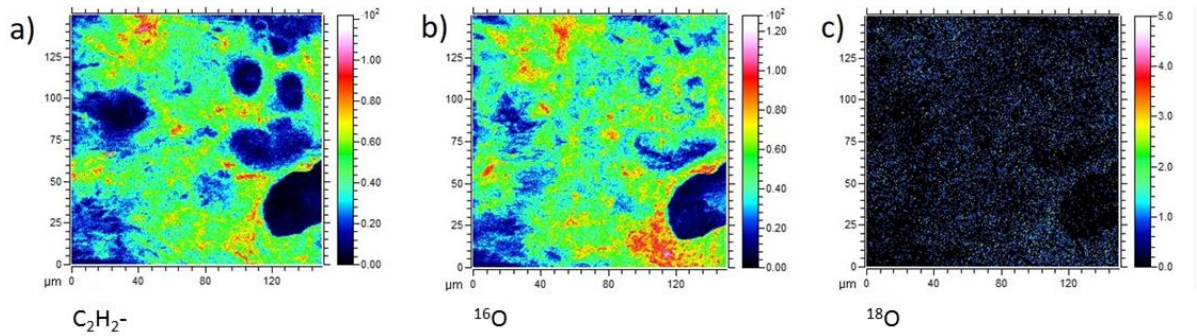

Figure 2. a) C_2H_2- biomass signal after 20 h of incorporation. **b)** ^{16}O signal after 20 h of incorporation time. **c)** ^{18}O signal with visible distinct features of the sample. The total ion dose was 8.4×10^{12} cm^{-2}. This measurement as well as the other shown measurements were performed in static SIMS conditions.

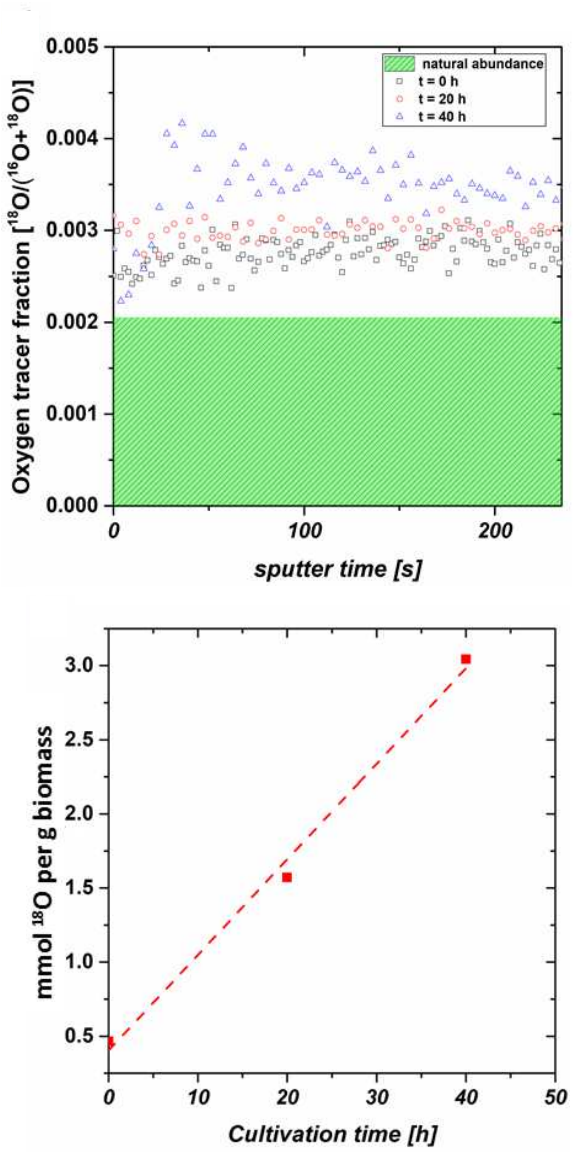

Figure 3. top) Time-dependence of ^{18}O-tracer incorporation by tracer marked glucose. No depth profile can be dedicated by the measurement, but rather the overall tracer incorporation. The offset at t=0 compared to the natural abundance is caused by the media, already containing tracer marked glucose. **bottom)** Amount of ^{18}O detected in 1 g of biomass over cultivation time with added linear fit.

Using higher marked glucose or a higher tracer concentration, a far more sensitive increase could be expected making exchange times of below 1 hour possible for highly resolved measurements. Expecting a factor 30 when using exclusively tracer oxygen with three marked oxygen atoms would result in a difference of a factor of 3 within 1 hour of exchange. To investigate these results in more quantitative terms, we can use again Equation 1 while employing the average biomass composition of the utilized strain: C=47%, N= 7.5%, H=6.5%, O=31%. With D-[1-18O] glucose present in the medium the ^{18}O amount in 1 g of biomass (BM) is 0.01 mmol/g_{BM} and eventually reaches 0.05 mmol/g_{BM} after 40 hours of cultivation time with roughly 2 g of biomass formed. As only 10 % of total glucose utilized in this experiment was in fact D-[1-18O] glucose and incorporation of oxygen through respiration into biomass is negligible (as shown in the previous section), we can further assume that the $^{18}O/(^{16}O+^{18}O)$ fraction would further increase by a factor of 10 if solely D-[1-18O] glucose were used. If we furthermore consider all six oxygen atoms, we can estimate the detection of 3.0 mmol ^{18}O in 1 g of biomass after 40 hours of cultivation time.

These calculations represent average values across the whole analysed area from one sample. As our method is capable of measuring much smaller areas in specific morphological regions, these numbers might change. Therefore, comparison between measurement of total sample area and reduced sample area including visualization of morphological regions within the same sample or between different samples is possible as demonstrated in Figure 4. This sensitive method of tracer-marked glucose in combination with ToF-SIMS analysis is capable of visualization of metabolically active biomass regions in filamentous biomass. Such information can be used to generate flux-based models for C-source incorporation in biomass and in secondary metabolites (antibiotics) in the different growth phases of the fungal cultivation. As of now, industrial processes tend to favour pellet morphology for reasons of facilitated process control. Therefore, detailed information on limitations within the pellet's core are may be accessible with this method. For this purpose, the workflow for sample preparation must include fixation with resin and cutting with ultramicrotomy and subsequent tracer analysis of the core sections.

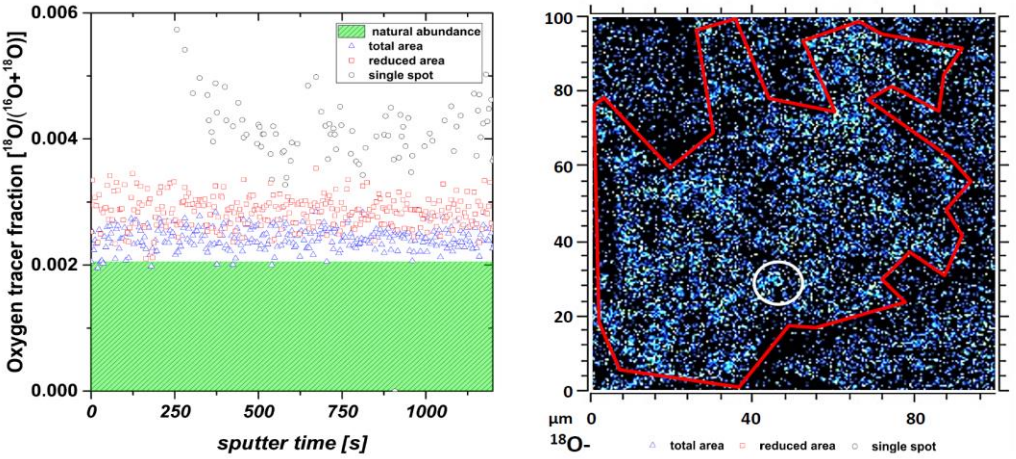

Figure 4. Measurement of oxygen tracer fraction $^{18}O/(^{18}O+^{16}O)$ in total sample area, reduced sample area and one single spot including visualization of measurement areas within the same sample.

Localisation of productive regions in *P. chrysogenum* biomass

In addition to oxygen diffusion and incorporation, we studied additional fragment masses obtained in measurement. Thereby we observed several prominent fragment masses apart from oxygen including the carbon backbone in various forms (11 C-, 25 C_2H_2-, 14 CH_2-), as well as a distinct 93 fragment mass consistently localised in the inner sections of the hyphal carbon backbone. This fragment mass varied in intensity according to sampling time, as well as penicillin and phenoxyacetic acid concentrations. Based upon this observation and in accordance with literature (Paul and Thomas 1998, Zangirolami et al. 1997, Wittler et al. 1986), we hypothesized that the observed 93 fragment mass must be related to penicillin production. To further verify this hypothesis, we acquired low-resolution mass spectra in negative-ion mode by means of electrospray ionization (ESI) of penicillin standard and phenoxyacetic acid in solid form and could identify the 93 fragment mass in both compounds.

In addition, we performed ToF-SIMS measurements of both compounds where we could also detect the 93 fragment mass. MS spectra of phenoxyacetic acid and penicillin V can be found in Supplementary Figure 2a and 2b. In Figure 5a the ratio of the aforementioned 93 fragment mass to the C_2H_2- carbon (26) signal is displayed for different sampling times integrated over the entire region of interest. HPLC measurements of the supernatant display increasing penicillin concentration with

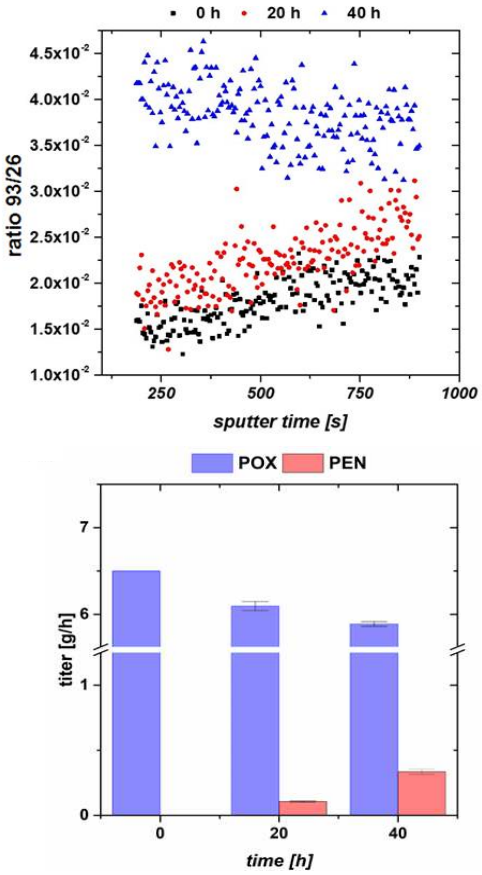

Figure 5. **top)** ToF SIMS measurements: secondary ion ratio of 93 signal to 26 signals [C_2-] across sputter time; Ratios between intensity of 93 signal (phenol) and 26 signal (C_2H_2-) demonstrate that the 93 signal is increasing in relation to the C_2H_2-carbon backbone with cultivation time and penicillin production. **bottom)** HPLC measurements: concentration of penicillin and phenoxyacetate in supernatant for different cultivation times (0, 20, 40 h).

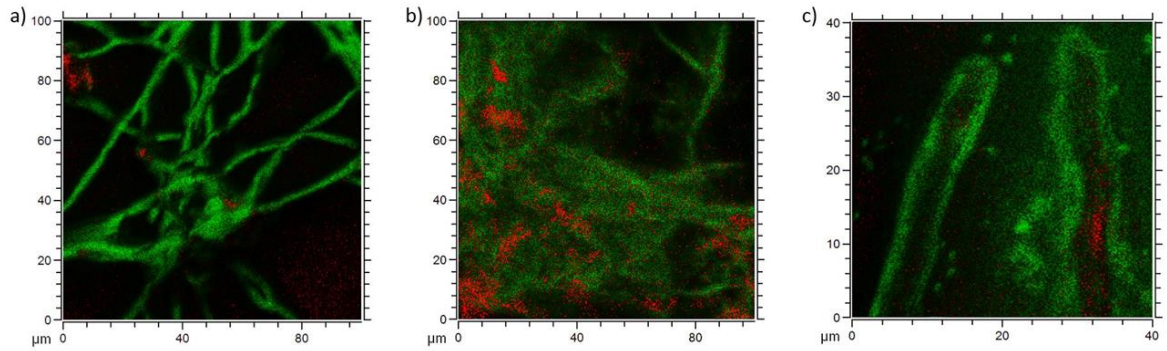

Figure 6. ToF SIMS measurements in spatial resolution: **a)** hyphal entanglement at 20 h cultivation time, overlay of 26 [C_2H_2-] (green) and 93 [C_6H_5O-] (red) signal. **b)** dense hyphal entanglement, overlay of 26 [C_2H_2-] and 93 [C_6H_5O-] signal at 40 h cultivation time. **c)** zoom into productive and non-productive hyphae at 20 h cultivation time, overlay of 26 [C_2H_2-] and 93 [C_6H_5O-] signal.

display increasing penicillin concentration with cultivation time., the ratio of 93/26 obtained from the biomass samples is following the same trend as observable in Figure 5b, as phenoxyacetic acid is incorporated by the biomass and penicillin is produced accordingly.

Obviously, an increased amount of both species is present in the fungal biomass at elevated cultivation times. Visualised results from ToF-SIMS measurements can be found in Figure 6. At elevated cultivation times productive zones are clearly indicated by 93 fragment mass signals, mainly in dense hyphal entanglements and can be furthermore spatially resolved.

The 93 m/z fragment in both cases most likely is phenol (C_6H_5O-) present in phenoxyacetic acid and penicillin. With this method is it possible to detect penicillin producing regions within the hyphal and pellet structure of *P. chrysogenum.* This is in accordance with literature, as these productive regions are not located in the hyphal tips, but rather occur in non-growing (subapical) regions (Paul and Thomas 1998, Zangirolami et al. 1997).

Discussion

We implemented a novel method for spatially resolved analysis of substrate and oxygen incorporation into biomass. The novelty of this approach lies in the application of Time-of-Flight Secondary Ion Mass Spectroscopy in combination with oxygen and glucose tracer substrates in a new context. In general, such techniques are only used in surface science. In this contribution, we demonstrate feasibility for more detailed analysis of substrate uptake in filamentous *P. chrysogenum* biomass with more complex morphology. Moreover, our results also suggest that biomass regions involved in penicillin production can be identified.

Advantages, disadvantages and comparability of the method

The method described here has been used in a novel context to study respiration and substrate incorporation in complex filamentous biomass. It employs ToF-SIMS in CBA operation mode (Kubicek et al. 2014), an imaging mode optimized for $^{18}O/^{16}O$ isotope analysis. The ~100 nm lateral resolution allows for detailed analysis of morphological sub-structures like hyphae. This method can clearly distinguish between metabolically active and non-active biomass zones, which is especially important for filamentous fungi processes featuring hyphal agglomerates or pellet structures. Incorporation of oxygen into hyphal structures can be detected when the sample is subjected to ^{18}O for sufficiently long-time intervals (> 12 hours). With the use of D-[1-18O] glucose we can visualize substrate uptake in different biomass regions. Furthermore, we can identify productive zones in detail as demonstrated by Figure 6 by zooming into productive and non-productive hyphae.

In this particular method ToF-SIMS analysis is carried out with Bi^+ ions. This mode of measurement was specifically chosen for $^{18}O/^{16}O$

isotope analysis, where fragmentation is helpful. We also found that we can obtain valuable information also from higher fragments. For sole analysis of organic mass fragments, higher Bi-clusters (e.g. Bi_3^+ or Bi_5^+) or gas cluster guns would be superior to ensure less fragmentation and higher secondary ion count (Kayser et al. 2013).

Comparing ToF-SIMS to NanoSIMS, the latter has a higher lateral resolution. However ToF-SIMS is still a valid compromise for our described method because of (i) the possibility to study large areas of several hundred µm across to study different hyphae simultaneously, and (ii) it offers the possibility to measure with low ion doses $<10^{13}$ cm^{-2} to retain static measurement conditions as done for the measurements presented here.

Applicability of the method

Filamentous fungi comprise several morphological forms, affecting biomass viability and productivity in different ways. Whenever the pellet form is favoured, detailed knowledge on the pellet's inherent viable, non-viable and productive zones is essential for process optimization. We envision our method as a tool to facilitate industrial process design and strain characterization by shedding light on C-source incorporation and respiratory limitations within complex fungal biomass agglomerates. This information could also be used in the generation of flux-based models. An additional benefit is the simultaneous localisation of productive biomass regions, which does not require further effort in sample preparation or measurement.

Acknowledgements

We thank the Austrian Federal Ministry of Science, Research and Economy in course of the Christian Doppler Laboratory for Mechanistic and Physiological Methods for Improved Bioprocesses for financial support. Strains for the experiments were gratefully provided by Sandoz GmbH (Kundl, Austria).

Authors' contributions

LVE and CSL designed the study. LVE and CSL performed the experiments and analysed the data. MKU performed and analysed ToF-SIMS measurements. EPI performed MS measurements. LVE and CSL wrote the paper. HHU gave valuable scientific input. CHE supervised the work.

Compliance with Ethical Standards

Funding: This study was funded by Austrian Federal Ministry of Science, Research and Economy in course of the Christian Doppler Laboratory for Mechanistic and Physiological Methods for Improved Bioprocesses (grand number 171).
Conflict of interest: The authors declare that they have no conflict of interest.
Ethical approval: This article does not contain any studies with human participants or animals performed by any of the authors.

References

Baumgartl H, Wittler R, Lubbers DW, Schugerl K (1984) Oxygen profiles and structure of *Penicillium chrysogenum* pellets. Adv Exp Med Biol 169:793-9

Cliff JB, Gaspar DJ, Bottomley PJ, Myrold DD (2002) Exploration of inorganic C and N assimilation by soil microbes with time-of-flight secondary ion mass spectrometry. Appl Environ Microbiol 68(8):4067-73

Couturier M, Navarro D, Chevret D, Henrissat B, Piumi F, Ruiz-Duenas FJ (2015) Enhanced degradation of softwood versus hardwood by the white-rot fungus *Pycnoporus coccineus*. Biotechnol Biofuels 8:216

Ehgartner D, Fricke J, Schroder A, Herwig C (2016) At-line determining spore germination of *Penicillium chrysogenum* bioprocesses in complex media. Appl Microbiol Biotechnol 100(20):8923-30

Fearn S (2015) Characterisation of biological material with ToF-SIMS: a review. Mater Sci Tech-Lond 31(2):148-61

Hille A, Neu TR, Hempel DC, Horn H (2005) Oxygen profiles and biomass distribution in biopellets of *Aspergillus niger*. Biotechnol Bioeng 92(5):614-23

Hille A, Neu TR, Hempel DC, Horn H (2009) Effective diffusivities and mass fluxes in fungal biopellets. Biotechnol Bioeng 103(6):1202-13

Holzlechner G, Kubicek M, Hutter H, Fleig J (2013) A novel ToF-SIMS operation mode for improved accuracy and lateral resolution of oxygen isotope measurements on oxides. J Anal Atom Spectrom 28(7):1080-9

Kayser S, Rading D, Moellers R, Kollmer F, Niehuis E (2013) Surface spectrometry using large argon clusters. Surf Interface Anal 45(1):131-3

Kubicek M, Holzlechner G, Opitz AK, Larisegger S, Hutter H, Fleig J (2014) A novel ToF-SIMS operation mode for sub 100 nm lateral resolution: Application and performance. Appl Surf Sci 289:407-16

Nielsen J, Krabben P (1995) Hyphal growth and fragmentation of *Penicillium chrysogenum* in submerged cultures. Biotechnol Bioeng 46(6):588-98

Nunez J, Renslow R, Cliff JB, Anderton CR (2017) NanoSIMS for biological applications: Current practices and analyses. Biointerphases 13(3):03B301

Paul GC, Thomas CR (1998) Characterisation of mycelial morphology using image analysis. Adv Biochem Eng Biotechnol 60:1-59

Posch AE, Herwig C (2014) Physiological description of multivariate interdependencies between process parameters, morphology and physiology during fed-batch penicillin production. Biotechnol Prog. 30(3):689-99

Veiter L, Rajamanickam V, Herwig C (2018) The filamentous fungal pellet - relationship between morphology and productivity. Appl Microbiol Biotechnol 102(7):2997-3006

Walisko R, Moench-Tegeder J, Blotenberg J, Wucherpfennig T, Krull R (2015) The Taming of the Shrew--Controlling the Morphology of Filamentous Eukaryotic and Prokaryotic Microorganisms. Adv Biochem Eng Biotechnol 149:1-27

Walker AV (2008) Why is SIMS underused in chemical and biological analysis? Challenges and Opportunities. Anal Chem 80(23):8865-70

Wittler R, Baumgartl H, Lubbers DW, Schugerl K (1986) Investigations of Oxygen-Transfer into *Penicillium chrysogenum* Pellets by Microprobe Measurements. Biotechnol Bioeng 28(7):1024-36

Zangirolami TC, Johansen CL, Nielsen J, Jorgensen SB (1997) Simulation of penicillin production in fed-batch cultivations using a morphologically structured model. Biotechnol Bioeng 56(6):593-604

Zhang J, Zhang J (2016) The filamentous fungal pellet and forces driving its formation. Crit Rev Biotechnol 36(6):1066-77

Supplementary Figures

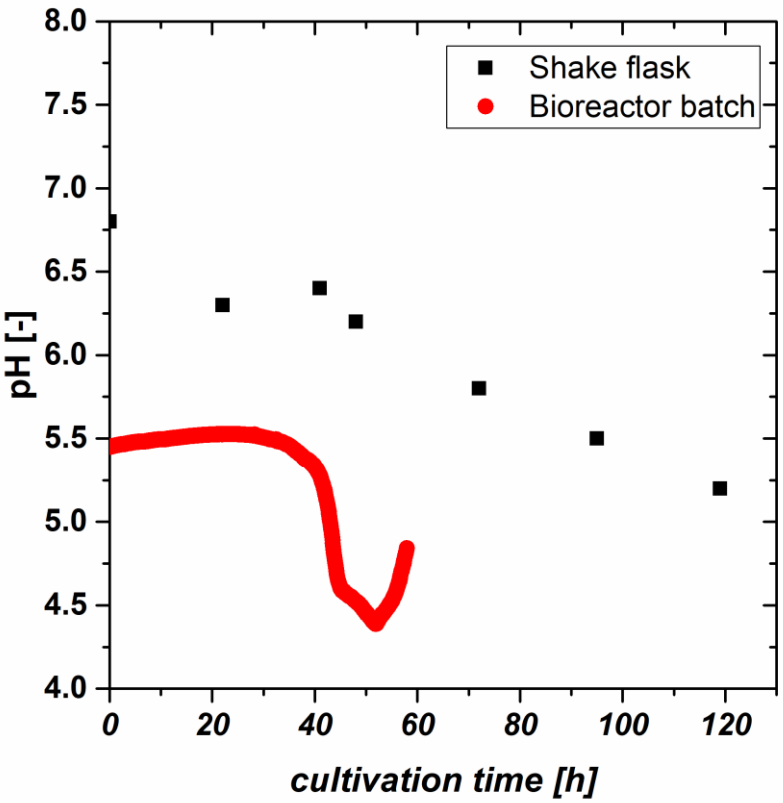

Supplementary Figure 1. pH range during shake flask and bioreactor experiments.

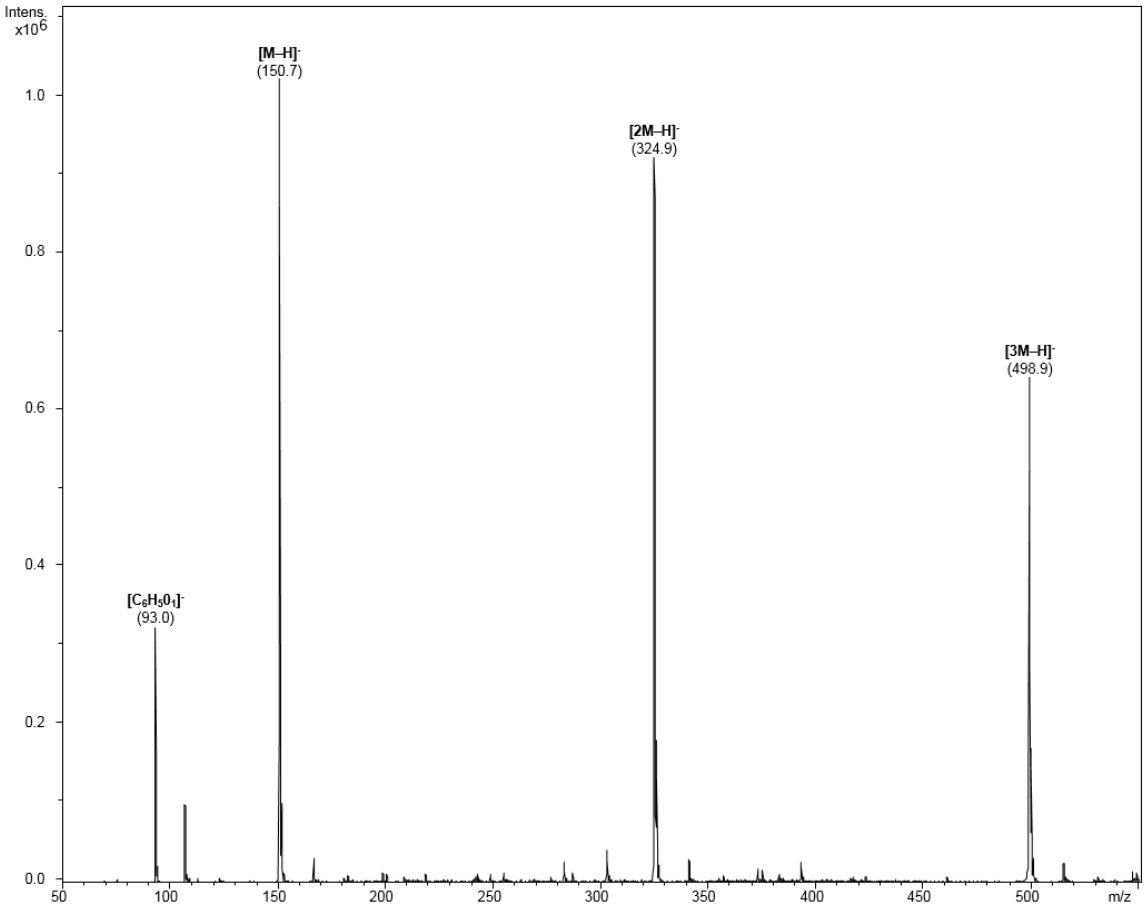

Supplementary Figure 2A. Low-resolution mass spectra and low-energy (LE) CID-MS2 spectra of phenoxyacetic acid acquired on an ion trap mass spectrometer in positive-and negative-ion mode by means of electrospray ionization (ESI).

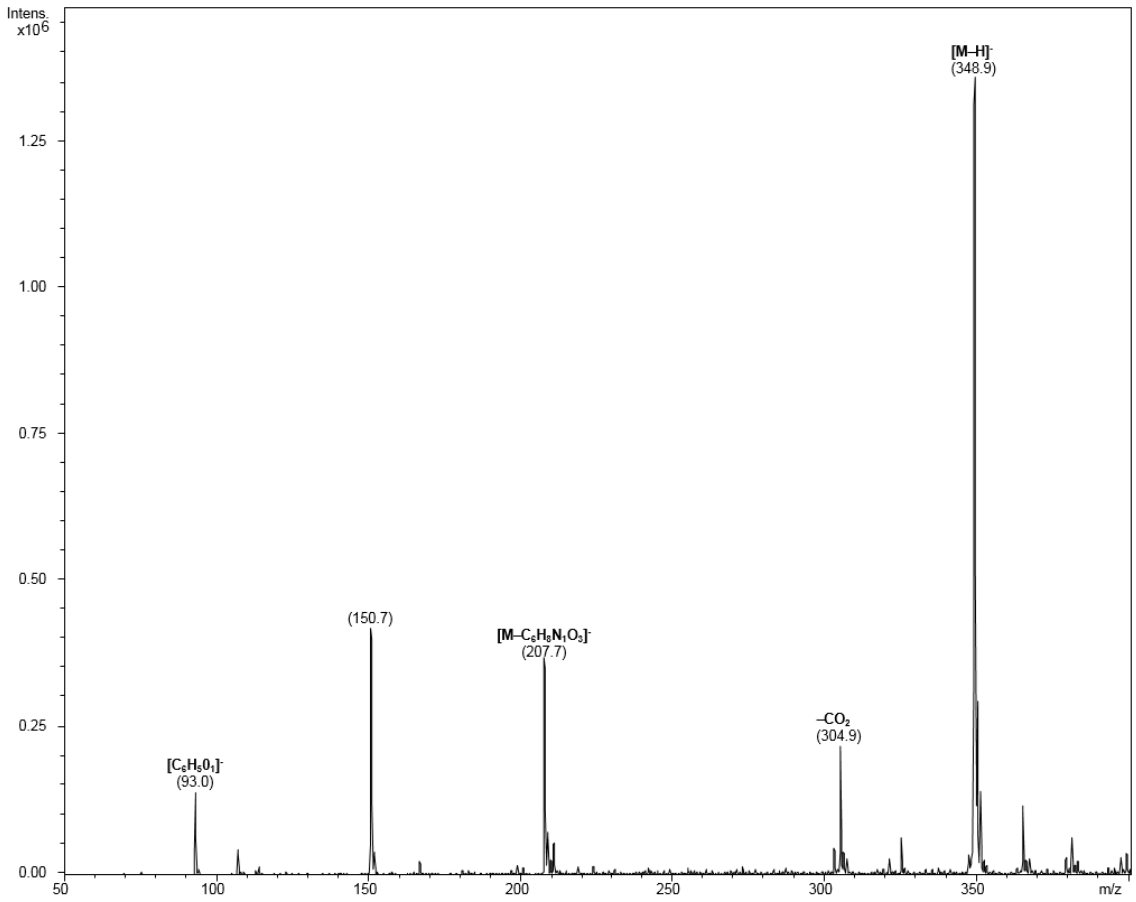

Supplementary Figure 2B. Low-resolution mass spectra and low-energy (LE) CID-MS2 spectra of penicillin V standard acquired on an ion trap mass spectrometer in positive-and negative-ion mode by means of electrospray ionization (ESI). The in-source generated fragment ion at m/z 207.7 represents a triple bond cleavage across the two rings of the penicillic acid-moiety. The ion at m/z 150.7 simply represents a background ion not related to Phenoxymethylpenicillin.

Chapter 6.
Control

Controlling the specific growth rate via biomass trend regulation in filamentous fungi bioprocesses

Daniela Ehgartner[1,2], Thomas Hartmann[1,2], Sarah Heinzl[1,2], Manuela Frank[1,2], Lukas Veiter[1,2], Julian Kager [1], Christoph Herwig[1,2] and Jens Fricke*[1,2]

[1] Technische Universität Wien, Institute of Chemical, Environmental and Bioscience Engineering, Research Area Biochemical Engineering, Gumpendorfer Strasse 1a, 1060 Vienna, Austria
[2] Christian Doppler Laboratory for Mechanistic and Physiological Methods for Improved Bioprocesses, TU Wien, Gumpendorfer Straße 1a, 1060 Vienna, Austria

* Correspondence: Jens Fricke
TU Wien, Institute of Chemical, Environmental and Bioscience Engineering, Research Area Biochemical Engineering, Gumpendorfer Strasse 1a

Published in 'Chemical Engineering Science'

Ehgartner D., Hartmann T., Heinzl S., Frank M., Veiter L., Kager J., Herwig C. and Jens Fricke (2017) 'Controlling the specific growth rate via biomass trend regulation in filamentous fungi bioprocesses.' Chem Eng Sci.

Highlights

- Viable biomass concentration is predicted online via dielectric spectroscopy.
- The method is applicable for filamentous fungi process in growth and decline phase.
- Holding growth rate on a constant level is based on controlling biomass trends.
- The control strategy adapts automatically to changing biomass yields.
- The method is robust to changing process parameters, physiology and morphology.

Abstract

Increasing pressure on product quality and quantity pushes solutions of process control to be a central issue in pharmaceutical bioprocesses. Especially online biomass estimation, and further control of the specific growth rate are of central importance because they describe the catalyst of the reaction. For penicillin producing bioprocesses with filamentous microorganisms, this was underlined by recent findings describing the influence of the specific growth rate on the specific production rate. Hence, the specific growth rate needs to be controlled on a certain level to achieve high productivity.
In this study, we developed a control strategy for the specific growth rate based on online estimation of viable biomass via dielectric spectroscopy. The method was verified using an at-line staining method for viability measurement. The online viable biomass estimation is applicable in the growth and decline phase, coping with physiological and morphological changes of filamentous fungi. Furthermore, the control strategy adapts to changing biomass yields, which is a big issue in the bioprocess for penicillin production applied in this study.

Two application runs were conducted, yielding in proper online viable biomass estimation and control of the specific growth rate at a constant level of 0.012 h^{-1}. We achieved biomass predictions with an average error of 1.5 g/l over the whole fed-batch process. In the decline phase, the control of specific growth rates was not possible due to physiological constrains. However, in the growth phase, a total specific growth rate of 0.013 h^{-1} was achieved, which met the pre-defined acceptance criterion for this method.
The method is thus ready for viable biomass estimation in the growth and in the decline phase of the penicillin production process. Furthermore, the method is applicable to control the specific growth rate during the growth phase.

Keywords

Penicillin, dielectric spectroscopy, bioprocess control, viability, online biomass estimation, filamentous fungi.

Introduction

Process control is of utmost importance in pharmaceutical bioprocesses to maximize productivity and to ensure product quality. The importance of the latter was underlined by the Quality by Design (QbD) initiative (FDA, 2006). One parameter which is often the focus is biomass growth. Various methods of biomass estimation for different processes and organisms have been applied (Mou and Cooney 1983a, Riesenberg et al. 1991, Sagmeister et al. 2013, Jenzsch et al. 2006). Studies presenting the influence of the specific growth rate, μ, on penicillin production (Douma et al. 2010, Pirt and Righelato 1967, van Gulik et al. 2000) underline the importance of μ-control strategies in filamentous fungi bioprocesses.

The basis for the control of μ is the availability of real-time biomass measurements. Hereby, two different principles can be distinguished: hard type sensors and soft sensors. The former are in-situ measurements of the biomass concentration, while soft sensors estimate the biomass based on mathematical models (Olsson and Nielsen, 1997). Commonly, soft sensors require high process knowledge and historical data for the development of mathematical models. Soft sensors were reportedly applied for biomass concentration and biomass growth estimation of filamentous organisms (Golabgir and Herwig 2016, Massimo et al. 1992, Thompson and Kramer 1994, Mou and Cooney 1983b). The online biomass estimation based on carbon balancing was already applied for the μ-control of penicillin processes (Mou and Cooney 1983a, Mou and Cooney 1983b). In situ biomass measurements applied for filamentous organisms were fluorescence probes (Haack et al. 2007) and dielectric spectroscopy (Fehrenbach et al. 1992, Mishima et al. 1991, Neves et al. 2000, Sarra et al. 1996). Fluorescence probes were found to be not applicable for penicillin-producing cultures in complex media, as changes in the medium composition influence fluorescence. Furthermore, penicillin is a fluorescent product which interferes with the measurement of fluorescence (Nielsen et al. 1994).

The principle for biomass measurement via dielectric spectroscopy is based on the function of cells as capacitors. The measured signal is a function of the volume fraction of the cells. Only cells with an intact membrane potential are recorded with dielectric spectroscopy. Hence, the method is insensitive to dead cells and only measures viable biomass (Dabros et al. 2009). This fact is of high importance for filamentous organisms who grow pellets, as the inner parts of these hyphal aggregates tend to die due to substrate and oxygen limitation, leading to considerable amounts of dead biomass (Bizukojc and Ledakowicz 2010, Hille et al. 2005, Manteca et al. 2008). In contrast to this dead biomass, only viable biomass is responsible for biomass growth and productivity (Bizukojc and Ledakowicz 2010, Paul et al. 1998). Most contributions, in which dielectric spectroscopy was applied on filamentous fungi for the estimation of biomass concentration, differentiate between a growth phase and a decline phase (at the end of cultivation). For the growth phase, biomass prediction via dielectric spectroscopy is reported to be highly applicable. However, biomass prediction in the decline phase still shows results that are very error-prone (Neves et al. 2000, Rønnest et al. 2011, Sarra et al. 1996).

Within this contribution, an online μ-control strategy in a penicillin production process based on viable biomass measurement via dielectric spectroscopy is established. So far, biomass estimation in the decline phase was reported to not work properly. We aim to predict the viable biomass concentration in the growth and the decline phase to further apply μ-control in both phases. The goal is to predict viable biomass in a similar error range as at-line and offline reference methods (6–12%). The control of the specific growth rate in filamentous cultures presents a special challenge as growth rate levels are rather low compared to other organisms as E. coli. These low specific growth rates make the control and the evaluation of the control strategy difficult as they have a lower signal-to-noise-ratio (Wechselberger et al. 2013). Furthermore, changing biomass yields during the penicillin production process appeared to be a main issue in μ-control. The developed control strategy aims to be applicable in the growth phase as well as in the decline phase and enables an automatic adaption to changing biomass yields. To avoid error propagation in the calculation of the specific growth rate, the control strategy focuses on biomass trends rather than the specific growth itself.

Nomenclature

Symbols

c	concentration [g/l]
ΔCap	delta Capacitance [pF/cm]
F	feed rate [g/h]
μ	specific growth rate [h^{-1}]
ρ	density [g/l]
r	rate [g/h]
t	time [h]
V_R	reactor volume [l]
Y_{PID}	output of PID controller [g/h]
$Y_{x/s}$	biomass yield [g/g]

Indices

tar	set-point; target value
est	predicted value based on the model
s	substrate
total	total biomass measured
viable	viable biomass measurements
X	biomass

Materials & Methods

Strains and inoculum

One strain of Penicillium chrysogenum (code BCB1_V2) was regenerated from an ancestor strain BCB1 and kindly donated by Sandoz GmbH (Kundl, Austria).

Bioreactor cultivation

Cultivations were performed in either of two Techfors S bioreactors (Infors HT, Bottmingen, Switzerland) with a maximum working volume of 10 L and 20 L respectively. The initial batch and fed-batch volumes were 6.5 L for the 10-l-bioreactor and 13 L for the bigger one. The stirrer was equipped with three six-bladed Rushton turbine impellers, of which two were submersed and one was installed above the maximum liquid level for foam destruction. The fermentation temperature was kept at 25 °C via a double jacket. Aeration was controlled at 1 vvm in batch and initial fed-batch with mass flow controllers (Vögtlin, Aesch, Switzerland). The concentration of dissolved oxygen was measured using a probe of dissolved oxygen (Hamilton, Bonaduz, Switzerland). If not stated otherwise, the pO2 was controlled via an adjustment of the stirrer speed at a level higher than 40%. The pH was measured using a pH probe (Hamilton, Bonaduz, Switzerland). CO_2 and O_2 concentrations were analysed with an off-gas analyser (M. Müller AG, Egg, Switzerland).

Dielectric spectroscopy was applied in dual frequency mode using a Biomass Monitor 220 (Aber Instruments, Aberstwyth, UK). Every minute the delta capacitance (ΔCap) was recorded for the following frequencies: 100/15,650 kHz. For further application, the signal was smoothed using a Savitzky-Golay-filter (first order, window of 60 data points).

The batch was carried out on a complex bioreactor medium similar to the one described in Posch et al. (2013). The culture was inoculated with a spore inoculum concentration of $2*10^8$ spores/l. During this phase, the pH was not controlled. The end of the batch was indicated by an increase in pH by 0.5. After the batch, a fed-batch was performed on a defined medium (similar to Posch et al. 2013). For this purpose, 10% of the batch broth were added to 90% of the initial fed-batch volume. The initial fed-batch volumes were 6.5 L and 13 L respectively. During the first 48 h, glucose was fed at a constant rate (1.01 ml/(l*h) of a 500 g/l glucose solution). During this phase, the pH was kept constant at 6.5 ± 0.1 by addition of 20% (w/v) KOH or 15% (v/v) H_2SO_4, respectively.

Fed-batch parameters

To achieve different viable biomass concentrations and trends, 13 fed-batches were run by varying the following parameters: spore inoculum concentration ($2*10^8$ spores/l and $2*10^9$ spores/l), feed profile starting after 48 h (constant, linearly increasing, exponentially increasing), feed rates at the start of the feeding profile (1.0 ml/(l*h), 3.0 ml/(l*h) of a 500 g/l glucose solution) and pO_2 (>40% vs.<10%). These runs were used for the development of the online biomass estimation strategy.

Additionally, two fed-batches were conducted to show the application of μ-control - fed-batch 1 and 2 (FB1&2). Apart from some minor changes described in the following, these two cultivations were conducted as previously stated. An initial constant feed of 1.01 ml/(l*h) of 500 g/l glucose solution was applied for only 24 h, then μ-control was started. The first biomass sample of these two fed-batches was used to analyse the viable biomass concentration at-line. This was necessary to calculate the offset of ΔCap, and thus to be able to apply the model for biomass prediction. All other steps of biomass estimation and μ-control were conducted online. During the first 24 h, both fed-batches were controlled at a pO_2 level higher than

40%. After 24 h, the pO_2 of FB1 was decreased to 4% by mixing the air flow with nitrogen.

Calculations

Calculations of yields, rates and specific rates like the specific growth rate were carried out as stated elsewhere (Sagmeister et al. 2012). This study focuses on the measurement of viable biomass. Thus, the viable biomass was used as a basis for all calculations.

Analytics

At-line viability measurement

To investigate the viability via propidium iodide (PI) staining, 200 µl of the sample were diluted 1:5 with phosphate buffered saline (PBS, see Ehgartner et al. 2016). In addition, 1 ml of the sample was diluted 1:5 with PBS and microwave-treated by leaving it in a M510 microwave oven (Philips, Netherlands) for 30s at 940 W. One millilitre of the microwave-treated sample was used for further investigation. In a next step, duplicates of all samples (including microwave-treated and untreated samples) were centrifuged for 15 min at 500 rpm. 800 µl of the supernatant were removed and 800 µl of PBS buffer were added. The pellet was resuspended and the washing step repeated. 100 µl of the resuspended sample was pipetted into a microtiter well and 1 µl of 200 µM PI solution (Sigma Aldrich, St. Louis, Missouri/USA) was added. The PI was prepared by diluting a 20 mM PI stock solution in DMSO, 1:100 in PBS. After an incubation time of 20 min at room temperature in darkness, the measurement was performed in a Tecan well-plate reader (Tecan, Männedorf, Switzerland; ex./em. 535/600 nm). Six aliquots of each sample were measured simultaneously using 96 well plates.

Total biomass concentration

Two methods for the determination of the total biomass concentration were applied. For the at-line determination of viable biomass, the wet weight was measured. Due to a lower degree of measurement error (4% vs. 10%), the total biomass concentration for offline use was determined through the dry cell weight (DCW). One exception was the decline phase in FB2, where wet weight data was also used for offline investigations. This was due to an increased and highly fluctuating DCW measurement caused by the crystallisation of salts from the highly conductive broth in this phase.

Measurements were carried out in quadruplicates by transferring 5 ml of fermentation broth into weighed glass eprouvettes and centrifuging them at 4800 rpm for 5 min at 4 °C. The supernatant was removed and stored at –20 °C for further analysis. The pellets were then resuspended in 5 ml of deionized water and the eprouvettes were centrifuged again at the conditions mentioned above. The supernatant was discarded. For wet weight determination, the eprouvettes were weighed and the biomass concentration was calculated using a predefined regression to the DCW. After the wet weight determination, the eprouvettes were dried at 105 °C for at least 72 h and weighed again, resulting in the DCW.

Confocal microscopy

Microscopic images of pellets were taken using a confocal fluorescence microscope (TE2000-E, Nikon, Tokio, Japan). Hence, 100 µl of the bioreactor sample were diluted with 900 µl of PBS buffer and then centrifuged for 2 min at 500 rpm at room temperature. 800 µl of the supernatant were discarded and replaced with 800 µl of PBS buffer. Afterwards, 10 µl of the 200 µM PI reagent (prepared as described in 2.3.1) were added and the sample was incubated for at least 10 min in the dark. Furthermore, 20 µl of the sample were applied on a cover slide and 50 mg/l FDA reagent (Sigma Aldrich, St. Louis, Missouri/USA; from 5 g/l stock solution by diluting 1:100 with PBS) were added. The measurements were conducted using two different lasers and filters: ex./em. 543/580 nm for PI and ex./em. 488/507 nm for FDA.

Light microscopy

A morphological analysis via scanning of microscopic images was conducted as described in Posch et al. 2012. To do so, 900 images per sample were recorded with a Leitz wide field microscope (Leitz, Stuttgart, Germany). It was equipped with a five megapixel microscopy CCD colour camera (DP25, Olympus, Tokio, Japan) and a fully automated x-y-z stage (Märzhäuser, Wetzlar, Germany). The software used for the image recording was analysis5 (Olympus, Tokio, Japan).

Sugar and metabolites

Gluconic acid, glucose and mannitol were quantified through ion chromatography. The analysis was carried out using a Dionox column (Thermo Fisher Scientific, Massachusetts, US) at a column temperature of 30 °C.

For detection, a Dionex PAD detector in quadrupole potential mode (Thermo Fisher Scientific, Waltham, Massachusetts, US) was used. A gradient profile was applied combining three different solvents (MQ water, 0.1 N NaOH and 1 N NaOH).

Results

Monitoring of viable biomass concentration

The application for the online determination of the viable biomass concentration was based on at-line viability measurements. This was a combination of total biomass determination via wet weight (or DCW for offline purposes) and viability determination. For this purpose, the viability stain PI, microwave treatment and the Tecan well-plate reader (Tecan, Männedorf, Switzerland) were used. As described in Section 2.3.1, one aliquot of the sample was microwave-treated, another one was used in its native state. Both were stained with PI and the ratio of red fluorescence described the viability of the culture (see Equation 1). In addition to quantitative viability measurements, confocal fluorescence microscopy in combination with the viability stains FDA and PI was conducted to support the quantitative methodology. Confocal fluorescence microscopy pictures taken during the process reveal the decrease of viability as shown in Figure A.1 in the appendix.

Equation 2 shows how the viable biomass concentration ($c_{x,viable}$) was calculated by using viability measurements. If not stated otherwise, biomass concentration refers to the viable biomass as determined by Equation 2. The viable biomass concentration ($c_{x,viable}$) is calculated from the total biomass concentration ($c_{x,total}$) and the viability. The total biomass concentration was either determined via wet weight (at-line application) or DCW (offline application).

(1)

$$\text{Viability } [-] = 1 - \frac{\text{red fluorescence original sample}}{\text{red fluorescence in microwaved sample}}$$

(2)

$$c_{x,viable} = \text{Viability} * c_{x,total}$$

Cultivations with the goal to achieve different viable biomass concentrations and trends were conducted, where the viability was measured at-line. The total biomass concentration, viable biomass concentration and viability are shown exemplarily for two cultivations in Figure 1. In both cultivations, a significant decrease in the viability after around 100 h could be observed. The cultivation shown in Fig. 1b depicts a strong decline of viability to a final value of 30 %.

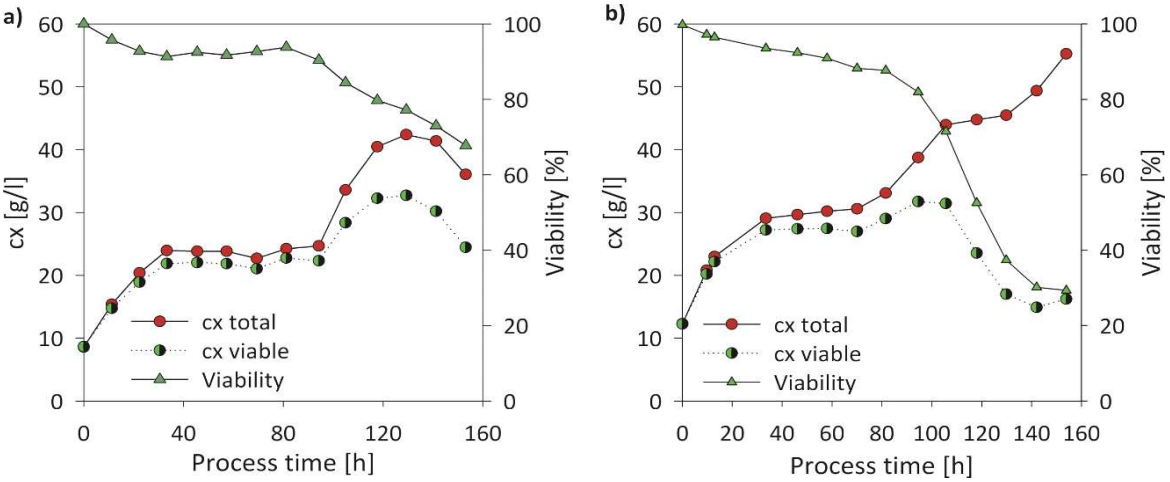

Figure 1. Time courses of the viability, viable and total biomass concentration for two fed-batch cultivations. The ultivations differed in their feeding profile. While the fed-batch in (**a**) had an exponential feeding profile (0.02 h−1) starting with 1.0 l/(l*h) of a 500 g/l glucose solution, the fed-batch in (**b**) was conducted with a feed starting with 3.0 ml/(l*h) of a 500 g/l glucose solution, which then constantly increased to a final rate of 9.0 ml/(l*h).

Distinction between process phases: growth phase vs. decline phase

In order to make a distinction between the different process phases, the aforementioned cultivations were examined. In most of the performed cultivations two different phases were observable: the growth phase and the decline phase. As it is shown exemplarily for one cultivation in Figure 2, two correlations between ΔCap and viable biomass could be distinguished.

The change from one phase (growth phase) to the second phase (decline phase) was indicated by the decrease of the ΔCap signal. This indication for the switch from the first to the second phase cannot be applied when μ is controlled on a constant level, because the biomass ought to increase with the intended specific growth rate. Thus, another indicator for the change of phases needed to be found.

Several permittivity probe parameters were investigated as indicators for the start of the decline phase. Certain trends were observed for typical capacitance measurement parameters like Fc and Cole Alpha (Dabros et al. 2009). However, these trends were not specific for the observed phase change. Opposed to this, an increase of conductivity was found to be distinctive for the start of the decline phase. The conditions that must be met for the increase of the conductivity signal to indicate the start of the decline phase are shown in Figure 3.

Exemplary trends of conductivity and the defined indication of phase change for two cultivations are shown in Figure 4. The increase of conductivity at the start of the fed-batch in Fig. 4a was caused by the addition of higher amounts of acid and base for the control at a constant pH and was hence no indicator for the start of the decline phase. This occurrence underlines the importance of condition 1 as described in Fig. 3, which must be met before condition 2 can be of significance. On the other hand, the decline phase of the fed-batch presented in Fig. 4b and c was successfully detected via conductivity measurement. The increase of the conductivity signal indicates a lysis of cells or the release of a metabolite into the surrounding medium at the onset of the decline phase. Furthermore, cell size and morphology were reported to influence the ΔCap-biomass-correlation (Ehgartner et al. 2015). Hence, there ought to be a morphological change resulting in the difference of correlation of viable biomass and ΔCap between these two phases. Thus, morphological parameters like the average size of morphological aggregates, the differentiation of morphological aggregates in fractions (e.g. pellets, smaller elements) and the parameters describing the pellet itself (e.g. fullness, roughness) were examined (data not shown).

The morphological parameters are described elsewhere (Golabgir et al. 2015, Posch et al. 2012). However, no significant correlation between morphology and phase change could be observed.

In summary, two different phases (growth and decline phase) were clearly distinguished based on the correlation ΔCap and cx,viable. The onset of the decline phase as a second phase in the process was detectable via an increase in the conductivity signal.

Model for online viable biomass estimation

The model for viable biomass estimation by using the capacitance signal is shown in Figure 5. Data to establish the model was taken from the 13 fed-batch cultivations as previously described. The model contains a correlation between the growth phase (a) and the decline phase (b).

Based on these correlations, the viable biomass can be estimated (cx,est) with Equation 3 (growth phase, GP) and Equation 4 (decline phase, DP) respectively. Calculation of the estimated viable biomass concentration ($c_{x,est}$) during growth phase

$$c_{x,est} = b_{0,GP} + b_{1,GP} * \Delta Cap \quad (3)$$

$$c_{x,est} = b_{0,DP} + b_{1,DP} * \Delta Cap \quad (4)$$

is based on the offset ($b_{0,GP}$) from the correlation of $c_{x,viable}$ and ΔCap during the growth phase and its slope ($b_{1,GP}$). During decline phase different offset ($b_{0,DP}$) and slope ($b_{1,DP}$) are used. The determined parameters for the linear correlation between $c_{x,viable}$ and ΔCap are:

$b_{0,GP} = 1.96$ $b_{1,GP} = 0.33$
$b_{0,DP} = 17.36$ $b_{1,DP} = 0.10$

The application of the growth phase model (Figure A.2a in the supplementary material) shows a slight overestimation of $c_{x,viable}$, as the correlation trend line does not cross the zero point (intercept 0.8 g/l).

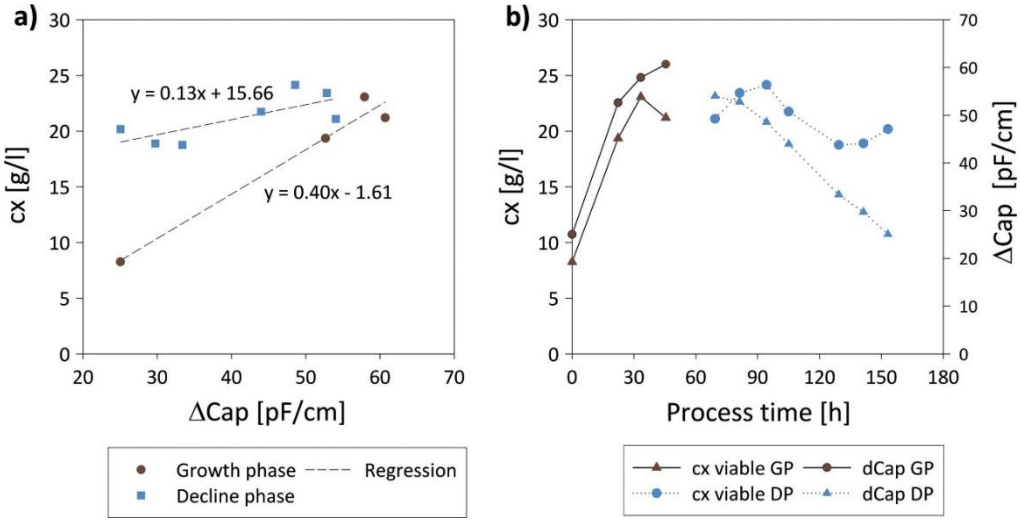

Figure 2. ΔCap and $c_{x,viable}$ in the two phases. (a) Correlation of ΔCap and $c_{x,viable}$ for growth and decline phase. (b) Time courses of ΔCap and $c_{x,viable}$ for growth phase (GP) and decline phase (DP).

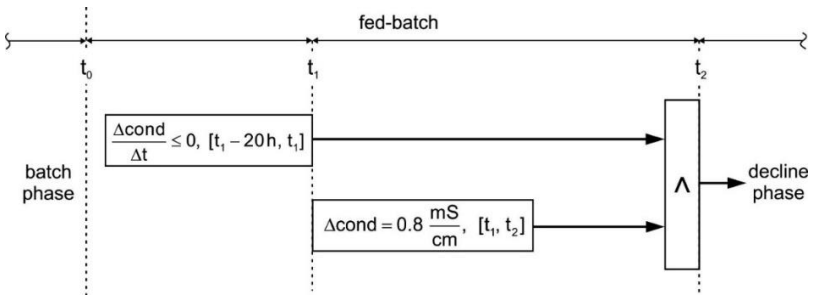

Figure 3. Decision scheme for the indication of the decline phase onset via conductivity (cond.) signal. The following points in the fed-batch are crucial: t0: start of fed-batch, t1: start increase of conductivity, t2: start decline phase. The conditions are (1) a constant or decreasing conductivity for a defined period of time before the signal starts increasing [t1-20 h, t1)] and (2) an increase of the conductivity (0.8 mS/cm).

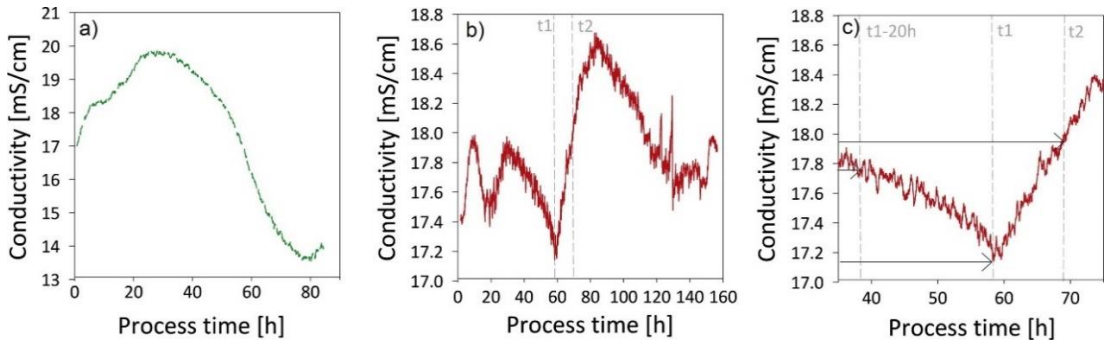

Figure 4. Conductivity of two fed-batch cultivations. (**a**) The conductivity signal in the first 30 h of the fed-batch shown here, increases. Still, there is no decline phase as condition 1 is not met (20 h before the beginning of the increase in conductivity, the value of the signal needs to be higher than at the start of the increase. This is not possible as the increase starts directly with the beginning of the fed-batch.). In (b-c) another fed-batch is shown. While in (**b**) the conductivity throughout the whole fed-batch is shown, (**c**) presents the phases t1-20 h to t2 in more detail. At the start of the increase in conductivity at t1 = 58.4 h, condition 1 as presented in Fig. 3 was accomplished: the value of the conductivity signal at t1-20 h was higher than it was at t1. Furthermore, the signal rose 0.8 mS/cm between t1 = 58.4 h and t2 = 68.6 h. Hence condition 2 was accomplished as well, indicating the start of the decline phase.

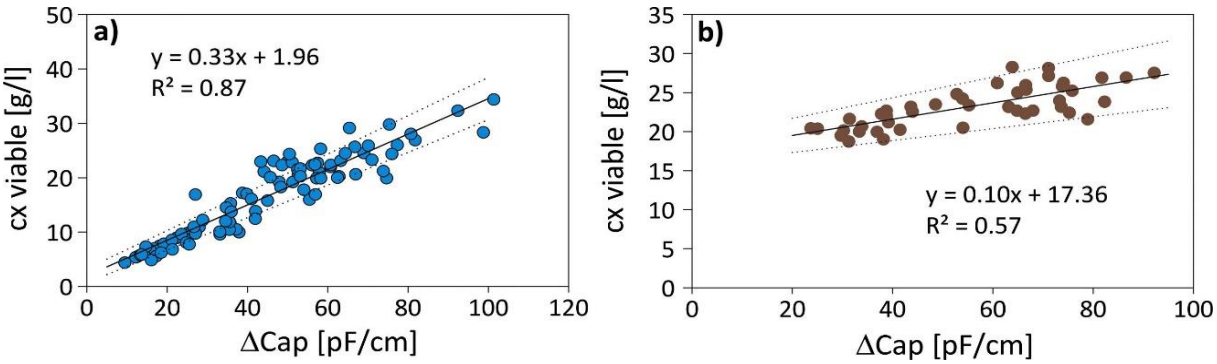

Figure 5. Correlation including a 95% confidence interval for ΔCap and c $_{x,viable}$ for growth phase (a) and decline phase (b).

Process control strategy

The applied control strategy is described in Figure 6. The process control system (Lucullus PIMS, Securecell AG, Schlieren, Switzerland) records the process signals and sends these to Matlab (MathWorks, Natick, Massachusetts, US). Therefor the equations shown in Equations 3, 4. Apart from the current $c_{x,est}$, the viable biomass concentration target ($c_{x,tar}$) is determined. These values are sent back to the process control system, where the current $c_{x,est}$ and $c_{x,tar}$ are fed into a PID controller.

The output of the controller acts on the feed rate FS to adjust for changes in the substrate yield. The feed flow calculation contains a constant value for the initial biomass yield ($Y_{x/s(t0)}$). This value changes according to the cultivation. It is evaluated in advance, using a data based regression model predicting $Y_{x/s}$ dependent on process time and µ.

Application of the method

The application of the control strategy is exemplarily shown in Figure 7, Figure 8 for FB1 and FB2, respectively. The specific growth rate µ in FB2 was controlled exactly as sketched in Figure 6. In the case of FB1, the control was conducted in a slightly different way. The inputs for the PID controller were not $c_{x,est}$ and $c_{x,tar}$, but µtar, and the current µ was calculated from $c_{x,est}$. In comparison to the slightly altered control strategy for FB1, the control strategy presented in Figure 6, has the advantage that the influence of the error of $c_{x,est}$ is not multiplied by calculating µ.

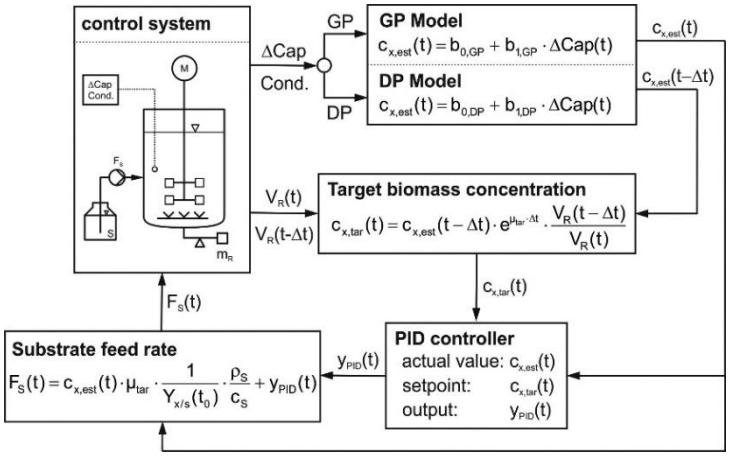

Figure 6. An overview of the process control strategy. The applied process control system records process data and transfers them to Matlab. The current process phase is determined via the conductivity signal (Cond.). Then the viable biomass concentration ($c_{x,est}$) based on the measured ΔCap signal is estimated. To do so, Equations (3), (4) are used. In addition to the current $c_{x,est}$, the viable biomass concentration target ($c_{x,tar}$) is determined. For $c_{x,tar}$, the specific growth rate target (μ_{tar}), Δt and the reactor volume (VR) are required. The process data is sent back to the process control system, where the current viable biomass $c_{x,est}$ and the viable biomass target $c_{x,tar}$ are fed into a PID controller. The output of the controller (y_{PID}) is added to the feed flow (Fs) to adjust for changes in the substrate yield ($Y_{x/s(t0)}$). In addition, the glucose concentration in the feed (c_s) and the density of the feed (ρ_s) are crucial for the calculation of the substrate feed rate. Δt is the set control interval, e.g. 1 h.

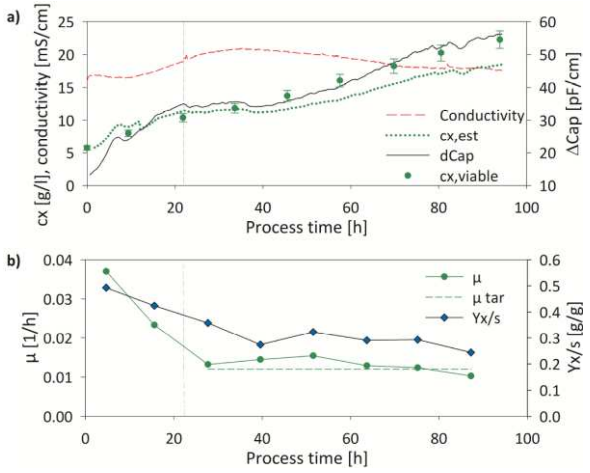

Figure 7. FB1. (a) Online signals and offline determined $c_{x,viable}$. (b) μtar as well as μ based on at-line and offline measurements. In addition, the biomass yield is presented. The start of μ-control is indicated by the vertical line at t = 22 h.

FB1 contained only a growth phase, lacking a decline phase, as the conductivity signal in Fig. 7 depicts. Although there is an increase in the conductivity signal before the start of μ-control, it does not indicate the beginning of the decline phase as the first condition, which compares the signal at t1-20 h and t1, is not fulfilled. This first condition would only be met at about 60 h, but consecutively no increase of the conductivity was observed, thus lacking the achievement of condition 2.

The prediction of the biomass concentration in the first 40 h of this cultivation worked well. After 40 h, $c_{x,viable}$ was constantly underestimated and the offset increased with time. While the deviation was 2 g/l after 45 h, it increased to more than 3 g/l at the end of fed-batch at 94 h. The average error of prediction was 2.1 g/l.

At t = 22 h the μ-control was started. While μ reached values of about 0.037 h^{-1} in the first 12 h, it decreased to an average of 0.013 ± 0.002 h^{-1} at the onset of μ-control. The μ target of 0.012 h^{-1} was missed by 0.002 h^{-1} on average. The total specific growth rate during μ-control (calculated between the first and last biomass sample of this period) was 0.013 h^{-1}.

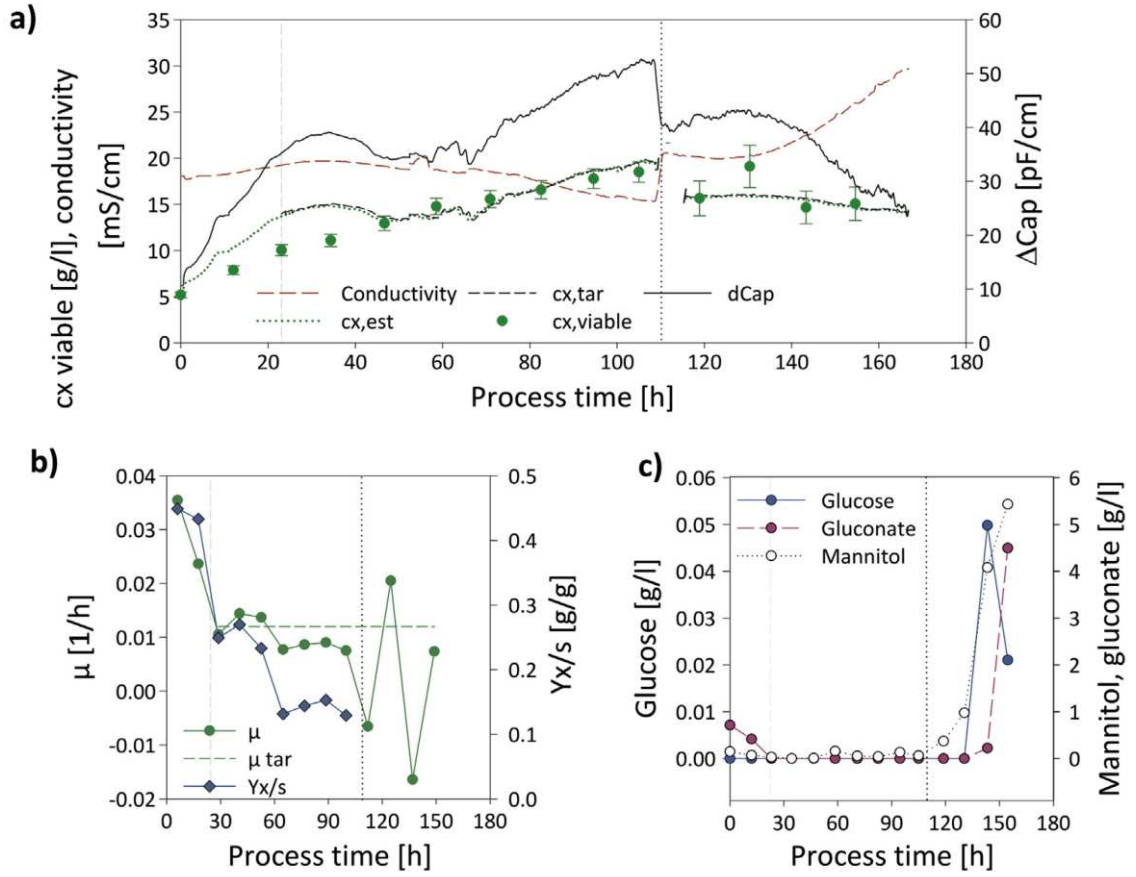

Figure 8. FB 2. **a)** online signals and measured $c_{x,viable}$. Between t = 109 h and t = 115 h the connection between the process control system and Matlab was cut. Hence, neither $c_{x,est}$ nor $c_{x,tar}$ are shown for this period. **b)** μ-control: μtar as well as μ based on at-line and offline measurements are shown. The former is only shown for the period of μ-control. Yx/s in this figure represents glucose as the only substrate and ignores the initial consumption of gluconate. **c)** Sugars and metabolites measured in the medium. The vertical lines at t = 23 h indicate start of μ-control, the ones at t = 111 h depict the onset of the decline phase.

FB2 consisted of a growth and a decline phase (see Figure 8). The decline phase – indicated by an increase of the conductivity signal – started at t = 111 h. The values of the viable biomass prediction are in good match to the measured viable biomass concentrations for both phases. The average error of prediction was 1.5 g/l during the growth phase, 1.2 g/l during the decline phase and 1.4 g/l for the whole fed-batch phase. During the growth phase, the measured specific growth rate deviated 0.003 h^{-1} on average from the μ target of 0.012 h^{-1}. The average specific growth rate during the growth phase was 0.010 ± 0.003 h^{-1}. The total specific growth rate during μ-control (calculated between the first and the last biomass sample of the control period in the growth phase) was 0.010 h^{-1}. Although viable biomass prediction worked well in the decline phase, it was not possible to maintain a constant μ level of 0.012 h^{-1}. Glucose accumulated after 130 h, resulting in gluconate build up, and from the start of the decline phase, the mannitol concentration increased considerably in the medium (see Figure 8c). The accumulation of glucose and metabolites depicts that more glucose is fed than consumed. Hence, the maximum specific growth rate decreased significantly during the decline phase, falling below 0.012 h^{-1}. Therefore, it was not possible to control the obtained μ during this phase. As already shown for FB1, the biomass yield from glucose also varied in FB2, with a tendency to decrease over process time. This is demonstrated in Figure 8. During μ-control, the maximal yield $Y_{x/s}$ was 0.27 g/g and the minimal one was 0.13 g/g.

Discussion

Morphological and biological changes

The biomass-ΔCap-correlation is the basis for a viable biomass prediction, distinguishing two process phases with different ΔCap-biomass-correlations – the growth and the decline phase. As the application runs FB1 and FB2 show, there are slight changes in ΔCap-biomass-correlation during the initial phase of fed-batch. Thus, the viable biomass is either overestimated in this initial phase or underestimated later in the growth phase. To find explanations for this occurrence, morphological parameters were investigated and compared to the biodensity, representing the ΔCap-biomass-correlation, which is described in more detail elsewhere (Ehgartner et al. 2015). In the early growth phase, first pellets are detectable and cells start to produce penicillin. Different trends in cell fractions and other morphological phases were observed (see Fig. A.3 in the appendix for morphological data of FB1). Yet, no clear relationship between one of these parameters and the changes in the ΔCap-biomass-correlation could be detected. The morphological changes may be too complex to be easily deducible.

Possibly, a third phase – an initial growth phase – ought to be necessary to increase accuracy in viable biomass prediction. However, this would make the prediction and control strategy more complex. In particular, an unambiguous indicator and clearly recognizable criteria for the change between these two phases would be needed. Nevertheless, viable biomass prediction worked well with an average deviation of 1.4 g/l for more than 160 h in FB2 and an average deviation of 2.1 g/l (12%) error in FB1. Even for *E. coli* processes, where a lot of work has been done in the area of biomass prediction, errors rates of 11–13% occur for single methods (Reichelt et al. 2016). The at-line method for viable biomass measurement applied here has an error rate of 12%.

Control strategy

The achieved specific growth rates tended to exceed the specific growth rate target of 0.012 h^{-1} at the start of µ-control and to remain below it at the end. This trend can be explained by the continuously decreasing biomass yield. The control strategy adapts to changing biomass yields, but the feed-back regulation could still be improved. Depending on the level of the growth rate target and the current biomass concentration, the control interval was set between 1 h and 4 h. Especially for low specific growth rates, the control interval is crucial. In fact, an interval of several hours is necessary to achieve significantly different biomass concentrations due to the high error rate of biomass estimation. To avoid an even higher impact of the error rate of the estimated biomass, the biomass concentration target $c_{x,tar}$ was invented as set-point for the PID controller in the final control strategy. Initially – as applied in FB1 – the set-point in the PID controller was μ_{tar}, which was compared to the current μ_{est}. This approach using μ_{tar} is significantly more affected by the error of biomass estimation than the approach using the biomass concentration target (Wechselberger et al. 2013).

When larger control intervals are applied, the system becomes more inert. For instance, if the biomass growth in the last few hours was too low, a higher feed rate would be required at a certain point. This would be necessary to achieve the overall specific growth rate target of this control interval, as µ had been too low before. Although the average specific growth rate ought to be close to the μ_{tar}, the specific growth rate in-between would fluctuate highly, thus not meeting the aim of obtaining a constant µ.

On average, the specific growth rate in FB1 slightly exceeded μ_{tar}, while the measured µ in FB2 was 0.002 h^{-1} beneath the set-point in total. The measured µ better matched the μ_{tar} in FB1. This was due to the overestimation of $c_{x,viable}$ during the final growth phase, which balanced the trend of a decreasing µ. The relatively low offline-determined µ is *inter alia* caused by neglecting dying biomass. This effect of neglecting dying biomass by using $c_{x,viable}$ for all calculations may be relevant when µ is calculated in a 12-h interval - contrary to the interval of approximately 1 h utilized for online calculation of the µ set-point. A considerable amount of biomass dies in this time span.

$$\mu = \frac{r_{x,\,viable}}{c_{x,\,viable} * V_R} \quad (5)$$

$$\mu = \frac{r_{x,\,total}}{c_{x,\,viable} * V_R} \quad (6)$$

Actual calculation of µ. $r_{x,viable}$ [g/h] is the biomass production rate calculated from viable biomass ($c_{x,viable}$). V_R represents the reactor volume [l]. Alternative calculation of µ. $r_{x,total}$ [g/h] is the bio -

mass production rate calculated from total biomass ($c_{x,total}$) measured via DCW or wet weight. V_R represents the reactor volume [l].

By calculating biomass rates for μ determination based on $c_{x,viable}$, dead cells are not taken into account (see Equation 5). An alternative calculation of μ considering dying biomass is shown in Equation 6. However, the offline calculation of μ using Equation (6) is not equivalent to the applied online control strategy, which is fully based on $c_{x,viable}$. Using dielectric spectroscopy, the evaluation of $c_{x,total}$ is not possible. Applying Equation 6 for calculating μ in the growth phase of FB2 results in an overall μ of 0.014 h^{-1}. Hence, μ_{tar} was exceeded by 0.002 h^{-1} while it was lower by 0.002 h^{-1} when using only viable biomass concentrations (Equation 5) for μ calculation.

Error propagation

The deviation of the offline-determined μ from the μ_{tar} is minimal, compared to the observed errors on the calculated specific growth rate. Using the combination of DCW and viability measurements as an offline method for viable biomass calculation results in an average error rate of 6% on $c_{x,viable}$. Due to error propagation, the maximal error on μ determined for an interval of 12 h is $0.01h^{-1}$. Thus, the deviation of an average of 0.002 h^{-1} (FB1) and 0.003 h^{-1} (FB2), respectively, is negligible. Even for larger intervals like the whole growth phase of the fed-batches, the maximal error on μ is still 0.002 h^{-1} for the 75 h interval of μ-control in FB1 and 0.001 h^{-1} for the 88 h interval in FB2.

One might thus question the approach of a μ-control strategy for bioprocesses with such low specific growth rates. Opposed to that, investigations such as the one carried out by Douma et al. 2010, describing the influence of μ on the productivity, underline the importance of controlled constant specific growth rates. With the control strategy developed here, we aimed to find a compromise by regulating μ indirectly via the control of a biomass trend ($c_{x,tar}$).

Benefits of the method

Advantages of dielectric spectroscopy: viable biomass

The proposed method is applicable for viable biomass estimation in the growth and the decline phase. Hence, it is adaptable to changes in physio - logy and morphology of cells due to the shift from hyphal elements to pellets and finally to cell degradation at the end of the bioprocess. The advantage of the dielectric spectroscopy only measuring the volume of viable biomass was exploited. By using viable biomass, e.g. for mechanistic model building, instead of taking total biomass measurements, the errors caused by taking a significant amount of dead, inactive biomass into account ought to be avoided.

Application in decline phase and high viscosities

Despite deviations in the decline phase due to physiological changes, where substrate accumulation, metabolite production and a strong decrease of the maximum growth rate could be observed, the prediction of viable biomass concentration was successful with an average error of 1 g/l (7%). This accuracy is comparable to the offline determination of viable biomass based on DCW. Moreover, the error is only half as high as the one of the at-line estimation of viable biomass based on wet weight determination. Prior investigations of dielectric spectroscopy for biomass prediction in filamentous bioprocesses stated this decline phase as their weak point (Neves et al. 2000, Rønnest et al. 2011, Sarra et al. 1996).

Especially for this late process phase, where the combination of high biomass concentration and significant hyphal background leads to immense viscosities, a method applicable online is of great advantage. The combination of broth viscosity with the occurrence of partially large hyphal aggregates hinders representative sample taking/preparation and pipetting is prone to error. Thus, analytical results are inaccurate. For elucidation, a picture of the cultivation broth in the last hours of the process is shown in Fig. A.4 in the appendix.

Robustness and flexibility

Further benefits of dielectric spectroscopy are reflected in the method presented here. Little process knowledge is necessary for the control strategy based on permittivity measurements. The method is robust to process changes like pO_2, spore inoculum concentrations or the feeding strategy and is thus easily transferable to other processes and process conditions. The development of this method for other strains/organisms, different processes and other probes/frequencies only requires some prior cultivations with different trends of viable biomass

concentrations where ΔCap is measured and $c_{x,viable}$ is determined. Furthermore, the regulation of μ by biomass trend control showed to be feasible for processes with high fluctuations in the biomass yield, which can be seen as a great advantage to other μ-control strategies (Jenzsch et al. 2006, Mou and Cooney 1983b).

Thus, the proposed control strategy in combination with the knowledge about μ-profiles for optimal productivity ought to increase the product titer of penicillin processes and hence the rentability of the process. First investigations about optimal specific growth rates for increased specific penicillin production have been recently published (Douma et al. 2010, van Gulik et al. 2000).

Conclusion

• A method to measure viable biomass online, by applying dielectric spectroscopy in dual frequency mode, was developed. The model underlying the method for online biomass estimation distinguishes two process phases - growth and decline phase – and is applicable in both. In the final run an average error of only 1.4 g/l (13%) viable biomass was achieved in almost 160 h of cultivation.

• The online method was evaluated using an at-line procedure including viability measurements. To do so, the verification was done by measuring viable biomass. Hence, dead biomass was not neglected.

• The online viable biomass estimation enabled μ-control during the growth phase with an average error of 0.002 h^{-1}. This μ-control strategy copes with changing process conditions, even varying biomass yields. During the decline phase, the biomass growth showed to be impaired, which made μ-control challenging.

• During the development process of this method, process parameters such as the spore inoculum concentration, the pO_2-level and the feeding strategy were varied. The application runs differed in their pO_2 set points (4% vs. >40%). The functionality of the developed control approach within these process parameter ranges shows its flexibility. Moreover, the method is applicable for typical physiological and morphological changes of the filamentous organism during fermentation.

• The method is ready to be applied for μ-control in the growth phase of *Penicillium chrysogenum* bioprocesses and for an online biomass estimation throughout the growth and decline phase.

Acknowledgements

We thank the Austrian Federal Ministry of Science, Research and Economy in course of the Christian Doppler Laboratory for Mechanistic and Physiological Methods for Improved Bioprocesses for their financial support (grant number 171). Strains for the experiments were kindly provided by Sandoz GmbH (Kundl, Austria).

References

Bizukojc M, Ledakowicz S (2010) The morphological and physiological evolution of *Aspergillus terreus* mycelium in the submerged culture and its relation to the formation of secondary metabolites. World Journal of Microbiology and Biotechnology 26:41-54. doi:10.1007/s11274-009-0140-1

Dabros M, Dennewald D, Currie DJ, Lee MH, Todd RW, Marison IW, von Stockar U (2009) Cole-Cole, linear and multivariate modeling of capacitance data for on-line monitoring of biomass. Bioprocess and biosystems engineering 32 (2):161-173. doi:10.1007/s00449-008-0234-4

Douma RD, Verheijen PJ, de Laat WT, Heijnen JJ, van Gulik WM (2010) Dynamic gene expression regulation model for growth and penicillin production in *Penicillium chrysogenum*. Biotechnology and bioengineering 106 (4):608-618. doi:10.1002/bit.22689

Ehgartner D, Fricke J, Schroder A, Herwig C (2016) At-line determining spore germination of *Penicillium chrysogenum* bioprocesses in complex media. Applied microbiology and biotechnology 100 (20):8923-8930. doi:10.1007/s00253-016-7787-y

Ehgartner D, Sagmeister P, Herwig C, Wechselberger P (2015) A novel real-time method to estimate volumetric mass biodensity based on the combination of dielectric spectroscopy and soft-sensors. J Chem Technol Biotechnol 90 (2):262-272. doi:10.1002/jctb.4469

FDA (2006) Guidance for industry: Q9 Quality risk management. Maryland

Fehrenbach R, Comberbach M, Petre JO (1992) On-line biomass monitoring by capacitance measurement. J Biotechnol 23 (3):303-314. doi:10.1016/0168-1656(92)90077-M

Golabgir A, Ehgartner D, Neutsch L, Posch AE, Sagmeister P, Herwig C (2015) Imaging Flow Cytometry and High-Throughput Microscopy for Automated Macroscopic Morphological Analysis of Filamentous Fungi. In: van den Berg MA, Maruthachalam K (eds) Genetic Transformation Systems in Fungi, vol 2. Fungal Biology. Springer International Publishing, pp 201-210. doi:10.1007/978-3-319-10503-1_17

Golabgir A, Herwig C (2016) Combining Mechanistic Modeling and Raman Spectroscopy for Real-Time Monitoring of Fed-Batch Penicillin Production. Chemie Ingenieur Technik 88 (6):764-776. doi:10.1002/cite.201500101

Haack MB, Lantz AE, Mortensen PP, Olsson L (2007) Chemometric analysis of in-line multi-wavelength fluorescence measurements obtained during cultivations with a lipase producing *Aspergillus oryzae* strain. Biotechnology and bioengineering 96 (5):904-913. doi:10.1002/bit.21170

Hille A, Neu TR, Hempel DC, Horn H (2005) Oxygen profiles and biomass distribution in biopellets of *Aspergillus niger*. Biotechnology and bioengineering 92 (5):614-623. doi:10.1002/bit.20628

Jenzsch M, Simutis R, Luebbert A (2006) Generic model control of the specific growth rate in recombinant *Escherichia coli* cultivations. J Biotechnol 122 (4):483-493. doi:10.1016/j.jbiotec.2005.09.013

Manteca A, Alvarez R, Salazar N, Yague P, Sanchez J (2008) Mycelium differentiation and antibiotic production in submerged cultures of *Streptomyces coelicolor*. Applied and environmental microbiology 74 (12):3877-3886. doi:10.1128/AEM.02715-07

Massimo C, Montague G, Willis M, Tham M, Morris A (1992) Towards improved penicillin fermentation via artificial neural networks. Computers Chemical Engineering 16 (4):283-291. doi:10.1016/0098-1354(92)80048-E

Mishima K, Mimura A, Takahara Y, Asami K, Hanai T (1991) On-Line Monitoring of Cell Concentrations by Dielectric Measurements. Journal of Fermentation and Bioengineering 72 (4):291-295. doi:10.1016/0922-338X(91)90166-E

Mou DG, Cooney CL (1983a) Growth monitoring and control in complex medium: a case study employing fed-batch penicillin fermentation and computer-aided on-line mass balancing. Biotechnology and bioengineering 25 (1):257-269. doi:10.1002/bit.260250119

Mou DG, Cooney CL (1983b) Growth monitoring and control through computer-aided on-line mass balancing in a fed-batch penicillin fermentation. Biotechnology and bioengineering 25 (1):225-255. doi:10.1002/bit.260250118

Neves A, Pereira D, Vieira L, Menezes J (2000) Real time monitoring biomass concentration in *Streptomyces clavuligerus* cultivations with industrial media using a capacitance probe. Journal of Biotechnology 84 (1):45-52. doi:10.1016/S0168-1656(00)00325-4

Nielsen J, Johansen C, Villadsen J (1994) Culture fluorescence measurements during batch and fed-batch cultivations with *Penicillium chrysogenum*. Journal of Biotechnology 38 (1):51-62. doi:10.1016/0168-1656(94)90147-3

Olsson L, Nielsen J (1997) On-line and in situ monitoring of biomass in submerged cultivations. Trends in Biotechnology 15 (12):517–522. doi:10.1016/S0167-7799(97)01136-0

Paul GC, Syddall MT, Kent CA, Thomas CR (1998) A structured model for penicillin production on mixed substrates. Biochemical Engineering Journal 2 (1):11-21. doi:10.1016/S1369-703X(98)00012-6

Pirt SJ, Righelato RC (1967) Effect of Growth Rate on the Synthesis of Penicillin by *Penicillium chrysogenum* in Batch and Chemostat Cultures. Applied microbiology 15 (6):1284-1290

Posch AE, Koch C, Helmel M, Marchetti-Deschmann M, Macfelda K, Lendl B, Allmaier G, Herwig C (2013) Combining light microscopy, dielectric spectroscopy, MALDI intact cell mass spectrometry, FTIR spectromicroscopy and multivariate data mining for morphological and physiological bioprocess characterization of filamentous organisms. Fungal genetics and biology : FG & B 51:1-11. doi:10.1016/j.fgb.2012.11.008

Posch AE, Spadiut O, Herwig C (2012) A novel method for fast and statistically verified morphological characterization of filamentous fungi. Fungal genetics and biology: FG & B 49 (7):499-510. doi:10.1016/j.fgb.2012.05.003

Reichelt W, Thurrold P, Brillmann M, Kager J, Fricke J, Herwig C (2016) Generic biomass estimation methods targeting physiologic process control in induced bacterial cultures. Engineering in Life Sciences 16 (8):720-730. doi:10.1002/elsc.201500182

Riesenberg D, Schulz V, Knorre WA, Pohl HD, Korz D, Sanders EA, Ross A, Deckwer WD (1991) High cell density cultivation of *Escherichia coli* at controlled specific growth rate. J Biotechnol 20 (1):17-27. doi:10.1016/0168-1656(91)90032-Q

Rønnest NP, Stocks SM, Lantz AE, Gernaey KV (2011) Introducing process analytical technology (PAT) in filamentous cultivation process development: comparison of advanced online sensors for biomass measurement. Journal of industrial microbiology & biotechnology 38 (10):1679-1690. doi:10.1007/s10295-011-0957-0

Sagmeister P, Wechselberger P, Herwig C (2012) Information Processing: Rate-Based Investigation of Cell Physiological Changes along Design Space Development. PDA journal of pharmaceutical science and technology / PDA 66 (6):526-541. doi:10.5731/pdajpst.2012.00889

Sagmeister P, Wechselberger P, Jazini M, Meitz A, Langemann T, Herwig C (2013) Soft sensor assisted dynamic bioprocess control: Efficient tools for bioprocess development. Chemical Engineering Science 96:190-198. doi:10.1016/j.ces.2013.02.069

Sarra M, Ison A, Lilly M (1996) The relationships between biomass concentration, determined by a capacitance-based probe, rheology and morphology of *Saccharopolyspora erythraea* cultures. Journal of Biotechnology 51 (2):157-165. doi:10.1016/0168-1656(96)01612-4

Thompson M, Kramer M (1994) Modeling Chemical Processes Using Prior Knowledge and Neural Networks. AIChE Journal 40 (8):1328-1340. doi:10.1002/aic.690400806

van Gulik WM, de Laat WT, Vinke JL, Heijnen JJ (2000) Application of metabolic flux analysis for the identification of metabolic bottlenecks in the biosynthesis of penicillin-G. Biotechnology and bioengineering 68 (6):602-618

Wechselberger P, Sagmeister P, Herwig C (2013) Model-based analysis on the extractability of information from data in dynamic fed-batch experiments. Biotechnology progress 29 (1):285-296. doi:10.1002/btpr.1649

Supplementary Material

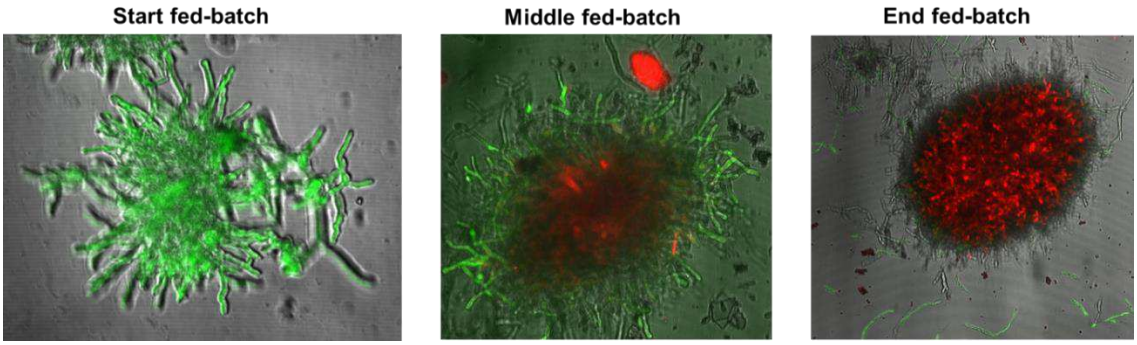

Figure A.1. Representing viability of pellets using confocal microscopy: beginning of fed-batch (after 27 h), middle of fed-batch (53 h) and end of fed-batch (125 h).

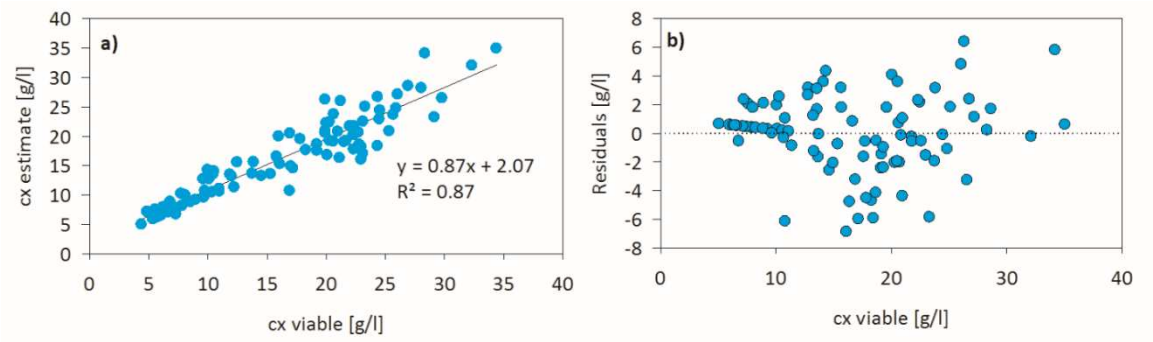

Figure A.2. Quality of the growth phase model. a) $c_{x,viable\ e}$ vs $c_{x,estimate}$ for the growth phase model. b) Residuals of viable biomass estimation.

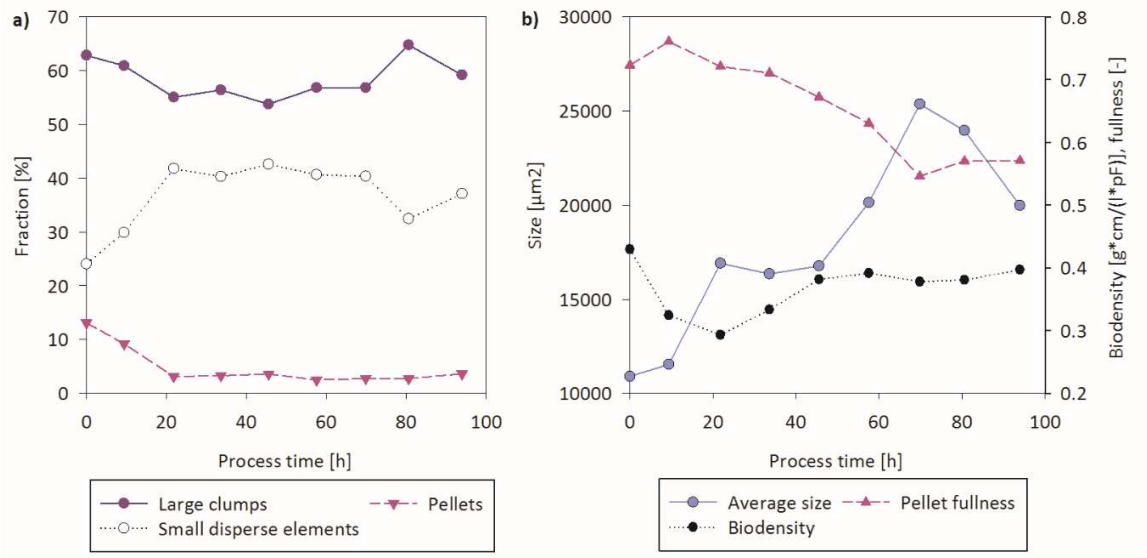

Figure A.3. Morphological data for FB1. a) Morphological fractions representing pellets, large clumps and small disperse elements. b) Single morphological parameter as the mean size of large elements and pellet average fullness are compared to biodensity representing the Cap-biomass-correlation.

Figure A.4. Cultivation broth at the end of fed-batch cultivation

Optimal process design space to ensure maximum viability and productivity in *Penicillium chrysogenum* pellets during fed-batch cultivations through morphological and physiological control

Lukas Veiter[1,2], Julian Kager[1] and Christoph Herwig*[,1,2]

[1] Technische Universität Wien, Institute of Chemical, Environmental and Bioscience Engineering, Research Area Biochemical Engineering, Gumpendorfer Strasse 1a, 1060 Vienna, Austria
[2] Christian Doppler Laboratory for Mechanistic and Physiological Methods for Improved Bioprocesses, TU Wien, Gumpendorfer Straße 1a, 1060 Vienna, Austria

[*] Correspondence: Christoph Herwig
TU Wien, Institute of Chemical, Environmental and Bioscience Engineering, Research Area Biochemical Engineering, Gumpendorfer Strasse 1a

Submitted to 'Microbial Cell Factories'

Abstract

Background

Biomass growth of *Pencillium chrysogenum* is characterised by a distinct pellet morphology consisting of compact hyphal agglomerates. Fungal pellets are advantageous in industrial process control due to rheological advantages but lead to biomass degradation due to diffusional limitations of oxygen and substrate in the pellet's core. Several fermentation parameters are known to affect key pellet characteristics regarding morphology, viability and productivity. Pellet morphology and size are affected by agitation. Biomass viability and productivity are tightly interlinked with substrate uptake and dissolved oxygen concentration.

Results

The goal of this study was the elucidation of the impact of the fermentation parameters power input, dissolved oxygen content and specific substrate uptake rate on morphology, biomass viability and productivity. A design of experiments (DOE) approach was conducted and corresponding responses were analysed using novel morphological descriptors analysed by a previously established flow cytometry method. Results clearly display inverse correlations between power input and pellet size, specific morphological parameters related to pellet density can be increased in direct proportion to power input. Biomass viability and productivity are negatively affected by high specific substrate uptake rates.

Conclusions

Based upon multiple linear regression, it was possible to obtain an optimal design space for enhanced viability and productivity at beneficial morphological conditions. We could maintain a high number of pellets with favourable morphology at a power input of 1500 W/m^3. A sound compromise between viability and productivity is possible at a specific glucose uptake rate of 0.043 g/g/h at dissolved oxygen levels of 40 % minimum.

Keywords

Filamentous fungi, *Penicillium chrysogenum*, design of experiments, flow cytometry, viability, morphology, pellets, multiple linear regression

Introduction

Cultivation strategies of filamentous fungi are characterized by specific fungal morphologies encompassing several forms ranging from homogeneously dispersed hyphae to dense agglomerates (Walisko et al. 2015, Zhang and Zhang 2016). Industrial bioprocesses using *Penicillium chrysogenum* favour the sphere-like pellet form where tightly packed mycelium forms a dense core surrounded by a looser 'hairy' region (Nielsen et al. 1995). These spherical pellets lead to advantages for process control such as lower viscosity of the cultivation broth as it contains less tangled mycelia (Zhang and Zhang 2016). Lower mixing times and facilitated gas-liquid mass transfer enable higher cell densities during cultivation. However, pellet morphology also calls for a segregated view of biomass. Different pellet regions feature different characteristics: the outer pellet region shows higher metabolic activity than the pellet's core which displays diffusional limitations mainly regarding oxygen (Walisko et al. 2015). For penicillin production, the pellet's outer region is also the productive zone (Paul and Thomas 1998). Consequently, the ideal pellet is characterised by i) the largest possible viable outer zone and ii) a rather loose morphology with a large 'hairy' region (Nielsen et al. 1995), at the same time iii) being dense and compact enough to ensure all the rheological advantages of pellet morphology.

From the perspective of morphology, effects of agitation have been extensively described (Walisko et al. 2015, Zhang and Zhang 2016, Veiter et al. 2018). Generally, pellet size as well as pellet quantity can be lowered by increased agitation (Vansuijdam and Metz 1981, (Nielsen et al. 1995) as well as morphological aspects such as compactness (Cui et al. 1997). Apart from influences on morphology, higher agitation also increases the power input into the system and by extend affects mixing time and k_La (Garcia-Ochoa and Gomez 2009).

The characteristics of diffusional limitations of oxygen and nutrients within fungal pellets are essential when dealing with pellet morphology. Hille et al. 2005 reported sharp decreasing oxygen concentration profiles along the pellet radius. Mass transport in pellets is commonly described by the effective diffusion coefficient D_{eff} according to equation 1 with diffusion factor f_D and molecular diffusion coefficient D_{mol}. D_{eff} is dependent on porosity ε_P whereas ε_P or f_D is changing along the pellet radius in the case of an inhomogeneous porosity (Hille et al. 2009).

$$(1)\ D_{eff} = f_D * D_{mol} = \varepsilon_P * D_{mol}$$

D_{eff}	effective diffusion coefficient [$m^2\ s^{-1}$]
D_{mol}	molecular diffusion coefficient [$m^2\ s^{-1}$]
f_D	diffusion factor [-]
ε_P	porosity [-]

These pellet characteristics can be defined by the terms porosity ε_P or 'pellet compactness' (Veiter and Herwig 2019), a more 'compact' pellet is fundamentally dense and features a smaller 'hairy' region. Studies in diffusivities and mass fluxes employing microelectrodes and evaluation of oxygen profiles indicate a negative correlation between compactness and D_{eff} (Hille et al. 2009).

Additionally, there are interlinks with substrate consumption: substrate oxidation inside the pellet causes rapid consumption of the diffused oxygen which makes substrate availability a critical process parameter with regard to oxygen limitation. During limiting substrate regimes oxygen penetration depth can be influenced based on different specific substrate uptake rates (Bodizs et al. 2007). Being the main trigger for productivity (Douma et al. 2010), substrate limiting regimes are widely used in state of the art production processes (Bodizs et al. 2007). Several articles describe the relation of specific growth rate, substrate availability and productivity (Douma et al. 2010, Tayeb and Lim 1986, Pirt and Righelato 1967). However, knowledge on the effect of oxygen penetration as a function of substrate availability is still scarce. By studying these influences, the aforementioned aspects and interlinks with pellet viability can be further addressed.

In this publication, our goal was to use a design of experiments (DOE) approach to analyse factors affecting pellet morphology and viability in *P. chrysogenum* fed-batch processes using novel morphological descriptors. Subsequently we performed optimization of said factors employing

multiple linear regression to achieve enhanced biomass viability and productivity. As potentially influencing factors we selected the power input (P/V), dissolved oxygen content (dO_2) and specific substrate uptake rate (q_s), morphological and physiological responses were analyzed by a previously established flow cytometry method. These responses depict pellet size and two novel morphological descriptors: pellet compactness (C) and viable pellet layer (vl). Statistical evaluation of fermentation results provided insights into the influence of examined factors on the measured responses. Combining the obtained information, optimal operating ranges for optimised pellet characteristics and productivity will be presented to define a design space ensuring an efficient and productive fed-batch process.

Material and methods

Strain

Spore suspensions of the P-14 *P. chrysogenum* candidate strain for penicillin production descending from the P-2 *P. chrysogenum* candidate strain (American Type Culture Collection with the access number ATCC 48271) were kindly provided by Sandoz GmbH (Kundl, Austria) and used for all experiments.

Bioreactor cultivations

All cultivations were performed in a DASGIP Mini parallel reactor system (working volume 4*2.0 L, Eppendorf, Germany). The batch was inoculated with approximately $2 \cdot 10^8$ spores/l. During batch phase pH was not controlled. The end of the batch was defined per default as an increase in pH of 0.5 by convention. After the batch, the broth was diluted with fed-batch medium (15% broth, 85% medium) and fed-batches were started. Details on batch and fed-batch media can be found in Posch and Herwig 2014.The fed-batch process lasted for approximately 150 - 170 h. Temperature was maintained at 25°C and pH was controlled at 6.5 via addition of KHO and H_2SO_4. During fed-batch phase, pH was kept constant at 6.5 ± 0.1 by addition of 20% (w/v) KOH or 15% (v/v) H_2SO_4, respectively. pH was measured using a pH probe (Hamilton, Bonaduz, Switzerland). After additional 12 h nitrogen and phenoxyacetate feeds were started at constant rates (6.5 ml/h for nitrogen and 2 ml/h for phenoxyacetate). A feed-forward controller was implemented to maintain a constant specific glucose uptake rate of biomass q_s.

The glucose feed was adjusted based on equation 2 which includes the actual biomass concentration within the bioreactor estimated by real-time model simulation of a literature model of *P. chrysogenum* (Paul et al. 1998), Paul and Thomas 1996). Further details on the biomass state estimation algorithm can be found in Stelzer et al. 2017, Kager et al. 2018.

$$(2)\ F_{(t)} = \frac{qs_{(t)} * X_{(t)} * V_{(t)}}{c_S} \qquad [L/h]$$

F(t)	feed flow rate [L/h] after time (t)
$q_s(t)$	biomass specific substrate uptake rate [g/g] at time point (t)
x(t)	Biomass concentration [g/L] at time (t)
V(t)	Reactor volume [L] at time (t)
c_s	substrate concentration in feed [g/L]

The stirrer was equipped with three six bladed Rushton turbine impellers, of which two were submersed and one was installed above the maximum liquid level for foam destruction. Aeration was controlled at 1 vvm in batch and initial fed-batch with mass flow controllers (Vögtlin, Aesch, Switzerland). Dissolved oxygen concentration was measured using a dissolved oxygen probe (Hamilton, Bonaduz, Switzerland) and controlled between 40% and 90% during batch and at the set-points 5.0, 22.5 % or 40.0% during fed-batch, via adjustment of the gas mix using pressurized air, nitrogen and oxygen. The agitation conditions were maintained at 325 rpm – 500 rpm stirring speed in the batch phase. For the duration of the entire fed-batch phase power input (P/V) was calculated according to equations by Rutherford et al. 1996, specifically equation (3) and (4), and controlled at the set-points 370, 1535 or 2000 W/m^3 via adjustment of stirrer speed.

$$(3)\ P/V = \rho * N_P * n^3 * d^5$$

$$(4)\ N_P = 6.57 - 64.771 * \left(\frac{b_t}{d}\right)$$

ρ	density medium [1022 kg/m^3]
N_P	Newton number [-]
n	agitation speed [rpm]
d	impeller diameter [45 mm]
b_t	blade thickness [1.25 mm]

CO_2 and O_2 concentration in the off gas were analysed with an off-gas analyser (DASGIP MP8, Eppendorf AG, Germany), using infrared and para-magnetic principle (Bluesens GmbH, Germany),

which were used as inputs for the biomass state observer as described in Stelzer et al. 2017, Kager et al. 2018.

Experimental design of bioreactor cultivations

A full factorial design including power input (P/V), dissolved oxygen (dO_2) concentration and availability of limiting substrate in the form of specific substrate uptake rate (q_s) was employed. The design for all bioreactor cultivations is depicted in Figure 1, in total 11+3 cultivations were performed. All relevant factors and respective nomenclature are summarized in Table 1. Multiple linear regression analysis was performed using the software MODDE10 (Umetrics, Umeå, Sweden).

The center point represents standard operation conditions (P/V = 1500 W/m^3, dO_2 = 22.5 %, q_s = 0.035 g/g/h). In order to generate a sufficient morphological response in the pellet fraction we used a wide range of P/V set-points based on preliminary experiments with 1500 W/m^3 as standard set-point. In two cultivations we exceeded the experimental boundary of 2000 W/m^3 to generate further morphological effects.

To maintain the P/V set-points the dO_2 was solely controlled via the in-flow gas mix composition. In addition, we employed various q_s and dO_2 set points to test our hypothesis: the specific substrate uptake rate affects the viable pellet layer due to inter-dependency of oxygen and substrate consumption.

Note that the highest q_s could not be sustained at low dO_2 for an entire cultivation (LHL and LLH as displayed in Figure 1).

Table 1. Multivariate experimental design of 11+3 bioreactor cultivations, nomenclature and factors with mean values over process time including standard deviation

Name	P/V [W/m^3]	q_s [$g_s/g_x/h$]	dO_2 [%]
LLL	370 ± 10	0.017 ± 0.003	5.0 ± 1.5
HLL	2012 ± 20	0.018 ± 0.001	5.0 ± 1.6
LHL	370 ± 12	0.040 ± 0.012	5.0 ± 3.1
HHH1	1900 ± 15	0.042 ± 0.004	40.0 ± 6.5
LLH	370 ± 11	0.015 ± 0.004	40.0 ± 5.2
MMH	1535 ± 20	0.038 ± 0.003	40.0 ± 4.1
LHH	370 ± 14	0.045 ± 0.004	40.0 ± 5.2
HHH2	2700 ± 15	0.049 ± 0.005	40.0 ± 7.5
CP1	1535 ± 11	0.034 ± 0.005	22.5 ± 6.6
CP2	1535 ± 11	0.033 ± 0.005	22.5 ± 5.0
CP3	1535 ± 12	0.035 ± 0.003	22.5 ± 6.9
MHH	1113 ± 14	0.054 ± 0.005	40.0 ± 5.4
CP4	1535 ± 32	0.026 ± 0.003	22.5 ± 3.9
HHH3	3000 ± 34	0.050 ± 0.005	40.0 ± 9.5

Flow cytometry

Samples from fed-batch cultivations were diluted 1:10 into phosphate buffered saline (50 g/l of 2.65 g/l $CaCl_2$ solution, 0.2 g/l KCl, 0.2 g/l KH_2PO_4, 0.1 g/l $MgCl \cdot 6\ H_2O$, 8 g/l NaCl and 0.764 g/l $Na_2HPO_4 + 2\ H_2O$) and stained with propidium iodide (Sigma Aldrich, St. Louis, Missouri/USA; 20 mM stock dissolved in DMSO ≥ 99.9 %, diluted with phosphate buffered saline to a final concentration of 20 µM) and fluorescein diacetate (Sigma Aldrich, St. Louis, Missouri, USA; stock solution of 5 g/l dissolved in acetone ≥ 99.9% to a final concentration of 5 mg/l).

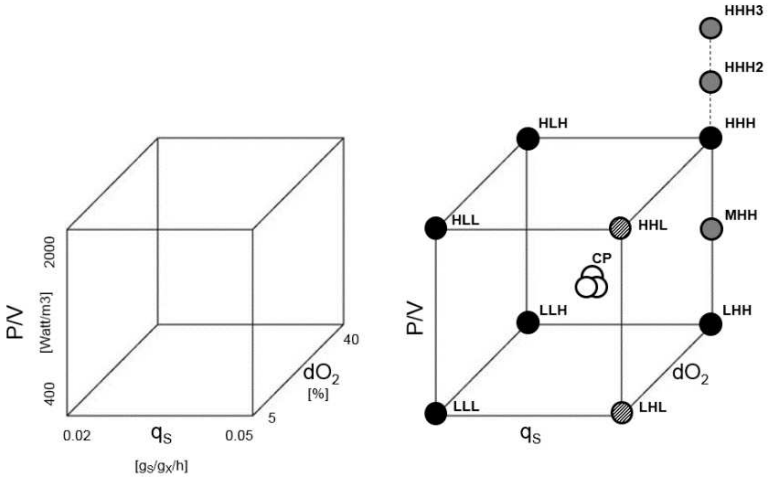

Figure 1. Experimental design of bioreactor cultivations (left). Factor ranges of bioreactor cultivations including nomenclature (right): additional cultivations exceeding the standard number of experiments along the P/V range (grey circles), centre-points (white circles), cultivations were set-points could not be sustained due to external constraints (painted circles).

A CytoSense flow cytometer (CytoBuoy, Woerden, Netherlands) with two forward scatter (FSC), one sideward scatter (SSC) and two fluorescence channels (green, red) was used for particle analysis. The implemented laser had a wavelength of 488 nm. The configuration of the filter set was 515-562 ± 5 nm for the green fluorescence channel (FL-green, used for fluorescein diacetate) and 605-720 ± 5 nm for the red fluorescence channel (FL-red, used for propidium iodide). The device was equipped with a PixeLINK PL-B741 1.3MP monochrome camera for in flow image acquisition. For data treatment, the software CytoClus3 (CytoBuoy, Woerden, Netherlands) and a custom-programmed Matlab 2016b script (MathWorks, Nattick, Massachusetts, USA) were used.

The flow cytometry method allows for determination of the following responses as depicted in Figure 2: volume ratio of pellets in relation to all morphological classes (= pellet ratio in %), average size of pellets (pellet size in µm), pellet compactness (no unit) and viable pellet layer (vl in µm). Further details on the method including data evaluation can be found in Veiter and Herwig 2019.

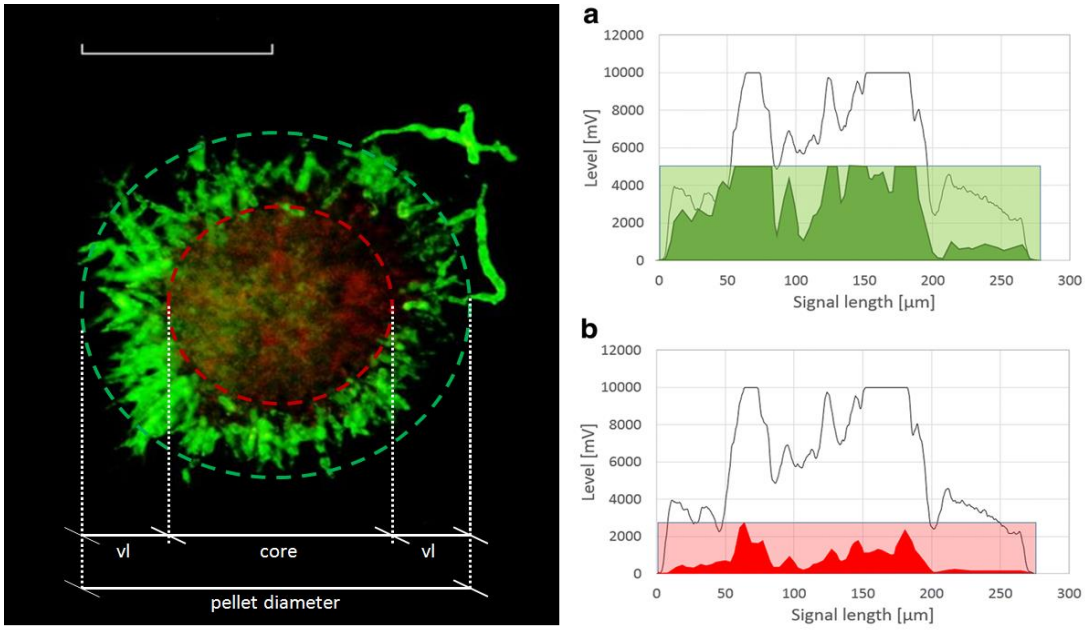

Figure 2. Left: confocal microscopy of pellet with enhanced contrast depicting pellet diameter, viable layer (vl), compact core region (red circle) and hairy outer region (green circle). White line = 50 µm. Right: corresponding signal profiles from flow cytometry depicting (a) viable area across pellet diameter and (b) degraded area in the pellet's core according to Veiter and Herwig 2019.

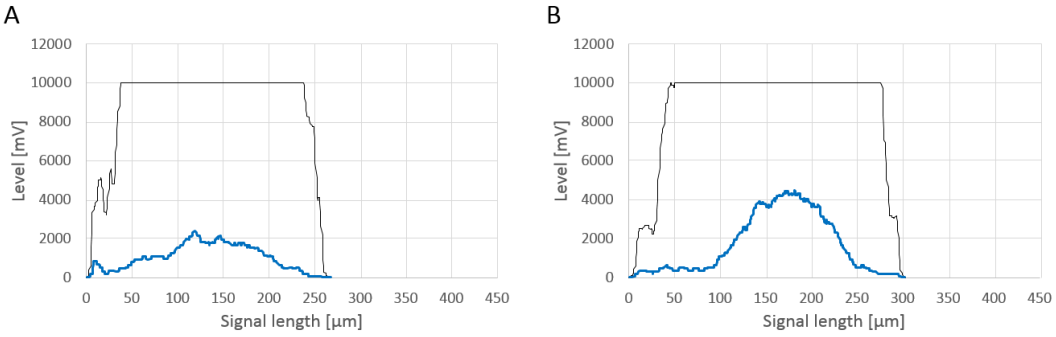

Figure 3. Spatially resolved pellet signal profiles, FSC signal (black) and SSC signal (blue). Pellet with low compactness (A) and high compactness (B) according to SSC signal.

As depicted in Figure 3, compactness can be obtained from the analysis of SSC signal length in combination with particle size, hereafter termed 'Compactness according to SSC' and calculated according to the following equation:

$$(5)\ \text{Compactness}_{SSC} = \frac{\text{Length of SSC signal [µm]}}{\text{Particle diameter [µm]}}$$

To further estimate pellet viability and demonstrate the relation of viable layer to pellet size, a viability factor was calculated according to equation 6.

$$(6)\ \text{viability factor vf}\,[-] = \frac{2 * \text{viable layer [µm]}}{\text{pellet size [µm]}}$$

HPLC analytics

High performance liquid chromatography (HPLC) using a Thermo Scientific UltiMate 3000 system (Thermo Fisher Scientific, Massachusetts, United States) with a Zorbax Eclipse AAA C18 column (Agilent Technologies, Santa Clara, USA) was used to quantify penicillin V and phenoxyacetic acid concentration with a buffer as described elsewhere (Ehgartner, Fricke (19)). A flow rate of 1.0 ml/min was applied and the temperature of the column oven was 30°C. The UV/VIS detector for determining penicillin and phenoxyacetic acid peaks via absorption was set to 210 nm.

Results and discussion

Multiple linear regression

The effects of process parameters on DoE responses across process time (see Table 1) are exemplarily displayed for cultivation LLH in Figure 4: Due to low a P/V distinct effects on pellet size and pellet compactness are visible. Furthermore, low q_s and simultaneously high dO_2 affect viability and productivity alike. All these interactions were analysed will be discussed in detail in the following section:

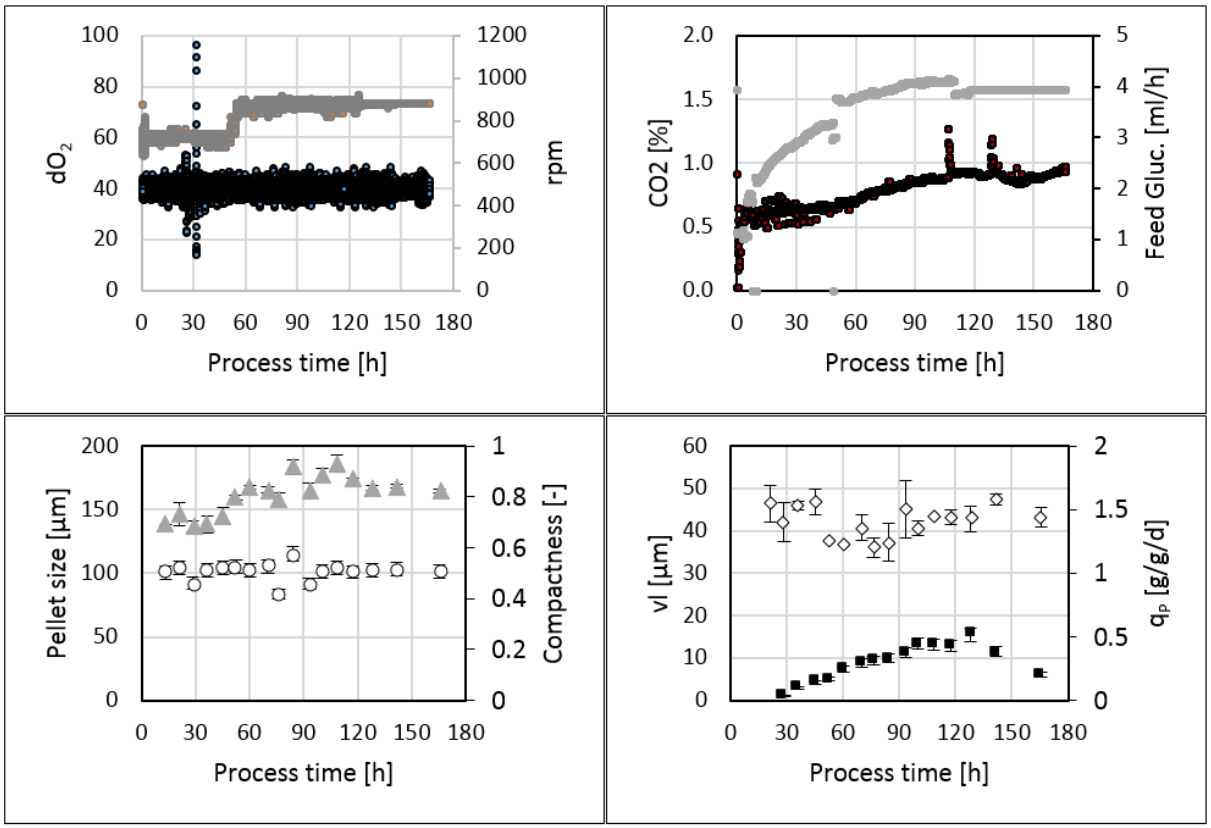

Figure 4. Top: process data across process time: dO_2 (black), agitation via rpm (grey), CO_2 in off-gas (black), glucose feeding rate (grey). Bottom: responses across process time: pellet size (grey triangles), compactness (circles), viable layer (circles) and specific productivity (black rectangles).

All responses were subjected to single factor ANOVA analysis ($\alpha = 0.05$) to test for statistically significant results rather than noise indicated by p-values of less than 0.05. For all responses the F-value is greater than the F-critical value for the alpha level selected (0.05), indicating significantly different means in the samples which thus belong to an entirely different population. Detailed information on the results from ANOVA analysis can be found in Table 2.

To subsequently analyse all morphological and physiological responses considered in this study in a combined fashion, multiple linear regression (MLR) was used to study the effects on responses: mean pellet size, mean pellet compactness (C), mean viable pellet layer (vl) and mean specific productivity (q_P). Mean values of each response over the entire process time were considered for this. Table 3 summarizes factors and responses generated from all 14 bioreactor cultivations performed in this study as depicted in Figure 1. Model statistics are summarised and specified as a summary-of-fit displayed in Table 4. Overviews detailing summary-of-fit for all responses are displayed in Supplementary Figures 1 – 5.

Morphological responses apart from pellet compactness are well described by MLR (see Table 3), these responses are dependent upon the factor power input. Issues in model fitting regarding pellet compactness can be explained by the low number of cultivations (only 3) featuring increased compactness due to a maximum power input over 2000 W/m^3 in the uppermost region of the design space far from the normal operating range. These outliers lead to statistically significant model problems and low model validity. The impact of power input on morphology will be discussed in the detail in the section: 'Impact of power input on morphology'.
Viability and productivity are foremost dependent on the factor q_s which will be examined below in the sections: 'Impact of factors on viability' and 'Interlink between productivity and specific substrate uptake'.

Table 2. Single-factor ANOVA analysis ($\alpha = 0.05$) of responses

Response	F - value	p – value	Critical F - value
Pellet size	71.0	$9.9 * 10^{-61}$	1.97
Pellet compactness C	529.3	$5.5 * 10^{-63}$	1.97
Viable layer vl	20.3	$9.4 * 10^{-23}$	1.98
Specific productivity q_P	8.9	$1.8 * 10^{-9}$	2.02

Table 3. Design space, factors and responses including standard deviations from full factorial study comprising 11 + 3 additional bioreactor cultivations.

Name	P/V [W/m^3]	q_s [$g_s/g_x/h$]	dO_2 [%]	mean pellet size [µm]	mean C [-]	mean vl [µm]	mean q_P [$g_P/g_X/d$]
LLL	370	0.017	5.0	150.7 ± 9.5	0.51 ± 0.02	31.5 ± 5.1	0.18 ± 0.12
HLL	2012	0.018	5.0	129.3 ± 4.5	0.88 ± 0.03	38.6 ± 3.0	0.19 ± 0.09
LHL	370	0.040	5.0	183.1 ± 9.3	0.52 ± 0.02	22.1 ± 9.8	0.02 ± 0.01
HHH1	1900	0.042	40.0	135.7 ± 9.0	0.61 ± 0.03	33.6 ± 3.1	0.41 ± 0.24
LLH	370	0.015	40.0	161.7 ± 9.0	0.48 ± 0.02	40.1 ± 4.2	0.29 ± 0.23
MMH	1535	0.038	40.0	136.5 ± 5.8	0.48 ± 0.01	33.1 ± 3.0	0.38 ± 0.17
LHH	370	0.045	40.0	142.3 ± 5.3	0.44 ± 0.03	28.9 ± 2.9	0.29 ± 0.17
HHH2	2700	0.049	40.0	128.7 ± 5.1	0.85 ± 0.02	31.7 ± 2.3	0.34 ± 0.21
CP1	1535	0.034	22.5	136.5 ± 8.0	0.49 ± 0.05	36.4 ± 3.1	0.44 ± 0.19
CP2	1535	0.033	22.5	136.1 ± 5.8	0.48 ± 0.02	33.3 ± 3.5	0.40 ± 0.16
CP3	1535	0.035	22.5	129.6 ± 4.5	0.49 ± 0.03	38.1 ± 3.0	0.48 ± 0.21
MHH	1113	0.054	40.0	128.0 ± 5.1	0.49 ± 0.02	28.0 ± 3.1	0.13 ± 0.09
MMM	1535	0.026	22.5	141.7 ± 6.9	0.50 ± 0.03	40.1 ± 4.2	0.29 ± 0.13
HHH3	3000	0.050	40.0	120.8 ± 5.1	0.88 ± 0.03	31.0 ± 3.2	0.30 ± 0.19

Table 4. Summary of fit for model responses. Ranges to differentiate good models according to MODDE: R2 (> 0.5), Q2 (> 0.1 for a significant model, > 0.5 for good model), Model validity (> 0.25), Reproducibility (> 0.5).

Model response	Model parameter (95 % significance level)	R2	Q2	Model validity	Reproducibility
Pellet size	P/V	0.60	0.43	0.50	0.93
Pellet compactness	P/V	0.58	0.45	-	0.99
Viable pellet layer	q_s, P/V, dO_2	0.78	0.58	0.88	0.71
Mean specific productivity	q_s	0.71	0.48	0.58	0.91

Impact of power input on morphology

Morphological classification was performed as previously established by Ehgartner et al. 2017. This method enables classification according to hyphae, small clumps, large clumps and pellets. Summarising, gate setting is based on particle size in combination with SSC total to account for particles form. In the following, pellets were analysed as most relevant morphological class as it encompasses 80 – 90 % in relation to other classes. Within Figure 5 time resolved responses of two extreme power input points are presented.

Both bioreactor cultivations are morphologically very diverse due to a considerably different power input controlled at either 400 W/m^3 or 2000 W/m^3. Average pellet size is increased by over 20 µm on average at lower power input. Compactness was calculated using SSC signals according to equation 4 as described by Veiter and Herwig 2019. Pellet compactness is greatly increased at power inputs exceeding 2000 W/m^3.

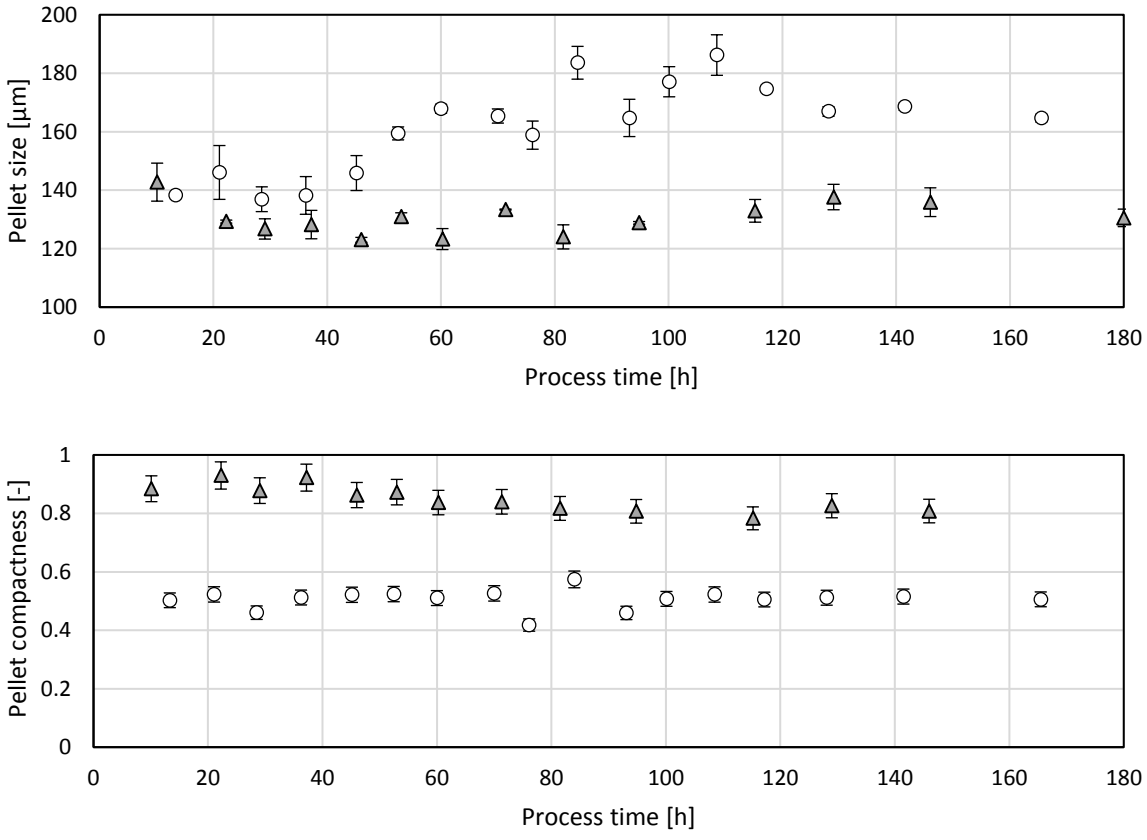

Figure 5. Morphological assessment of two bioreactor cultivations differing in power input. High power input at over 2000 W/m^3 (triangles), low power input at 400 W/m^3 (circles). Top: size of pellets, bottom: compactness of pellets across process time.

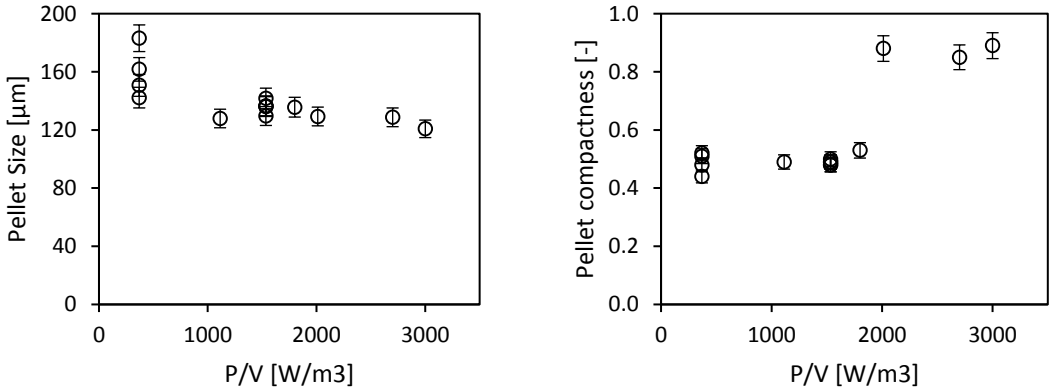

Figure 6. Dependence of morphological responses on power input, mean values from all bioreactor cultivations. Left: pellet size, right: pellet compactness.

When looking at the entirety of bioreactor cultivations, Figure 6 clearly demonstrates that all measured morphological responses are highly affected by the power input. Specifically, pellet fraction (in relation to all morphological classes) and pellet size are inversely proportional to power input while pellet compactness reacts proportionally. This is in accordance with literature (Cui et al. 1997), where agitation effects have been reported which can either break up the pellet (i), or shave-off the pellet's hairy region (ii). Our results on pellet compactness are in accordance with the latter phenomenon. The impact of these morphological effects on viability will be further explained in the section 'Impact of factors on viability'.

Impact of factors on viability

As described in the introduction, we expected dependencies of the viable pellet layer on q_s and dO_2. Trajectories of viable layer for two cultivations clearly display degradation of pellet biomass at high q_s and low dissolved oxygen content across process time (see Figure 7).

These results clearly indicate that on the one hand the viable layer depends on dO_2, however on the other hand oxygen and glucose consumption are very much interconnected: oxygen consumption is likely triggered by glucose consumption as described in the introduction ((Bodizs et al. 2007).

Multiple linear regression further reveals the effects of q_s and dO_2 on pellet viability. The coefficient plot (see Figure 8) on the response viable layer reveals the negative impact of q_s, which also represents the largest effect of all the factors. Consequently, the viable pellet layer is indirectly proportional to q_s as depicted in Figure 8. As expected, we also observe a positive effect of dO_2. Regarding the depicted advantageous effects of higher power inputs, we can remark that although dO_2 was controlled via the gas mix, its control is still facilitated by a high power input with advantageous effects on mixing time and k_La (Garcia-Ochoa and Gomez 2009).To further estimate pellet viability and demonstrate the relation of viable layer to pellet size, a viability factor was calculated according to equation 6.

The effect of increased pellet compactness on diffusional limitations can be depicted in a correlation between compactness and diffusion factor adapted from Hille et al. 2009 whereas a so-called hyphal gradient in the pellet periphery was established comparable to pellet compactness. For the here presented data, the impact of increasing compactness on diffusion and furthermore viability is depicted in Supplementary Figure 1. Results suggest that compactness levels exceeding 0.8 have negative effects on viability, however most bioreactor cultivations considered in this study feature lower compactness levels due to more moderate power inputs in the standard operating range.

These interlinks between substrate uptake and diffusional limitations not only affect viability but can be exploited favourably in order to increase productivity, which will be discussed in the following section.

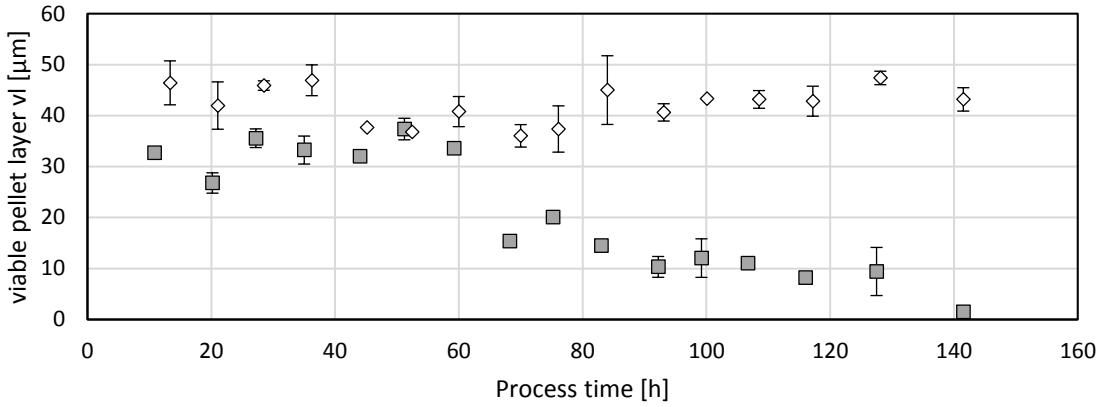

Figure 7. Viable layer of two bioreactor cultivations across process time. High q_s of 0.04 $g_S/g_X/h$ and low dO_2 content of 5 % (grey rectangles), low q_s of 0.015 $g_S/g_X/h$ and dO_2 content of 40 % (white diamonds).

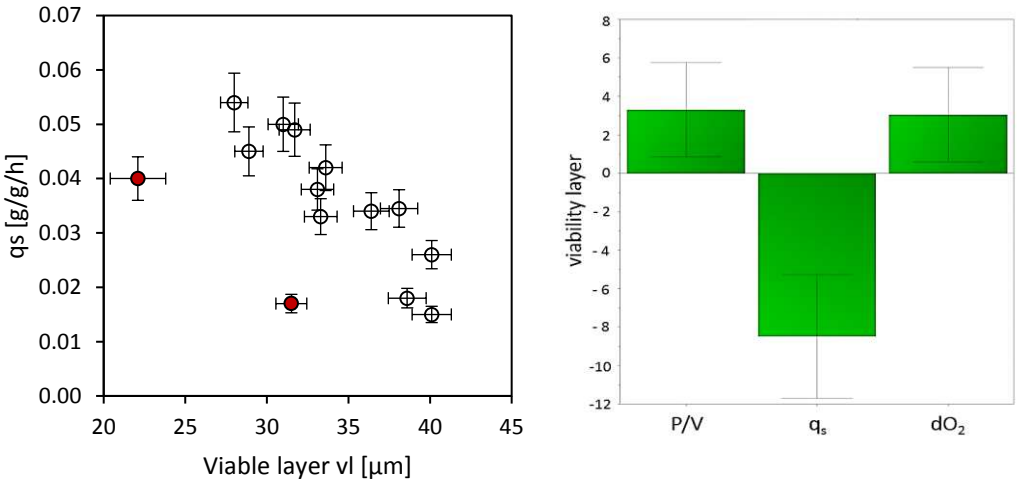

Figure 8. Dependence of viable layer on specific substrate uptake rate. Red triangles indicate bioreactor cultivations at low dissolved oxygen set-points (left). Coefficient plot of the factors 'P/V', 'q_s' and 'dO_2' and their effects on the viable pellet layer (right). Interaction terms were omitted because they were not significant according to MODDE.

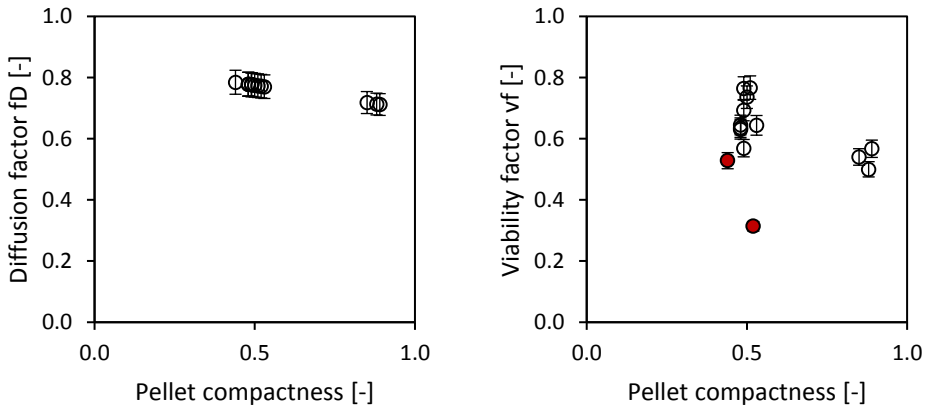

Figure 9. Impact of compactness on diffusion factor (top) and viability factor (bottom). Red circles indicate bioreactor cultivations at low dO_2 set-points.

Interlink between productivity and specific substrate uptake

As demonstrated in Supplementary Figure 2, the trajectories of specific productivity (q_p) reach a maximum and subsequently start to decline within 10 – 20 hours of cultivation time. Each trajectory is dependent on the corresponding q_s. As a consequence, cultivations employing a high q_s reach their productivity maximum faster but also start to decline much earlier. This earlier decline phase is also reflected in a loss in viability as previously demonstrated in Figure 6.

When plotting the mean q_p against q_s, a positive correlation is shown at low growth levels as depicted in Figure 9. However, q_p declines at increasing q_s values. Literature suggests interlinks to the rate-limiting enzyme isopenicillin-N synthase, which is essential to penicillin production (Douma et al. 2010). Our data indicates that the threshold for this decline in q_P is at a q_s of 0.04 g/g/h as already discussed in the MLR section.

The response viable pellet layer is foremost dependent on q_s. Similarly, q_s has also a considerable impact on q_p. Both aspects can be used to determine an optimal operating range as depicted in the following section.

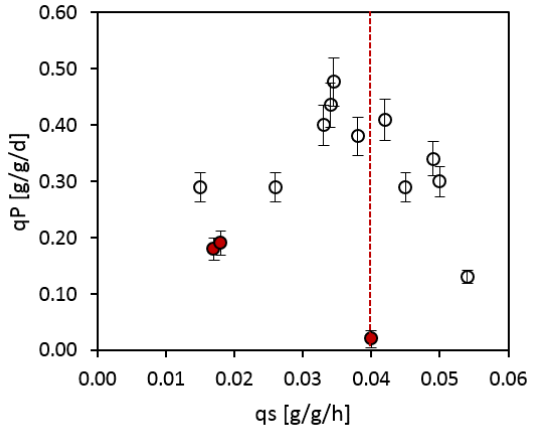

Figure 10. Dependence of specific productivity q_p on substrate uptake rate q_s. Red triangles indicate bioreactor cultivations at low dissolved oxygen set-points. Red dotted line indicates q_s threshold of q_P decline.

Optimal process design space

Due the high number of interdependencies, optimisation efforts need to be performed with all DOE factors and corresponding responses in mind. A 'sweet spot' plot generated by MODDE displaying the optimum of q_s and P/V for a dO_2 level of 40 % is depicted in Figure 10. Response ranges for this plot were set as: viable layer: 31 – 40 µm, mean q_p: 0.45 – 0.48, compactness: 0.5 – 0.6. Note that the 'sweet spot' at these response ranges can only be achieved at the higher dO_2 level of 40 %.

Cultivation MMH meets the optimal operating range criteria, an overview on this cultivation is provided in Figure 11. Mean pellet size was 136.5 ± 5.8 µm, mean compactness was 0.48 ± 0.02, mean viable layer was 33.1 ± 3.0 µm and mean specific productivity was 0.38 g/g/d. With a considerable standard deviation across process time of ± 0.17 q_p values of 0.7 g/g/d were well exceeded in this cultivation.

Conclusions

From an industrial point of view, several aspects contribute to ensuring the maximum of process efficiency. The highest possible space-time-yield can be achieved via an optimised operating range of several factors: a feed regime dependent on q_s ensures a sound compromise between productivity and viability, at the same time favourable morphological conditions can be ensured through controlled power input.

The optimal design space was identified as follows: We were able to maintain a high number of pellets with favourable pellet compactness at a power input of 1500 W/m^3. As demonstrated in section 'Optimal operating range' (see Figure 9), the compromise between viability and productivity is represented by a q_s of 0.040 – 0.045 g/g/h at the dO_2 level of 40 %. We were able to identify these advantageous fermentation parameters through a DoE approach in combination with novel morphological descriptors identified by flow cytometry analysis.

For further process optimization, we envision a feeding profile with several q_s levels across process time starting with a high q_s of 0.05 g/g/h to quickly reach optimal q_p-phases. To maintain a high q_p and viability, q_s should be decreased below 0.02 g/g/h for the remainder of the cultivation process.

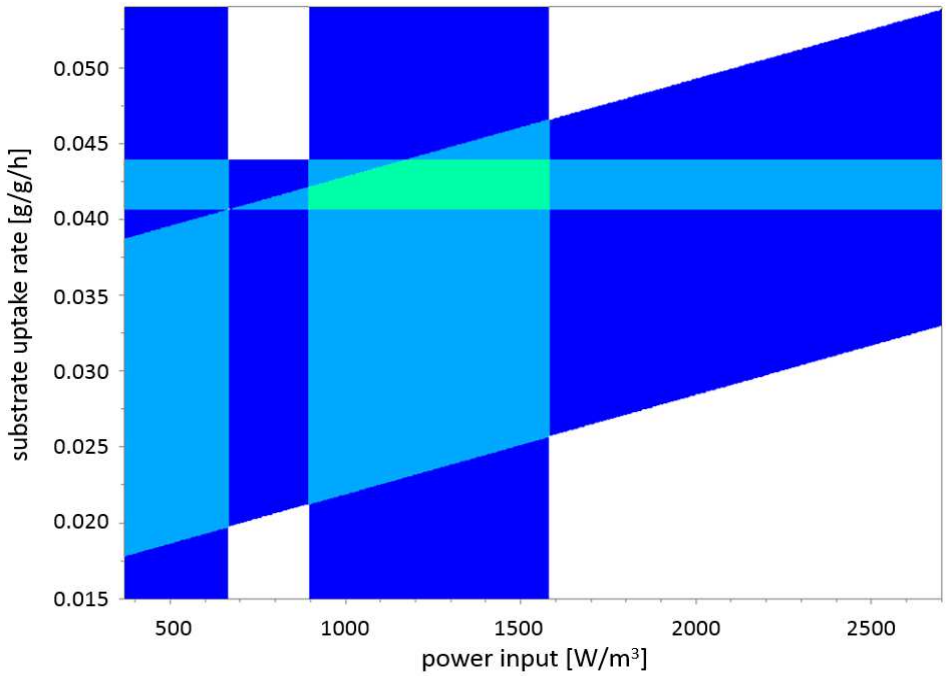

Figure 11. Sweet spot plot (green area) based on the following properties: viability factor: 0.6 – 0.75, viable layer: 31 – 40 µm, mean q_p: 0.45 – 0.48, compactness: 0.5 – 0.6 at a pellet fraction: 75 – 95 % of the whole biomass according to morphological classification. Dissolved oxygen content: 40 %. Dark blue areas signify that two criteria are met, light blue areas signify that three criteria are met.

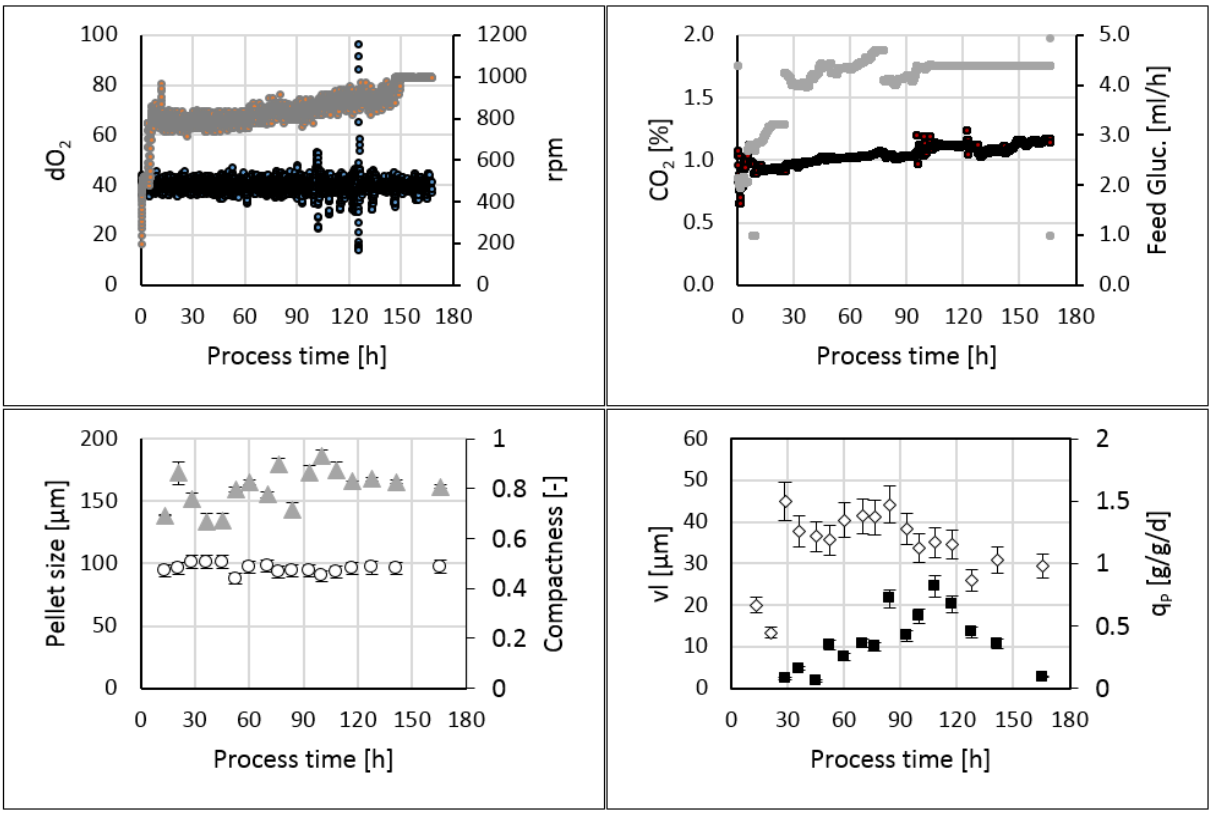

Figure 12. Cultivation MMH. Top: process data across process time: dO_2 (black), agitation via rpm (grey), CO_2 in off-gas (black), glucose feeding rate (grey). Bottom: responses across process time: pellet size (grey triangles), compactness (circles), viable layer (circles) and specific productivity (black rectangles).

Author's contributions

LVE, JKA and CHE designed the study. LVE and JKA performed all cultivation experiments and analysed the data. LVE designed the underlying flow cytometry method and evaluated morphological and viability data from flow cytometry measurements. JKA designed the q_s control. LVE and JKA wrote the paper. CHE guided the study and gave valuable scientific input.

Acknowledgements

We thank the Austrian Federal Ministry of Science, Research and Economy in course of the Christian Doppler Laboratory for Mechanistic and Physiological Methods for Improved Bioprocesses for financial support. Strains for the experiments were gratefully provided by Sandoz GmbH (Kundl, Austria).

Compliance with Ethical Standards

Funding: This study was funded by Austrian Federal Ministry of Science, Research and Economy in course of the Christian Doppler Laboratory for Mechanistic and Physiological Methods for Improved Bioprocesses (grand number 171).
Conflict of Interest: The authors declare that they have no conflict of interest.

Ethical approval: This article does not contain any studies with human participants or animals performed by any of the authors.

References

Bodizs L, Titica M, Faria N, Srinivasan B, Dochain D, Bonvin D (2007) Oxygen control for an industrial pilot-scale fed-batch filamentous fungal fermentation. J Process Contr 17: 595-606

Cui YQ, van der Lans RG, Luyben KC (1997) Effect of agitation intensities on fungal morphology of submerged fermentation. Biotechnol Bioeng 55: 715-726

Douma RD, Verheijen PJ, de Laat WT, Heijnen JJ, van Gulik WM (2010) Dynamic gene expression regulation model for growth and penicillin production in *Penicillium chrysogenum*. Biotechnol Bioeng 106: 608-618

Ehgartner D, Herwig C, Fricke J (2017) Morphological analysis of the filamentous fungus *Penicillium chrysogenum* using flow cytometry-the fast alternative to microscopic image analysis. Appl Microbiol Biotechnol 101: 7675-7688

Garcia-Ochoa F, Gomez E (2009) Bioreactor scale-up and oxygen transfer rate in microbial processes: an overview. Biotechnol Adv 27, 153-176

Hille A, Neu TR, Hempel DC, Horn H (2005) Oxygen profiles and biomass distribution in biopellets of *Aspergillus niger*. Biotechnol Bioeng 92: 614-623

Hille A, Neu TR, Hempel DC, Horn H (2009) Effective diffusivities and mass fluxes in fungal biopellets. Biotechnol Bioeng 103, 1202-1213

Kager J, Herwig C, and Stelzer IV (2018) State estimation for a penicillin fed-batch process combining particle filtering methods with online and time delayed offline measurements. Chem Eng Sci 177: 234-244

Nielsen J, Johansen CL, Jacobsen M, Krabben P, Villadsen J (1995) Pellet formation and fragmentation in submerged cultures of *Penicillium chrysogenum* and its relation to penicillin production. Biotechnol Prog 11: 93-98

Paul GC, Syddall MT, Kent CA, Thomas CR (1998) A structured model for penicillin production on mixed substrates. Biochem Eng J 2: 11-21

Paul GC, Thomas CR (1996) A structured model for hyphal differentiation and penicillin production using *Penicillium chrysogenum*. Biotechnology and Bioengineering 51: 558-572

Paul GC, Thomas CR (1998) Characterisation of mycelial morphology using image analysis. Adv Biochem Eng Biotechnol 60: 1-59

Pirt SJ, Righelato RC (1967) Effect of Growth Rate on the Synthesis of Penicillin by *Penicillium chrysogenum* in Batch and Chemostat Cultures. Appl Microbiol 15: 1284-1290

Posch AE, Herwig C (2014) Physiological description of multivariate interdependencies between process parameters, morphology and physiology during fed-batch penicillin production. Biotechnol Prog 30: 689-699

Rutherford K, Mahmoudi SMS, Lee KC, Yianneskis M (1996) The influence of Rushton impeller blade and disk thickness on the mixing characteristics of stirred vessels. Chem Eng Res Des 74: 369-378

Stelzer IV, Kager J, Herwig C (2017) Comparison of Particle Filter and Extended Kalman Filter Algorithms for Monitoring of Bioprocesses. Comput-Aided Chem En 40b: 1483-1488

Tayeb YJ, Lim HC (1986) Optimal Glucose Feed Rates for Fed-Batch Penicillin Fermentation - an Efficient Algorithm and Computational Results. Ann Ny Acad Sci 469: 382-403

Vansuijdam JC, Metz B (1981) Fungal Pellet Breakup as a Function of Shear in a Fermenter. J Ferment Technol 59: 329-333

Veiter L, Herwig C (2019) The filamentous fungus *Penicillium chrysogenum* analysed via flow cytometry-a fast and statistically sound insight into morphology and viability. Appl Microbiol Biotechnol

Veiter L, Rajamanickam V, Herwig C (2018) The filamentous fungal pellet-relationship between morphology and productivity. Appl Microbiol Biotechnol 102: 2997-3006

Walisko R, Moench-Tegeder J, Blotenberg J, Wucherpfennig T, Krull R (2015) The Taming of the Shrew--Controlling the Morphology of Filamentous Eukaryotic and Prokaryotic Microorganisms. Adv Biochem Eng Biotechnol 149: 1-27

Zhang J, Zhang J (2016) The filamentous fungal pellet and forces driving its formation. Crit Rev Biotechnol 36: 1066-1077

Supplementary Figures

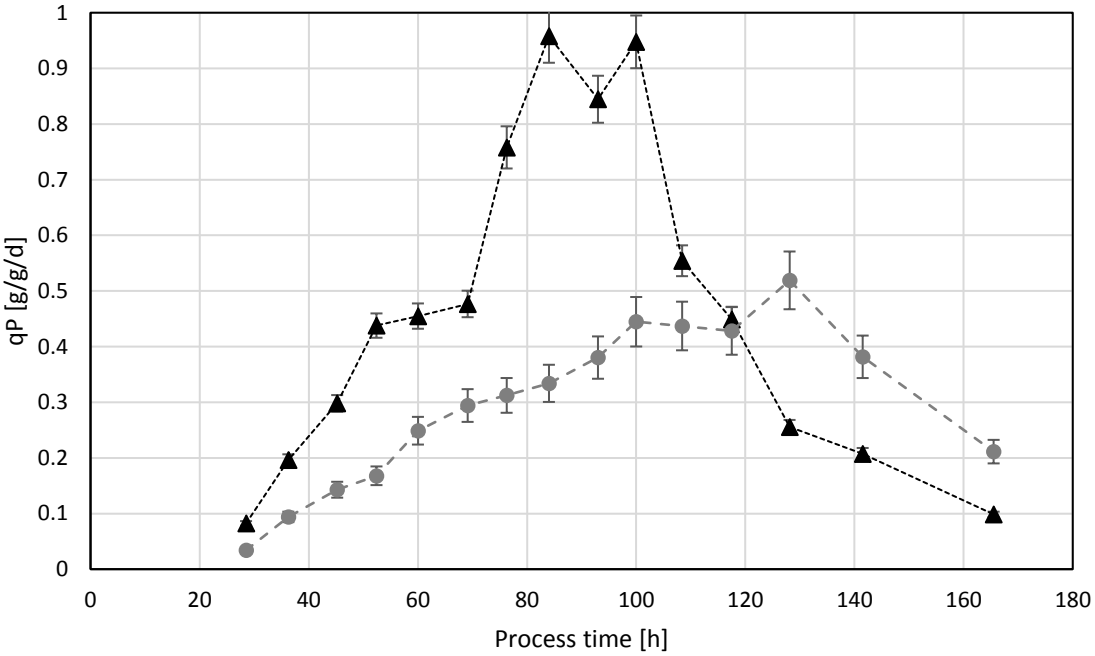

Supplementary Figure 1. Trajectories of specific productivity over process time for cultivations at high specific substrate uptake rate q_s (black triangles) and low q_s (grey circles).

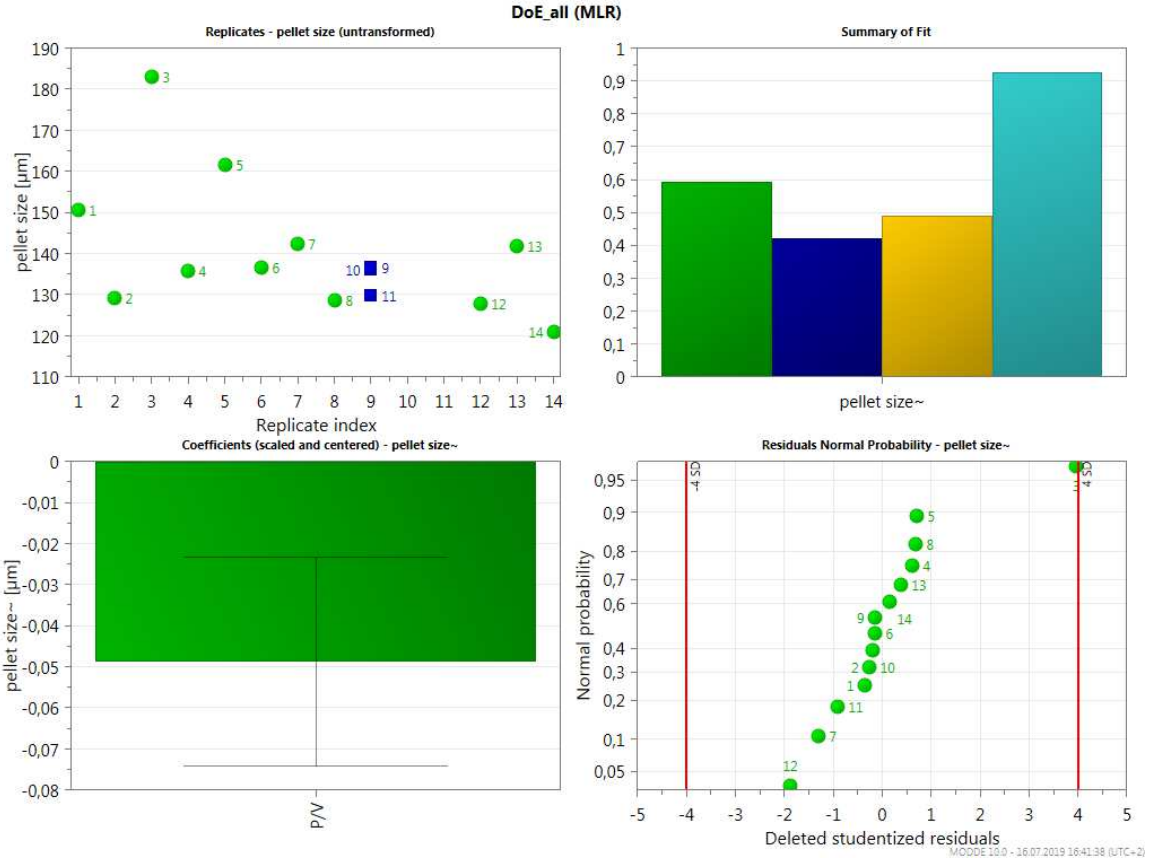

Supplementary Figure 2. Overview for response pellet size: replicates, summary of fit, coefficients, residuals normal probability.

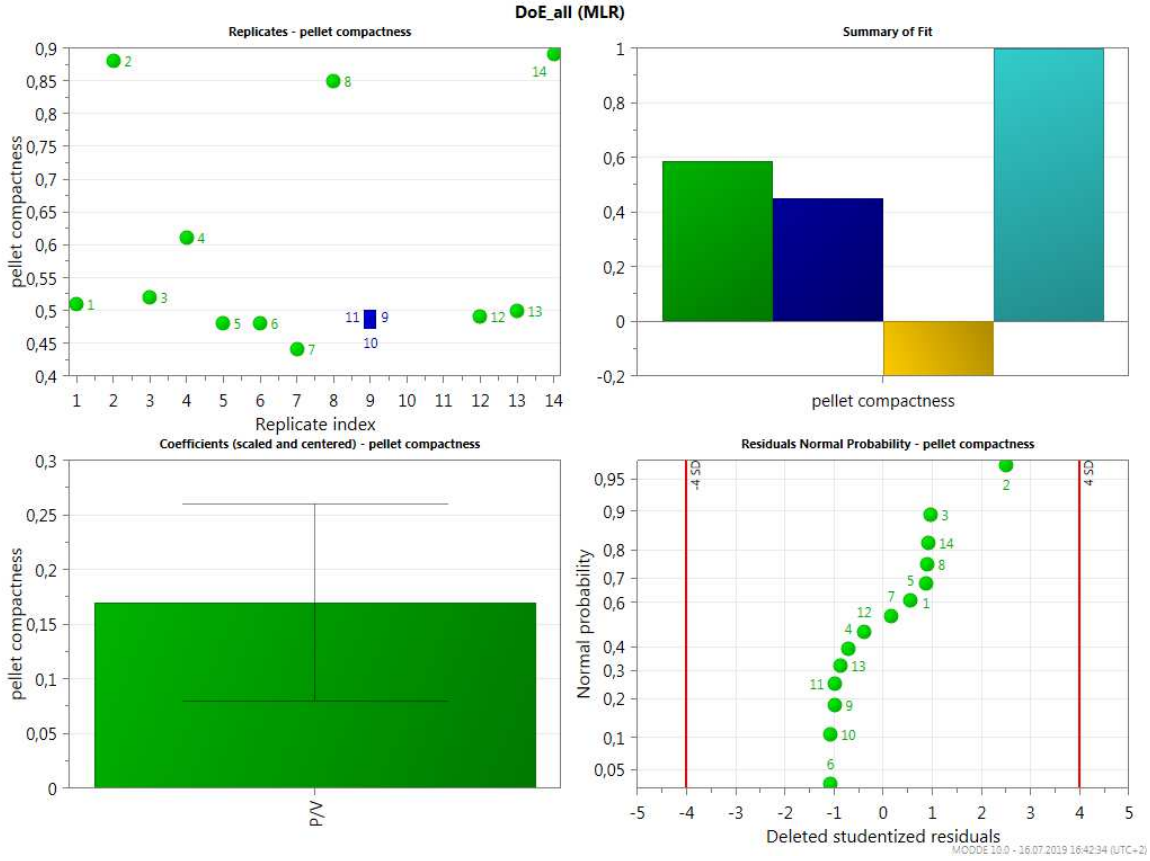

Supplementary Figure 3. Overview for response pellet compactness: replicates, summary of fit, coefficients, residuals normal probability.

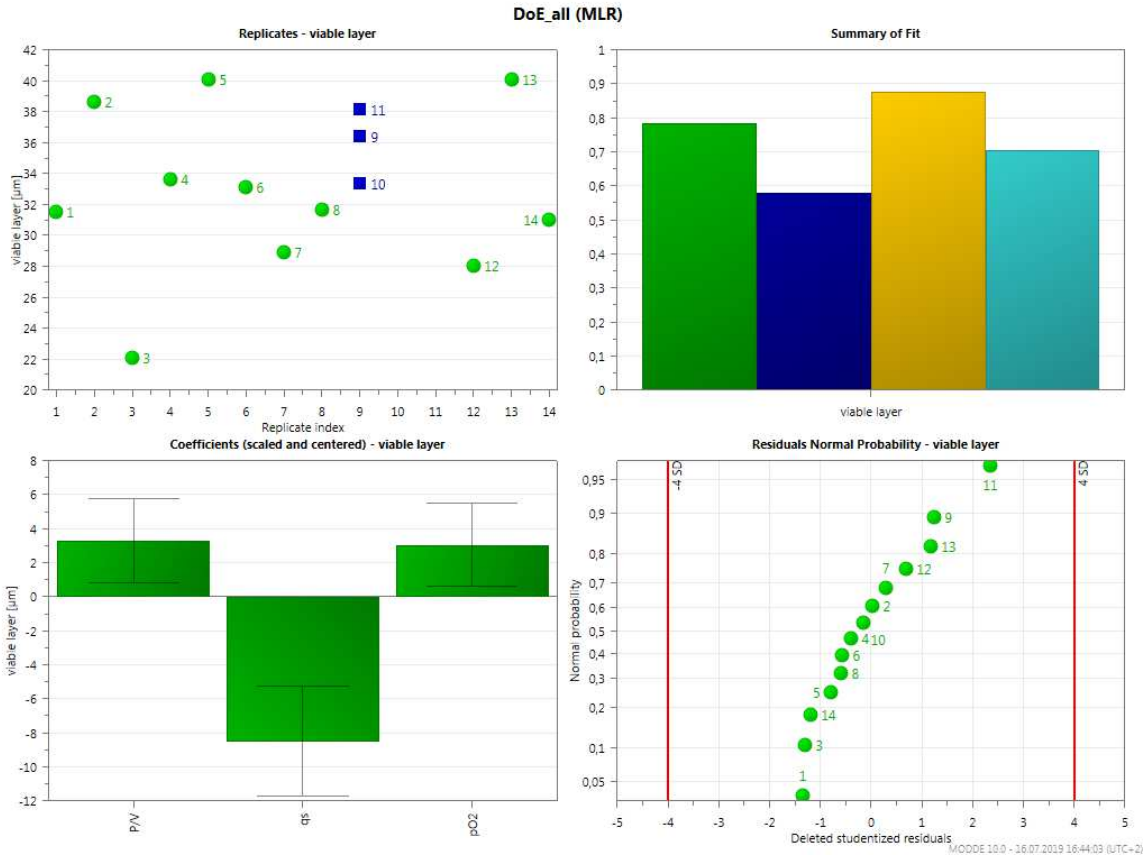

Supplementary Figure 4. Overview for response viable layer: replicates, summary of fit, coefficients, residuals normal probability.

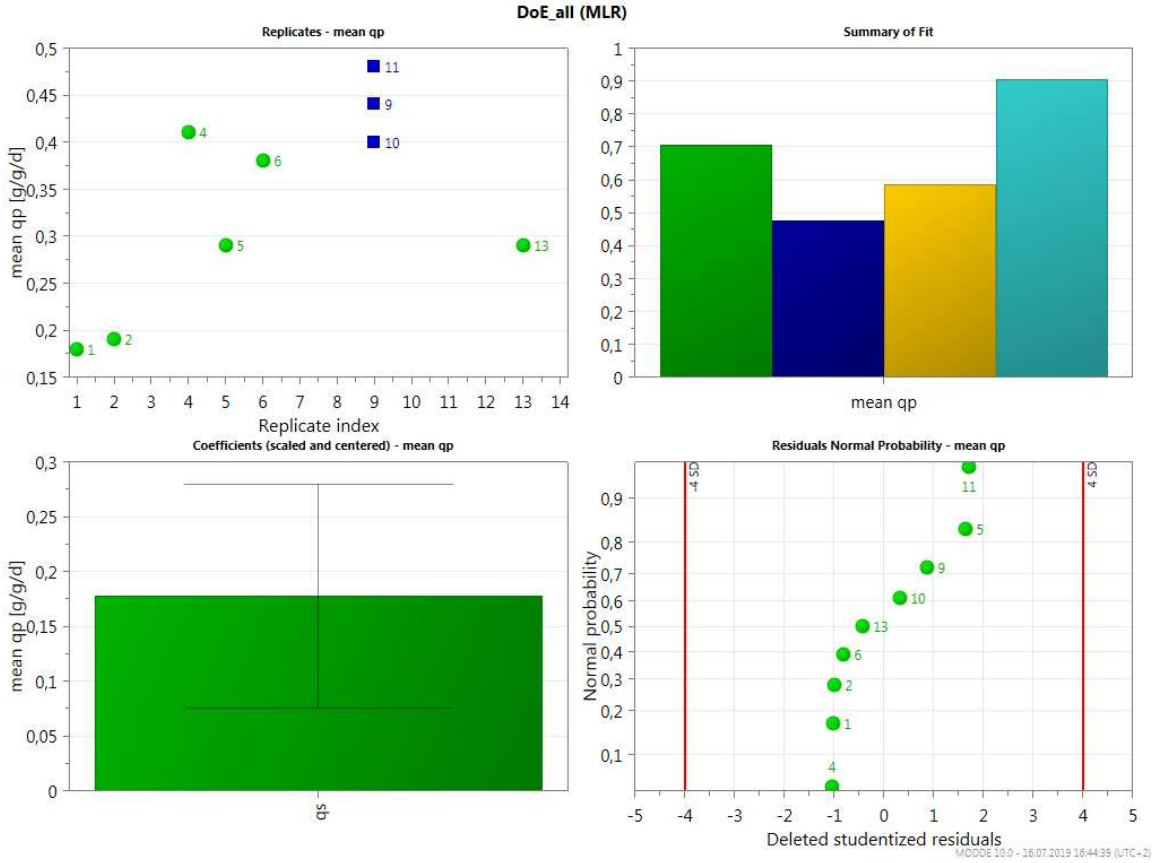

Supplementary Figure 5. Overview for response mean q_P: replicates, summary of fit, coefficients, residuals normal probability.

Chapter 7.
Impact

Scientific and industrial impact

Biochemical engineering is inherently a field dealing with applied science. We have outlined the challenges of PAT in filamentous bioprocesses in the introduction of this Thesis. The approach and findings of our research fits well into these challenges:

Our method development compiled in 'Chapter 5. Analytics' provides alternative solutions to existing challenges in filamentous fungi or leads to novel morphological insight through measurement of previously unknown morphological and physiological responses. Subsequently we have employed these analytical methods in the field of process control: several approaches to timely assess viable biomass were used to control the specific growth rate of filamentous biomass, novel morphological responses were studied to define optimised operating ranges to ensure high viability and productivity in *P. chrysogenum* bioreactor cultivations.

The basis for all our work is an industrial project. Therefore, our goals and hypothesis were specifically tailored to industrial needs, including:

- Filamentous organisms exhibit a complex morphological behaviour and undergo several stages of morphological transformation, from hyphae to clumps and pellets. Hence, the interactions between morphology, physiology and productivity must be understood in order to achieve robust processes.
- The impact of process parameters on viable biomass and process performance needs to be understood.
- Recent findings regarding *P. chrysogenum* bioprocesses are describing interlinks between specific growth rate and specific production rate (Ehgartner et al. 2017). Hence, the specific growth rate (μ) needs to be controlled on a certain level to achieve high productivity.
- Filamentous fungi show a large variety of morphological forms in submerged cultures. These range from dispersed hyphae, to interwoven mycelial aggregates, to denser hyphal aggregates, the so-called pellets. Depending on the objective of the bioprocess, different characteristics of morphology are favourable and need to be quantified accurately.
- The most common method to quantitatively characterize morphology is image analysis based on microscopy. This method is work intensive and time consuming and statistically compromised. Therefore, a faster, at-line applicable alternative method based on flow cytometry would be a promising alternative.
- There is considerable merit in assessing viability in individual particles, morphological classes as well as overall sample. Obtained information could be used for model verification or real-time (model based) control of bioprocesses.

Following up on our focus on industrial needs, all research articles collected in this Thesis were published in scientific journals that focus on applied research such as 'Microbial Cell Factories' and 'Applied Microbiology and Biotechnology'. Furthermore, we have strived to bridge the gap towards engineering through publication of an article in 'Chemical Engineering Science'.

Finally, we have demonstrated transferability of methods from ‘Chapter 5’ through additional research focusing on morphological and physiological analysis of glycol-engineered *P. pastoris* strains. These strains form physiologically impaired clusters during cultivations that behave similarly to filamentous fungal pellets regarding viability decline in the cluster core. Consequently, we have shown that our flow cytometry method is also applicable for other agglomerate forming organisms such as yeast. This research was published in ‘Microbial Cell Factories’ and is included in full form in this chapter.

Production of a recombinant peroxidase in different glycol-engineered *Pichia pastoris* strains: a morphological and physiological comparison.

Alexander Pekarsky[1,+], Lukas Veiter[1,2,+], Vignesh Rajamanickam[1,2], Christoph Herwig[1,2], Clemens Grünwald-Gruber[3], Friedrich Altmann[3] and Oliver Spadiut[1*]

1 Technische Universität Wien, Institute of Chemical, Environmental and Bioscience Engineering, Research Area Biochemical Engineering, Gumpendorfer Strasse 1a, 1060 Vienna, Austria
2 Christian Doppler Laboratory for Mechanistic and Physiological Methods for Improved Bioprocesses, TU Wien, Gumpendorfer Straße 1a, 1060 Vienna, Austria
3 Department of Chemistry, University of Natural Resources and Life Sciences, Muthgasse 18, 1190 Vienna, Austria

+ Equal contribution

* Correspondence: Oliver Spadiut, TU Wien, Institute of Chemical, Environmental and Bioscience Engineering, Research Area Biochemical Engineering, Gumpendorfer Strasse 1a, 1060 Vienna, Austria. Tel: +43 1 58801 166473, Fax: +43 1 58801 166980, Email: oliver.spadiut@tuwien.ac.at

Published in 'Microbial Cell Factories'

Pekarsky A., Veiter L., Rajamanickam V., Herwig C., Grünwald-Gruber C., Altmann F. and Oliver Spadiut (2018). 'Production of a recombinant peroxidase in different glyco-engineered *Pichia pastoris* strains: a morphological and physiological comparison.' Microb Cell Fact.

Abstract

Background

The methylotrophic yeast *Pichia pastoris* is a common host for the production of recombinant proteins. However, hypermannosylation hinders the use of recombinant proteins from yeast in most biopharmaceutical applications. Glyco-engineered yeast strains produce more homogeneously glycosylated proteins, but can be physiologically impaired and show tendencies for cellular agglomeration, hence are hard to cultivate. Further, comprehensive data regarding growth, physiology and recombinant protein production in the controlled environment of a bioreactor are scarce.

Results

A $Man_5GlcNAc_2$ glycosylating and a $Man_{8\text{-}10}GlcNAc_2$ glycosylating strain showed similar morphological traits during methanol induced shake-flask cultivations to produce the recombinant model protein HRP C1A. Both glyco-engineered strains displayed larger single and budding cells than a wild type strain as well as strong cellular agglomeration. The cores of these agglomerates appeared to be less viable. Despite agglomeration, the $Man_5GlcNAc_2$ glycosylating strain showed superior growth, physiology and HRP C1A productivity compared to the $Man_{8\text{-}10}GlcNAc_2$ glycosylating strain in shake-flasks and in the bioreactor. Conducting dynamic methanol pulsing revealed that HRP C1A productivity of the $Man_5GlcNAc_2$ glycosylating strain is best at a temperature of 30°C.

Conclusion

This study provides the first comprehensive evaluation of growth, physiology and recombinant protein production of a $Man_5GlcNAc_2$ glycosylating strain in the controlled environment of a bioreactor. Furthermore, it is evident that cellular agglomeration is likely triggered by a reduced glycan length of cell surface glycans but does not necessarily lead to lower metabolic activity and recombinant protein production. $Man_5GlcNAc_2$ glycosylated HRP C1A production is feasible, yields active protein similar to the wild type strain, but thermal stability of HRP C1A is negatively affected by reduced glycosylation.

Keywords

Pichia pastoris, SuperMan$_5$, *OCH1*, bioreactor, cellular agglomeration, flow cytometry, glycosylation, horseradish peroxidase, morphology.

Background

The methylotrophic yeast *Pichia pastoris*, also known as *Komagataella phaffii*, is widely used for the production of recombinant proteins, due to its high productivity, the ability to grow on defined and inexpensive media and its capacity to perform post-translational modifications (e.g. (Cregg et al. 2000)). Protein glycosylation is one of the most critical aspects in the recombinant production of proteins, especially of biopharmaceuticals, as it affects protein properties such as solubility, stability, biological activity, pharmacokinetics (e.g. Cregg et al. 2009), clearance from the body and efficacy (e.g. (Parekh 1991). In *P. pastoris* protein O-glycosylation still must be fully understood, but is expected to consist of variable short, unphosphorylated or phosphorylated α-1,2- and β-1,2-mannose chains (e.g. (Lommel and Strahl 2009).

First approaches to alter O-glycosylation in *P. pastoris* showed promising results (Hamilton et al. 2013). Protein N-glycosylation in yeasts, which is characterized by hypermannosylation, has been thoroughly investigated and is well understood (e.g. (Hamilton and Gerngross, 2007). Initially, N-glycans are linked to the amido group of asparagine residues that are recognized by glycosyltransferases in the endoplasmatic reticulum (ER) at the sequence motif N-X-S/T of the proteins, where X is any amino acid but proline. After the ER, the proteins carry a $Man_8GlcNAc_2$ glycan chain, which is then subjected to hypermannosylation. The first reaction in hypermannosylation is catalyzed by an α-1,6-mannosyltransferase (Och1), which was first discovered and characterized in *S. cerevisiae* (Nagasu et al. 1992, Nakayama et al. 1992). Notably, its glycosylation activity of secreted and membrane proteins makes it also a key enzyme for cell wall maintenance and integrity in yeast (J. et al. 1999, Krainer et al. 2013, Li et al. 2002, Tang et al. 2016). However, hypermannosylation hinders the use of recombinant proteins from yeasts in most biopharmaceutical applications, which is why numerous efforts focused on the efficient 'humanization' of the yeast glycosylation machinery (Choi et al. 2003, Hamilton et al. 2006, Hamilton and Gerngross 2007, Jacobs et al. 2009, Nett et al. 2011, Vervecken et al. 2004). Although the 'humanization' of yeast was accomplished over 10 years ago, only a few studies are known, in which biopharmaceutically relevant products with glyco-engineered strains were produced. Most of the strains have an *och1* deficiency and retain a recombinant α-1,2-mannosidase in the ER to yield mainly $Man_5GlcNAc_2$ structures (Baeshen et al. 2016, Choi et al. 2003, De Meyer et al. 2015, Effenberger et al. 2017, Jacobs et al. 2009, Liu et al. 2018, Maciola et al. 2017; Smith et al. 2014, Vervecken et al. 2004). First studies by Vervecken *et al.* (Vervecken et al. 2004) and Jacobs *et al.* (Jacobs et al. 2009) reported higher stress sensitivity of such strains leading to reduced growth but leading to homogeneously (>90 %) $Man_5GlcNAc_2$ glycosylated products. In most cases, only shake-flask experiments were performed, in which comparisons to other strains or impact of product glycosylation patterns can be biased, due to the uncontrolled behavior in terms of process control (e.g. pH, dissolved oxygen) (Baeshen et al. 2016, De Meyer et al. 2015; Liu et al. 2018; Maciola et al. 2017).

In literature, environmental stressors are known to affect a protein's post-translational processing (Puxbaum et al. 2015), which highlights the importance of analyzing a protein's properties during the controlled production in bioreactors. To our knowledge, only a few studies exist, which analyzed the behavior of $Man_5GlcNAc_2$ glycosylating *P. pastoris* strains in the controlled environment of a bioreactor (Effenberger et al. 2017, Jacobs et al. 2010, Smith et al. 2014). Jacobs *et al.* (Jacobs et al. 2010) were able to produce a maximum of 760 $mg \cdot L^{-1}$ of a murine granulocyte-macrophage colony-stimulating factor (mGM-CSF) at high cell densities upon MeOH induction of alcohol oxidase 1 promoter (P*AOX1*). Although they successfully produced almost homogeneously (>90 %) $Man_5GlcNAc_2$ glycosylated mGM-CSF, a comparison of performance to a mGM-CSF expressing wild-type strain would have been interesting. Furthermore, a decrease in productivity was observed after 40 h of MeOH induction but was not further discussed. In another study by Smith et al. (Smith et al., 2014), the researchers successfully produced recombinant human mast cell chymase (rhChymase) under the control of a glyceraldehyde-3-phosphate dehydrogenase promoter (P*GAP*). During their glycerol fed-batch cultivation, they detected chymase-like proteolytic activity after 72 h of induction, which might have resulted from physiological stress. Recently, the cotton plant

proteins GbDIR2 and GhDIR3 were produced with > 90 % $Man_5GlcNAc_2$ glycosylation homogeneity, but the researchers observed an increased MeOH toxicity for their glyco-engineered strain compared to conventional wild-type strains (Effenberger et al. 2017). Concluding, all three research groups experienced a decrease in process performance over time. We speculate that their glyco-engineered yeast strains were physiologically impaired, due to the altered glycosylation machinery. As we have shown previously for a horseradish peroxidase C1A (HRP C1A) expressing *P. pastoris* strain, where we knocked out *OCH1* (Krainer et al. 2013), an altered glycosylation machinery can have significant impacts: We found that the *OCH1* knockout strain was characterized by slow growth, increased temperature sensitivity and formation of cellular agglomerates, compared to the HRP C1A expressing wild-type strain. Further analysis of this cellular agglomeration showed a decrease in cell surface glycosylation, a negatively affected budding process and indicated covalently bound cells. The recombinant protein was still produced and carried a much more homogeneous surface glycosylation, with the majority being $Man_8GlcNAc_2$ and $Man_9GlcNAc_2$ structures.

In this study, we shed more light on the physiological impairment accompanied by glyco-engineered strains, by performing a morphological investigation and analyzing the size distribution of cellular agglomerates of differently glycosylating *P. pastoris* strains by microscopy and flow cytometry. Furthermore, we physiologically characterized a recombinant $SuperMan_5$ strain in a bioreactor during un-induced phases and MeOH induced phases, produced HRP C1A as a model product and biochemically characterized it. The used strain is based on the GlycoSwitch® plasmids and is able to yield $Man_5GlcNAc_2$ glycosylated products by harboring an *OCH1* disruption and an α-1,2-mannosidase from *Trichoderma reesei* with a C-terminal HDEL signal sequence for ER retention (Jacobs et al. 2009). Due to its shortened glycan pattern, a comparable morphology to the *och1* deficient strain was expected. We compared all results of the $SuperMan_5$ strain to a recombinant *P. pastoris* wild type (wt) (hypermannosylated product) as well as to a recombinant *P. pastoris* *OCH1* knockout strain (Δ*OCH1*) ($Man_{8-10}GlcNAc_2$). Summarizing, in this study we investigated different glyco-engineered *P. pastoris* strains for morphological differences and recombinant protein production. To our knowledge, we provide the first study in literature that comprehensively describes the physiology and growth behavior of a $Man_5GlcNAc_2$ glycosylating *P. pastoris* strain in the controlled environment of a bioreactor.

Results and discussion

Strain characterization in shake-flask screening

Glyco-engineered strains often show a decrease in productivity over time (Effenberger et al. 2017, Jacobs et al. 2010, Smith et al. 2014), which might be linked to their altered glycosylation machinery and therefore a stressed metabolism. Based on our recent findings with the Δ*OCH1* strain (Gmeiner et al. 2015, Krainer et al. 2013), we found that cellular agglomeration and therefore an altered morphology, affected process performance over time. Therefore, we initially hypothesized that an altered glycosylation machinery can be the trigger for morphological deviations, due to an overall decrease in glycan length on the cell surface resulting in cellular agglomeration, as it has also been shown for glyco-proteins (Høiberg-Nielsen et al. 2009). Based on this hypothesis, we performed a shake-flask screening under inducing conditions to produce HRP C1A as recombinant model product in different *P. pastoris* strains and monitored cellular morphology by microscopy and flow cytometry. A hypermannosylating wt strain, the ΔOCH1 strain ($Man_{8-10}GlcNAc_2$ glycans) and the $SuperMan_5$ strain ($Man_5GlcNAc_2$ glycans) were compared.

We observed that the wt and $SuperMan_5$ strain grew similarly in terms of OD_{600} over the whole induction time of 71 h but observed stagnating growth for the Δ*OCH1* strain (see Supplementary Figure 3 for OD_{600} growth curve). At low cell densities (OD_{600} ~ 10) and after 47 h of induction, when samples for the glycosylation analysis were taken, we observed similar volumetric HRP C1A activity for all three strains, however the Δ*OCH1* strain showed a significantly lower specific HRP C1A activity compared to the wt and $SuperMan_5$ strain (see Table 1). This highlighted two aspects: First, due to the lower specific activity and a stagnating growth, the Δ*OCH1* strain seemed to have a stressed metabolism that probably resulted in a decreased viability over time. As foam formation was more prominent for the Δ*OCH1*, partial cell lysis and higher abundance of host cell proteins in the cultivation broth was likely and was also observed in our previous studies (Gmeiner et al. 2015, Kriner

et al. 2013). Second, the shake-flask screening data in Table 1 suggested that the performance of the SuperMan$_5$ strain was not negatively affected by its altered glycosylation machinery as its performance was comparable to the wt strain.

Table 1. Volumetric activity of HRP C1A from wt, Δ*OCH1* and SuperMan$_5$ strains from shake-flask screening, measured in duplicates.

	Volumetric activity (U mL^{-1}) at OD_{600} of 10	Volumetric activity (U mL^{-1}) after 47 h of induction
wt	2.20 ± 0.04	3.20 ± 0.10
Δ*OCH1*	2.02 ± 0.05	2.78 ± 0.08
SuperMan$_5$	2.13 ± 0.05	3.01 ± 0.09

In order to investigate strain morphology and previously observed agglomerate formation for a glyco-engineered strain (Gmeiner et al. 2015), shake-flask samples were analysed via microscopy as well as flow cytometry.

Microscopy

The average cell size for *P. pastoris* lies between 4–6 µm in average cell diameter (Alain et al., 1995). However, conventional budding cells can also encompass two or more cells. Therefore, we defined structures smaller than 15 µm as single or budding cells and structures larger than 15 µm as agglomerates (Gmeiner et al., 2015). In Figure 1, microscopic pictures from shake-flask samples during MeOH induction are displayed, which enable a clear distinction between the strains. The wt strain shows typical single and budding cells. Strong agglomerate formation was seen for both glyco-engineered strains, but the SuperMan$_5$ strain seemed to have a higher degree of agglomeration. Observed agglomerates clearly exhibited multi-budded cells and spanned up to agglomerate diameters over 25 µm. Although the microscopic analysis supported our initial hypothesis that glyco-engineered strains tend to cellular agglomeration, we aimed to analyze this phenomenon with additional methods to minimize biased results. As cellular agglomeration can be triggered by sedimentation during microscopic analysis, we also used flow cytometry to analyze cell morphology under fluid conditions, which approximated the moving environment in a bioreactor or shake-flask better.

Flow cytometry

By using flow cytometry, not only sedimentation and possibly biased cellular agglomeration was minimized, but also a false-positive detection of loosely agglomerated cells could be minimized, due to the in-flow velocity of the cell suspension and the resulting force on the cells. Therefore, the detected cell agglomerates were thought to consist of cells, being attached to each other by strong non-covalent forces through their surface glycosylation or even covalent bonds through an inefficient budding process (Krainer et al. 2013). These agglomerates were termed ‘cluster’ in the evaluation of flow cytometry data.

Signal curve properties of various detector signals were used to differentiate morphological classes. As explained by Dubelaar and Gerritzen, forward scatter (FSC) and sideward scatter (SSC) signals represent size, shape and overall morphology of measured elements (Dubelaar and Gerritzen 2000). By using the flow cytometer, it was possible to distinguish between budding cells and cellular agglomerates. Furthermore, fluorescence signals derived from staining with propidium iodide (PI) and fluorescein diacetate (FDA) provided the means for biomass viability assessment (Ehgartner et al. 2016). Hereby, metabolic activity is detected by FDA treatment resulting in green fluorescence through esterase activity (Söderström 1977). PI fluorescence is a result from DNA intercalation in cells with compromised membranes (28). Based on initial measurements of induction medium with and without cells, a distinction of yeast cells from media background was possible and only particles above a threshold of maximum green fluorescence higher than 200, representing FDA staining, were set as viable yeast cells. In the next step, scatter plots were created and gates were set for classification. Gate setting was based on particle size in accordance with microscopic image analysis as discussed in the previous section and on our prior results with a cell agglomerate forming strain (Gmeiner et al., 2015).

The image-in-flow feature supported the visual identification of morphological classes, as single or budding cells and cluster could be distinguished. An increase in red fluorescence from PI staining indicated viability-declined agglomerates, because PI cannot cross the membrane of healthy cells (see Supplementary Figure 4 for cluster analysis).

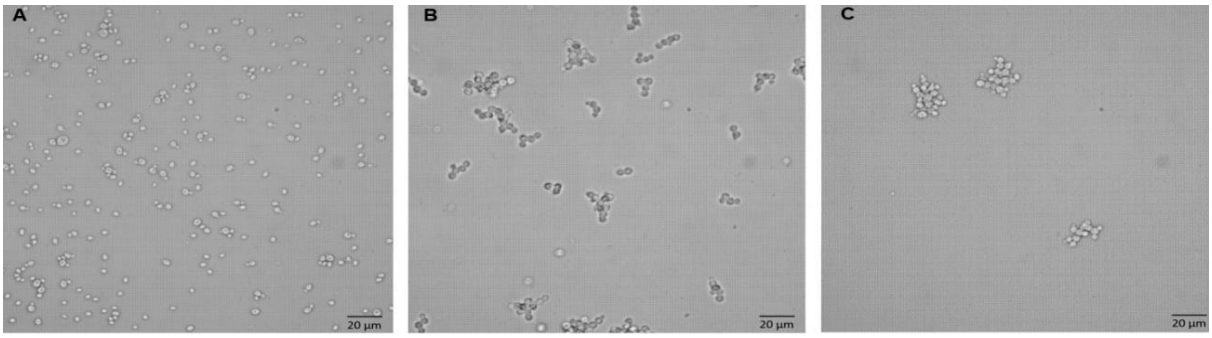

Figure 1. Light microscopy images taken from shake flask experiment at induction time of 11h. (A) wt, (B) Δ*OCH1*, (C) SuperMan$_5$. Black bar signifies 20 µm.

Again, it was possible to set the threshold for viability-declined cluster, based on initial experiments, in which we deliberately induced cell death by heat treatment and compared the scatter plots of treated and untreated cells (data not shown). Therefore, a threshold of total red fluorescence of 1000 was set to distinguish between living and viability-declined cells. The definition of the used morphological classes for flow cytometry analysis is summarized in Figure 2. Based on the pre-set ranges for the morphological classes, a proper distinction between different particles was possible. First, all viable yeast cells were detected, then these cells were divided into single and budding yeast cells or clusters. In a further step, these clusters were analyzed in depth, which revealed viability-declined clusters harboring a significant amount of PI permeable cells. These cells likely underwent substrate or oxygen limitation, hence the agglomerate formation led to a decrease in viability of these cells.

The process of morphological distinction through flow cytometry is demonstrated exemplarily for the SuperMan$_5$ strain from the MeOH induced shake-flask cultivation (Figure 3). According to the classes set in Figure 2, viable yeast cells (3A. yellow), single and budding cells (3B. green) clusters (3C. blue) as well as viability-declined clusters (3D. red) could be distinguished. Interestingly, 23 h after induction start all three strains already showed different morphological distributions for single and budding cells and for clusters in the shake-flasks (Figure 4A). The size distribution of wt strain single and budding yeast was visibly narrower than compared to the glyco-engineered strains. This might indicate that wt cells were less stressed. In literature, it has been reported that yeast cell size can still increase, when cellular proliferation is hindered by stress, leading to larger cells (Tripathi et al. 2011). Furthermore, the size distribution of Δ*OCH1* clusters was narrower distributed and generally smaller in contrast to SuperMan$_5$ clusters, hence Δ*OCH1* clusters were more tightly packed. As seen in Figure 4B, also the wt strain was found to yield a small percentage of cluster forming cells, but with a negligible amount when compared to the glyco-engineered strains. Cluster formation of the SuperMan$_5$ strain and the Δ*OCH1* strain might be triggered by the decrease in glycan length on the cell surface. It is likely that cell surface glycans help to sustain repulsive electrostatic interactions of the cells and thus prevent agglomeration, which has also been shown for glycosylated proteins in high concentrations (Høiberg-Nielsen et al. 2009). In addition, both glyco-engineered strains showed viability-declined clusters, which correlated well to our hypothesis that cellular agglomeration can lead to limitations for inner core cells. A representative signal profile of a SuperMan$_5$ viability-declined cluster can be seen in Figure 5A together with the corresponding image-in-flow of the measured cluster in Figure 5B. The signal profile shows an increase in susceptibility to PI staining (see Supplementary Figure 4 for comparison between viable and viability-declined clusters), resulting in an increase of red fluorescence that corresponds to a decrease in viability of these cells. Interestingly, the SuperMan$_5$ strain exhibited a stronger proportion of viability-declined clusters at the beginning of the MeOH induced shake-flask experiments (Figure 5C). Over time, this trend diminished as the Δ*OCH1* strain increased its proportion in viability-declined clusters (Figure 5). These results together with the fact that mean cluster size of the glyco-engineered strains remained similar over the whole induction time (Supplementary Figure 1), supported morpho -

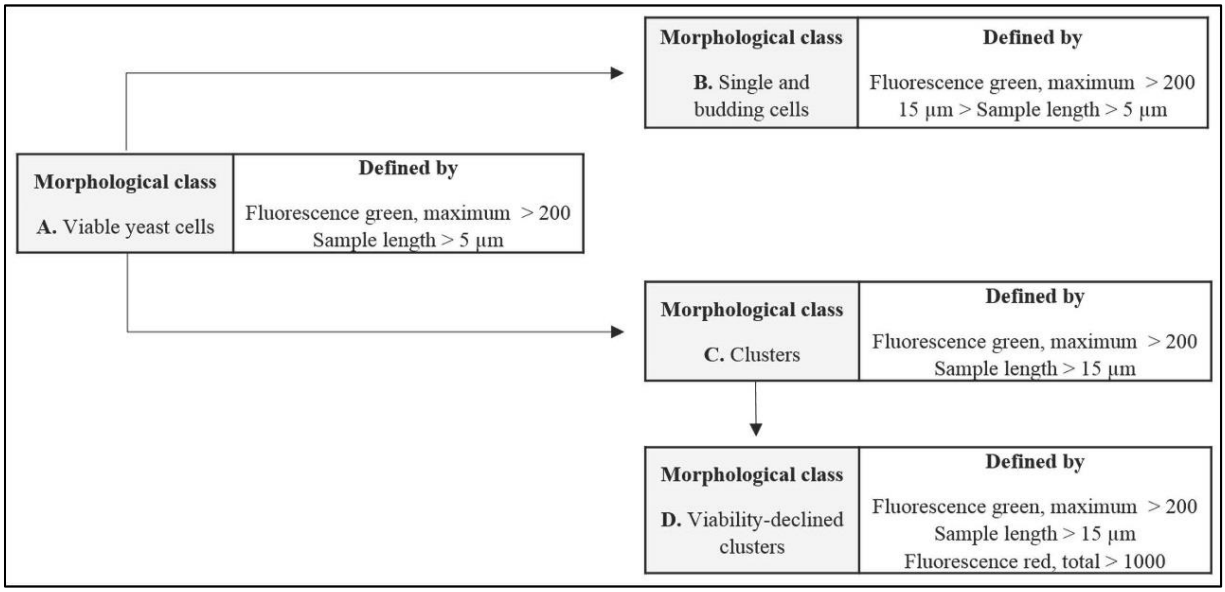

Figure 2. Definition of morphological classes for flow cytometry analysis.

logical similarity between these two strains. However, while the overall morphology between the Δ*OCH1* and SuperMan$_5$ strain was similar, the SuperMan$_5$ strain appeared to be fitter, due to its better HRP C1A production and no visible growth stagnation in the shaking flasks. We hypothesized that the glyco-engineered strains differed in performance neither due to their altered glycosylation machinery nor due to their tendency to agglomerate. Both glyco-engineered strains strongly agglomerated and both were *OCH1* deficient, which suggested another reasons for the decreased performance of the Δ*OCH1* strain. Although not tested, we hypothesized that the different methods of *OCH1* inactivation could be responsible for the observed difference in performance. The Δ*OCH1* strain was generated by a knock-out procedure (Krainer et al. 2013), but the SuperMan$_5$ strain with an *OCH1* knock-in procedure (Jacobs et al. 2009; Vervecken et al. 2004). Therefore, most of the *OCH1* gene and promoter remained present, but inactive in the knock-in strain (Vervecken et al., 2004).

In literature, not only the Och1 protein, but also the *OCH1* gene and its promoter region are described as important factors for cell wall integrity (Tang et al. 2016), oxidative- and hypo-osmotic stress tolerance (J. et al. 1999; Li et al. 2002). For example, Li and colleagues showed that the transcription factor Skn7p, is important in stress response pathways in *S. cerevisiae*, binds upstream of the *OCH1* open reading frame and they also further suggested that successful Skn7p binding, promotes activation of other transcription factors. Therefore, it might be possible that binding/activation of Skn7p or other important factors was hindered in the *OCH1* knock-out strain (Δ*OCH1*), which diminished its stress tolerance, but future research has to elucidate this theory. Overall, the SuperMan$_5$ strain seemed to be fit for a further characterization in the bioreactor and a proper production strain for Man$_5$GlcNAc$_2$ glycosylated HRP C1A. Additional analysis of the glycosylation pattern of HRP C1A from the different strains also indicated that the destined glycosylation was present for each of the different HRP C1A enzymes (Supplementary Figure 2).

Summarizing, we investigated the HRP C1A production in three different *P. pastoris* strains that yielded differently glycosylated products and analysed strain morphological properties by microscopy and flow cytometry. The Δ*OCH1* and SuperMan$_5$ strain showed similar morphological traits. Both glyco-engineered strains had larger single and budding cells than the wt strain and showed strong cellular agglomeration. This phenomenon of agglomeration is believed to be triggered by the shorter glycan structures on the cell surface and a disturbed budding process.

We also found that inner core cells of these agglomerates appeared to be less viable, possibly due to limitations, hence one should consider this

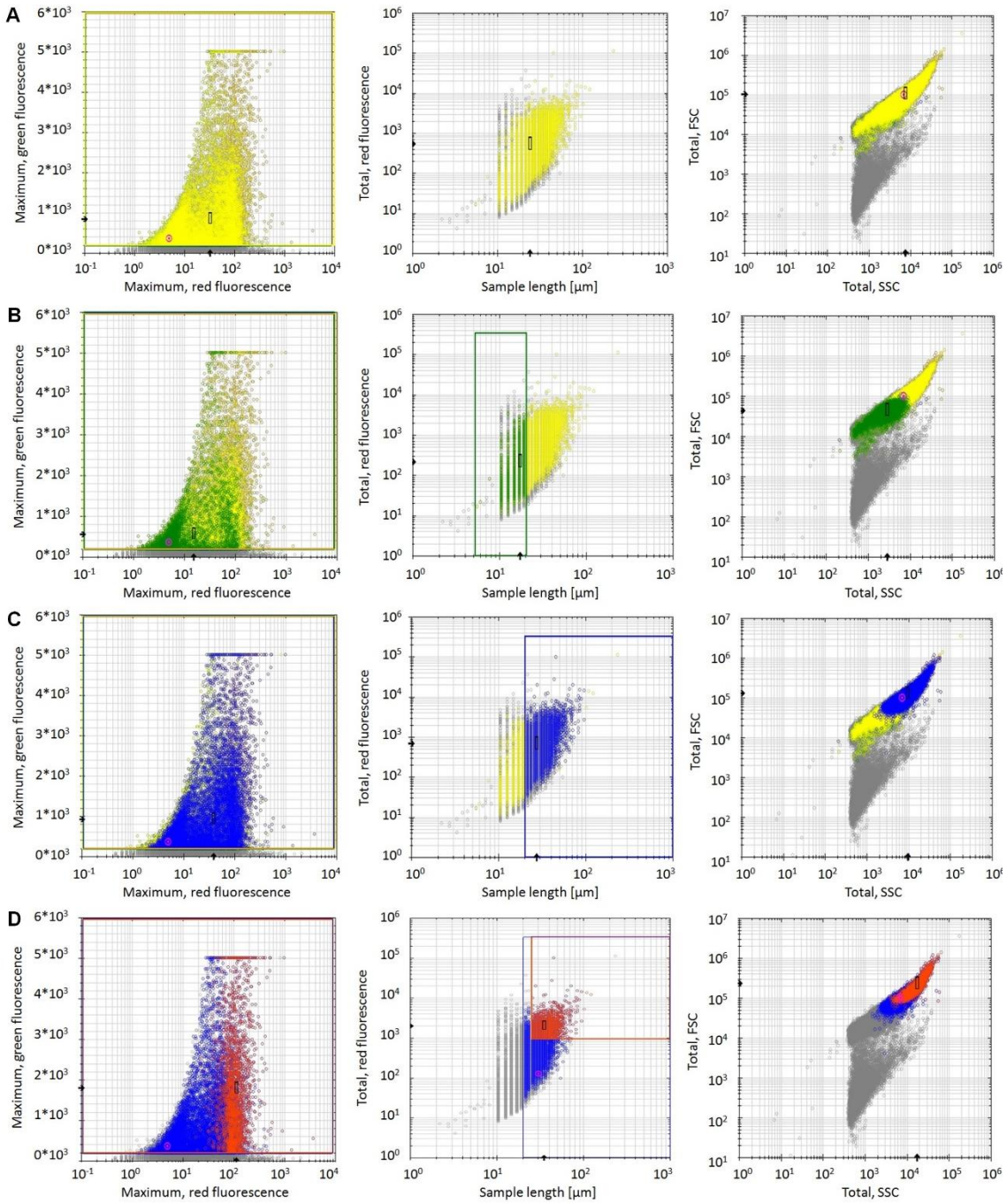

Figure 3. Exemplary flow cytometry scatter plots of SuperMan5 strain from shake-flask during induction at 23 h. From left to right: fluorescence green vs. fluorescence red, fluorescence red vs. sample length, FSC total vs. SSC total. From top to bottom: (A) viable yeast cells (yellow), (B) single and budding cells (green), (C) clusters (blue) and (D) viability-declined clusters (red). Rectangles signify chosen gates according to morphological classification.

fact when working with any other glyco-engineered strains. Additionally, our results suggested that the diminished performance of the Δ*OCH1* strain resulted not from the altered glycosylation machinery, but rather from other phenomena, likely including hindered stress tolerance pathways. Nevertheless, a high specific activity of HRP C1A was found for the SuperMan$_5$ strain, which made a further characterization with defined medium in the bioreactor interesting.

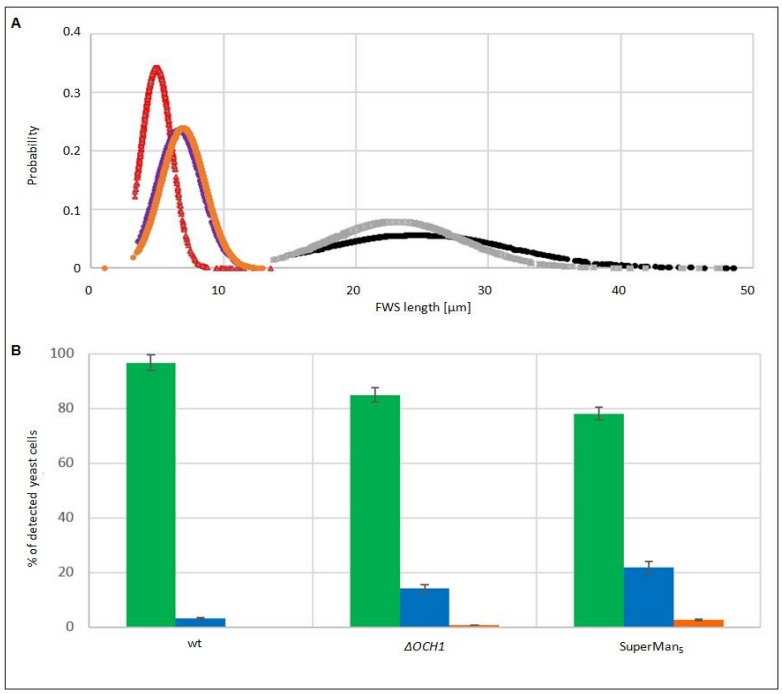

Figure 4.
(A) Normal distribution of particle FSC length of single and budding cells and cluster for wt, ΔOCH1 and SuperMan5 strains at cultivation time of 23h from shake-flask screening. Distribution of wt single and budding cells (red), ΔOCH1 single and budding cells (violet), SuperMan5 single and budding cells (orange), ΔOCH1 cluster distribution (grey), SuperMan5 cluster distribution (black).
(B) Morphological classes in percentages of detected yeast cells at induction time of 23h from shake-flask screening for wt, ΔOCH1 and SuperMan5 strain. Bar plot shows single and budding cells (green), clusters (blue), viability-declined cluster (red).

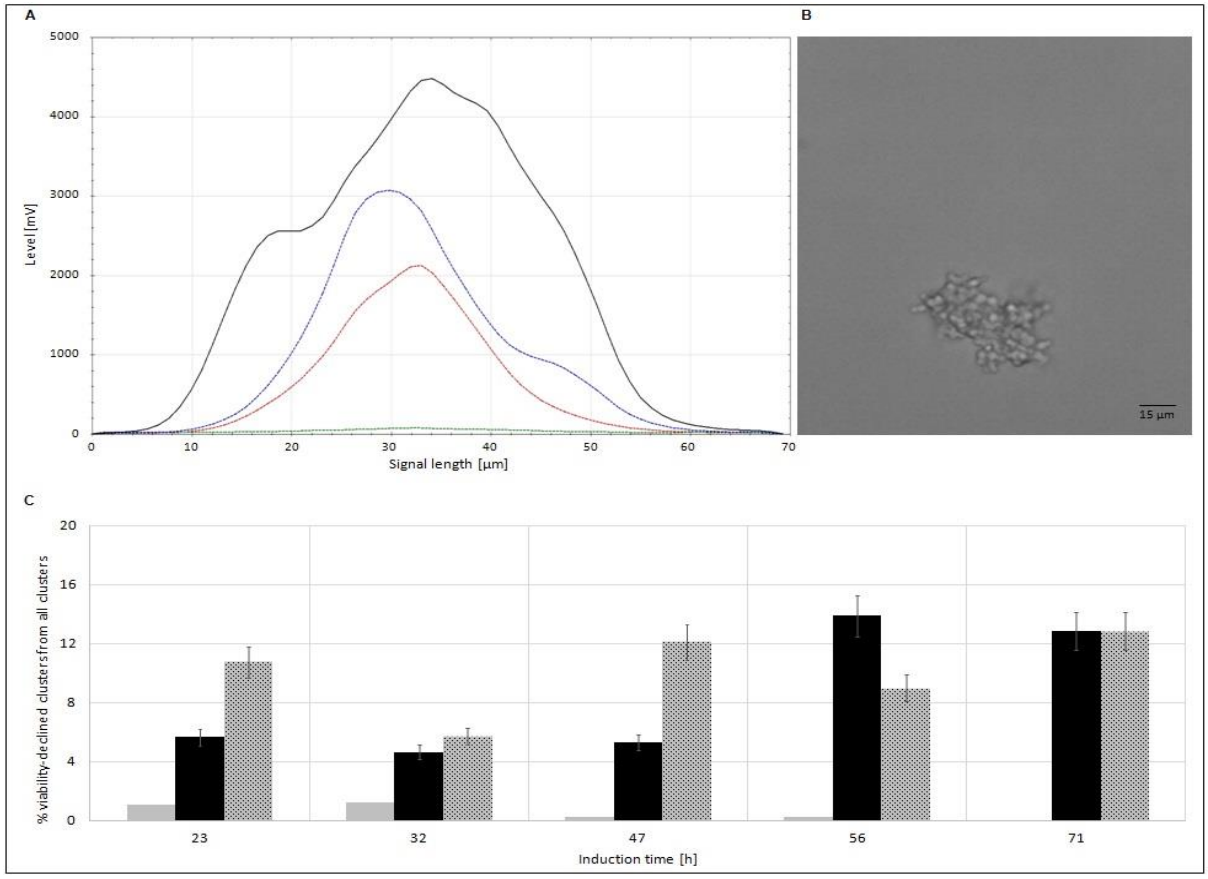

Figure 5. (A) Exemplary signal profile from flow cytometer of SuperMan5 cluster after 23 h induction time in shake-flasks. FSC (black line -), SSC (blue line --), green (green line --) and red (red line --) fluorescence signals with corresponding image-in-flow picture (B). (C) Percentages of viability-declined clusters from all detected clusters over induction time from shake-flask screening. wt (grey bars), ΔOCH1 (black bars), SuperMan5 (dotted grey bars).

Table 2. Strain specific parameters of SuperMan5

				SuperMan$_5$
max. μ_{Gly} (h^{-1})				0.28 ± 0.03
$Y_{X/Gly}$ (Cmol Cmol^{-1})				0.55 ± 0.03
$Y_{CO_2/Gly}$ (Cmol Cmol^{-1})				0.47 ± 0.02
$\Delta time_{adapt}$ (h)				4.85
	15 °C	**20 °C**	**25 °C**	**30 °C**
q_{MeOH} (mmol g^{-1} h^{-1})	0.76 ± 0.12	1.17 ± 0.05	1.41 ± 0.18	1.52 ± 0.11
$Y_{X/MeOH}$ (Cmol Cmol^{-1})	0.037 ± 0.001	0.024 ± 0.002	0.022 ± 0.006	0.033 ± 0.001
$Y_{CO_2/MeOH}$ (Cmol Cmol^{-1})	0.924 ± 0.001	0.923 ± 0.048	0.961 ± 0.046	0.972 ± 0.033
C-balance	0.961 ± 0.003	0.947 ± 0.071	0.983 ± 0.074	1.005 ± 0.048
q_p (U g^{-1} h^{-1})	0.62 ± 0.06	0.94 ± 0.07	1.01 ± 0.06	1.05 ± 0.05

The batch phase on glycerol and the adaptation to methanol were performed at 30 °C. Subsequent methanol pulses were added at different temperatures. Parameters are defined in the footnote

max. μ_{Gly} maximum specific growth rate on glycerol, q_{Gly} specific uptake rate of glycerol during the batch, $Y_{X/Gly}$ biomass yield on glycerol, $Y_{CO_2/Gly}$ CO_2 yield on glycerol, $\Delta time_{adapt}$ time from first addition of methanol to a maximum in offgas activity, q_{MeOH} average specific uptake rate of methanol during consecutive methanol pulses, q_p specific product formation rate, $Y_{X/MeOH}$ biomass yield on methanol, $Y_{CO_2/MeOH}$ CO_2 yield on methanol, *C-balance* sum of biomass and CO_2 yields

Physiological strain characterization in the bioreactor

Based on the prior shake-flask screening, the SuperMan$_5$ strain was seen as a suitable strain for the production of $Man_5GlcNAc_2$ glycosylated HRP C1A in the controlled environment of a bioreactor. First, we characterized the SuperMan$_5$ strain with our published method of conductingdynamic experiments with pulse-wise feeding during batch cultivations in the bioreactor (Capone et al. 2015, Dietzsch et al. 2011a, b, Krainer et al. 2012, Krainer et al. 2013) and to our knowledge, this study represents the first comprehensive analysis of the temperature dependent physiology and growth behavior of a $Man_5GlcNAc_2$ glyco-engineered *P. pastoris* strain. The strain specific physiological parameters of SuperMan$_5$ for the batch phase and the MeOH induction phase at different temperatures are summarized in Table 2.

As shown in Table 2, the specific uptake rate for MeOH (q_{MeOH}) increased with increasing temperature as also did the specific productivity (q_p). Therefore, 30°C was seen as the optimal cultivation temperature for future fed-batch cultivations. To assess the physiology of the SuperMan$_5$ strain in a more comprehensive way, we compared its strain specific physiological parameters at 30°C to our published results for a HRP C1A producing wt strain and Δ*OCH1* strain under the same conditions (Table 3).

As shown in Table 3, the HRP C1A expressing *P. pastoris* strains showed differences in physiological parameters during batch on glycerol at 30°C, hence their growth behaviour was already distinguishable. The SuperMan$_5$ strain showed a similar maximum specific growth rate (μ_{max}) to the wt strain, but the ΔOCH1 strain clearly exhibited slower growth. The above discussed shake-flask screening showed that both glyco-engineered strains have similar morphology and thus, cellular agglomeration does not seem to trigger the slow growth of the Δ*OCH1* strain, but rather hindered stress tolerance pathways. More interestingly, glyco -engineered strains had a better conversion of substrate to biomass, as seen by a higher biomass yield and produced less CO_2 per substrate compared to the wt strain. We hypothesized that this might be connected to the altered glycosylation machinery in both strains that led to smaller glycans. Smaller glycans also mean that less carbon is used to build sugar molecules, hence the carbon can be re-routed for biomass conversion.

Table 3. Strain specific physiological parameters of the different glyco-engineered P. pastoris Mut^S strains expressing HRP C1A at 30°C.

	wt	**Δ*OCH1***	**SuperMan$_5$**
max. μ_{Gly} (h^{-1})	0.31	0.20	0.28 ± 0.03
$Y_{X/Gly}$ (Cmol Cmol^{-1})	0.41	0.54	0.55 ± 0.03
$Y_{CO_2/Gly}$ (Cmol Cmol^{-1})	0.64	0.44	0.47 ± 0.02
$\Delta time_{adapt}$ (h)	19.9	8.90	4.85
q_{MeOH} (mmol g^{-1} h^{-1})	0.70	0.43	1.52 ± 0.11
$Y_{X/MeOH}$ (Cmol Cmol^{-1})	0.071	0.046	0.033 ± 0.001
$Y_{CO_2/MeOH}$ (Cmol Cmol^{-1})	1.02	Constantly decreasing	0.97 ± 0.03
C-balance	1.09	Constantly decreasing	1.01 ± 0.05
q_p (U g^{-1} h^{-1})	0.77	0.50	1.05 ± 0.05

All three strains behaved very differently during adaptation to MeOH and induction with MeOH. The decrease in glycan length correlated with the adaptation time ($\Delta time_{adapt}$) for MeOH, but cause

of this faster adaptation has to be elucidated in future studies. As also seen during the shake-flask screening, the SuperMan$_5$ strain was superior during induction by yielding the best results for HRP C1A productivity and the highest q_{MeOH}. Whereas Δ*OCH1* lost metabolic activity over time, shown in a constantly decreasing $Y_{CO2/S}$ (Krainer et al. 2013). The wt and SuperMan$_5$ strain were easily cultivated at 30°C for a prolonged induction time. Closing C-balances for wt and SuperMan$_5$ underlined the validity of the calculated strain specific physiological data.

Summarizing, it was possible to characterize the Man$_5$GlcNAc$_2$ glycosylating SuperMan$_5$ strain in the controlled environment of a bioreactor during un-induced batch on glycerol and induced batches on MeOH. The use of dynamic substrate pulsing made it possible to characterize the SuperMan$_5$ strain at 30°C, 25°C, 20°C and 15°C during induction with MeOH in only one experiment. HRP C1A productivity was best at 30°C. Furthermore, a comparison between the SuperMan$_5$, Δ*OCH1* and wt strain was possible at 30°C to yield comprehensive data on the impact of glyco-engineering on growth behaviour and HRP C1A productivity. The SuperMan$_5$ strain exhibited similar μ_{max} as the wt strain during batch, but the glyco-engineered strains seemed to have a more efficient substrate to biomass conversion. We hypothesized that this resulted from decreased carbon demand for the glycosylation machinery. The decrease in glycan length of protein and cell surface glycosylation of the SuperMan$_5$ strain did not lead to a lower metabolic activity, growth or protein productivity compared to the wt strain.

Enzyme characterization

Biochemical enzyme characterization

To check whether the kinetic constants and the stability of the protein were affected by the altered glycosylation pattern, we characterized the 2x concentrated and diafiltrated HRP C1A from the SuperMan$_5$ bioreactor cultivation.

We compared published results for substrate affinity and thermal stability of HRP C1A produced in the wt or Δ*OCH1* strain from our recent study (Table 4) (Krainer et al. 2013). The affinity towards the substrate ABTS was not significantly affected by altered protein glycosylation. However, the thermal stability of HRP C1A decreased clearly together with the amount of sugars attached to the protein surface, hence structural protein integrity seemed to be affected by its glycosylation pattern. This phenomenon has already been described in literature for glycosylated proteins (Tams and Welinder 1998, Wang et al. 2018, Zou et al. 2012).

Summarizing, we analysed enzyme kinetics and thermal stability of HRP C1A from the SuperMan$_5$ strain. Although enzyme affinity towards ABTS was comparable to wt and Δ*OCH1* products, the thermal stability was diminished 3-fold compared to the HRP C1A from the wt strain, hence proofing that HRP C1A stability is strongly affected by glycosylation.

Conclusion

In this study, we report the first comprehensive evaluation of growth, physiology and recombinant protein productivity of a Man$_5$GlcNAc$_2$ glycosylating *P. pastoris* strain (SuperMan$_5$) in the controlled environment of a bioreactor. The strain showed superior growth, physiology and HRP C1A productivity compared to a Man$_{8\text{-}10}$GlcNAc$_2$ glycosylating Δ*OCH1* strain and a hypermannosylating wt strain.

Additionally, we shed more light on the often-seen impairment in process performance of glyco-engineered strains in a detailed morphological study: Flow cytometry and microscopic analysis revealed the formation of cellular agglomerates with impaired viability of inner core cells. Although agglomeration was prominent in both glyco-engineered strains, our results suggest that a decreased process performance might not necessarily derive from the altered glycosylation machinery. It can be rather attributed to additional metabolic burdens, like hindered stress tolerance pathways, which can make strains more sensitive to environmental stressors.

Methods

Chemicals

Enzymes, deoxynucleotide triphosphates and Phusion™ High-Fidelity DNA-polymerase was obtained from ThermoFisher Scientific (Vienna, Austria). 2,2'-azino-bis(3-ethylbenzthiazoline-6-sulfonic acid) diammonium salt (ABTS) and hemin were purchased from Sigma-Aldrich (Vienna, Austria). Difco™ yeast nitrogen base w/o amino acids (YNB), Difco™ yeast nitrogen base w/o amino acids and ammonia sulfate (YNB2), Bacto™

tryptone and Bacto™ yeast extract were purchased from Becton Dickinson (Vienna, Austria). Zeocin™ was purchased from InvivoGen (Toulouse, France) via Eubio (Vienna, Austria).

Microorganisms

For this study, a *HRP C1A* gene, codon-optimized for *P. pastoris*, was ordered from GenScript (Nanjing, China) and cloned into a pPICZαC vector, providing a Zeocin™ (Zeo) resistance gene as well as an α-prepro mating signal sequence from *Saccharomyces cerevisiae* for product secretion, using standard methods. Correct integration was verified by sequencing. The pPICZαC vector was successfully integrated in a *P. pastoris* GS115 strain (*HIS*$^+$*, pep4Δ, aox1*Δ), provided by Biogrammatics, Inc. (California, United States) and should yield mainly $Man_5GlcNAc_2$ glycosylated HRP C1A after transformation (SuperMan$_5$) (Jacobs et al., 2009). The Och1 deficiency of the SuperMan$_5$ strain is based on the disruption, but not deletion of the *OCH1* gene. The strain CBS 7435 (identical to NRRL Y-11430 or ATCC 76273) was chosen as a benchmark wild type strain (wt), which yields natively hypermannosylated HRP C1A (Krainer et al. 2013) . As described in our previous study, we used a genetically engineered wt strain harboring a knock-out deletion of the *OCH1* gene (Δ*OCH1*) to avoid hypermannosylation that yielded mainly $Man_{8\text{-}10}GlcNAc_2$ glycosylated HRP C1A upon transformation (Krainer et al. 2013). Both, the wt and Δ*OCH1* strain contained a pPpT4_S, which contained the codon-optimized *HRP C1A* gene under equal conditions (Krainer et al., 2013; Naatsaari et al., 2012). Therefore, all resulting strains had a Mut^S phenotype, expressed and secreted HRP C1A upon induction of the *AOX1* promoter with MeOH.

Culture Media

The growth medium (buffered medium with glycerol for yeast (BMGY)) for the shake-flask screenings contained: 10 g·L^{-1} yeast extract, 20 g·L^{-1} peptone, 13.4 g·L^{-1} YNB2, 4 mg·L^{-1} D(+)-Biotin, 10 g·L^{-1} glycerol and 100 mL of a 1 M potassium phosphate buffer pH 6.0. The induction medium (buffered medium with MeOH for yeast (BMMY)) for the shake-flask screenings contained: 10 g·L^{-1} yeast extract, 20 g·L^{-1} peptone, 13.4 g·L^{-1} YNB2, 4 mg·L^{-1} D(+)-Biotin, 5 g·L^{-1} MeOH and 100 mL of a 1 M potassium phosphate buffer pH 6.0. The preculture medium for the bioreactor cultivations (Yeast nitrogen base medium (YNBM)) contained: 20 g·L^{-1} α-D(+)-glucose monohydrate, 3.4 g·L^{-1} YNB2, 10 g·L^{-1} $(NH_4)_2SO_4$, 0.4 g·L^{-1} D(+)-Biotin, 0.1 M potassium phosphate buffer, pH 6.0. Trace element solution (PTM1) for the bioreactor cultivation contained: 6 g·L^{-1} $CuSO_4.5H_2O$, 0.08 g·L^{-1} NaCl, 3 g·L^{-1} $MnSO_4·H_2O$, 0.2 g.L^{-1} $Na_2MoO_4·2H_2O$, 0.02 g·L^{-1} H_3BO_3, 0.5 g·L^{-1} $CoCl_2$, 20 g·L^{-1} $ZnCl_2$, 65 g·L^{-1} $FeSO_4·7H_2O$, 0.2 g·L^{-1} D(+)-Biotin, 5 mL·L^{-1} 95-98 % H_2SO_4. Basal salt medium (BSM) for the bioreactor cultivations contained: 60 g·L^{-1} glycerol, 1.17 g·L^{-1} $CaSO_4·2H_2O$, 18.2 g·L^{-1} K_2SO_4, 14.9 g·L^{-1} $MgSO_4.7H_2O$, 4.13 g·L^{-1} KOH, 26.7 mL·L^{-1} 85 % (v/v) o-phosphoric acid, 0.2 mL·L^{-1} Antifoam Struktol J650, 4.35 mL·L^{-1} PTM1, NH_4OH as N-source. pH was maintained by using 12.5% $NH_{3,\,aq}$. Throughout all shake-flask cultivations, Zeocin™ was used in a concentration of 50 µg·mL^{-1}.

Strain selection

After transformation, 10 Zeo resistant clones were picked and grown overnight in 10 mL BMGY-Zeo medium in 100 mL baffled shake-flasks at 230 rpm and 30°C. Then, cells were harvested by centrifugation (1,800 g, 4°C, 10 min) and re-suspended in BMMY-Zeo for adaptation of the cells to MeOH. Again, cells were grown at 230 rpm and 30°C. Recombinant protein production was induced by adding 1.5% (v/v) pulses of pure MeOH supplemented with 12 mL PTM1/L MeOH to the culture each day, for 5 days. Each day, a sample was taken and analyzed for OD_{600}, total protein content in the cell-free cultivation broth (Bradford assay) as well as the presence of recombinant HRP C1A by SDS-PAGE. A recombinant *P. pastoris* strain carrying the empty pPICZαC vector was included as negative control in all experiments.

Analysis of strain morphology and glycosylation

To understand a possible impact of the genotype and phenotype on overall strain physiology and productivity, an initial shake-flask screening, including morphological analysis was performed. The strain morphology was analyzed under inducing conditions for the wt, ΔOCH1 and SuperMan$_5$ strain. In parallel, growth and product formation were monitored to assure product presence for later glycosylation pattern analysis.

Shake-flask screening

A fresh cryo tube (-80°C) was thawed for each HRP C1A containing strain, added to 200 mL BMGY-Zeo medium in a 1000 mL shake-flask and incubated at 28°C and 230 rpm overnight. The next

day, 50 mL of each culture were transferred to 450 mL BMMY-Zeo, including also 10 µM Hemin (Heme) to ease HRP C1A induction (Gmeiner and Spadiut, 2015). Induced cultures were grown in 2.5 L baffled flasks and a working volume of 500 mL. For comparability, HRP C1A induction was performed at 28°C for all 3 strains. To assure complete depletion of the initial C-source (glycerol) and accurate adaptation to the inducing C-source in the shake-flasks (MeOH), cells were grown for 23 h in BMMY-Zeo-Heme before the first MeOH pulse was given. MeOH pulses were given each day as 1 % (v/v) with PTM1 (12 mL/L MeOH). Sampling of the cultures was done approximately every 12 h. After 47 h of induction, 100 mL of each culture were harvested, centrifuged (4000 g, 10 min, 4°C), the cell free supernatant was concentrated 20x with a 10 kDa centrifugal filter membrane (Amicon®Ultra - 15) tube (Merck Millipore Ltd., Carrigtwohill, IRL) and stored at -20°C for further analysis. Enzyme activity and total protein content of the concentrates were measured and aliquots of the concentrates were used for identification of the respective HRP C1A glycosylation pattern of each strain. However, the total induction time of the shake-flask cultures was 71 h to further monitor growth and the morphological behavior of the different strains.

Microscopy
20 µL of the cultivation broth were pipetted onto a standard glass slide (25 x 75 mm) and then covered with an extra-large cover slide (24 x 60 mm). Images were recorded at a 40x magnification with a five megapixel microscopy CCD colour camera (Olympus, Austria). These images were used as a rough estimation of cell agglomerate formation and agglomerate diameter.

Flow cytometry
Samples of the shake-flask screening were diluted in phosphate buffered saline (PBS) (2.65 g/L $CaCl_2$ solution, 0.2 g/L KCl, 0.2 g/L KH_2PO_4, 0.1 g/L $MgCl{\cdot}6\ H_2O$, 8 g/L NaCl and 0.764 g/L $Na_2HPO_4{\cdot}2\ H_2O$ at pH 6.5) to an OD_{600} of 1. Then, 0.5 µL of 20 mM propidium iodide stock in dimethyl sulfoxide (both from Sigma Aldrich, St. Louis, United States) and 5 µL of 12 mM fluorescein diacetate (Sigma Aldrich, St. Louis, United States) stock in acetone were added to 0.5 mL of the cell suspension. After 10 min incubation in the dark at room temperature, the sample was further diluted (1:10 in PBS) for flow cytometric analysis.

A CytoSense flow cytometer (CytoBuoy, Woerden, Netherlands) with two forward scatter (FSC), one sideward scatter (SSC) and two fluorescence channels (green, red) was used for single cell analysis. The implemented laser had a wavelength of 488 nm. The configuration of the emission wavelength filter set was 515-562 ± 5 nm for the green fluorescence channel (used for fluorescein diacetate) and 605-720 ± 5 nm for the red fluorescence channel (used for propidium iodide). The flow cytometer was equipped with a PixeLINK PL-B741 1.3MP monochrome camera for image-in-flow acquisition, which made real-time imaging of cell agglomerates possible. For data evaluation, the software CytoClus3 (CytoBuoy, Woerden, Netherlands) was used.

The CytoSense flow cytometer provides multiple spatially resolved data points per channel per particle. This signal is achieved for both scatter channels as well as for green and red fluorescence channels (Dubelaar and Gerritzen 2000), which is the basis for multiple curve parameters. Except for length parameters in µm, all parameters are in arbitrary units, as the user can set the sensitivity of the detector. The following parameters were used for the distinction of morphological classes: Maximum (maximum of signal curve), Total (area under curve), Length (length of the signal) and Sample length (length of signal above trigger level). Furthermore, image-in-flow feature enabled visual identification of yeast agglomerates, termed clusters. It should be noted that while FSC signals are closely linked to particle size (sample length), FSC length signals do not always correspond entirely to sample length due to overlays of other signals, which was seen during calibration with defined beads.

Glycosylation Analysis

A glycopeptide analysis using an LC-ESI-MS system was performed (Gruber and Altmann 2015). The concentrated samples of the shake-flask screening were digested in solution. The proteins were S-alkylated with iodoacetamide and digested with Trypsin (Promega, Madison, United States). The peptide mixtures were loaded on a BioBasic C18 column (BioBasic-18, 150 x 0.32 mm, 5 µm; ThermoFisher Scientific, Vienna, Austria) using 80 mM ammonium formiate buffer as the aqueous solvent. A gradient from 5% B (B: 80% acetonitrile) to 40% B in 45 min was applied, followed by a 15 min gradient from 40% B to 90% B that facilitates elution of large peptides, at a flow rate of 6 µL/min.

Detection was performed with a QTOF MS (Bruker maXis 4G) equipped with the standard ESI source in positive ion, DDA mode (= switching to MSMS mode for eluting peaks). MS - scans were recorded (range: 150-2200 Da) and the 3 highest peaks were selected for fragmentation. Instrument calibration was performed using an ESI calibration mixture (Agilent, Santa Clara, United States). The nine possible glycopeptides were identified as sets of peaks consisting of the peptide moiety and the attached N-glycan varying in the number of HexNAc, hexose and phosphate residues. The theoretical masses of these glycopeptides were determined with a spreadsheet using the monoisotopic masses for amino acids and monosaccharides. Manual glycopeptide searches were made using DataAnalysis 4.0 (Bruker, Billerica, United States).

Bioreactor cultivations

After conducting the shake-flask screening, we characterized the recombinant SuperMan$_5$ strain in terms of physiology, biomass growth and productivity using a dynamic strategy of conducting MeOH pulses during batch cultivations in the controlled environment of a bioreactor, which we have described several times before (Capone et al. 2015, Dietzsch et al. 2011a,b, Krainer et al. 2012; Krainer et al. 2013). This cultivation was used for subsequent purification to perform product kinetics and thermal stability analysis.

Preculture

Frozen stocks (-80 °C) from working cell banks were incubated in 100 mL of YNBM-Zeo in 1 L shake-flasks at 30°C and 230 rpm for 24 h. The preculture was transferred aseptically to the respective culture vessel. The inoculation volume was 10 % of the final starting volume.

Cultivation

Batch cultivation was carried out in a 5 L working volume Labfors glass bioreactor (Infors, Bottmingen, Switzerland). BSM was sterilized in the bioreactor and pH was adjusted to pH 5.0 by using 12.5 % $NH_{3,\ aq}$ after autoclavation. Sterile filtered PTM1 was transferred to the reactor aseptically. pH and dissolved oxygen probes were calibrated prior to cultivation start. Dissolved oxygen (dO_2) was measured with a sterilizable polarographic dissolved oxygen electrode (Mettler Toledo, Vienna, Austria) and maintained above 20 % throughout the cultivation. The pH was measured with a sterilizable electrode (Mettler Toledo, Vienna, Austria) and maintained constant at pH 5.0 with a step controller using 12.5 % $NH_{3,\ aq}$. Base consumption was determined gravimetrically. Agitation was fixed to 1495 rpm. The culture was aerated with 2.0 vvm dried air and offgas was measured by using an infrared cell for CO_2 and a paramagnetic cell for O_2 concentration (Servomax, Egg, Switzerland). Temperature, pH, dO_2, agitation as well as CO_2 and O_2 in the offgas were measured on-line and logged in a process information management system (PIMS Lucullus; Applikon Biotechnology, Delft, Netherlands).

The end of the initial batch phase at 30°C and therefore complete glycerol consumption was indicated by an increase in dO_2, a drop in offgas CO_2 and an increase in offgas O_2. The first MeOH pulse (adaptation pulse) of a final concentration of 0.5 % (v/v) was conducted with MeOH supplemented with 12 mL PTM1 per 1 L of added MeOH (MeOH/PTM1 pulse). Subsequently, at least three MeOH/PTM1 pulses were given to 1 % (v/v) at 30°C, then 25°C, 20°C and finally 15°C. For each pulse, at least two samples were taken to determine the concentrations of MeOH and product as well as dry cell weight (DCW) and OD_{600} to calculate the strain specific physiological parameters. Induction was carried out in the presence of 1 mM hemin, that was added prior to the adaptation pulse (Krainer et al. 2015).

Sample analysis

Analysis of growth- and expression-parameters

Dry cell weight (DCW) was determined by centrifugation of 5 mL culture broth (4,000 g, 4°C, 10 min), washing the pellet twice with 5 mL water and subsequent drying for 72 h at 105°C. Determination was performed in triplicates. OD_{600} of the culture broth was measured using a spectrophotometer (Genesys 20; ThermoFisher Scientific, Austria). The activity of HRP C1A in the cell free supernatant was determined with a CuBiAn XC enzymatic robot (Optocell, Bielefeld, Germany). Cell free samples (60 µL) were added to 840 µL of 1 mM ABTS in 50 mM potassium phosphate buffer, pH 6.5. The reaction mixture was incubated for 5 min at 37°C and was started by the addition of 100 µL of 0.078 % H_2O_2. Changes of absorbance at 420 nm were measured for 180 s and rates were calculated. Calibration was done by using commercially available horseradish peroxidase (Type VI-A, P6782; Sigma-Aldrich, Vienna, Austria,) as standard at six different concentrations (0.02; 0.05; 0.1; 0.25; 0.5 and 1.0 U·mL^{-1}).

Protein concentration of cell free supernatant was determined at 595 nm using the Bradford Protein Assay Kit (Bio-Rad Laboratories GmbH, Vienna, Austria) with bovine serum albumin (Protein standard; micro standard, liquid; P0914; Sigma Aldrich, Vienna, Austria) as standard.

Substrate concentrations
Concentration of glycerol and MeOH was determined in cell free samples of the bioreactor cultivation by HPLC (Agilent Technologies, Santa Clara, United States) equipped with a Supelco guard column, a Supelco gel C-610H ion-exchange column (Sigma-Aldrich, Vienna, Austria) and a refractive index detector (Agilent Technologies, Santa Clara, United States). The mobile phase was 0.1 % H_3PO_4 with a constant flow rate of 0.5 $mL \cdot min^{-1}$ and the system was run isocratically. Calibration was done by measuring standard points in the range of 0.1 to 10 $g \cdot L^{-1}$ glycerol and MeOH.

Data analysis
Strain characteristic parameters of the bioreactor cultivation were determined at a carbon dioxide evolution rate (CER) above 2.5 $mmol \cdot g^{-1} \cdot h^{-1}$ during each MeOH pulse. Along the observed standard deviation for the single measurement, the error was propagated to the specific rates (q_s and $q_{p)}$ as well as to the yield coefficients. The error of determination of the specific rates and the yields was therefore set to 10 % and 5 %, respectively (Dietzsch et al. 2011a).

Enzyme characterization

Kinetic constants
A cell free bioreactor supernatant with HRP C1A from the $SuperMan_5$ strain was 2x concentrated and diafiltrated with buffer (500 mM NaCl, 20 mM NaOAc, pH 6.0) (Krainer et al. 2014, Spadiut et al. 2012). Protein concentration of the HRP C1A preparation was determined at 595 nm using the Bradford Protein Assay Kit (Bio-Rad Laboratories GmbH, Austria) with bovine serum albumin as standard. The kinetic constants for ABTS and H_2O_2 were determined. The reaction was started by adding 10 µL enzyme solution (1.0 $mg \cdot mL^{-1}$) to 990 µL reaction buffer containing either ABTS in varying concentrations (0.01 - 5 mM) and 1 mM H_2O_2 or H_2O_2 in varying concentrations (0.001 – 0.5 mM) and 5 mM ABTS in 50 mM potassium phosphate buffer at pH 6.5. The change in absorbance at 420 nm was recorded in a spectrophotometer UV-1601 (Shimadzu, Japan) at 30°C. Absorption curves were recorded with a software program (UVPC Optional Kinetics; Shimadzu, Japan).

Thermal stability
The purified enzyme solution was incubated at 60°C. At different time points, aliquots were withdrawn, the solutions were immediately cooled and centrifuged (20,000 g, 15 min) to pellet precipitated proteins and the remaining catalytic activity in the supernatants was measured.

Abbrevations

FSC	Flow cytometry forward scatter signal [-]
SSC	Flow cytometry sideward scatter signal [-]
$max.\mu_{Gly}$	maximum specific growth rate glycerol $[h^{-1}]$
$Y_{X/Gly}$	biomass yield on glycerol $[Cmol \cdot Cmol^{-1}]$
$Y_{CO2/Gly}$	CO_2 yield on glycerol $[Cmol \cdot Cmol^{-1}]$
$\Delta time_{adapt}$	time from first MeOH addition to maximum offgas activity[h]
q_{MeOH}	average specific uptake rate of MeOH during MeOH pulses $[mmol \cdot g^{-1} \cdot h^{-1}]$
q_P	specific product formation rate $[U \cdot g^{-1} \cdot h^{-1}]$
$Y_{X/MeOH}$	biomass yield on MeOH $[Cmol \cdot Cmol^{-1}]$
$Y_{CO2/MeOH}$	CO2 yield on MeOH$[Cmol \cdot Cmol^{-1}]$

Declarations

Ethics approval and consent to participate

Not applicable. The manuscript does not contain data collected from humans or animals.

Consent of publication

Not applicable.

Availability of data and materials

The dataset(s) supporting the conclusions of this article are all included within the article. The datasets used and/or analyzed during the current study, if not shown in the text or additional files, are available from the corresponding author on reasonable request.

Competing interest

The authors declare that they have no competing interests.

Funding

The authors are very grateful to the Austrian Science Fund (FWF): project P30872-B26.

Authors' Contributions

OSP, APE and LVE planned the experiments. APE, LVE and VRA performed the experiments and analyzed the data. LVE analyzed the flow cytometry data. CGG and FAL conducted and analyzed the ESI-MS measurements. CHE gave valuable scientific input. APE, LVE and OSP wrote the manuscript.

References

Alain R, Yves C, Ludmila O, Francois K (1995) Three-dimensional structure of tubular networks, presumably Golgi in nature, in various yeast strains: A comparative study. The Anatomical Record 243: 283-293

Baeshen MN, Bouback TA, Alzubaidi MA, Bora RS, Alotaibi MA, Alabbas OT, Alshahrani SM, Aljohani AA, Munshi, RA, Al-Hejin A, Ahmed MM, Redwan EM, Ramadan HA, Saini KS, Baeshen NA (2016) Expression and Purification of C-Peptide Containing Insulin Using *Pichia pastoris* Expression System. Biomed Res Int 3423685

Capone S, Horvat J, Herwig C, Spadiut O (2015) Development of a mixed feed strategy for a recombinant *Pichia pastoris* strain producing with a de-repression promoter. Microb Cell Fact 14: 101

Choi BK, Bobrowicz P, Davidson RC, Hamilton SR, Kung DH, Li HJ, Miele RG, Nett JH, Wildt S, Gerngross TU (2003) Use of combinatorial genetic libraries to humanize N-linked glycosylation in the yeast *Pichia pastoris*. PNAS 100: 5022-5027.

Cregg JM, Cereghino JL, Shi JY, Higgins DR (2000) Recombinant protein expression in *Pichia pastoris*. Molecular Biotechnology 16: 23-52

Cregg JM, Tolstorukov I, Kusari A, Sunga J, Madden K, Chappell T (2009) Expression in the yeast *Pichia pastoris*. Methods in enzymology 463: 169-189

De Meyer T, Laukens B, Nolf J, Van Lerberge E, De Rycke R, De Beuckelaer A, De Buck S, Callewaert N, Depicker A (2015) Comparison of VHH-Fc antibody production in *Arabidopsis thaliana*, *Nicotiana benthamiana* and *Pichia pastoris*. Plant Biotechnol J 13: 938-947

Dietzsch C, Spadiut O, Herwig C (2011)a A dynamic method based on the specific substrate uptake rate to set up a feeding strategy for *Pichia pastoris*. Microb Cell Fact 10: 14

Dietzsch C, Spadiut O, Herwig C (2011)b A fast approach to determine a fed batch feeding profile for recombinant *Pichia pastoris* strains. Microb Cell Fact 10: 85

Dubelaar GBJ, Gerritzen PL (2000) CytoBuoy: a step forward towards using flow cytometry in operational oceanography. Scientia Marina 64: 255-265

Effenberger I, Harport M, Pfannstiel J, Klaiber I, Schaller A (2017) Expression in *Pichia pastoris* and characterization of two novel dirigent proteins for atropselective formation of gossypol. Appl Microbiol Biotechnol 101: 2021-2032

Ehgartner D, Herwig C, Neutsch L (2016) At-line determination of spore inoculum quality in *Penicillium chrysogenum* bioprocesses. Appl Microbiol Biotechnol 100: 5363-5373

Gmeiner C, Saadati A, Maresch D, Krasteva S, Frank M, Altmann F, Herwig C, Spadiut O (2015) Development of a fed-batch process for a recombinant *Pichia pastoris* Deltaoch1 strain expressing a plant peroxidase. Microb Cell Fact 14: 1

Gmeiner C, Spadiut O (2015) Effects of different media supplements on the production of an active recombinant plant peroxidase in a *Pichia pastoris Δoch1* strain. Bioengineered 6: 175-178

Gruber C, Altmann F (2015) Site-Specific Glycosylation Profiling Using Liquid Chromatography-Tandem Mass Spectrometry (LC-MS), in: Castilho, A. (Ed.), Glyco-Engineering: Methods and Protocols. Springer New York, New York, NY, pp. 407-415.

Hamilton SR, Cook WJ, Gomathinayagam S, Burnina I, Bukowski J, Hopkins D, Schwartz S, Du M, Sharkey NJ, Bobrowicz P, Wildt S, Li H, Stadheim TA, Nett JH (2013) Production of sialylated O-linked glycans in *Pichia pastoris.* Glycobiology 23: 1192-1203

Hamilton SR, Davidson RC, Sethuraman N, Nett JH, Jiang Y, Rios S, Bobrowicz P, Stadheim TA, Li H, Choi BK, Hopkins D, Wischnewski H, Roser J, Mitchell T, Strawbridge RR, Hoopes J, Wildt S, Gerngross TU (2006) Humanization of yeast to produce complex terminally sialylated glycoproteins. Science 313: 1441-1443.

Hamilton SR, Gerngross TU (2007) Glycosylation engineering in yeast: the advent of fully humanized yeast. Current opinion in biotechnology 18: 387-392

Høiberg-Nielsen R, Westh P, Skov LK, Arleth L (2009) Interrelationship of Steric Stabilization and Self-Crowding of a Glycosylated Protein. Biophysical Journal 97: 1445-1453

Godon C, Lagniel G, Spector S, Garin J, Labarre J (1999) Yap1 and Skn7 Control Two Specialized Oxidative Stress Response Regulons in Yeast. The Journal of biological chemistry 274: 16040 - 16046

Jacobs PP, Geysens S, Vervecken W, Contreras R, Callewaert N (2009) Engineering complex-type N-glycosylation in *Pichia pastoris* using GlycoSwitch technology. Nature protocols 4: 58-70

Jacobs PP, Inan M, Festjens N, Haustraete J, Van Hecke A, Contreras R, Meagher MM, Callewaert N (2010) Fed-batch fermentation of GM-CSF-producing glycoengineered *Pichia pastoris* under controlled specific growth rate. Microb Cell Fact 9: 93

Krainer FW, Capone S, Jager M, Vogl T, Gerstmann M, Glieder A, Herwig C, Spadiut O (2015) Optimizing cofactor availability for the production of recombinant heme peroxidase in *Pichia pastoris*. Microb Cell Fact 14: 4.

Krainer FW, Dietzsch C, Hajek T, Herwig C, Spadiut O, Glieder A (2012) Recombinant protein expression in *Pichia pastoris* strains with an engineered methanol utilization pathway. Microb Cell Fact 11: 22.

Krainer FW, Gmeiner C, Neutsch L, Windwarder M, Pletzenauer R, Herwig C, Altmann F, Glieder A, Spadiut O (2013) Knockout of an endogenous mannosyltransferase increases the homogeneity of glycoproteins produced in *Pichia pastoris*. Scientific reports 3: 3279-3279

Krainer FW, Pletzenauer R, Rossetti L, Herwig C, Glieder A, Spadiut O (2014) Purification and basic biochemical characterization of 19 recombinant plant peroxidase isoenzymes produced in *Pichia pastoris*. Protein Expression and Purification 95: 104-112

Li S, Dean S, Li Z, Horecka J, Deschenes RJ, Fassler JS (2002) The eukaryotic two-component histidine kinase Sln1p regulates OCH1 via the transcription factor, Skn7p. Mol Biol Cell 13: 412-424

Liu CP, Tsai TI, Cheng T, Shivatare VS, Wu CY, Wu CY, Wong CH (2018) Glycoengineering of antibody (Herceptin) through yeast expression and in vitro enzymatic glycosylation. Proc Natl Acad Sci USA 115: 720-725

Lommel M, Strahl S (2009) Protein O-mannosylation: conserved from bacteria to humans. Glycobiology 19: 816-828

Maciola AK, Pietrzak MA, Kosson P, Czarnocki-Cieciura M, Smietanka K, Minta Z, Kopera E (2017) The Length of N-Glycans of Recombinant H5N1 Hemagglutinin Influences the Oligomerization and Immunogenicity of Vaccine Antigen. Front Immunol 8: 444

Naatsaari L, Mistlberger B, Ruth C, Hajek T, Hartner FS, Glieder A (2012) Deletion of the *Pichia pastoris* KU70 homologue facilitates platform strain generation for gene expression and synthetic biology. PLoS One 7: e39720.

Nagasu T, Shimma Y, Nakanishi Y, Kuromitsu J, Iwama K, Nakayama K, Suzuki K, Jigami Y (1992) Isolation of new temperature-sensitive mutants of *Saccharomyces cerevisiae* deficient in mannose outer chain elongation. Yeast 8: 535-547

Nakayama K, Nagasu T, Shimma Y, Kuromitsu J, Jigami Y (1992) OCH1 encodes a novel membrane bound mannosyltransferase: outer chain elongation of asparagine-linked oligosaccharides. The EMBO journal 11: 2511-2519.

Nett JH, Stadheim TA, Li H, Bobrowicz P, Hamilton SR, Davidson RC, Choi BK, Mitchell T, Bobrowicz B, Rittenhour A, Wildt S, Gerngross TU (2011) A combinatorial genetic library approach to target heterologous glycosylation enzymes to the endoplasmic reticulum or the Golgi apparatus of *Pichia pastoris*. Yeast 28: 237-252

Parekh R (1991) Automation of glycosylation analysis: a way forward for recombinant therapeutics. Glycoconjugate journal 8: 63-65

Puxbaum V, Mattanovich D, Gasser B (2015) Quo vadis? The challenges of recombinant protein folding and secretion in *Pichia pastoris*. Appl Microbiol Biotechnol 99: 2925-2938

Smith ET, Perry ET, Sears MB, Johnson DA (2014) Expression of recombinant human mast cell chymase with Asn-linked glycans in glycoengineered *Pichia pastoris*. Protein Expr Purif 102: 69-75

Söderström BE (1977). Vital staining of fungi in pure cultures and in soil with fluorescein diacetate. Soil Biol. Biochem. 9, 59 - 63

Spadiut O, Leitner C, Salaheddin C, Varga B, Vertessy BG, Tan TC, Divne C, Haltrich D (2009) Improving thermostability and catalytic activity of pyranose 2-oxidase from *Trametes multicolor* by rational and semi-rational design. FEBS J 276: 776-792

Spadiut O, Rossetti L, Dietzsch C, Herwig C (2012) Purification of a recombinant plant peroxidase produced in *Pichia pastoris* by a simple 2-step strategy. Protein Expression and Purification 86, 89-97

Tams JW, Welinder KG (1998) Glycosylation and thermodynamic versus kinetic stability of horseradish peroxidase. Febs Lett 421: 234-236

Tang H, Wang S, Wang J, Song M, Xu M, Zhang M, Shen Y, Hou J, Bao X (2016) N-hypermannose glycosylation disruption enhances recombinant protein production by regulating secretory pathway and cell wall integrity in *Saccharomyces cerevisiae*. Scientific reports 6: 25654

Tripathi K, Matmati N, Zheng WJ, Hannun YA, Mohanty BK (2011) Cellular Morphogenesis Under Stress Is Influenced by the Sphingolipid Pathway Gene ISC1 and DNA Integrity Checkpoint Genes in *Saccharomyces cerevisiae*. Genetics 189: 533-547

Wang Z, Guo C, Liu L, Huang H (2018) Effects of N-glycosylation on the biochemical properties of recombinant bEKL expressed in *Pichia pastoris*. Enzyme Microb Technol 114: 40-47.

Supplementary Material

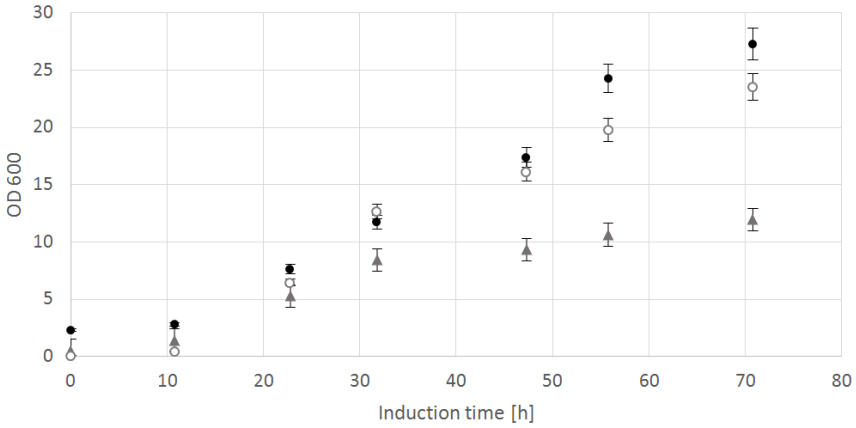

Supplementary Figure 1: OD_{600} over induction time in shake-flask experiment, black-filled circle = wt, unfilled white circle = SuperMan5, grey triangle = Δ*OCH1*.

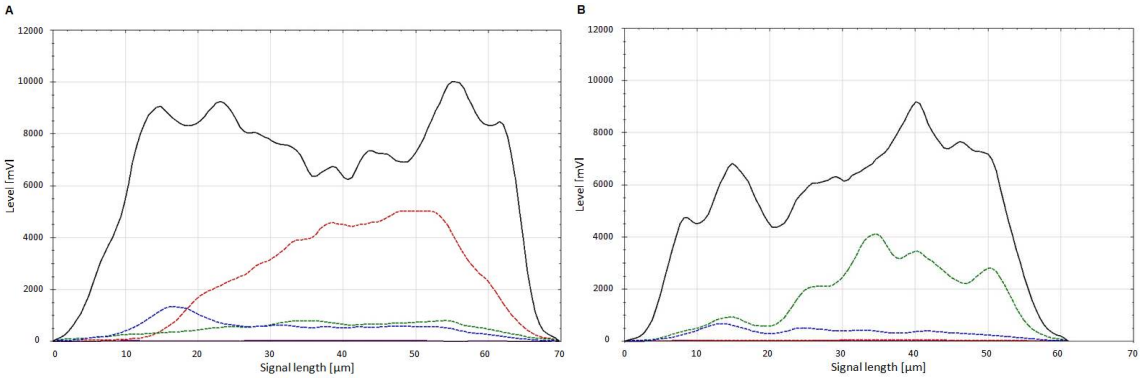

Supplementary Figure 2: Comparison of signal profiles from flow cytometer. FSC (black line -), SSC (blue line --), green (green line --) and red (red line --) fluorescence signals of SuperMan$_5$ clusters after 23 h induction time in shake-flasks. In viability-declined cluster (A) a clear increase in red fluorescence is visible from PI staining in contrast to the viable cluster (B).

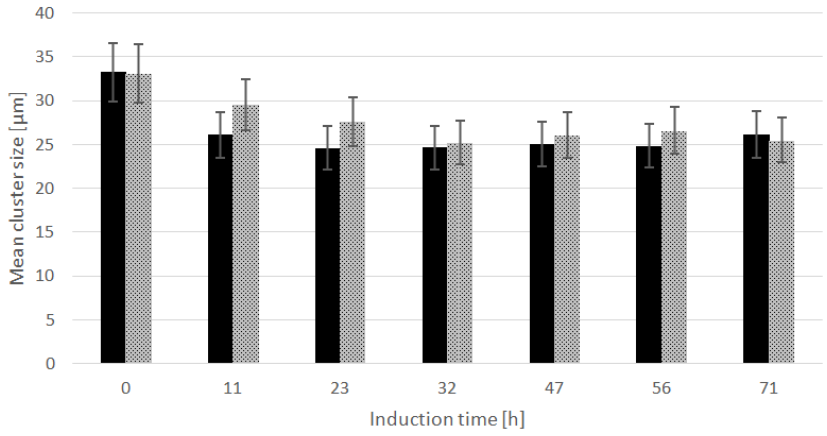

Supplementary Figure 3: Mean cluster size of Δ*OCH1* (black bars) and SuperMan$_5$ (dotted grey bars) over induction time in shake-flask cultivation. Standard deviations are derived from multiple measurements (at least 3) of single culture shake-flask samples.

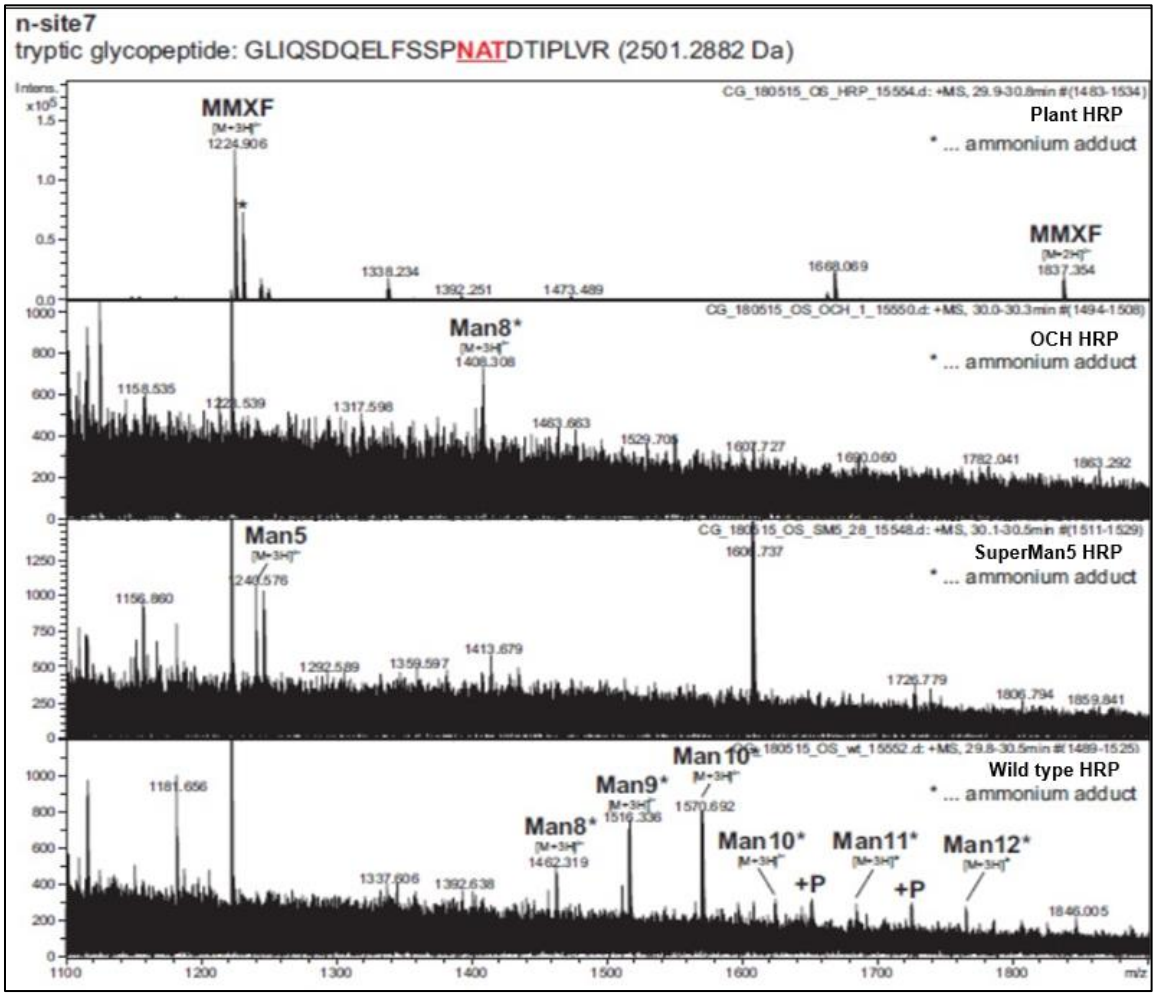

Supplementary Figure 4: ESI-MS spectra of HRP glycopeptides at n-glycosylation site 7. The triply (or doubly) charged site 7 N-glycopeptide GLIQSDQELFSSP**NAT**DTIPLVR of natural HRP and HRP produced in a ΔOCH1, in SuperMan$_5$ and in wt *P. pastoris* are shown. The wt_HRP exhibits also phosphorylated versions (P) of the oligomannosidic glycans.

To avoid interference by glycoproteins other than HRP, the glycosylation status of the HRP variants was deduced from glycopeptides, as shown for glycosite 7 (GLIQSDQELFSSPNATDTIPLVR). While natural HRP carries the plant typical MMXF structure with xylose and fucose and only 3 mannose residues, HRP C1A produced by wt *P. pastoris* exhibited a very heterogeneous pattern in which Man$_9$ and Man$_{10}$ glycans predominated and some phosphorylated glycans were also found. HRP C1A from the ΔOCH1 strain contained mainly the Man$_8$ structure and HRP C1A from the SuperMan$_5$ strain was modified by Man$_5$ as expected.

Chapter 8.
Summary, Conclusion and Outlook

Summary

Within this Thesis, PAT is defined as a framework for 'designing, analysing, and controlling manufacturing through timely measurements of critical quality and performance attributes' (Simon et al. 2015). In the scope of filamentous bioprocesses these critical attributes can be defined as 'biomass quality', comprising favourable morphologic characteristics and high biomass viability. The stepwise approach to achieve an optimised morphology for enhanced biomass viability can be summarised as follows:

Comprehensive insight into the relationship between filamentous fungal pellets, morphology and productivity is compiled in 'Chapter 4. State of the Art' in the form of a published review.

To employ PAT in the scope of filamentous bioprocesses, the first challenge was the development of analytical methods to obtain physiological responses specific to fungal morphology. A variety of analytical methods for this purpose is compiled in 'Chapter 5. Analytics'. In the following these methods and scientific achievements will be briefly summarized:

- A plate-reader method for viability assessment of fungal biomass via propidium iodide staining was developed and refined. This method was successfully transferred to our project partner's labs.
- A flow cytometry method for analysis of pellet morphology and viability was introduced, published and transferred to our project partner's labs.
- Spatially resolved characterisation of metabolism and productive zones in filamentous biomass was successfully conducted and published via a novel application of time-of-flight secondary ion mass spectrometry (ToF-SIMS). This method sheds further light individual morphological characteristics of fungal biomass.

'Chapter 6. Control' deals with the application of said analytical methods in process optimization.

- Dielectric spectroscopy and plate-reader viability assessment were employed for control of the specific growth rate in *P. chrysogenum* fed-batch processes featuring on-line quantification of viable biomass.
- Novel morphological responses were analysed using flow cytometry to obtain an optimal operating range in *P. chrysogenum* fed-batch processes ensuring high viability and productivity.

'Chapter 7. Impact' outlines the scientific and industrial impact of this work. Transferability of methods from 'Chapter 5' is demonstrated through an additional publication focusing on successful morphological and physiological analysis of glycol-engineered *P. pastoris* strains.

List of publications

As first author, published

Veiter L., Kubicek M., Hutter H., Pittenauer E., Herwig C. and Christoph Slouka 'Study of metabolism and identification of productive regions in filamentous fungi via spatially-resolved Time-of-Flight Secondary Ion Mass Spectrometry.' Anal Bioanal Chem., 2019.

Veiter L. and Christoph Herwig 'The filamentous fungus *Penicillium chrysogenum* analysed via flow cytometry - a fast and statistically sound insight into morphology and viability.' Appl Microbiol Biotechnol., 2019.

Pekarsky A.*, Veiter L.*, Rajamanickam V., Herwig C., Grünwald-Gruber C., Altmann F. and Oliver Spadiut 'Production of a recombinant peroxidase in different glyco-engineered *Pichia pastoris* strains: a morphological and physiological comparison.' Microb Cell Fact. 2018.
*equal contribution

Veiter L., Rajamanickam V. and Christoph Herwig 'The filamentous fungal pellet - relationship between morphology and productivity.' Appl Microbiol Biotechnol., 2018.

As co-author, published

Ehgartner D., Hartmann T., Heinzl S., Frank M., Veiter L., Kager J., Herwig C. and Jens Fricke 'Controlling the specific growth rate via biomass trend regulation in filamentous fungi bioprocesses.' Chem Eng Sci., 2017.

As first author, manuscripts submitted for publication

Veiter L., Kager J. and Christoph Herwig 'Optimal process design space to ensure maximum viability and productivity in *Penicillium chrysogenum* pellets during fed-batch cultivations through morphological and physiological control.' submitted to Microbial Cell Factories.

Posters and Scientific Presentations

Oral Presentation: 'Monitoring of Biomass Agglomerates in Filamentous Fungi via Flow Cytometry'. PYFF7 Conference on Physiology of Yeast & Filamentous Fungi - Milan 2019

Posters: 'Flow Cytometry as a versatile tool to monitor biomass agglomerates'. ECAB 5 European Congress of Applied Biotechnology - Florence 2019, RPP 10 Conference on Recombinant Protein Production - Crete 2019, BioProduction Congress - Dublin 2018

Conclusion

In filamentous bioprocesses the term 'quality' does not necessarily encompass quality of product but rather quality of the productive biomass itself. The reason for this lies in the specific morphological characteristics of fungal biomass, which has been thoroughly addressed in 'Chapter 4. State of the Art' of this Thesis.

The aim of this Thesis was to develop several PAT tools that specifically deal with application challenges in filamentous fungi cultivations. All our efforts can be summarized as an attempt to take fungal morphology into account when developing these PAT tools and analytical methods.

The goal of this Thesis is to provide analytical methods enhanced for fungal morphology as monitoring tools to be used in fermentation to ensure optimal morphology, viability and productivity through optimization of cultivation parameters.

Morphology, viability and productivity are to be:

- depicted via analytics
- predicted via data-driven modelling
- controlled through adaption of fermentation parameters

Based upon the Hypotheses described in 'Chapter 2. Hypotheses and Goal of the Thesis' we can conclude the following:

<u>Hypotheses 1 and 2</u>

1. There is a close relationship between morphology, viability and productivity.
2. Morphology and viability are affected by fermentation parameters and assessable via advanced analytical methods enhanced for fungal morphology.

We have addressed these points in the development of the following PAT tools:

- At-line determination of overall viability (Veiter and Herwig 2019)
- Assessment of pellet specific morphology and viability (Veiter and Herwig 2019)
- Demonstrate applicability of methodology for yeast (Pekarsky et al. 2018)

<u>Hypothesis 3</u>

3. Morphology, viability and productivity can be controlled through optimisation of fermentation parameters.

Process control strategies based on physiological or morphological aspects were introduced:

- Control of specific growth rate in *P. chryosogenum* bioprocesses (Ehgartner et al. 2017)
- Optimal process design space to ensure maximum viability and productivity in *Penicillium chrysogenum* pellets during fed-batch cultivations through morphological and physiological control (submitted to Microb Cell Fact.)

We can define several success factors that helped us in dealing with challenges in method development for filamentous bioprocesses:

Focused development of analytical methods
All methods depicted in 'Chapter 5. Analytics' and 'Chapter 6. Control' are tailored to specific industrial needs. The definition of a clear goal and individual industrial needs is extremely valuable in the design and development of applied science. We have strived to incorporate the viewpoint of industry in our research to ensure future applications of our work in industrial process development.

Close co-operation with industrial partner
As our goal was to provide methods for applied science, close communication with industry was of prime importance. In our efforts to transfer methods from university labs to industry we had to deal with previously unknown challenges and attempt to resolve them according to our project partner's needs. This led to a comprehensive account of potential problems when applying our methods which could be discussed in detail in our publications. On several occasions we could add a section dealing with 'Advantages, disadvantages and comparability to other methods', thereby our methods were thoroughly and honestly characterised.

Interdisciplinary approach
The general focus in our research division has always been an interdisciplinary one. The goals within this Thesis could only be achieved through co-operation with other research fields, such as:

- Control of specific growth rate (Ehgartner et al. 2017) was achieved through a control loop combining at-line and online viability assessment. Realisation of the real-rime data access with Matlab and controller implementation was done in co-operation with 'modelling' team members.
- Control of specific substrate uptake rate was achieved through implementation of mechanistic models on filamentous biomass growth in co-operation with 'modelling' team members.
- ToF-SIMS measurements to study metabolism and identify productive biomass regions was done in co-operation with Markus Kubicek, who performed and analysed ToF-SIMS measurements (Veiter et al. 2019).

Table 8.1 summarises some goals and success factors in the scope of this Thesis. The main scientific impact of this Thesis lies in the application of novel morphological descriptors obtained from robust and transferable analytical methods for subsequent bioprocess optimisation. Individual novelty aspects are also discussed in Table 8.1.

Table 8.1. Goals and success factors in method development

Goal	Achievement	Success factor	Scientific novelty
Analytics			
Assessment of individual and overall biomass viability in various process phases	Flow cytometry method (Veiter and Herwig 2019)	Focused development of analytical methods tailored to industrial need	Viability assessment of individual fungal pellets
Physiological and morphological pellet characterisation	Flow cytometry method (Veiter and Herwig 2019)	Focused development of analytical methods: close co-operation with industrial partner	Novel morphological descriptors for fungal pellets: viable layer, compactness
Spatially resolved characterisation of meta-bolism and productive zones in *P. chrysogenum*	ToF-SIMS method (Veiter et al. 2019b)	Interdisciplinary approach: assistance, co-operation with other research divisions	Novel insight into morphology dependent metabolism and productivity
Control			
Control of specific growth rate in *P. chrysogenum* bioprocesses	Combining plate reader method and dielectric spectroscopy (Ehgartner et al. 2017)	Focused development of analytical methods tailored to industrial need	Control of specific growth rate based on online measurement of viable biomass considering growth and decline phase of filamentous culture
Optimal operating range ensuring high viability and productivity in a *P. chrysogenum* bioprocess	Combining flow cytometry, design of experiments and data driven modelling (submitted to Microb Cell Fact.)	Interdisciplinary approach: assistance, co-operation; comprehensive research on fermentation parameters affecting morphology	Use of novel morphological descriptors in filamentous bioprocess optimisation
Impact and Transferability towards other organisms			
Physiological and morphological study of glycol-engineered *P. pastoris* strains	Flow cytometry method (Pekarsky et al. 2018)	Interdisciplinary approach: assistance, co-operation	First evaluation of growth, physiology, morphology and recombinant protein production of a $Man_5GlcNAc_2$ glycosylating strain in a bioreactor

Outlook

Within this Thesis a number of analytical methods applicable as PAT tools are complied. To a lesser extent, we have employed several of these analytical methods to obtain morphological and physiological responses in the optimization of fermentation process design spaces. Finally, we could demonstrate that an analytical method developed for *P. chryosogenum* is also applicable for *P. pastoris* with minimal adaption steps.

Naturally, there is still room for further work and improvements.

- The flow cytometry method for morphological and physiological analysis of *P. chryosogenum* displays issues regarding size-exclusion effects and fluorescence detector over-saturation as discussed in Veiter and Herwig 2019.
  Some of these issues could be addressed by developing a standard operating procedure for detector settings to customize the method for different strains and other organisms.
- Several methods compiled in 'Chapter 5. Analytics' were only tested at-line, but some of them could be used in an on-line capacity. In the field of PAT applications, more on-line applications would be desirable.
- The manuscript 'Optimal operating range ensuring high viability and productivity in *P. chrysogenum* bioprocesses' fundamentally deals with optimizations in the main-culture phase of the process. In filamentous fungi also a pre-culture phase is necessary to ensure pellet growth, while production of penicillin is happening in the subsequent main-culture stages. Additional efforts to optimize the pre-culture could lead considerable improvement regarding viability and productivity in later process stages.
- All *P. chrysogenum* cultivations were performed with strains provided by Sandoz GmbH. Obviously, these strains were very different in behavior compared to the most recent production strains. Consequently, some of our findings must be tested in industrial conditions to ensure comparability and transferability of our control approaches.
- Several analytical methods could also be tested using other filamentous or agglomerate forming organisms. We are currently working on applications for *Trichoderma*, *Lentzea* and *P. pastoris* to characterize the morphology or distinguish between single and budding yeast cells.

In addition to the efforts depicted in this Thesis, I believe that further use of modelling and model based experimental design would greatly benefit the understanding of interlinks between biomass growth, morphology, viability and finally productivity.

Such a model based experimental design would require several modelling stages:

- For control of the growth rate during cultivation, an exponential growth model with varying substrate yield coefficient would be sufficient. Online biomass estimation though permittivity probes could verify this model in a timely fashion as already demonstrated in Ehgartner et al. 2017.

- To maintain a constant specific glucose uptake rate of biomass q_s, the glucose feed can be was adjusted based on the actual biomass concentration within the bioreactor estimated by real-time model simulation of a literature model of *P. chrysogenum* as described in 'Chapter 6. Control'
- For model-based experimental design, a diffusion model would be needed in order to estimate limiting substrates beforehand through diffusion coefficients. Subsequently, the experimental design for additional verification runs in fermentation could be obtained.
- As mentioned in 'Chapter 4. State of the Art' and 'Chapter 6. Control' a diffusion model must take morphological aspects of pellets into account. This might be just simple description dependent on pellet size. However, in my estimation certain morphological descriptors like pellet porosity, the hyphal gradient (Hille et al. 2005, Hille et al. 2009) or pellet compactness (Veiter et al. 2019a) would be needed for a more thorough and valuable description of diffusion. Naturally, the effects of power input and resulting shear stress on morphology must be considered as well.

These modelling efforts are currently being advanced, a comprehensive diffusion model was already developed in the course of the CD Laboratory. Therefore, the potential upcoming task as envisioned in this Thesis would be to further combine all available methods in modelling and morphological analytics. These findings could also be used in experimental design, in order to obtain additional datasets for model verification and process optimization.

References

Ehgartner D, Hartmann T, Heinzl S, Frank M, Veiter L, Kager J, Herwig C, Fricke J (2017) Controlling the specific growth rate via biomass trend regulation in filamentous fungi bioprocesses. Chem Eng Sci 172: 32-41

Hille A, Neu TR, Hempel DC, Horn H (2005) Oxygen profiles and biomass distribution in biopellets of *Aspergillus niger*. Biotechnol Bioeng 92(5): 614-623

Hille A, Neu TR, Hempel DC, Horn H (2009) Effective diffusivities and mass fluxes in fungal biopellets. Biotechnol Bioeng 103(6): 1202-1213

Pekarsky A, Veiter L, Rajamanickam V, Herwig C, Grunwald-Gruber C, Altmann F, Spadiut O (2018) Production of a recombinant peroxidase in different glyco-engineered *Pichia pastoris* strains: a morphological and physiological comparison. Microb Cell Fact 17: 183

Simon LL, Pataki H, Marosi G, Meemken F, Hungerbuhler K, Baiker A, Tummala S, Glennon B, Kuentz M, Steele G, Kramer HJM, Rydzak JW, Chen ZP, Morris J, Kjell F, Singh R, Gani R, Gernaey KV, Louhi-Kultanen M, O'Reilly J, Sandler N, Antikainen O, Yliruusi J, Frohberg P, Ulrich J, Braatz RD, Leyssens T, von Stosch M, Oliveira R, Tan RBH, Wu HQ, Khan M, O'Grady D, Pandey A, Westra R, Delle-Case E, Pape D, Angelosante D, Maret Y, Steiger O, Lenner M, Abbou-Oucherif K, Nagy ZK, Litster JD, Kamaraju VK, Chiu MS (2015) Assessment of Recent Process Analytical Technology (PAT) Trends: A Multiauthor Review. Org Process Res Dev 19: 3-62

Veiter L, Herwig C (2019) The filamentous fungus *Penicillium chrysogenum* analysed via flow cytometry-a fast and statistically sound insight into morphology and viability. Appl Microbiol Biotechnol 103: 6725-6735

Veiter L, Kubicek M, Hutter H, Pittenauer E, Herwig C, Slouka C (2019) Study of metabolism and identification of productive regions in filamentous fungi via spatially resolved time-of-flight secondary ion mass spectrometry. Anal Bioanal Chem.

Appendix

Poetry, Posters & CV

A selection of poems written for special occasions during my doctorate.

Das Einhorn beim Bowling*

Das Einhorn stets das Bowling mied,
da ihm das Spiel dort oft missriet,
denn so ist es schnell erraten,
das Horn ist oft in'd Quer geraten.
Doch seit statt Kopf benutzt es Huf,
spielt's besser gar als war sein Ruf!

* Referenz: Eugen Roth

Hiasl's Abschied

If king, or beggar, if men or mice,
it's always nice when looking nice!
Long has been known, man's beauty lies,
in muscles of substantial size.

That's why Matthias being smart,
within the gym is training hard.
He also was right from the start,
highly advanced in martial art,
where 'spite of moves and trickery,
the road can still get slippery.
In any sport that isn't fake,
the athletes' bodies often ache!

Hias also knows that looking stale,
has to do with being pale.
And superior attraction,
comes with nice and rich complexion.
Though when sunrays aren't flat,
beware the skin could turn towards red.
Then even the most dangerous mobster,
seems tame when looking like a lobster.

So careful! Full attractiveness,
comes from sometimes doing less.
Avoided should be injury,
of shoulders, skin, or arms, or knee!
So sometimes stop and better fold,
it doesn't mean you're getting old.
It only means you're getting smart,
and that's the goal in any art!

Der Grummelbär auf Urlaub*

Der Grummelbär stolz tut den Schritt,
den Urlaub er verdient antritt,
denn ewig hat er abgewartet,
ob ihm der Olli gut geartet.
Nun denn, vorm Urlaub, wahrt er das Haus,
dreht überall die Lichter aus,
sind Kühlschrank, Äkta erst versorgt,
sperrt rasch er ab, fährt heiter fort.

Doch später beim Passieren der Grenze,
scheint Heiterkeit verloren zur Gänze,
wild steigert er sich in den Wahn,
er hätte vieles nicht getan.
Voll Schaudern sieht er dann im Geiste,
wie aufgetaut und warm das meiste,
die Tür des Kühlschranks offen weit,
das Licht entflammt die ganze Zeit!

Zu klären solchen Sinnestrug,
Fährt heim er mit dem nächsten Zug
Und ist schon dankbar, bloß zu sehn:
Bauteil BH scheint noch zu stehn!
Wie er hinauf die Treppe keucht:
Kommt aus der Labor kein Geleucht?
Und plötzlich scheint's dem Grummelbär,
die Stickstoff-Flasche wäre leer!

Doch alle Ängste unermessen:
der Grummelbär hat nichts vergessen!
Er schnuppert, fühlt und lauscht und äugt
Und ist mit Freuden überzeugt,
obgleich er hat es nicht gedacht,
zu Unrecht Sorgen sich gemacht.
Er fährt zurück und ist nicht bang.-
jetzt brennt das Licht vier Wochen lang.

* Referenz: Eugen Roth

Hymn to Black Dynamite by Batman

A warrior with tiger roots,
who's drinking milk and eating fruits.
In myths and stories being told,
his glory can't be weighted in gold.

A monolith in times of trouble,
a knight that shines in smoke and rubble.
If dark and endless feels the night,
Black Dynamite will make it right!

No dataset is set in ink,
all peaks shall form the fingerprint,
illuminate the knowledge's path,
to answers firmly in our grasp.

I've seen it all from day to day,
seen Post-Docs come and walk away,
but now will dawn a brighter day,
Black Dynamite is here to stay.

As Doctor now he holds the dam,
fights tyranny of evil man,
within our world of troubledness,
he's Shepard for the righteousness.

If dynamite lies in the dark,
it only takes the smallest spark,
and up it roars our guiding light,
Hail to you Black Dynamite!

Sincerely,
Your devoted Batman!

Präludium zum wurmstichigen Maibaum

Wenn landläufig vom Wurm die Rede,
dann ist das in der Regel blöde,
doch manchmal wenn der Wurm ist drin,
dann kann's auch seien ein Gewinn.

Ballade vom wurmstichigen Maibaum

Emsig pirschend sieht der Wurm,
sich lange schon im Walde um,
denn jener Baum, der bald wird fallen,
der soll als Maibaum wohl gefallen.

Doch damit nicht erschöpft sein Sinn,
der Baum, er soll zur Liebsten hin,
zum Anhalten um Lisas Hand,
empfiehlt's der Brauch im Burgenland.

Nach langem Spähen in jede Richtung,
endlich erblickend auf der Lichtung,
denn altbekannt, dass viele Birken,
besonders schön und prächtig wirken.

Wie David ist sie groß und schlank,
wie Lisa ist sie schlank und rank.
Ein Wunderwerk aus der Natur,
es muss jetzt aus dem Walde nur.

Von starker Hand die Sägen wetzen,
die Äste baumeln, es flieg'n die Fetzen,
und in taumeligem Reigen,
beginnt sich rasch der Baum zu neigen.

Der Baum wird aus dem Wald gekarrt,
die Rinde wird ihm abgeschabt,
und als die Sonne dann aufgeht,
der Baum vor Baders Haustür steht.

Doch Sonnenlicht, das macht im Harz
jetzt Löcher sichtbar, klein und schwarz.
Der Wurm, er seufzt, er glaubt es kaum,
wurmstichig, so scheint der Baum.

Und jäh durchzuckt ihn jetzt der Schreck,
hurtig, rasch, der Baum muss weg,
doch als er ihn beginnt zu heben,
im Haus die Jalousien sich regen.

Und was ihm auch noch nicht gefällt,
er scheint enttarnt, denn Diego bellt,
Bevor vom Höllenhund entdeckt,
er rasch sich im Gebüsch versteckt.

Dort denkt er nun, 'Ich armer Tor,
Der Maibaum morsch vor Lisas Tor,
wird fallen auf Fenster, Auto, Dach,
in einem fürchterlichen Krach.

Welch unglücklicher Unglückstag,
ob mich die Lisa jetzt noch mag?
Der Baders Gespött nun ich bin,
das hat doch alles keine Sinn!'

Und bald beginnt zu hören er Stimmen,
die lauter werdend zu ihm dringen.
als ob die Baders rufen forsch,
'Der Baum taugt nichts, der ist ja morsch.'

Doch als er dann genau hinhört,
langsam verschwindet, was ihn stört,
in Wahrheit ist zu hören nichts Grobes,
die Stimmen die sind voll des Lobes.

Des Baumes Größe wird gepriesen,
'ob er gefällt durch Hand von Riesen?'
Nur die Lisa muss nicht raten,
der Wurm im Stamm hat's ihr verraten!

Ode an den Sloukulus

Ein Hoch auf Slouki, stoßet an,
den zweiten Doktor er bezwang,
obwohl beim Doktor, kann man sagen,
da muss man viel Verdruß ertragen!

Studiert hat er schon lang Chemie,
jüngst auch erlernt Biologie,
seit neuem die Juristerei,
sein Resumé fast einwandfrei.

Denn trotz der allerbesten Bildung,
verwirrt des Kohlenstoffes Bindung.
Ein Anker der muss sein die Vier,
sonst wird der Gärtner glatt zum Stier!

Weithin zu hören ist sein Schmatzen,
Slouki isst nicht nur gern Krapfen,
auch jene zu legen macht ihn froh,
notfalls auch am Damenklo.

Verfehlungen muss prompt er rügen,
für schönen Schein mag er nicht lügen,
denn wer nicht schimpft in Simmering,
gilt oftmals gar als Kümmerling.

Legendär ist auch fürwahr,
des Sloukis wallend blondes Haar,
der Butterzopf in vollem Glanze,
er zeigt sich elegant beim Tanze!

Im Labor sein Genie besteht,
sein Herz jedoch im Ballsaal schlägt,
dies festzustellen hat nichts Bigottes,
denn Tänzer sind Athleten Gottes!

Flow cytometry as a versatile tool to analyse the morphology of viable biomass agglomerates

Lukas Veiter, Christoph Herwig
TU Wien - Institute of Chemical, Environmental and Bioscience Engineering - Research Division Biochemical Engineering - Vienna, Austria
contact: lukas.veiter@tuwien.ac.at

Motivation

Performance of specific bioprocesses depends on biomass morphology:

- pelleted growth of filamentous fungi *Penicillium chrysogenum* enables enhanced process control
- glycol-engineered *Pichia pastoris* strains tend to form agglomerates with reduced viability.

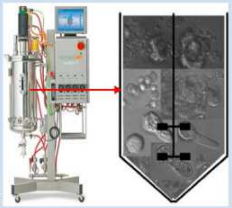

Various morphological classes in bioreactor cultivations of filamentous organisms ▸

Goal

- Method for **determination of morphology in turbid media** to discriminate cells, media particles and further analyze the morphology of biomass agglomerates.
- Method to determine **viability** within various morphological classes.

Measuring agglomeration in *P. pastoris* strains

- Distinction between 3 classes of yeast cells based on forward-scatter signals (FWS) and sample length, verifyable via microscopy and integrated camera

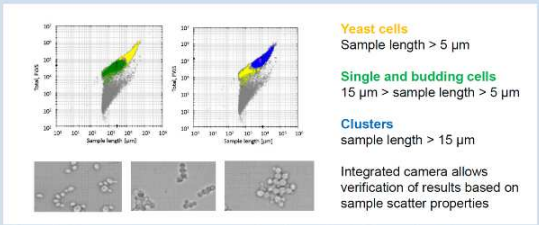

Figure 1. Flow cytometric measurement of agglomeration in *P. pastoris* strains

Measuring agglomeration in *P. chrysogenum*

- Complex morphology visualized in scatter plots

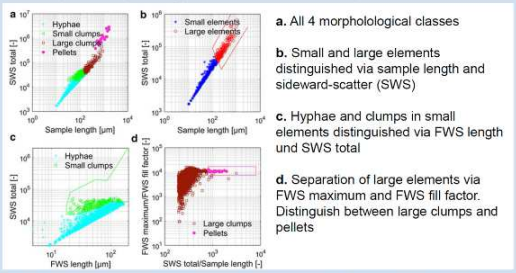

a. All 4 morpholological classes

b. Small and large elements distinguished via sample length and sideward-scatter (SWS)

c. Hyphae and clumps in small elements distinguished via FWS length und SWS total

d. Separation of large elements via FWS maximum and FWS fill factor. Distinguish between large clumps and pellets

Figure 2. Complex *P. chrysogenum* morphology analyzed via scatter properties

Exemplary analysis of viability in *P. pastoris* strains via fluorescent staining

- Use of fluorescent stains enables determination of viability in complex biomass agglomerates
- Fluorescein diacetate (FDA) measures enzymatic activity producing green fluorescence, thereby viable cells are detected.
- Propidium iodide (PI) is a DNA stain not permeant to live cells, dead cells are detected via red fluorescence.

Viable yeast cells distinguised from media background via green fluorescence

Viability-declined clusters distinguised from clusters via green fluorescence, thereby distinction between 4 classes of yeast cells

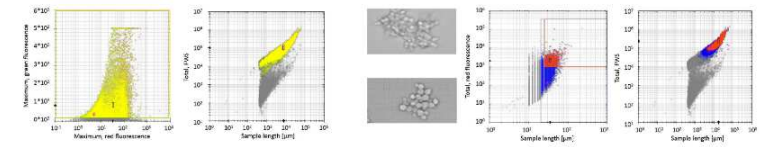

Morphological class	Defined by
Viable yeast cells	Fluorescence green, maximum > 200 Sample length > 5 µm
Single and budding cells	Fluorescence green, maximum > 200 15 µm > Sample length > 5 µm
Clusters	Fluorescence green, maximum > 200 Sample length > 15 µm
Viability-declined clusters	Fluorescence green, maximum > 200 Sample length > 15 µm Fluorescence red, total > 1000

Figure 3. Further distinction of yeast cells through employment of fluorescent staining, detection of media background (left) and viability-declined clusters (right)

Conclusion

Method for analysis of agglomerates in different organisms:

- Agglomerates in glycol-engineered *P. pastoris* strains
- Morphological classification of filamentous fungus *P. chrysogenum*

Method for investigation of viability in *P. pastoris* agglomerates

- Viability-declined clusters distinguised from viable agglomerates

Outlook

- Expand morphological classification of *P. chrysogenum* towards distinct pellet characteristics
- Expand viability determination to *P. chrysogenum*, specifically pellets
- Adapt and expand method to other agglomerate forming organisms

***P. Pastoris* and *P. chrysogenum* stories can be found in…**

Ehgartner et al. (2017) Morphological analysis of the filamentous fungus *Penicillium chrysogenum*. Appl Microbiol Biotechnol:1-14 doi:10.1007/s00253-017-8475-2
Veiter et al. (2018) Recombinant protein production in different glyco-engineered *Pichia pastoris* strains. Microb Cell Fact. 2018; 17: 183. doi: 10.1186/s12934-018-1032-6

Acknowledgments

Dr. Oliver Spadiut and Alexander Pekarsky for co-operation in *P. pastoris* experiments

RPP10 April 2019 **Crete, Greece**

Flow cytometry as a versatile tool to analyse the morphology of viable biomass agglomerates

Lukas Veiter, Christoph Herwig
TU Wien - Institute of Chemical, Environmental and Bioscience Engineering - Research Division Biochemical Engineering - Vienna, Austria
contact: lukas.veiter@tuwien.ac.at

Motivation

Performance of specific bioprocesses depends on biomass morphology:

- Pelleted growth of filamentous fungi *Penicillium chrysogenum* enables enhanced process control.
- Glycol-engineered *Pichia pastoris* strains tend to form agglomerates with reduced viability.

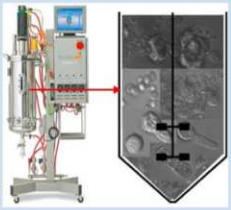

Various morphological classes in bioreactor cultivations of filamentous organisms ▸

Goal

- Method for **determination of morphology in complex media** to discriminate cells, media particles and further analyze the morphology of biomass agglomerates
- Method to determine **viability** within various morphological classes

Measuring agglomeration in *P. pastoris* strains

- Distinction between 3 classes of yeast cells based on forward-scatter signals (FWS) and sample length, verifyable via microscopy and integrated camera

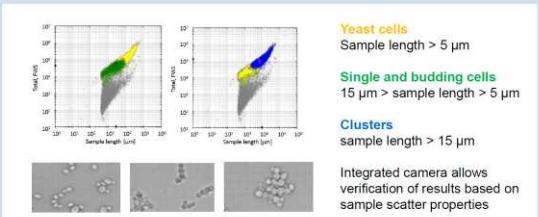

Figure 1. Flow cytometric measurement of agglomeration in *P. pastoris* strains

Measuring agglomeration in *P. chrysogenum*

- Complex morphology visualized in scatter plots

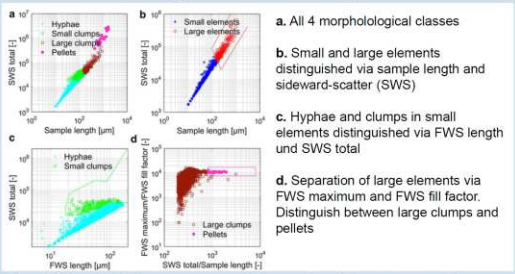

a. All 4 morpholological classes

b. Small and large elements distinguished via sample length and sideward-scatter (SWS)

c. Hyphae and clumps in small elements distinguished via FWS length und SWS total

d. Separation of large elements via FWS maximum and FWS fill factor. Distinguish between large clumps and pellets

Figure 2. Complex *P. chrysogenum* morphology analyzed via scatter properties

Information gain from measurement of distinct fungal morphology

- Use of fluorescent stains enables determination of viability in complex biomass agglomerates
- Fluorescein diacetate (FDA) measures enzymatic activity producing green fluorescence, thereby viable cells are detected.
- Propidium iodide (PI) is a DNA stain not permeant to live cells, dead cells are detected via red fluorescence.

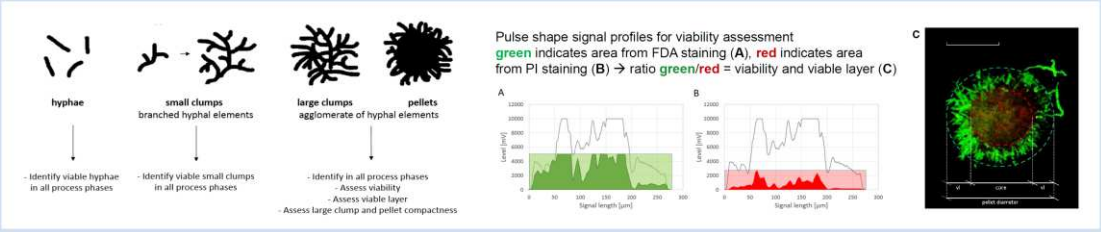

Figure 3. Further assessment of viability in individual particles - from morphological classification towards analyzing the viable layer in individual pellets.

Conclusion

Method for analysis of agglomerates in different organisms:

- Agglomerates in glycol-engineered *P. pastoris* strains
- Morphological classification of filamentous fungus *P. chrysogenum*

Method for investigation of viability for both organisms

- Detection of viability-declined clusters and individual pellet viability

Outlook

- Adapt and expand method to other agglomerate forming organisms
- At-line characterisation of complex fungal biomass in process development and routine manufacturing processes, with the clear potential for online application through automated sampling systems

***P. Pastoris* and *P. chrysogenum* stories can be found in…**

Pekarsky, Veiter et al. (2018) Production of a recombinant peroxidase in different glyco-engineered *Pichia pastoris* strains: a morphological and physiological comparison. Microb Cell Fact.17: 183. doi: 10.1186/s12934-018-1032-6

Veiter et al. (2019) The filamentous fungus *Penicillium chrysogenum* analysed via flow cytometry. Appl Microbiol Biotechnol 103:6725–6735. https://doi.org/10.1007/s00253-019-09943-4

Acknowledgments

Dr. Oliver Spadiut and Alexander Pekarsky for co-operation in *P. pastoris* experiments

ECCE 12, ECAB 5 2019 **Florence, Italy**

Curriculum vitae

Dipl.-Ing. Lukas Veiter
15.10.1989

Stolzenthalergasse 16/3
A - 1080 Wien
+ 43 (0) 676 88575 1125
lukas.veiter@gmx.at

Professional experience and Internships

2016 - present	Project Assistant 'Christian Doppler Laboratory for Mechanistic and Physiological Methods for Improved Bioprocesses', TU Wien, Vienna • Industrial project, working on filamentous fungi • Development and implementation of analytical methods • Planning and experimental realisation Tutoring and teaching, TU Vienna • Supervision of bachelor and master students: planning of theses and corresponding supervision of experiments, correction of theses • Laboratory courses: Biochemistry and Biotechnology
July/August 2014	Internship: production of virus deletion mutants for animal vaccines Boehringer Ingelheim Veterinary Research Center, Hannover
July 2013	Internship: oxide ceramics for dental prosthesis Treibacher Industrie AG, Althofen
July 2012	Internship: sample preparation for mass spectroscopy Treibacher Industrie AG, Althofen
July/August 2010	Internship: sample preparation for scanning electron microscopy Borealis GmbH, Advanced Polymer Characterisation, Linz

Academic Education

2016 - present	Doctoral program in the field of biochemical engineering under the supervision of Prof. Christoph Herwig at the TU Wien, Vienna
June 2016	Diplom Ingenieur (**Dipl.-Ing.**) in Technical Chemistry
2015	Diploma Thesis at the Institute of Chemical Engineering in the research division Biochemical Engineering, TU Wien 'The pET expression system revisited - how to boost soluble recombinant protein expression in *E. coli*'

2013 - 2016	Master program Technical Chemistry with focus on Biotechnology and Bioanalytics, TU Wien
June 2013	Bachelor of Science (**BSc**) in Technical Chemistry
2009 - 2013	Bachelor program Technical Chemistry, TU Wien

Scientific contributions, publications

Veiter L., Kubicek M., Hutter H., Pittenauer E., Herwig C. and Christoph Slouka „Study of metabolism and identification of productive regions in filamentous fungi via spatially-resolved Time-of-Flight Secondary Ion Mass Spectrometry.' Anal Bioanal Chem., 2019.

Veiter L. and Christoph Herwig 'The filamentous fungus *Penicillium chrysogenum* analysed via flow cytometry - a fast and statistically sound insight into morphology and viability.' Appl Microbiol Biotechnol., 2019.

Pekarsky A., **Veiter L.**, Rajamanickam V., Herwig C., Grünwald-Gruber C., Altmann F. and Oliver Spadiut 'Production of a recombinant peroxidase in different glyco-engineered *Pichia pastoris* strains: a morphological and physiological comparison.' Microb Cell Fact., 2018.

Veiter L., Rajamanickam V. and Christoph Herwig 'The filamentous fungal pellet - relationship between morphology and productivity.' Appl Microbiol Biotechnol., 2018.

Ehgartner D., Hartmann T., Heinzl S., Frank M., **Veiter L.**, Kager J., Herwig C. and Jens Fricke 'Controlling the specific growth rate via biomass trend regulation in filamentous fungi bioprocesses.' Chem Eng Sci., 2017.

Wurm D., **Veiter L.**, Ulonska S., Eggenreich B., Herwig C. and Oliver Spadiut 'The *E. coli* pET expression system revisited - mechanistic correlation between glucose and lactose uptake.' Appl Microbiol Biotechnol., 2016.

Presentations: PYFF7 Conference on Physiology of Yeast and Filamentous Fungi - Milan 2019,
RPP 10 Conference on Recombinant Protein Production - Crete 2019,
BioProduction Congress - Dublin 2018

Peer reviewing for scientific journals: Journal of Biotechnology

Skills and interests

Biochemical Engineering
Fermentation, design of experiments (DOE), HPLC, gel electrophoretic methods, enzymatic assays, blotting, flow cytometry, mass spectrometry, spectroscopic techniques, capacitance/permittivity, microscopy, PCR, cloning, filamentous fungi, yeast, bacteria

Languages
German (mother tongue), English (fluent), French (basic knowledge)

IT
Microsoft Office, Lucullus (Process Information Management System), DataLab, Matlab, MODDE